

UNCLASSIFIED

AD NUMBER

AD376669

CLASSIFICATION CHANGES

TO: unclassified

FROM: confidential

LIMITATION CHANGES

TO:  
Approved for public release, distribution unlimited

FROM:  
Distribution authorized to U.S. Gov't. agencies and their contractors; Administrative/Operational Use; 10 MAY 1966. Other requests shall be referred to Federal Aviation Administration, Washington, DC.

AUTHORITY

FAA ltr, 10 Oct 1972; FAA ltr, 10 Oct 1972

THIS PAGE IS UNCLASSIFIED

# **SECURITY**

---

# **MARKING**

**The classified or limited status of this report applies to each page, unless otherwise marked.**

**Separate page printouts MUST be marked accordingly.**

---

**THIS DOCUMENT CONTAINS INFORMATION AFFECTING THE NATIONAL DEFENSE OF THE UNITED STATES WITHIN THE MEANING OF THE ESPIONAGE LAWS, TITLE 18, U.S.C., SECTIONS 793 AND 794. THE TRANSMISSION OR THE REVELATION OF ITS CONTENTS IN ANY MANNER TO AN UNAUTHORIZED PERSON IS PROHIBITED BY LAW.**

**NOTICE: When government or other drawings, specifications or other data are used for any purpose other than in connection with a definitely related government procurement operation, the U. S. Government thereby incurs no responsibility, nor any obligation whatsoever; and the fact that the Government may have formulated, furnished, or in any way supplied the said drawings, specifications, or other data is not to be regarded by implication or otherwise as in any manner licensing the holder or any other person or corporation, or conveying any rights or permission to manufacture, use or sell any patented invention that may in any way be related thereto.**

AD-376 669

Best Available Copy

Best Available Copy

**Best  
Available  
Copy**



## NOTICES

When Government drawings, specifications, or other data are used for any purpose other than in connection with a definitely related Government procurement operation, the United States Government thereby incurs no responsibility nor any obligation whatsoever; and the fact that the Government may have formulated, furnished, or in any way supplied the said drawings, specifications, or other data, is not to be regarded by implication or otherwise as in any manner licensing the holder or any other person or corporation, or conveying any rights or permission to manufacture, use, or sell any patented invention that may in any way be related thereto.

Copies have been placed in the DDC collection. U.S. Government agencies may obtain copies from DDC. Other qualified DDC users may request, by submission of a DDC Form 1, through:

Director of Supersonic Transport Development  
Federal Aviation Agency  
Washington, D.C. 20553

Defense Documentation Center release to the Clearinghouse for Federal, Scientific, and Technical Information (CFSTI) and foreign announcement and dissemination are not authorized. The distribution of this report is limited because it contains technology identifiable with items excluded from export by the Department of State (U.S. Export Control Act of 1949 as amended).

**CONFIDENTIAL**

PWA FR-1855  
10 MAY 1966

(UNCLASSIFIED TITLE)  
**MONTHLY PROGRESS REPORT NO. 10**

**DEVELOPMENT OF  
A SUPERSONIC TRANSPORT  
AIRCRAFT ENGINE**

**PHASE II-C**

**1 APRIL THROUGH 30 APRIL 1966**



**CONTRACT NO. FA-55-66-8**

**(Competitive Data)**

THIS DOCUMENT CONTAINS INFORMATION AFFECTING THE NATIONAL DEFENSE OF THE UNITED STATES WITHIN THE MEANING OF THE ESPIONAGE LAWS, TITLE 18, U. S. C. SECTION 793 AND 794, IS TRANSMITTED OR THE REVELATION OF THE CONTENTS OF WHICH IN ANY MANNER TO AN UNAUTHORIZED PERSON IS PROHIBITED BY LAW.

**Pratt & Whitney Aircraft** DIVISION OF UNITED AIRCRAFT CORPORATION  
FLORIDA RESEARCH AND DEVELOPMENT CENTER

**U  
A<sup>®</sup>**

DECLASSIFIED AFTER 12 YEARS FROM 1966-10-10

**CONFIDENTIAL**

CONTENTS

SECTION		PAGE
I	SUMMARY OF PROGRESS. . . . .	I-1
II	PROBLEM REPORT . . . . .	II-1
III	DESCRIPTION OF TECHNICAL PROGRESS. . . . .	III-A-1
	A. Engine Design. . . . .	III-A-1
	B. Engine Test. . . . .	III-B-1
	C. Compressor . . . . .	III-C-1
	D. Primary Combustor. . . . .	III-D-1
	E. Turbine. . . . .	III-E-1
	F. Augmentor. . . . .	III-F-1
	G. Exhaust System . . . . .	III-G-1
	H. Controls . . . . .	III-H-1
	I. Bearings and Seals . . . . .	III-I-1
	J. Fuels and Lubricants . . . . .	III-J-1
	K. Inlet System Compatibility . . . . .	III-K-1
	L. Noise. . . . .	III-L-1
	M. Mockups. . . . .	III-M-1
	N. Coordination . . . . .	III-N-1
	O. Maintainability. . . . .	III-O-1
	P. Value Engineering. . . . .	III-P-1
	Q. Configuration Management . . . . .	III-Q-1
	R. Quality Assurance. . . . .	III-R-1
	S. Reliability. . . . .	III-S-1
IV	AIRLINE COMMENTS . . . . .	IV-1
V	STATE-OF-THE-ART . . . . .	V-1
	APPENDIX A - Augmentor Development Review	
	APPENDIX B - Fuels Activity Review	

SECTION I  
SUMMARY OF PROGRESS

The first experimental engine completed 11.68 hours of testing, including 27 minutes operation with the duct heater lit. Subsequent disassembly revealed no major problems. Objectives for the first build of the engine were attained. Engine parameters obtained included  $N_2$  speeds from idle to 90% of design speed, and airflows from idle to 88% of design flow. The maximum demonstrated corrected thrust was 22,850 pounds with duct heater lit and 18,060 pounds nonaugmented. The highest turbine inlet temperature was 1760°F. Rebuild of this engine is in process and is scheduled to resume testing the latter part of May. The second experimental engine build is in progress.

The rebuilt high compressor rig testing was continued with simulated Build No. 5 fan discharge profiles at the high compressor inlet. No adverse effect was observed in overall compressor performance or stress level. The rig is being rebuilt with reoperated parts to increase the work load in the middle stages.

Testing of the 0.6-scale fan rig with the recambered 2nd-stage blades, the original design 1st-stage blades, and the "drooped" splitter has shown that the 2nd-stage blades were not passing the desired airflow at high corrected speeds. The 2nd-stage blades are being redesigned to increase airflow, and parts will be procured for testing in the 0.6-scale fan rig.

A Preliminary Engine Specification for the JTF17A-21L was issued for Lockheed's application of an increased airflow study version of the JTF17A-20 engine.

Pratt & Whitney Aircraft SST program personnel attended or conducted meetings with representatives of The Boeing Company, Lockheed California Company, the Federal Aviation Agency, aviation jet fuel supplier, Booz-Allen Applied Research, Inc., Research Analysis Corporation, Delta Airlines, and National Airlines on subjects of SST fuel requirements, current tubing technology, design details, growth studies, noise attenuation studies, SST economics, engine/airframe interface activities, and general SST discussions.

SECTION II  
PROBLEM REPORT

Teardown of the first experimental engine, FX-161, revealed several cracks in a labyrinth air seal ahead of the 1st-stage turbine disk as reported in paragraph III-B. A redesigned seal to eliminate this problem is being incorporated in the rebuild of the first experimental engine.

Detailed inspection of the engine oil system and bearing compartments revealed no defective parts nor connection leaks to account for intermittent oil loss noted during the first runs. Analysis of the system indicated possible leakage past the No. 2 face carbon seal as the result of poor drainage of oil through holes in the No. 2 bearing support. Corrective action in the form of increased number and size of drain holes and a 30% increase in spring force on the carbon seal has been incorporated into parts for the second build of FX-161 and the second experimental engine, FX-162.

SECTION III  
DESCRIPTION OF TECHNICAL PROGRESS

A. ENGINE DESIGN

1. Fan

A design study was completed for the Lockheed inlet to provide a means of attachment for the trailing edge portion of the flow divider. Vertical assembly requirements necessitate that this attachment be done prior to installation of the engine.

An initial design study of the Boeing front mount system was completed. An alternative front mount system was investigated.

Evaluation of design changes for the prototype engine was continued.

2. Fan Rig

Design layout and detail drawings were completed for a sheet metal inlet bellmouth as a replacement for the fiberglass bellmouth that failed on the 0.6-scale fan rig.

A redesigned 2nd-stage fan rig blade was completed and detail drawings will be completed in May.

3. High Compressor

Design changes were completed to improve the end wall condition of the variable stators. End gaps were reduced by selective fitting.

The design layout for independent actuation of the 7th-stage stator on the experimental engines was completed.

Design and detail drawings were completed for redesigned 3rd-, 4th-, and 5th-stage blades. See paragraph III-C for aerodynamic description.

The telemetry instrumentation design for high rotor at the No. 3 bearing compartment is scheduled for completion early in May.

A design change was completed to provide more clearance between the damper weight and the disk lug to preclude binding of the blade damper weights.

4. Primary Combustor

Incorporation of primary combustor design changes for the prototype engine is continuing. The status of the primary combustor rig is reported in paragraph III-D.

5. Duct Heater

Incorporation of duct heater design changes for the prototype engine is continuing.

5. Turbine

Incorporation of turbine design changes for the prototype engine is continuing. The status of the turbine rigs is reported in paragraph III-E.

7. Shafts, Bearings, and Seals

Incorporation of the bearing compartments design changes for the prototype engine is continuing.

Redesigns to prevent oil leakage from the No. 1 and No. 2 seal compartment were completed. This included improved drainage from the upper tower shaft (starter gearbox), from the cavity between the No. 2 bearing and seal and from the cavity between the No. 1 bearing and the forward seal.

8. Accessory Drives

Design of a power takeoff gearbox and decoupler for the Lockheed installation is continuing based on currently available airframe information. Two feasibility studies of a combination power takeoff and airframe hydraulic pump drive gearbox for the Boeing installation were completed and submitted for airframe comment. These differ in the orientation of the pump and power takeoff pads.

Design modifications were made to increase the oil drainage passage for the experimental engine starter adapter gearbox (to permit use of existing J58 starters) to avoid flooding the gearbox. This gearbox is not a component of the prototype engine. It is a test stand component that is engine-mounted.

9. Fuel System

A schematic drawing of the fuel and hydraulic systems depicting proposed plumbing connections between control components and between components and manifolds has been initiated for the prototype Boeing engine and is approximately 75% complete.

10. Control System

a. Experimental Engine

Design work for an alternative system for automatic duct nozzle control was completed in this report period. The completion of detail drawings is scheduled in May.

Design work on duct nozzle and clamshell actuator plumbing for the final experimental engine was continued and is scheduled for completion early in the next period.

b. Prototype Engine

The component rearrangement study for the Boeing engine is approximately 80% complete. In conjunction with this study, new envelope drawings were initiated for the unitized fuel control, main fuel pump, and the hydraulic pump.

Mockups of quick-disconnect fuel controls for the Lockheed configuration were received from two vendors and are being evaluated.

11. Electrical and Instrumentation System

A preliminary electrical diagram was completed and sent to Boeing.

12. Reverser-Suppressor

Studies of the prototype reverser-suppressor are continuing. Effort is being directed to simplify and foolproof the actuation, synchronization, and interlocking of the suppressor blow-in and clamshell reverser doors.

Minor design modifications are being made to facilitate the manufacture of the reverser-suppressor for the initial experimental engines. These modifications are primarily to simplify tooling and material procurement, and to eliminate components that would not be functional in the initial test period.



No single suitable system has yet been devised which will satisfy the installation requirements of both airframes without major modification. It is becoming increasingly apparent that this section of the engine must be designed specifically for a particular installation.

Design was completed of a more universal wind tunnel model of the reverser-suppressor for performance studies. This model will allow simple interchange of components to allow evaluation of various configurations and settings.

## B. ENGINE TEST

	April	Phase II-C Total
FX-161	11.60 hours	11.68 hours

## 1. Experimental Engine

## a. FX-161 Testing

Testing of the first JTP17A-20 experimental engine (FX-161) was continued through completion of the scheduled test program in the first week of April. The engine accumulated 11.68 hours of which 0.45 hour was duct heating time. The test attained all the objectives of the initial test program. A chronological list of significant events during the test on FX-161 is as follows:

- 31 March Made initial start on engine and recorded functional and performance data at idle thrust.
- 1 April Confirmed starting schedule. Checked operation of variable stator actuation system at 5200 high rotor ( $N_2$ ) rpm.
- 2 April Performance calibration was obtained up to 6550  $N_2$  rpm including variable stator rotation to sea level takeoff position. Shut down to repair oil leak in top-mounted starter gearbox.
- 4 April Continued performance calibration through 90% of design  $N_2$  speed.
- 5 April Lit duct heater at 7250  $N_2$  rpm to check light-off fuel flows and operation of systems. Shut down to inspect engine and -VI systems. Conducted performance calibration with duct heater lit.
- 6 April Removed engine from test stand for teardown and inspection.

The engine teardown was accomplished with the engine in a horizontal position to take maximum advantage of all visual condition indications; i.e., oil stains, seal positions, residual oil volumes in compartments, etc. Visual, x-ray, and dimensional inspection of all major parts revealed that all parts were in excellent condition, and were acceptable for rebuild of the engine. One labyrinth air seal ahead of the last-stage turbine disk had cracked in several places across the knife edges, as shown in Figure III-B-1. Analysis of the seal indicated that the cracking was caused by a high order resonance (approximately 6000 cps). The seal has been redesigned to increase the clearance and to incorporate a stiffener and damper.

Several times during the test runs evidence of oil leakage from the overboard ambient vents was noted. Visual inspection of the oil system and bearing compartments during disassembly and detailed part inspection revealed no defective parts nor loose connections in the oil system. Analysis of the oil supply system, oil scavenging system, compartment breather system, and seal ambient vent system indicated that additional scavenge drain area through holes in the No. 2 bearing support should avoid flooding the No. 2 face seal. Parts for the rebuild of FX-161, and for subsequent engines, have been prepared to increase the number and size of these holes to improve oil drainage down to the gearbox scavenge pump. The spring force on the face seals of the No. 1 and No. 2 compartment were increased by 30% to provide better sealing at idle conditions when fan discharge pressure outboard of the seals is at a minimum. It is significant that the seal overboard vent system worked as intended and no trace of oil was found in the gas path leading to the cabin air bleed ports.

Rebuild of the engine is underway and delivery of the engine to test is scheduled for late May 1966.

#### b. Engine FX-161 Performance Analysis

The following performance evaluations were made from the first test of the JTF17A-20 engine:

1. Engine FX-161 essentially met the performance predictions for this engine.

2. Maximum demonstrated corrected thrust was 22,850 lb with duct heater lit, and 18,060 lb without duct heating.
3. A high rotor ( $N_2$ ) speed of 7290 rpm was achieved; this represents 90% of the design sea level  $N_2$  rpm of the engine.
4. Maximum average turbine inlet temperature of 1760°F was measured at 7290 rpm.
5. Duct heater operation was conducted in Zone I only, and to a maximum fuel-air ratio of 0.013. Duct heater light-offs were made at a fuel-air ratio of 0.002 with no noticeable pressure perturbation.
6. Operation with the variable compressor stators was as predicted from the high compressor rig.
7. Maximum corrected airflow in the engine was 570 lb/sec at the 7290 rpm speed. The engine bypass ratio was 1.74.
8. The TSFC corresponding to the 7290 rpm ( $N_2$ ) duct heating point was 0.774.

#### c. Engine PX-161 Vibration Analysis

Analysis of the engine resonance speeds for the first demonstrator engine was completed during the initial design. The analysis that was used incorporates the Timoshenko differential equations for a rotating shaft, together with the Prohl method of integration to derive sets of difference equations. The complete engine and mount structure can be accurately represented in this system, and the analysis is programmed for large-scale digital computer solution. Solution of the difference equations yields the natural frequencies that are used to compute the normalized deflection curves. The Pratt & Whitney Aircraft design criterion is to allow 20% stiff bearing margin in all supports to limit shaft deflections.

A resonance may theoretically be excited by either rotor in a two-spool engine; however, the rotor with significant bending is generally considered to cause the excitation. The inertial effects caused by difference in high and low speed rotors are included in the analysis through the use of Euler's equations of motion.

Modes of vibration were calculated for a completely elastic engine as shown in figures III-B-2 through III-B-11, and are as follows:

- 1st mode - Pitching and bouncing of engine on its support structure (figure III-B-2).
- 2nd mode - Cantilevered gas generator moving out of phase with main engine case (figure III-B-3).
- 3rd mode - Pitching of the engine on the stand support (figure III-B-4).
- 4th mode - First bending of the entire engine case (figure III-B-5).
- 5th mode - Low rotor bending and turbine bounce (figure III-B-6).
- 6th mode - Turbine moving out of phase with inner engine case (figure III-B-7).
- 7th mode - Fan mode (figure III-B-8).
- 8th mode - High compressor bending and pitching about the No. 4 bearing (figure III-B-9).
- 9th mode - Inner and outer engine cases in phase (figure III-B-10).
- 10th mode - Inner and outer engine cases out of phase (figure III-B-11).

A comprehensive vibration analysis was conducted on the initial test of engine PX-161. A deceleration transient from 7250  $N_2$  rpm and 5220  $N_1$  rpm was recorded and is shown graphically in figures III-B-12 through III-B-17.

Steady-state vibration data taken at 7250  $N_2$  rpm and 5220  $N_1$  rpm are also shown graphically in figures III-B-18 through III-B-25.

The forced vibrations produced by the high and low rotor residual unbalance can be readily distinguished as displacement peaks at the respective frequencies of the rotors. The low order of displacements evidenced in the steady-state plots and the lack of significant response to shaft speed in the transient plots gives good indication of the proper interaction between shafts, bearing supports, and engine cases, and confirms the design integrity of the engine concept.

d. Engine FX-162

Procurement of parts for the second experimental engine (FX-162) is nearing completion, and assembly of subassemblies is underway. Completion of the engine build is now scheduled for June.

The parts list for FX-162 is essentially identical to engine FX-161 except for improved aerodynamics in the fan (Build 7), which allows operation at an increased fan pressure ratio.

2. Material and Fabrication

The results of long-time stress rupture and creep rupture testing of current alloys (TD nickel, TD nichrome) Waspaloy, titanium, Astroloy, I-718, Hastelloy X, L-605, IN-100, and SM-302 are plotted in figures III-B-26 through III-B-46. The results are used to verify current design material property curves; when they are not in agreement, the design curves are modified. On new material, the results are used to generate design curves.

3. Sulfidation Testing

Sulfidation testing of current materials and coatings has continued. The test conditions were 1.0 ppm NaCl content in air and maximum sulfur content allowed (0.3%) by fuel specification PWA 533. The metal temperatures of the specimens were maintained at 1800°F.

PWA 47 coating applied on the entire PWA 658 material specimen provided protection from sulfidation attack for 450 hours. Two specimens of TD nickel (PWA 1035) coated with PWA 62 (applied by two different sources) showed acceptable sulfidation protection after testing for 150 hours on one specimen and 300 hours on the other specimen. PWA 658 with a newly developed coating continued to show excellent sulfidation resistance after 1300 hours of testing. (See figures III-B-47 and III-B-48.) Testing is continuing on the PWA 658 and PWA 1035 specimen.

4. LCF Testing of Film Cooling Slots

A report of the LCF testing is presented in paragraph III-E.

## 5. Advanced Material and Manufacturing Processes

Related technology to the manufacture and process control evaluation and development is as follows:

1. The development program on an alloy with the strength of L-605 and oxidation resistance of Hastelloy X is continuing. Material has been ordered with modified alloy chemistry to improve the oxidation resistance while maintaining the elevated temperature mechanical properties. Additional testing will be conducted when these specimens are received.
2. Astroloy Sheet Program - Testing has been completed on both the hot rolled and cold rolled sheet. Preliminary analysis of data is promising; a complete analysis of testing results is in process.
3. UX-1500 Program - Evaluation of forgeability on subscale ingots is in process.
4. Extrusion Forgings of IN-100 and Modified SM-200 Alloys for Turbine Blade Application - Complete analysis of the original heat treat specimens showed low prior elongation (less than 1% creep rupture). Heat treat cycles are being modified and evaluations are continuing.

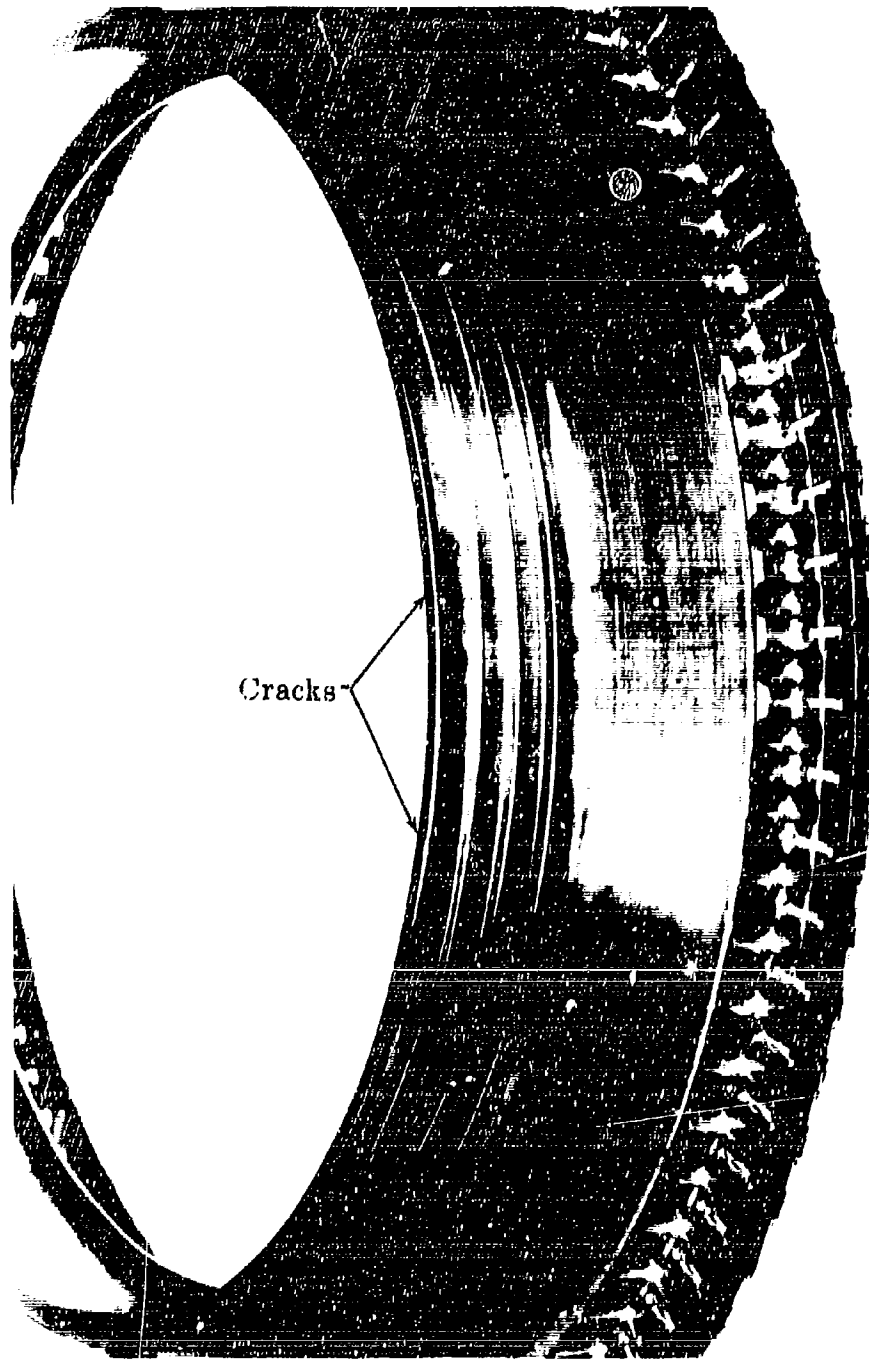
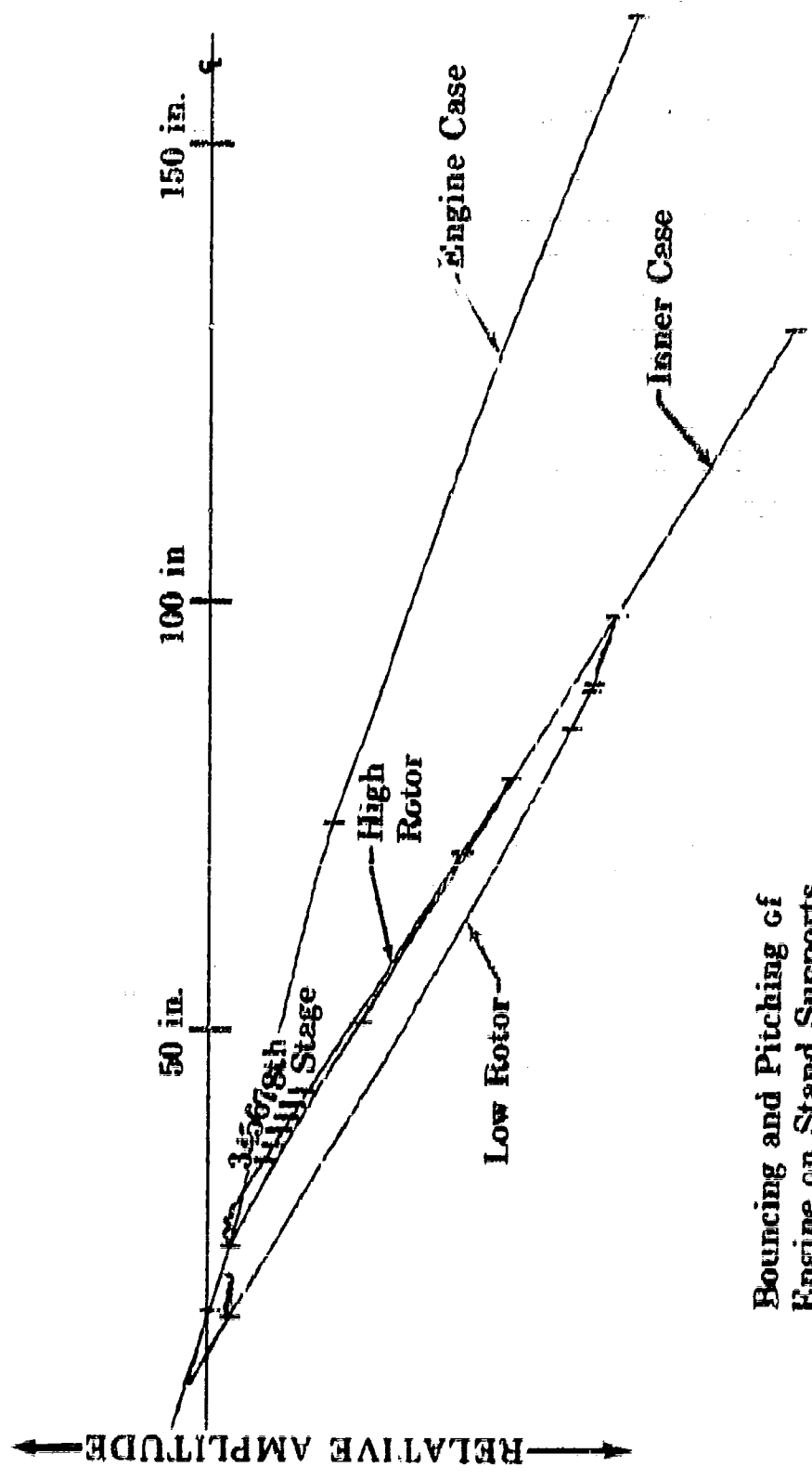


Figure III-B-1. Labyrinth Air Seal Ahead of  
1st-Stage Turbine Disk

FD 15615

III-B-7

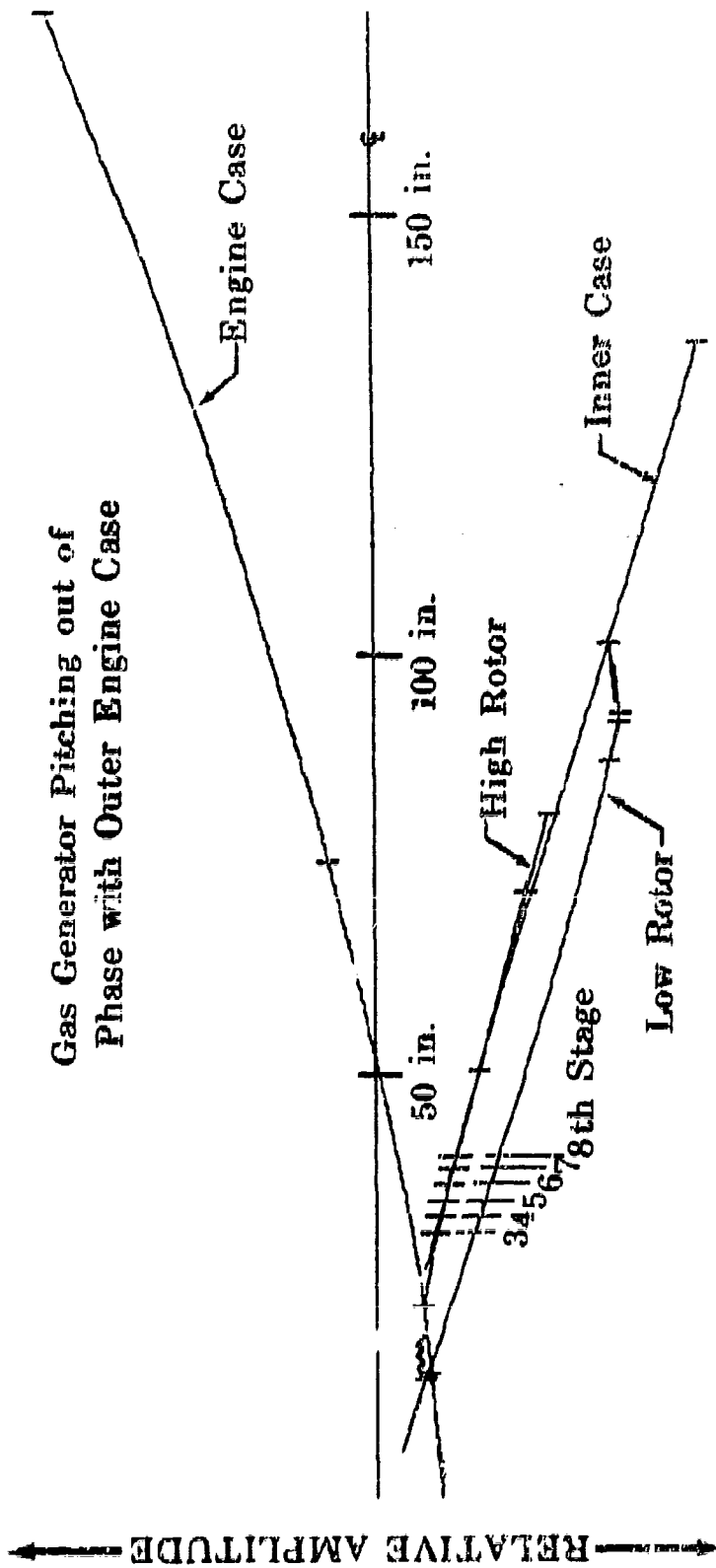




Bouncing and Pitching of  
Engine on Stand Supports

Figure III-B-2. Calculated JTF17A-20 Engine Vibrational Mode at 690 rpm

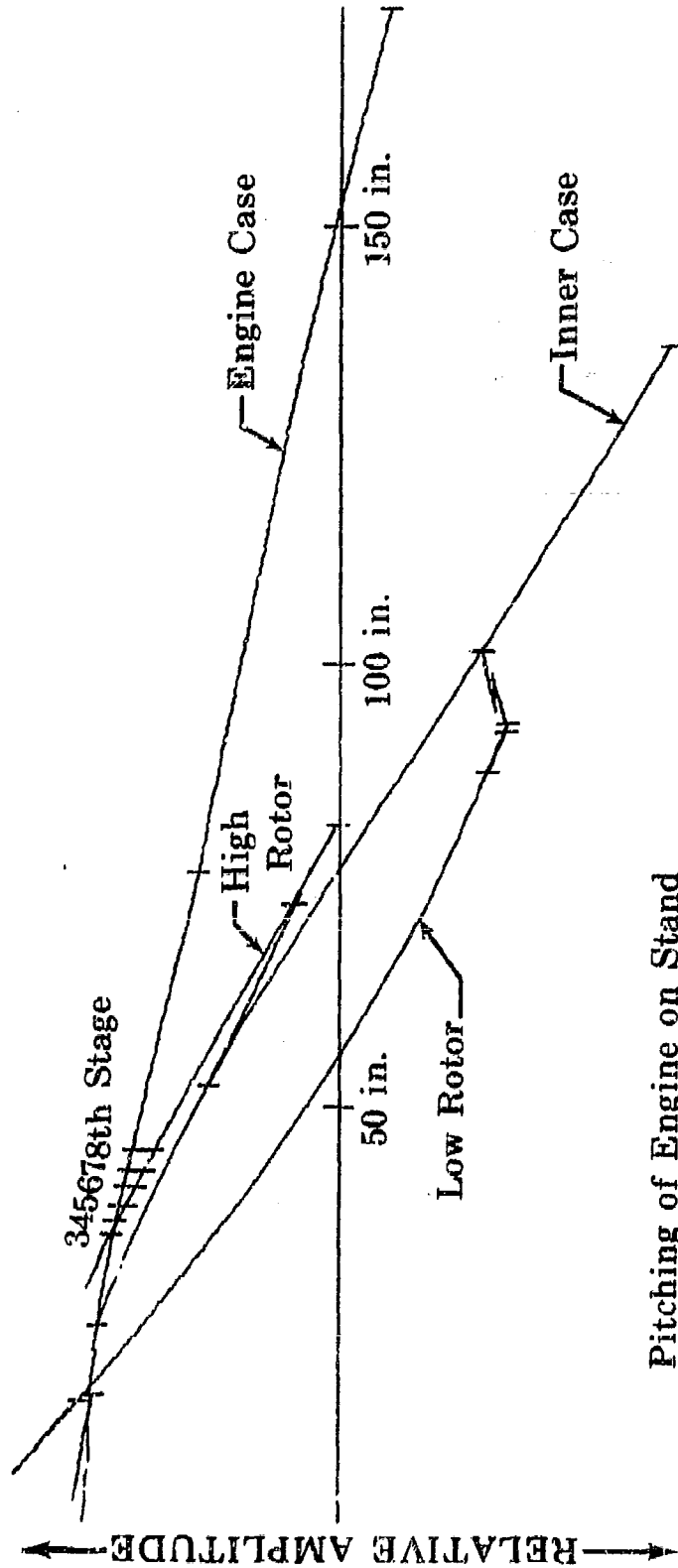
ED 15167



6-8-111

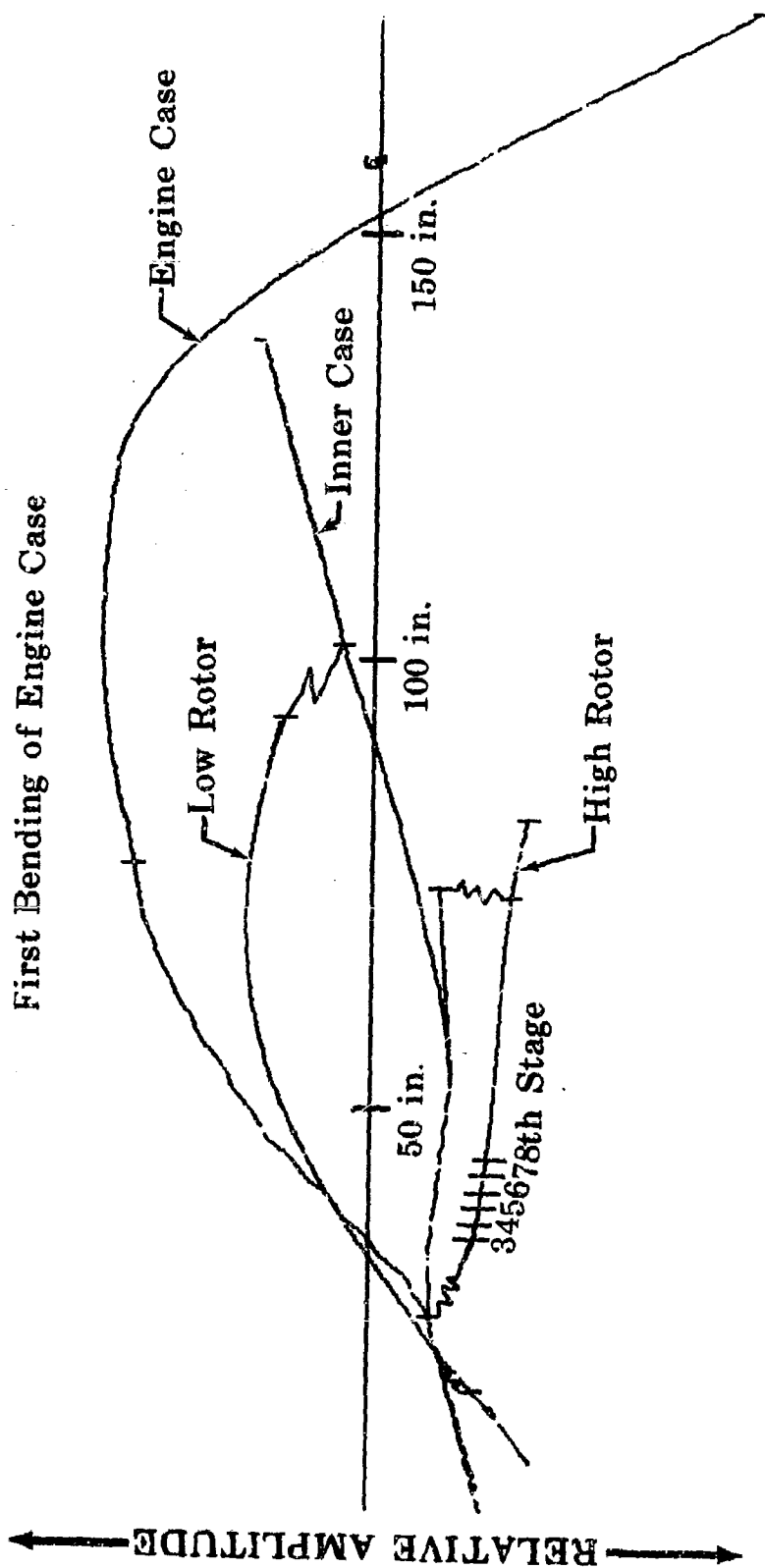
Figure III-B-3. Calculated JTF17A-20 Engine Vibrational Mode at 1090 rpm

FD 15173



Pitching of Engine on Stand

Figure III-B-4. Calculated JT17A-20 Engine Vibrational Mode at 1960 rpm

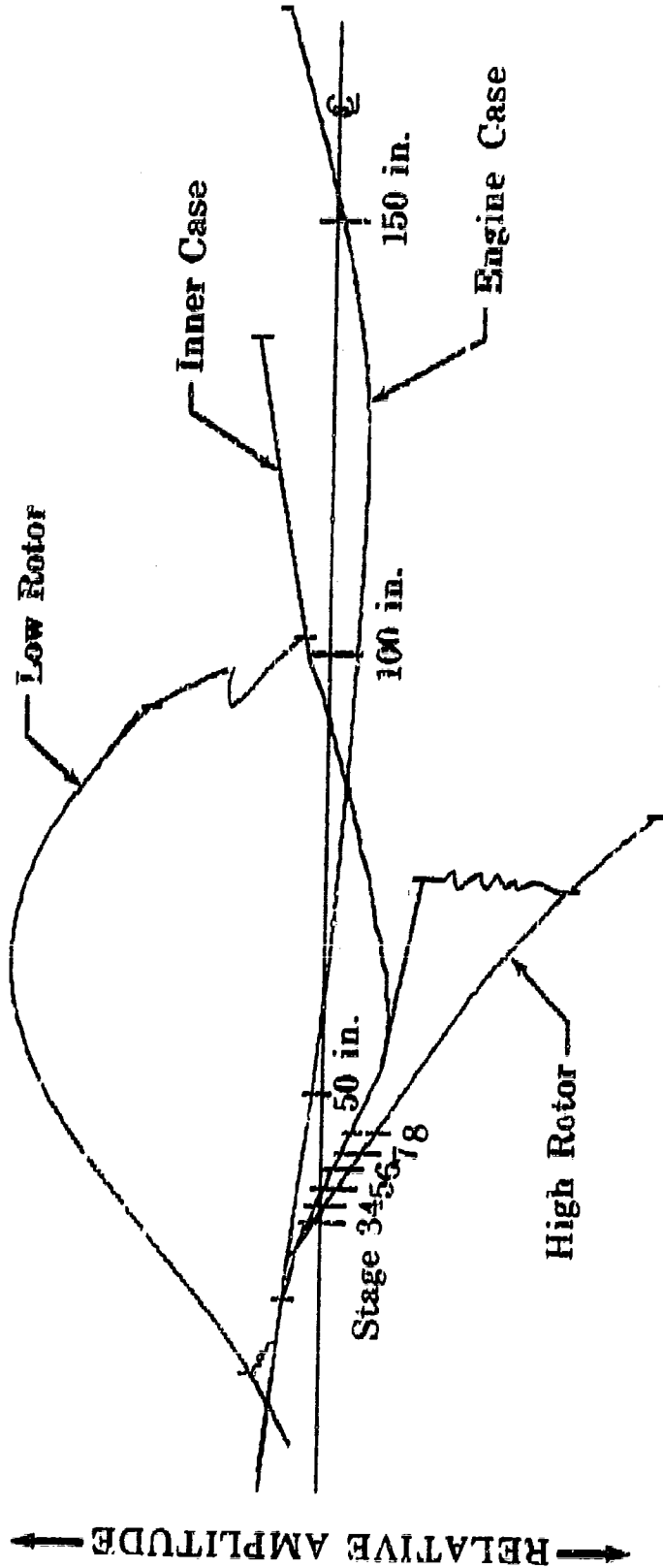


First Bending of Engine Case

Figure III-B-5. Calculated JTF17A-20 Engine Vibrational Mode at 4460 rpm

FD 15174

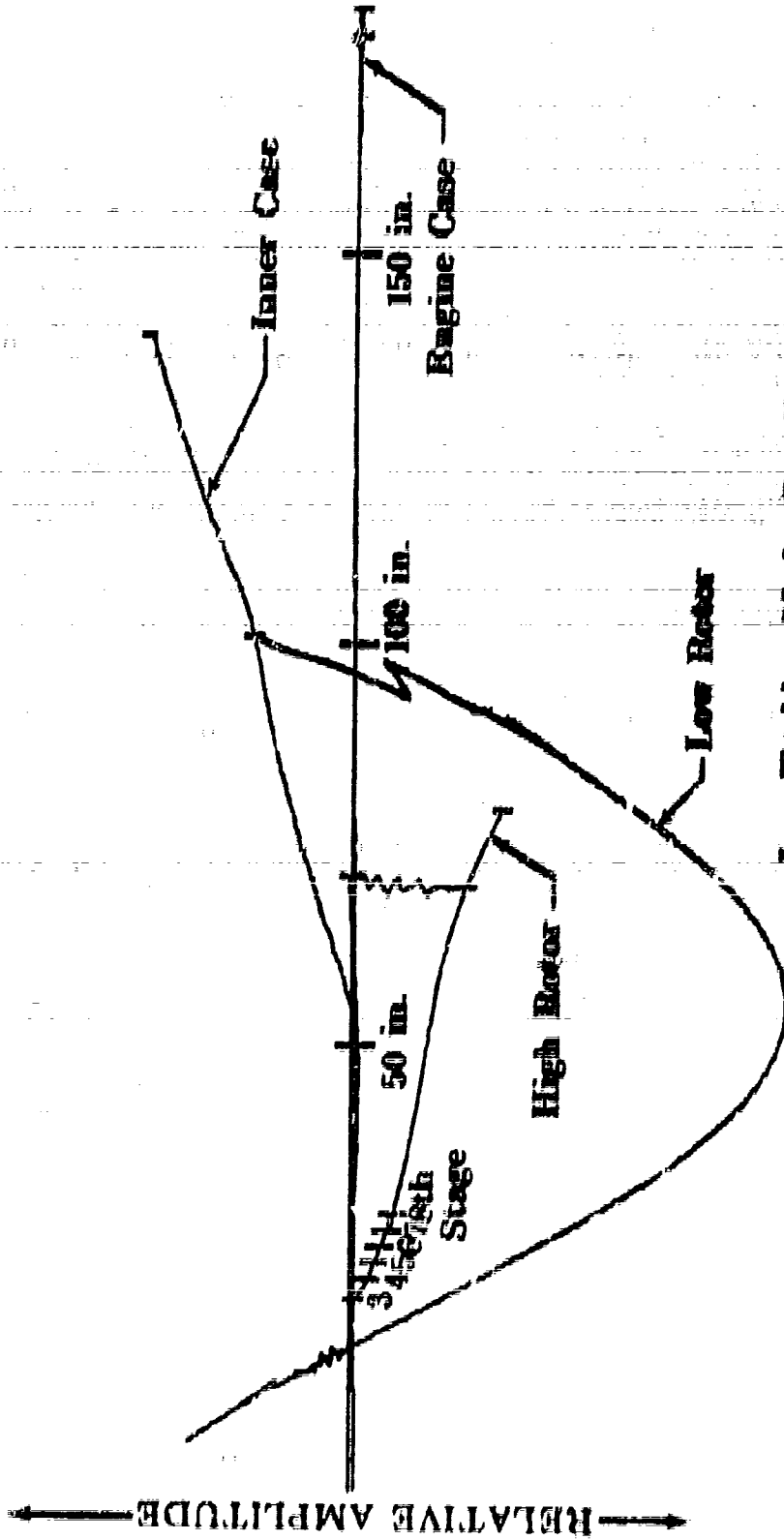
First Bending of Low Rotor



III-B-12

Figure III-B-6. Calculated J417A-20 Engine Vibrational Mode at 5090 rpm. (Low Rotor)

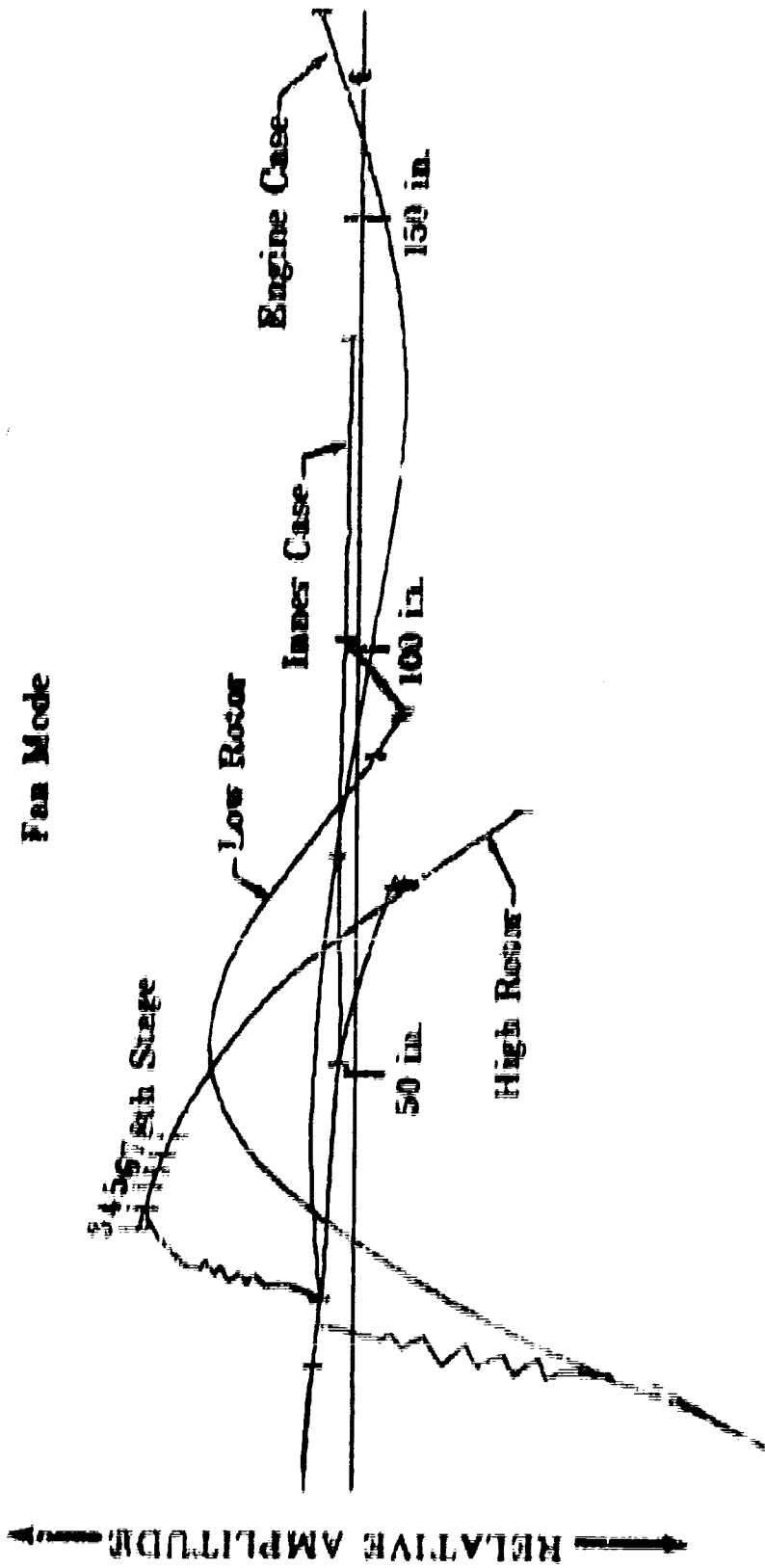
59 15169



Low Turbine Mode (Bending of the Turbine  
Shaft out of Phase with Inner Case)

FIGURE III-4-7. Calculated JTFM-20 Engine Vibrational Mode at 6150 rpm (Low Rotor)

FD 15166

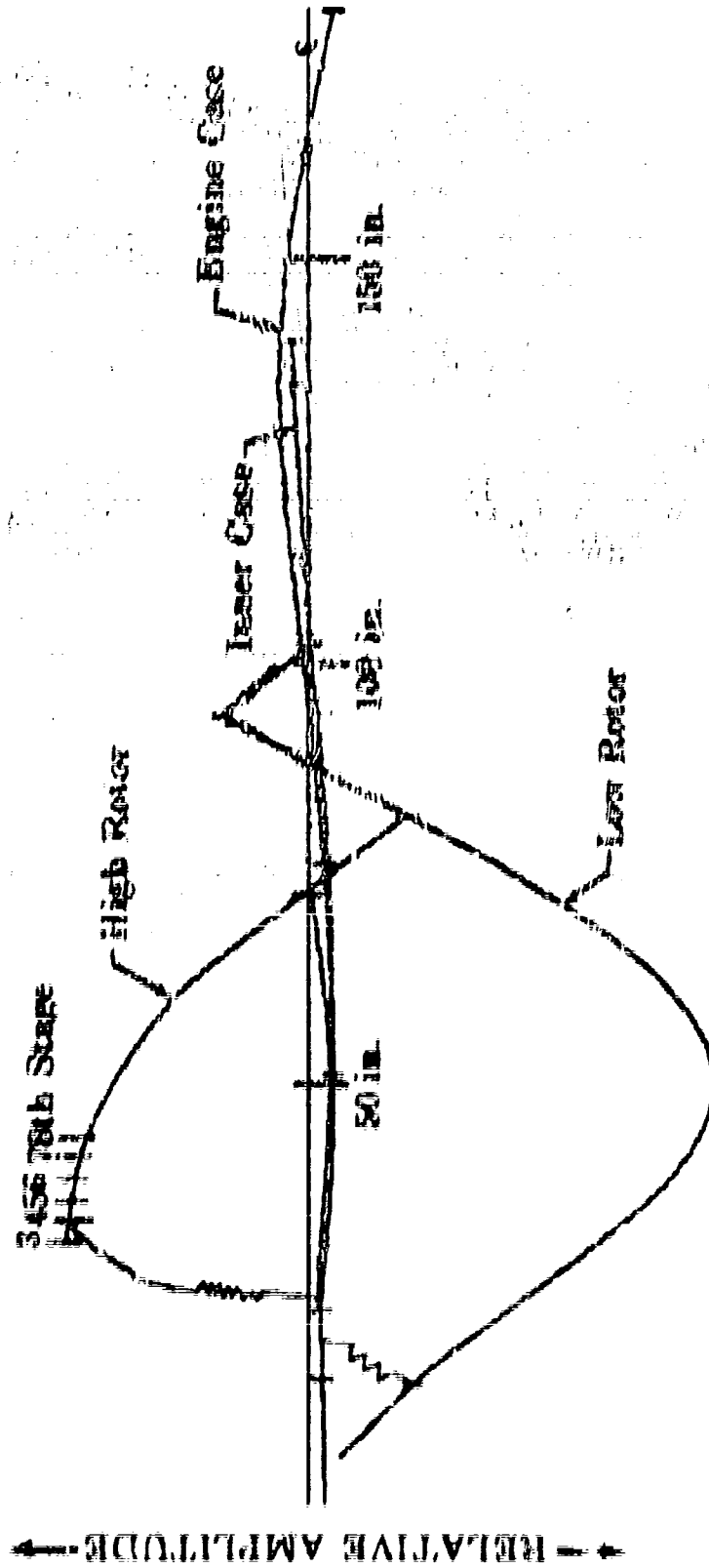


91 9-111

Figure 111-3-a. Calculated 111-20 Engine Vibration Mode at 7200 rpm (Case Linear)

FD 15168

High Compressor Mode



51-B-111

Pratt & Whitney Aircraft, Inc., 1000 Broadway, New York, N.Y. 10003 (High Rotor)

FD 15139



### Second Bending of Engine Case (Inner Case in Phase)

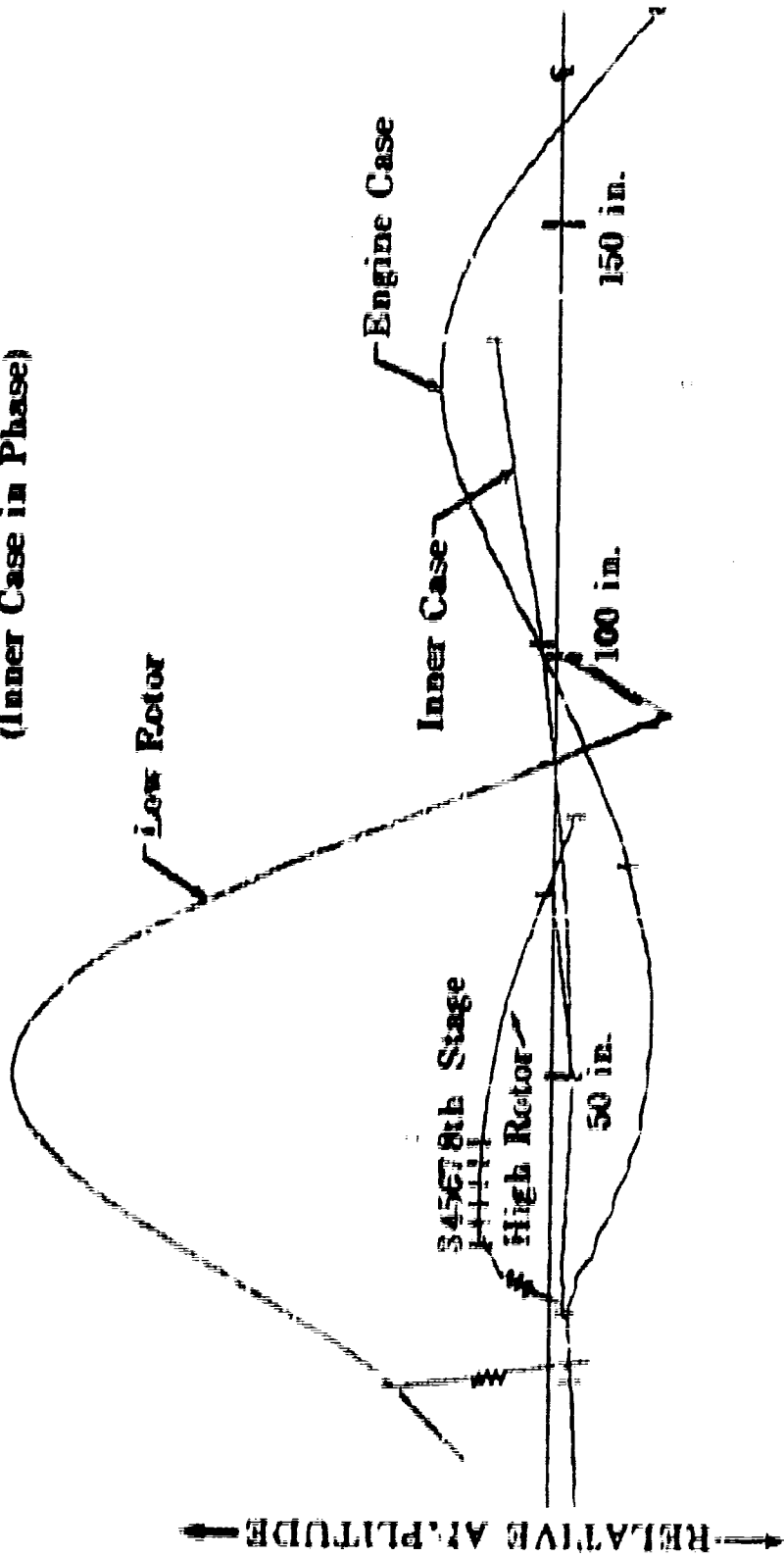
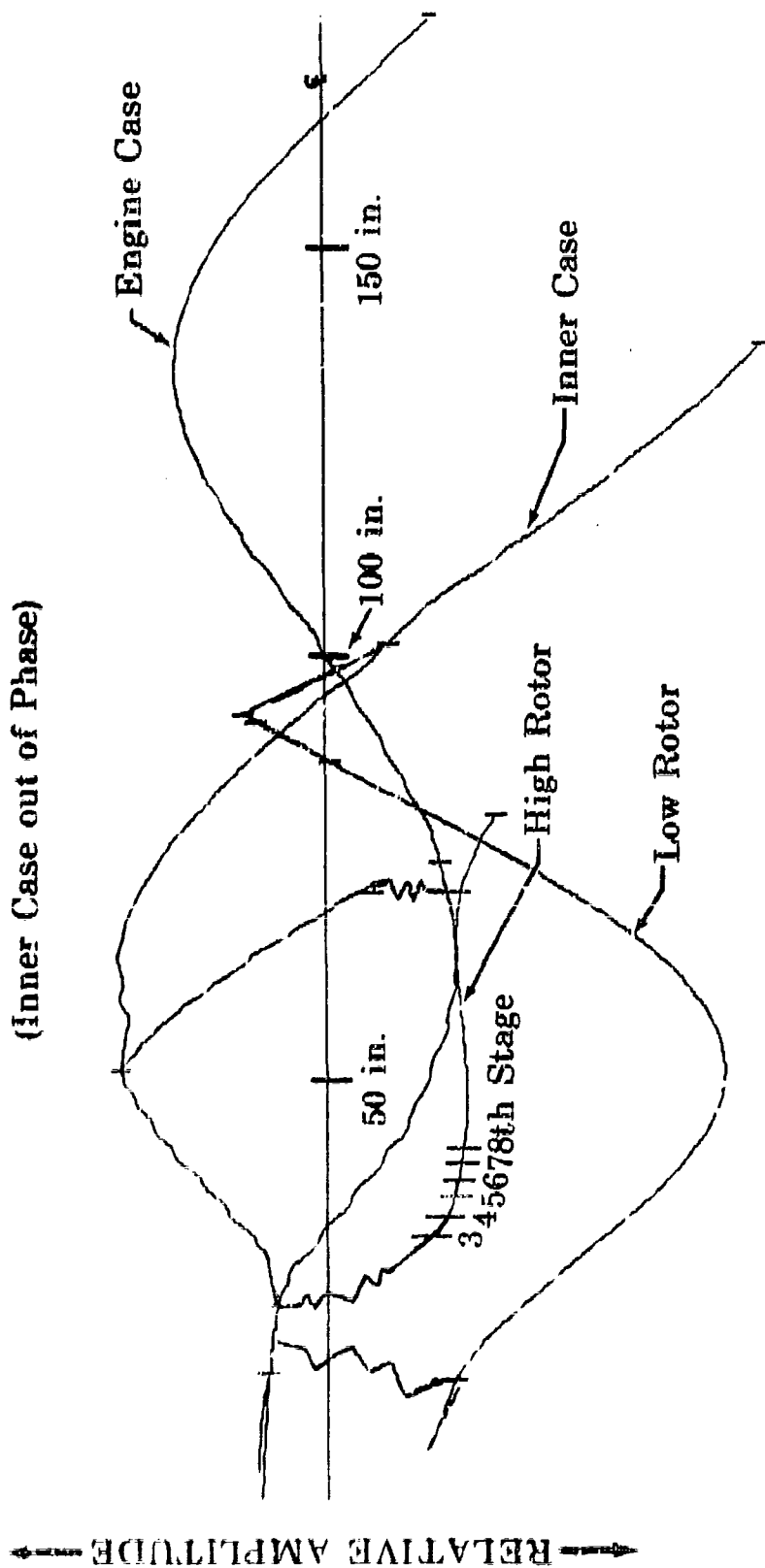


Figure 11-B-10. Calculated JTFI 24-20 Engine Vibrational Mode at 8100 rpm (High Rotor)

FD 15176

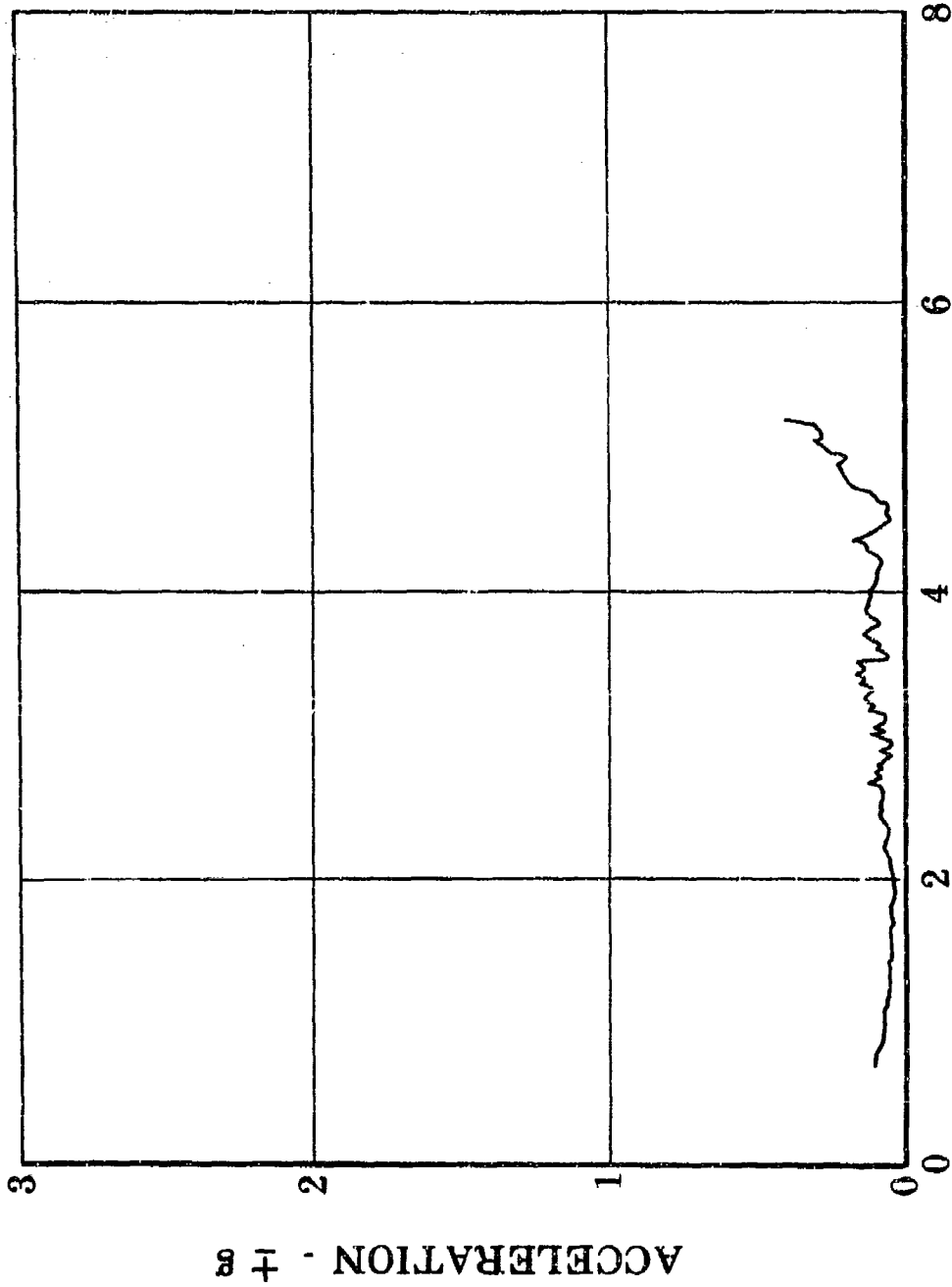
Second Bending of Engine Case  
(Inner Case out of Phase)



FD 15171

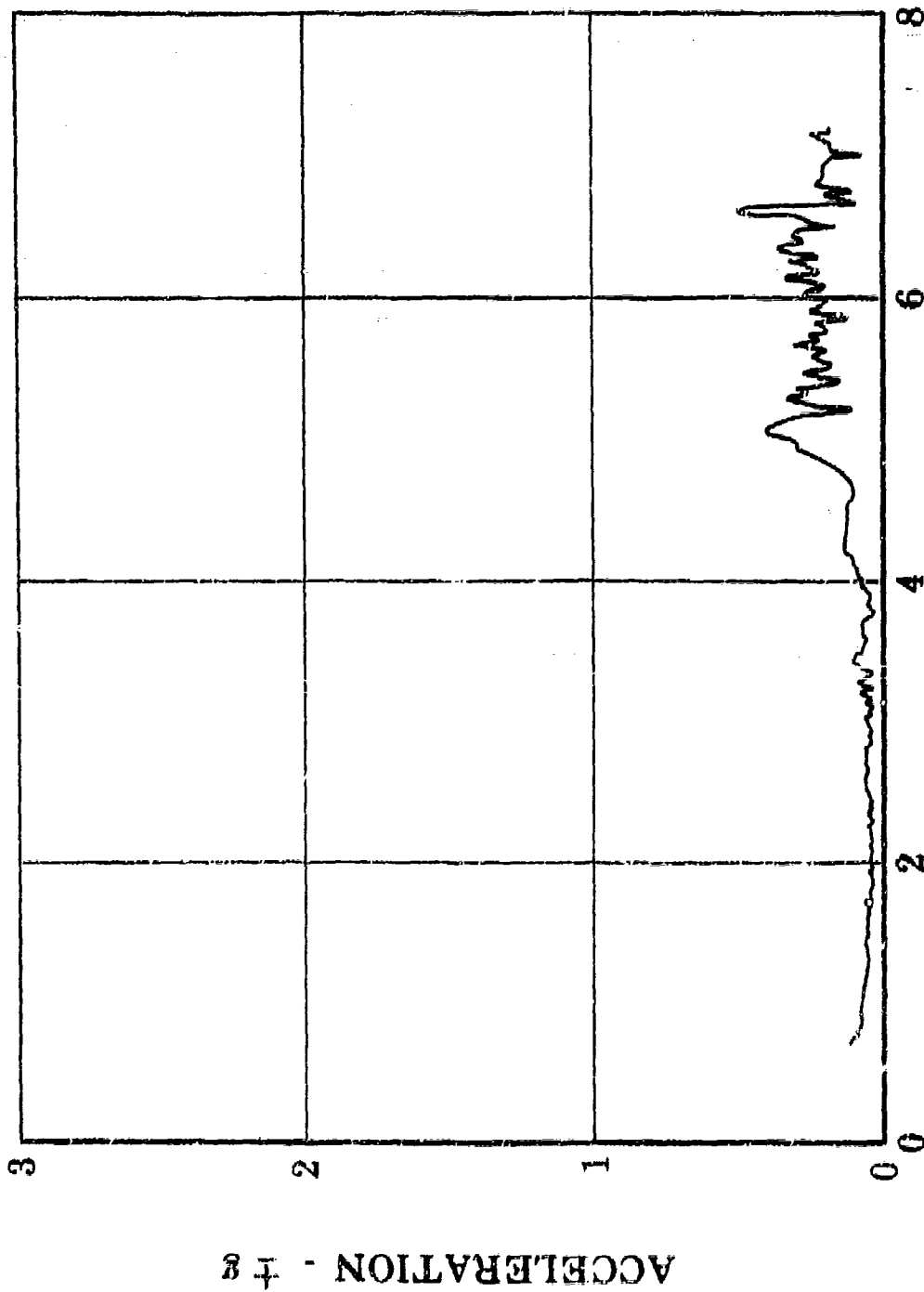
Figure III-B-11. Calculated JTF17A-20 Engine Vibrational Mode at 8700 rpm (High Rotor)

FD 15602



**LOW ROTOR SPEED - rpm(Thousand)**

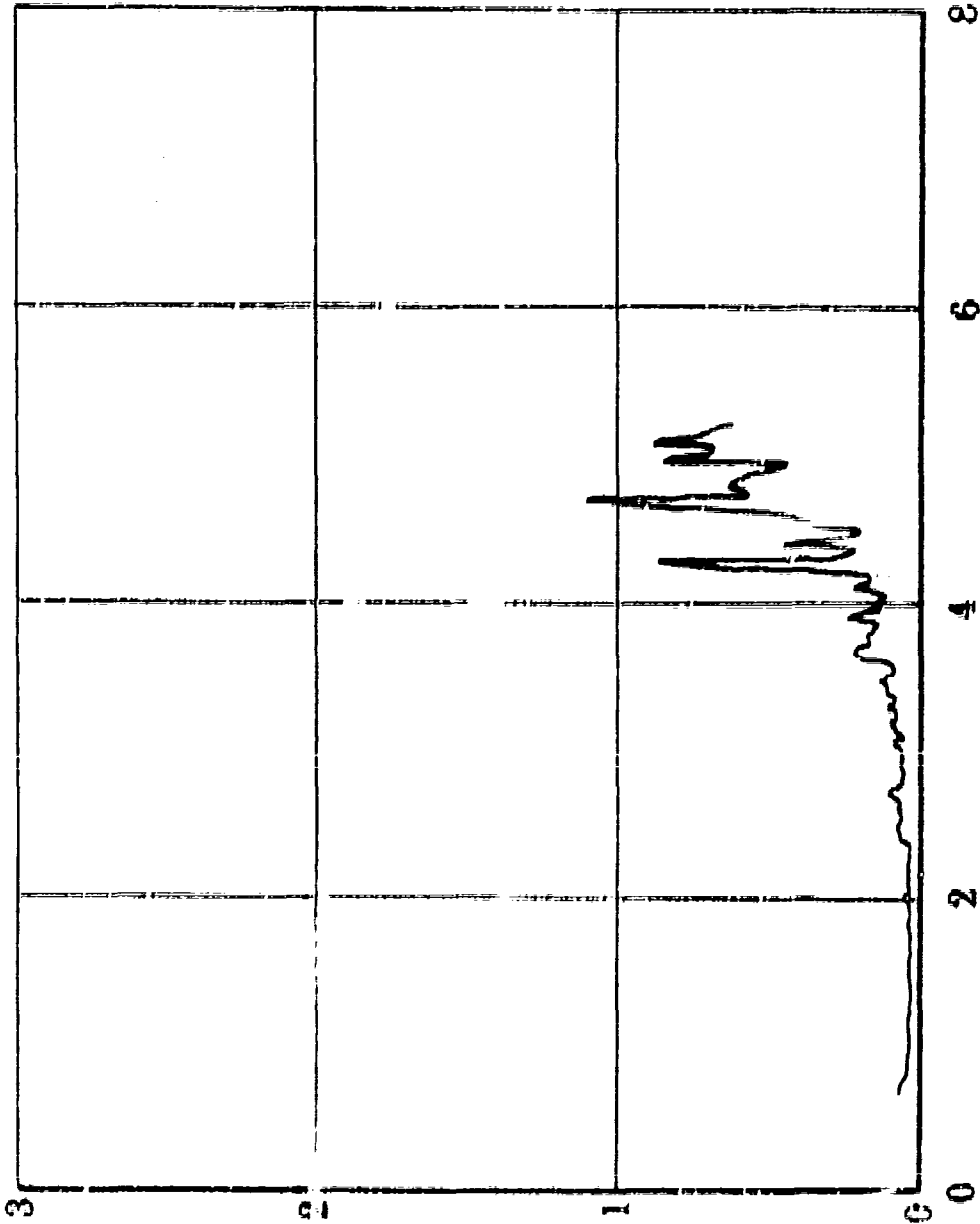
Figure III-B-12. Low Rotor (1E) Forced Vibration (Horizontal) of No. 2 Bearing Support



### HIGH ROTOR SPEED - rpm(Thousand)

Figure III-B-13. High Rotor (1E) Forced Vibration (Horizontal) of No. 2 Bearing Support

FD 15601



LOW ROTOR SPEED - rpm(Thousand)

Figure III-B-14. Low rotor (IE) Forced Vibration (Vertical) of Intermediate Case

ACCELERATION - ± g

FD 15596

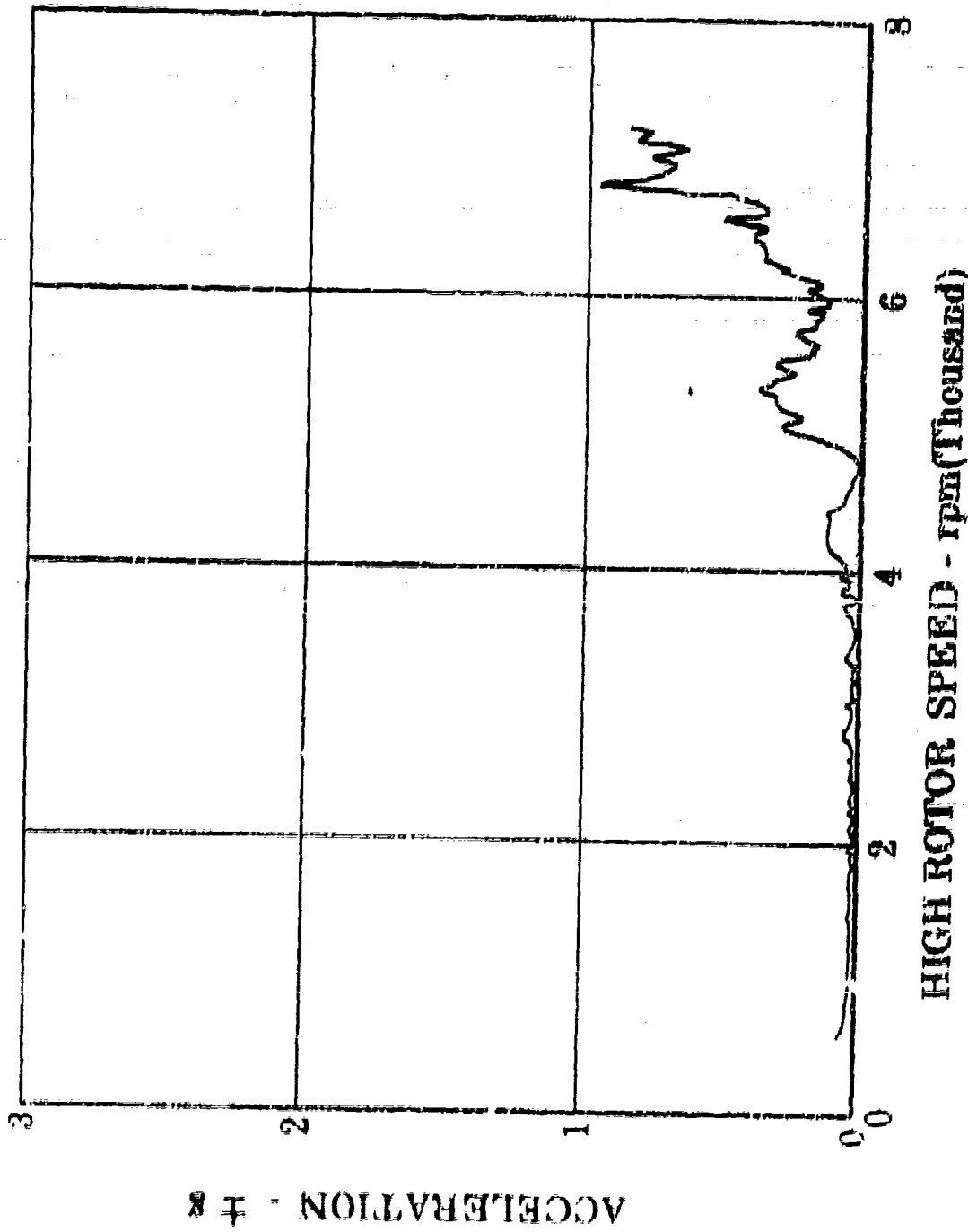
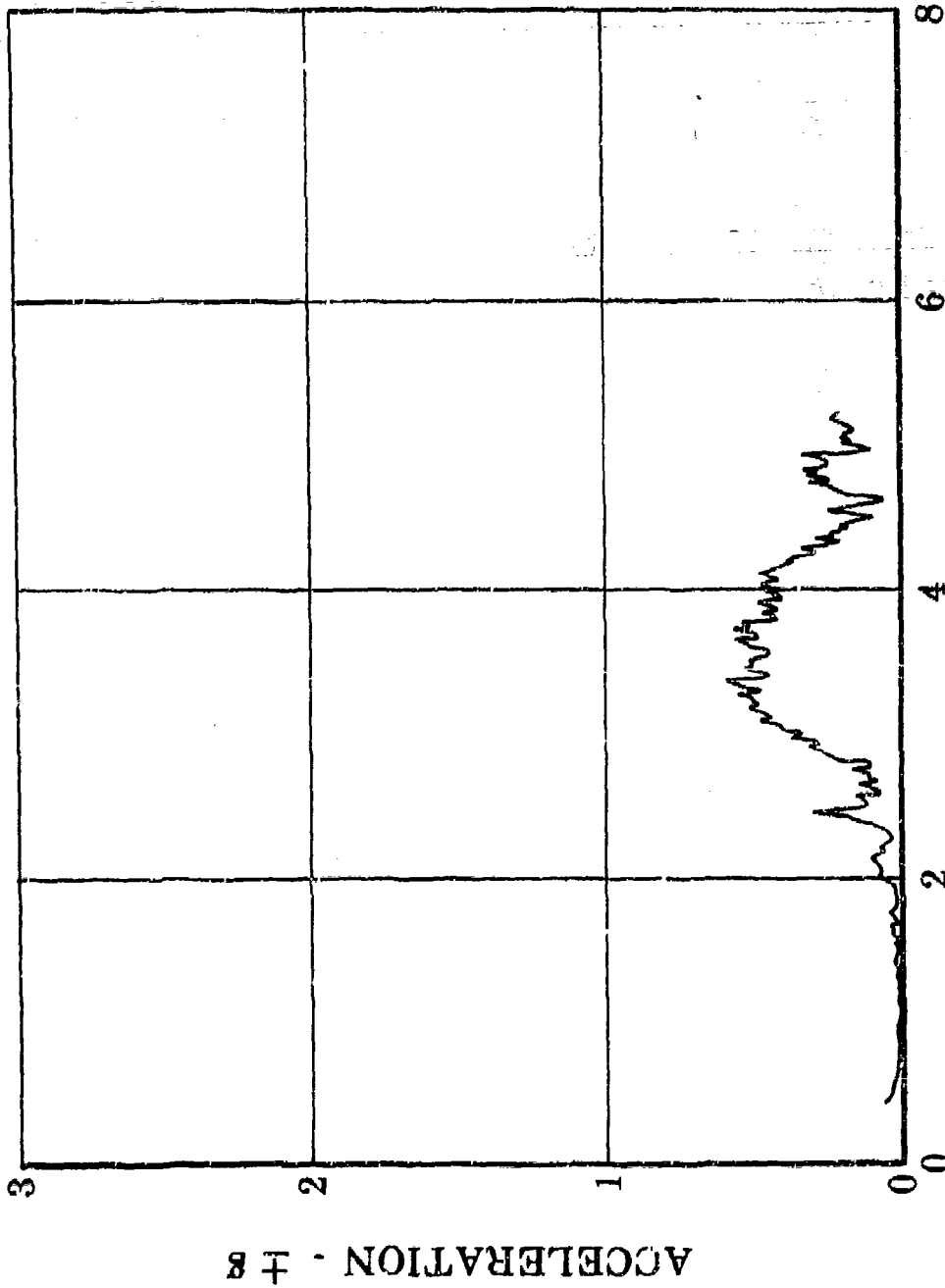


Figure III-B-15. High Rotor (IE) Forced Vibration (Vertical) of Intermediate Case

FD 15599



LOW ROTOR SPEED - rpm (Thousand)

Figure III-E-16. Low Rotor (1E) Forced Vibration (Vertical) of Turbine Exhaust Case

FD 15603

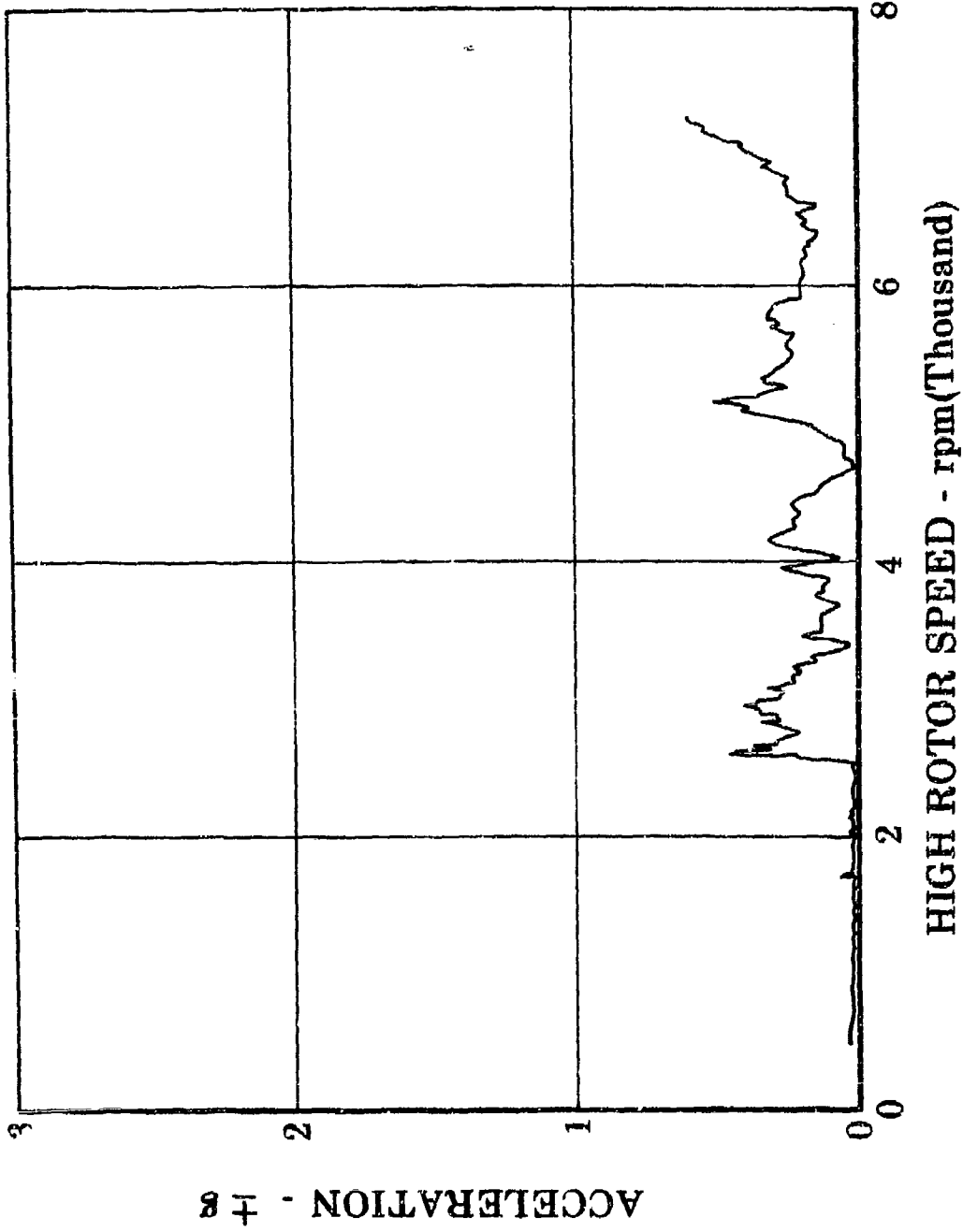
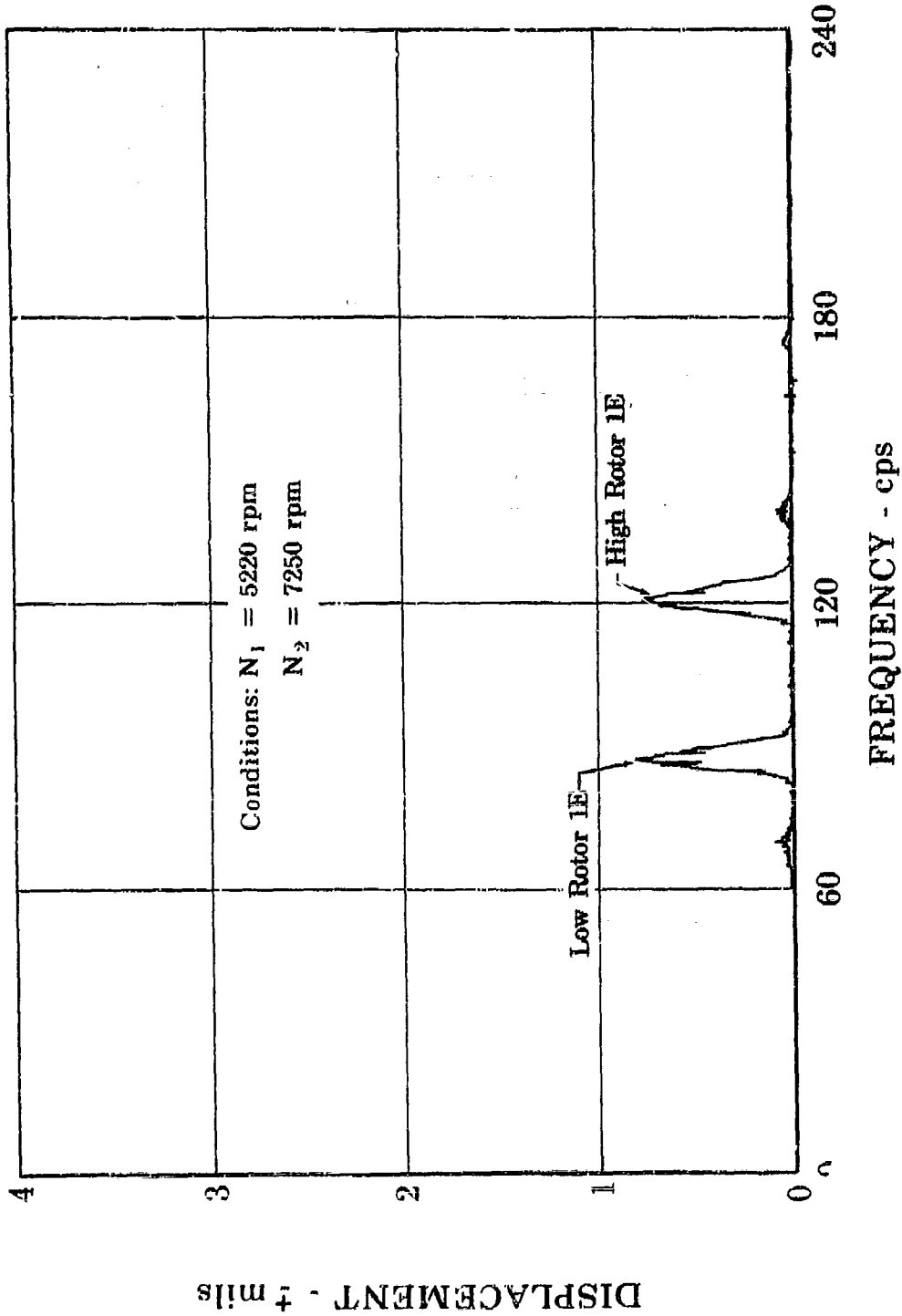


Figure III-B-17. High Rotor (IE) Forced Vibration (Vertical) of Turbine Exhaust Case





DISPLACEMENT - mils

FREQUENCY - cps

Figure III-B-18. Front Mount Case Horizontal Vibration vs Frequency

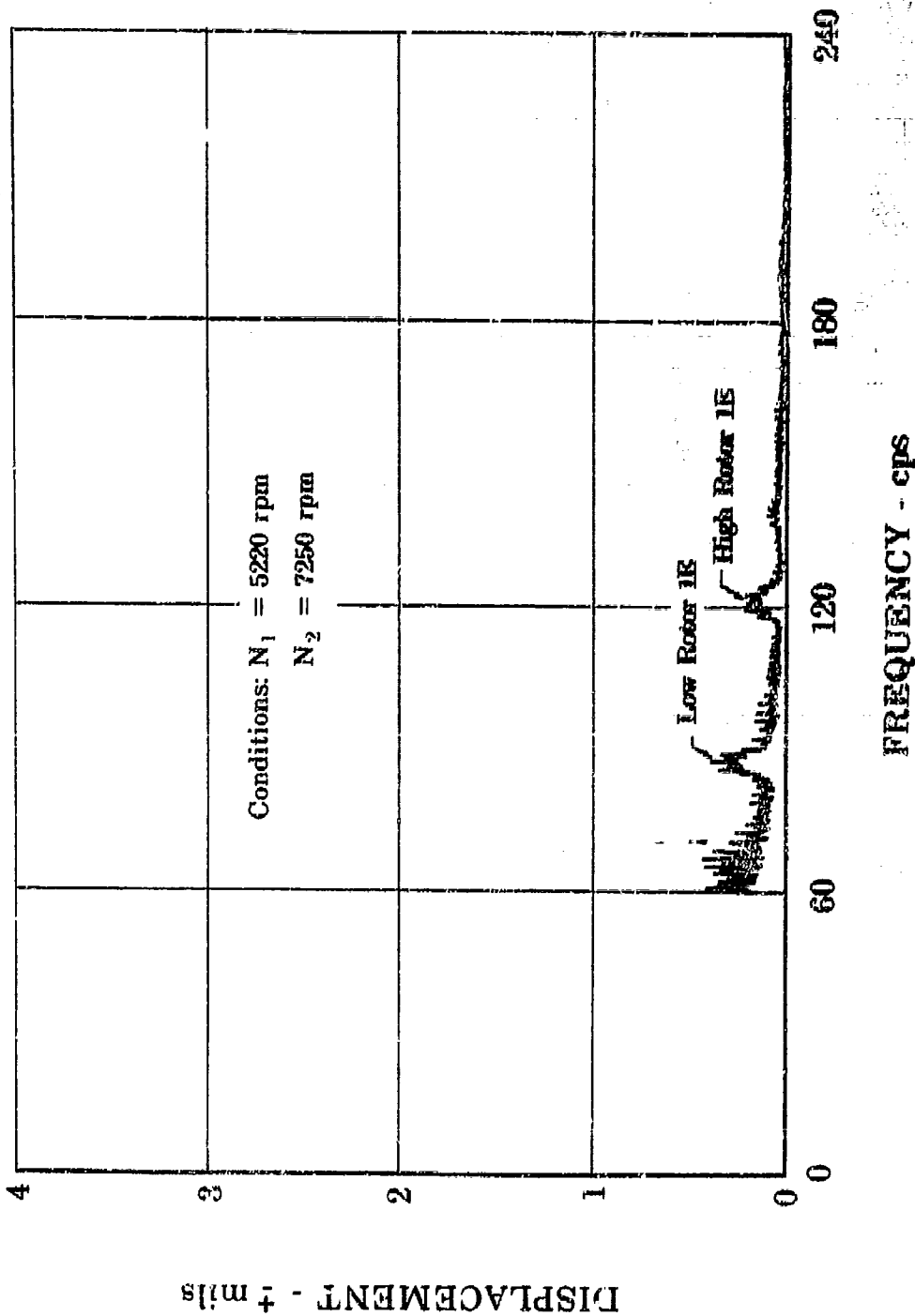


Figure III-B-19. Front Mount Case Vertical Vibration vs Frequency

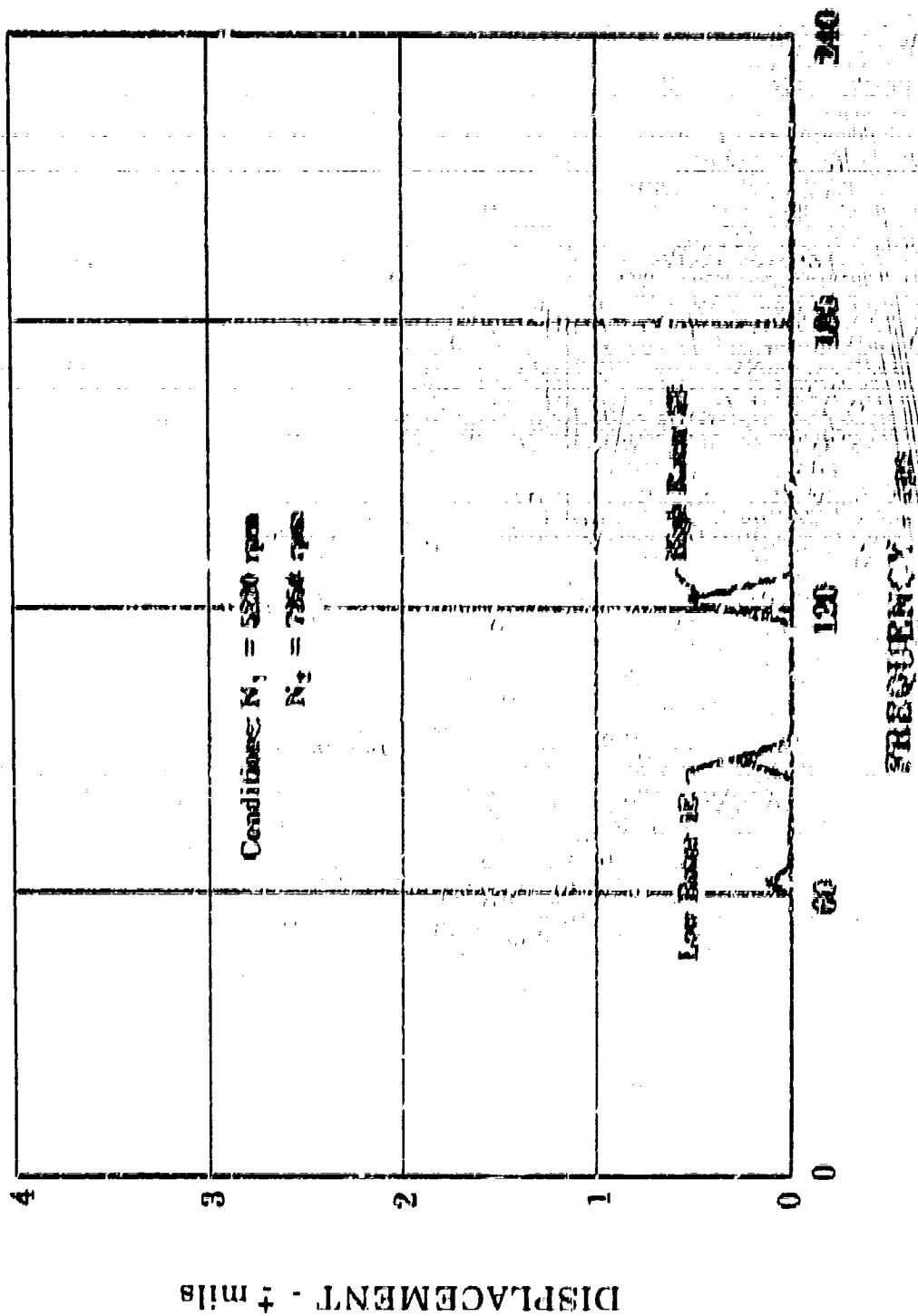


Figure III-B-20. Number 2 Bearing Horizontal Vibration vs Frequency

EB 15679

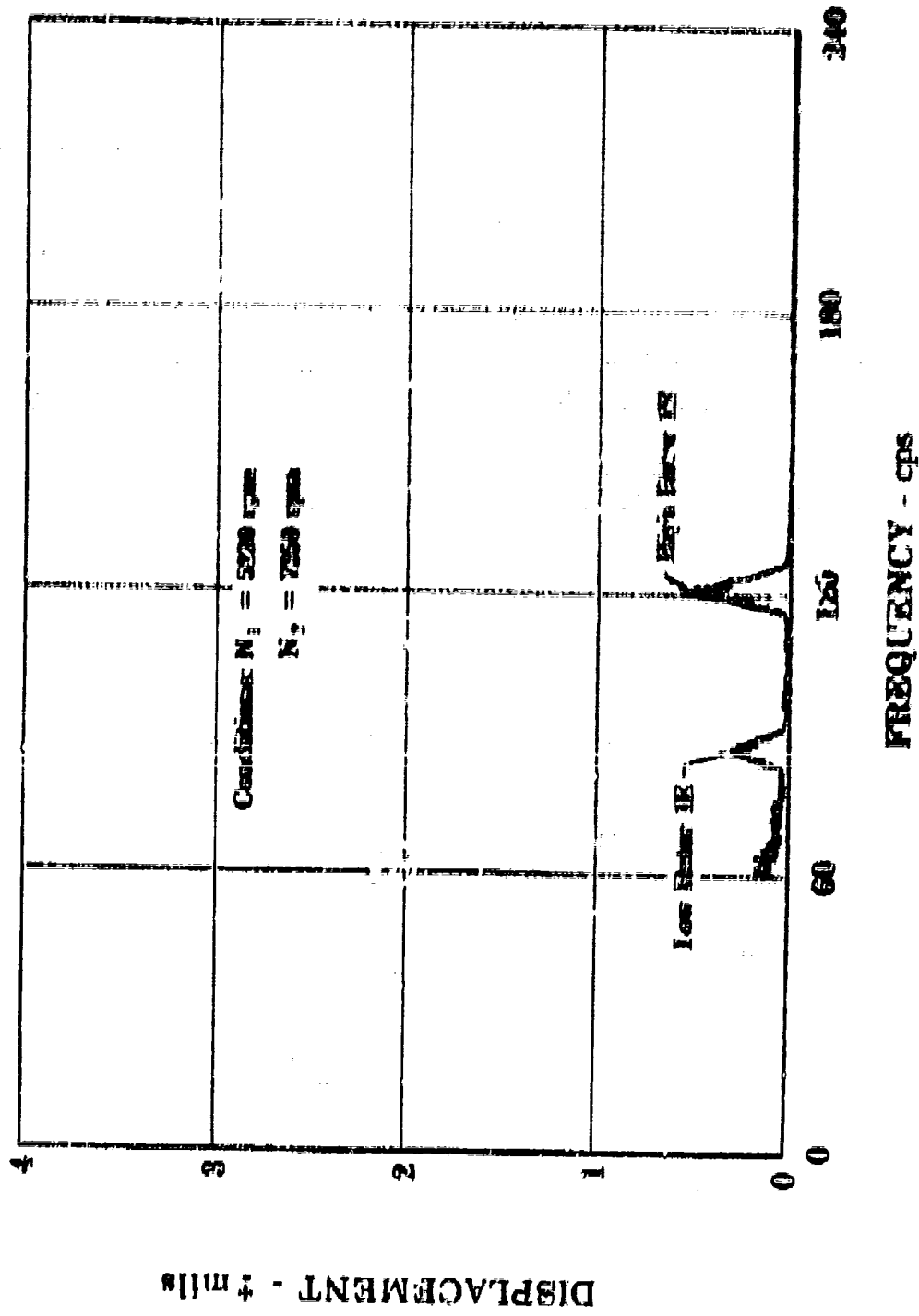


Figure III-B-21. Number 2 Bearing Vertical Vibration vs Frequency

FD 15616

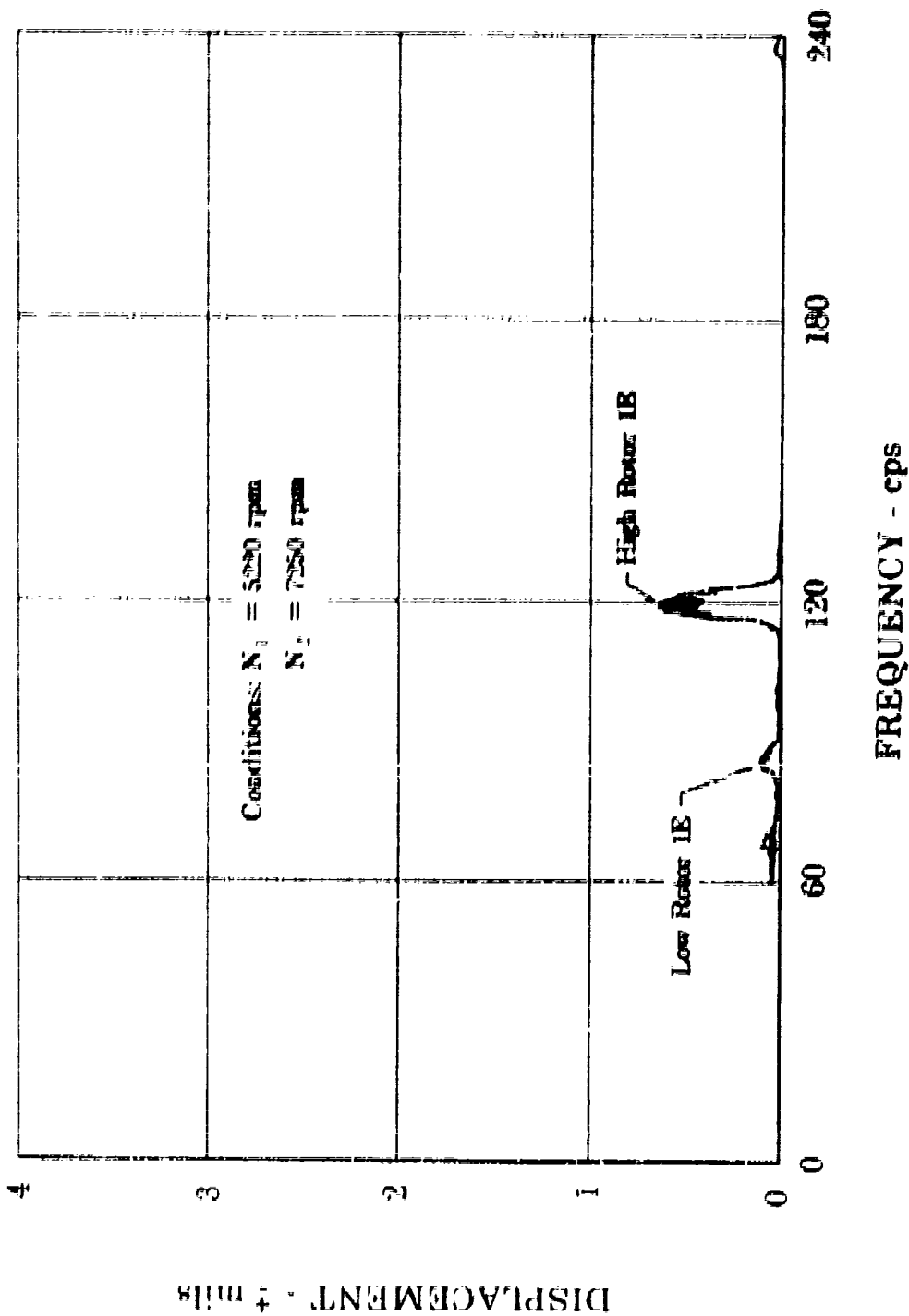


Figure III-B-22. Diffuser Horizontal Vibration vs Frequency

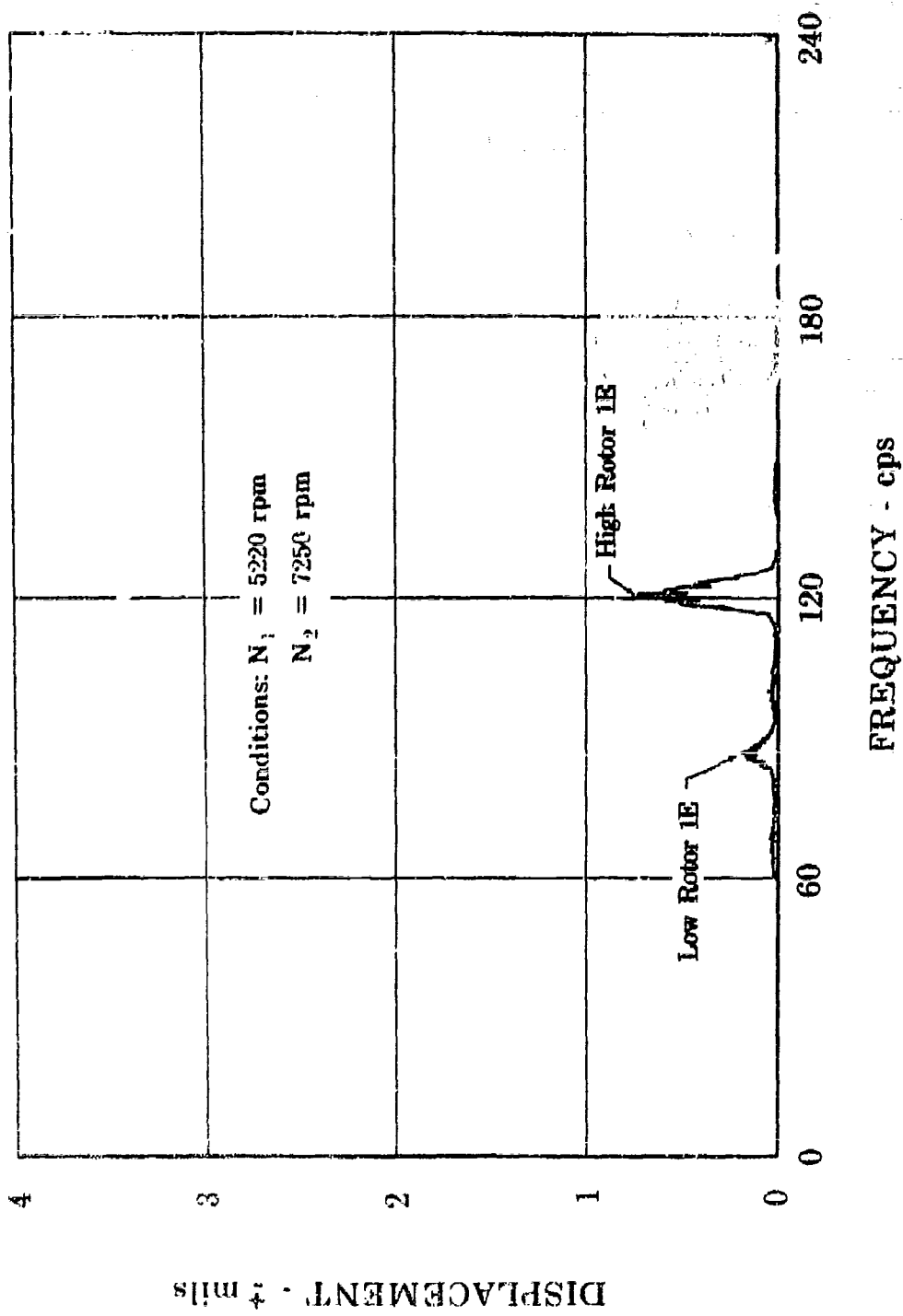


Figure III-B-23. Diffuser Vertical Vibration vs Frequency

FD 15622

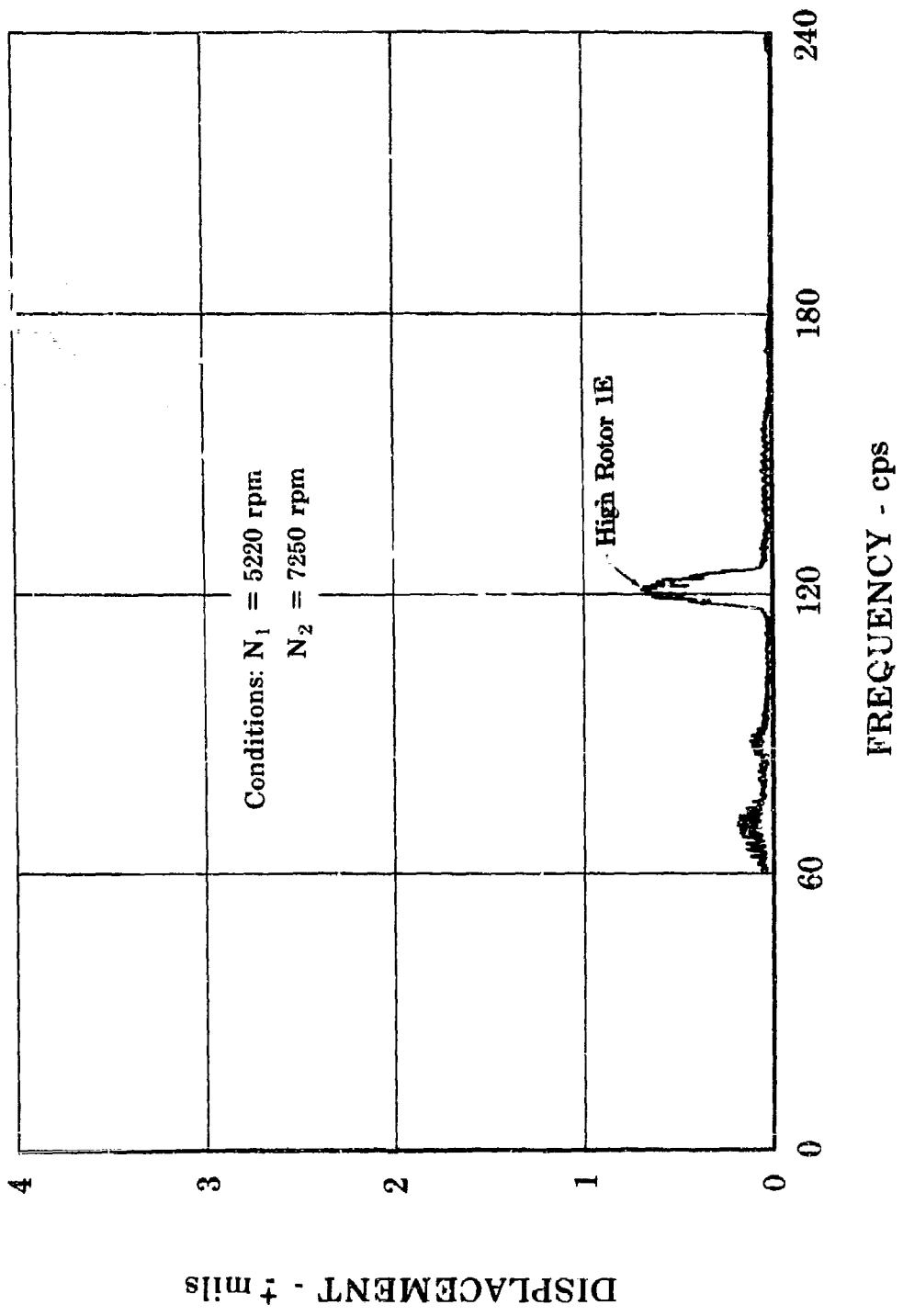


Figure III-B-24. Turbine Exhaust Horizontal Vibration vs Frequency

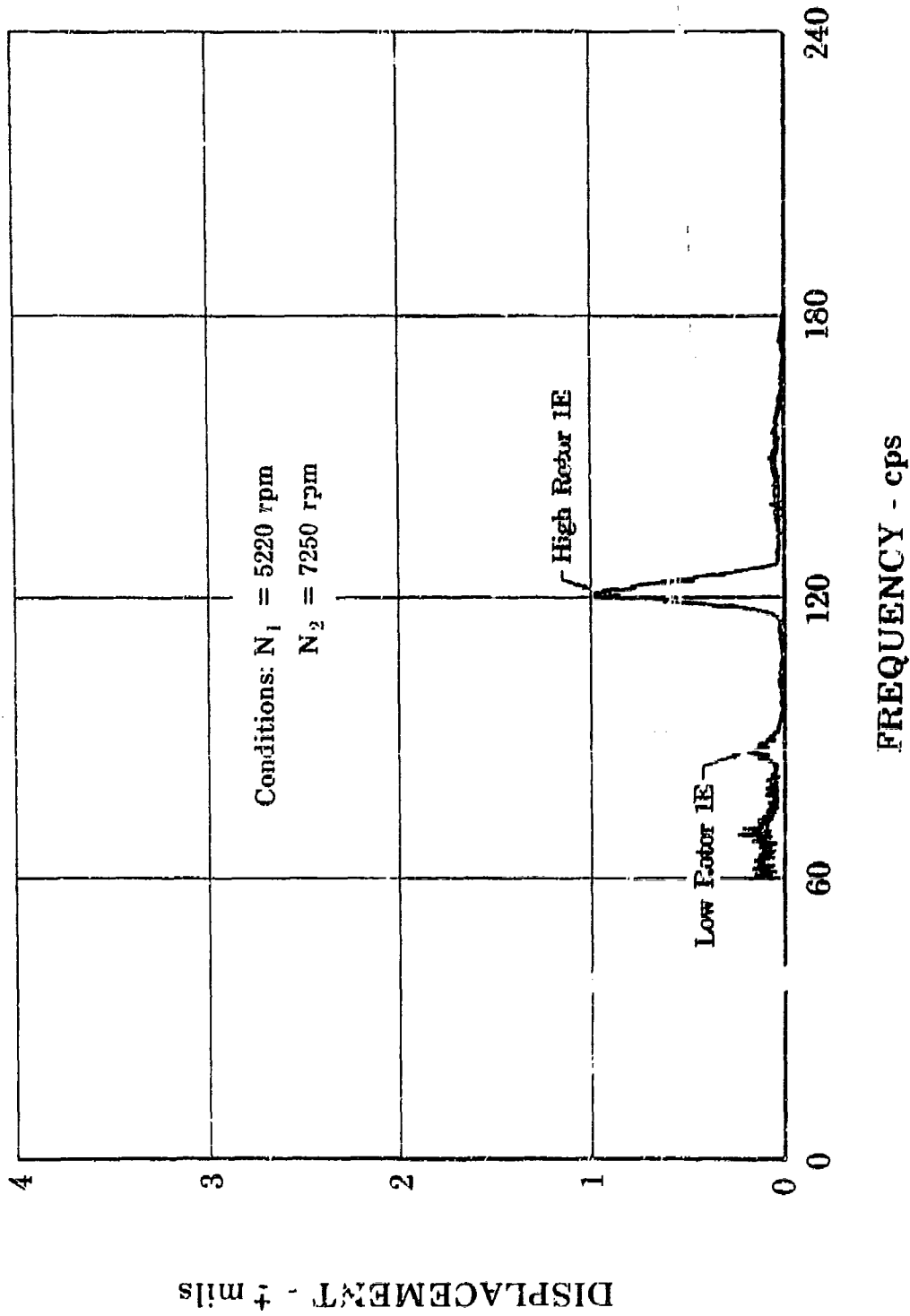


Figure III-B-25. Turbine Exhaust Vertical Vibration vs Frequency



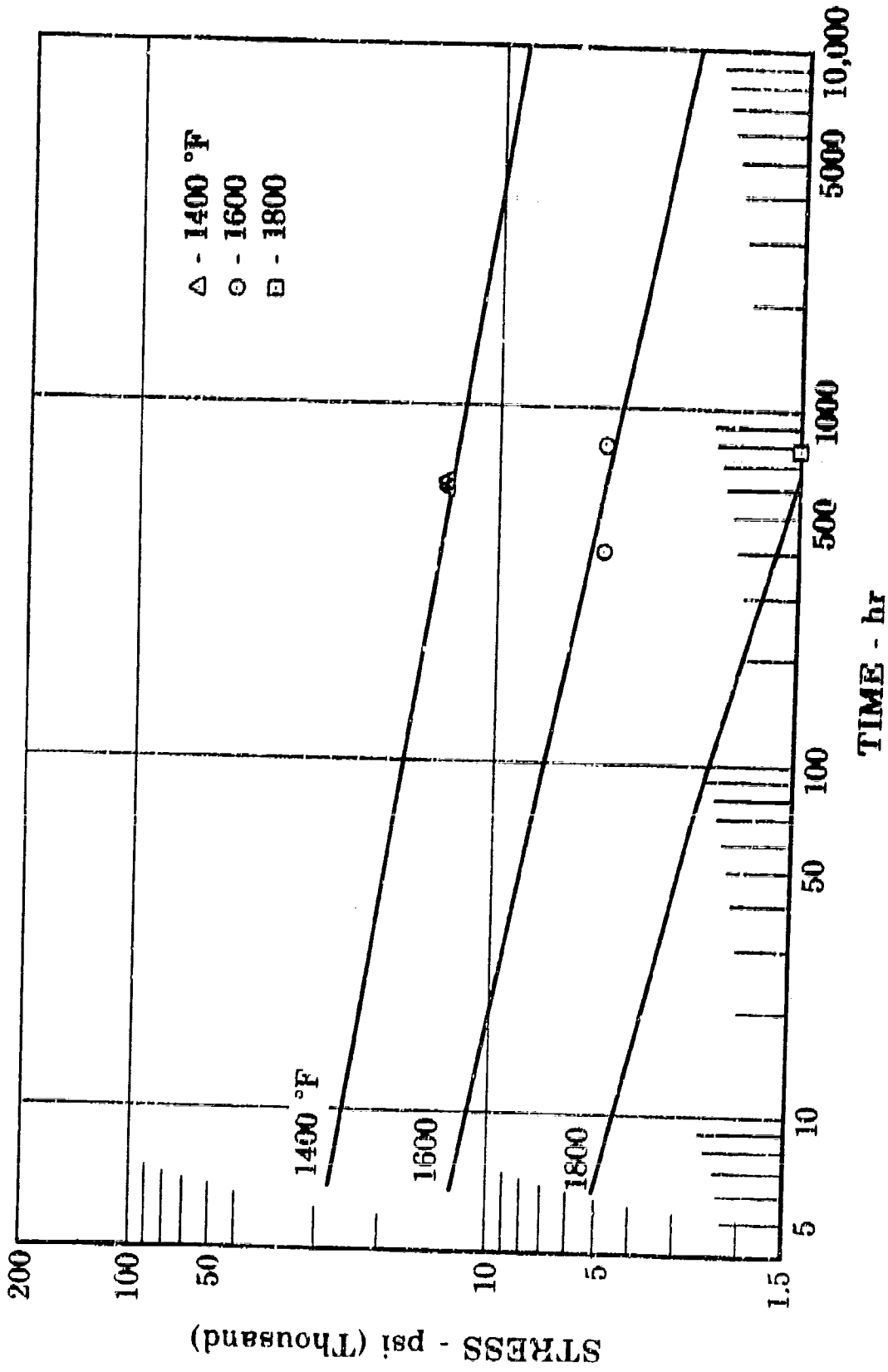


Figure III-B-26. Hastelloy X Sheet (AMS 5536) Stress Rupture Test vs Design Curves

ED 15588

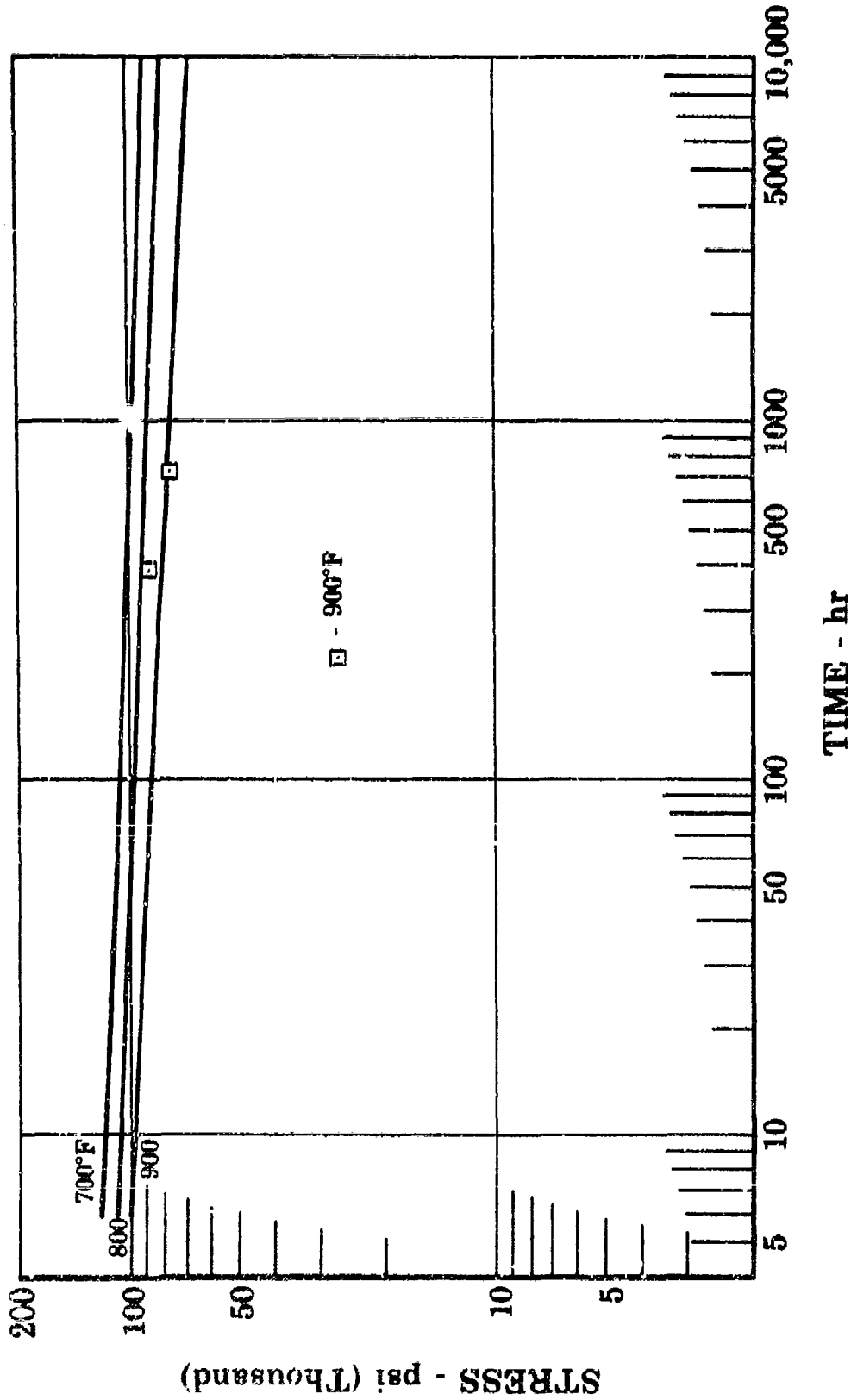


Figure III-B-27. Titanium (PWA 1205) Stress Rupture Test vs Design Curves

FD 15560

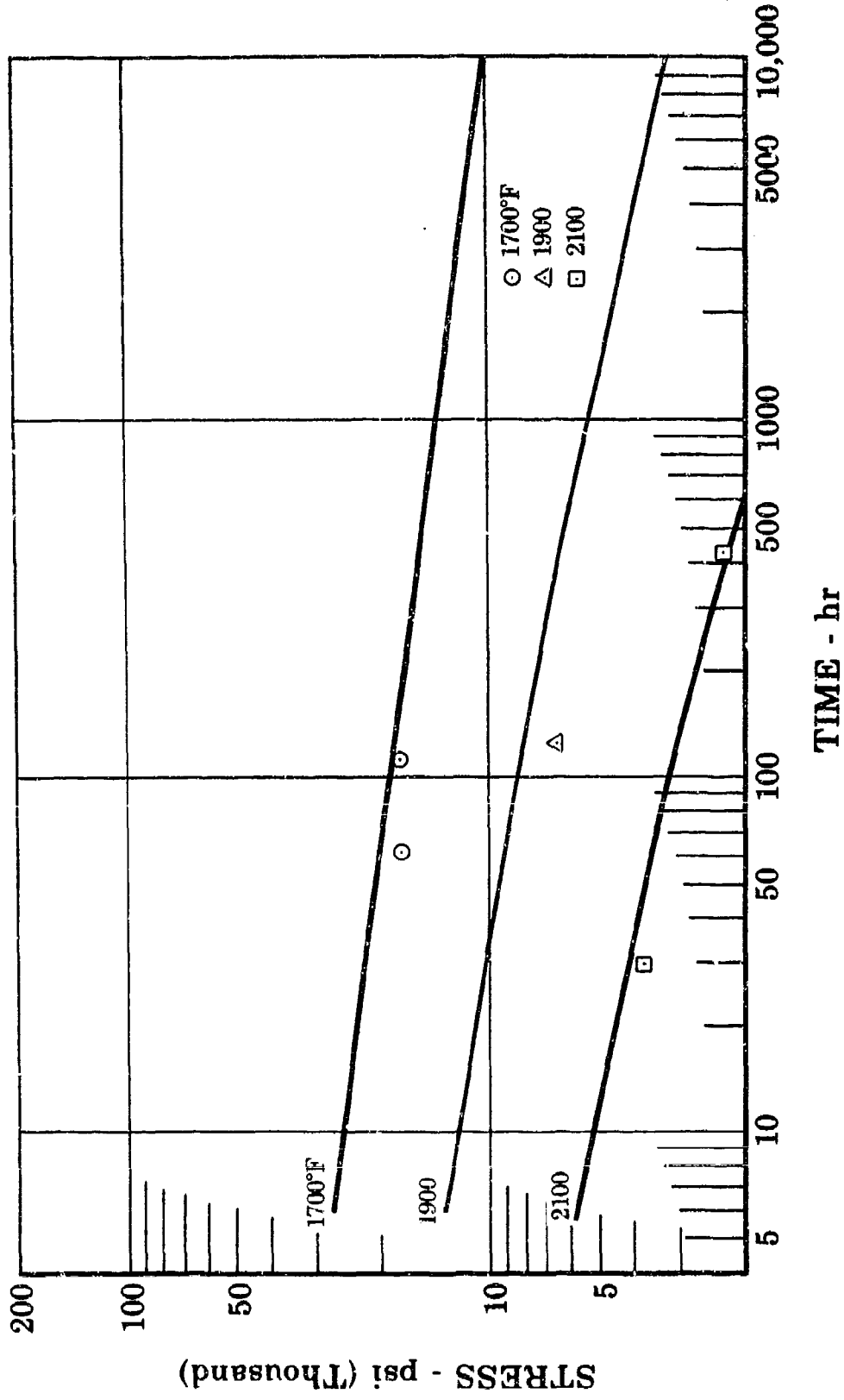


Figure III-B-28. SM 302 (PWA 657) Stress Rupture Test vs Design Curves

FD 15589

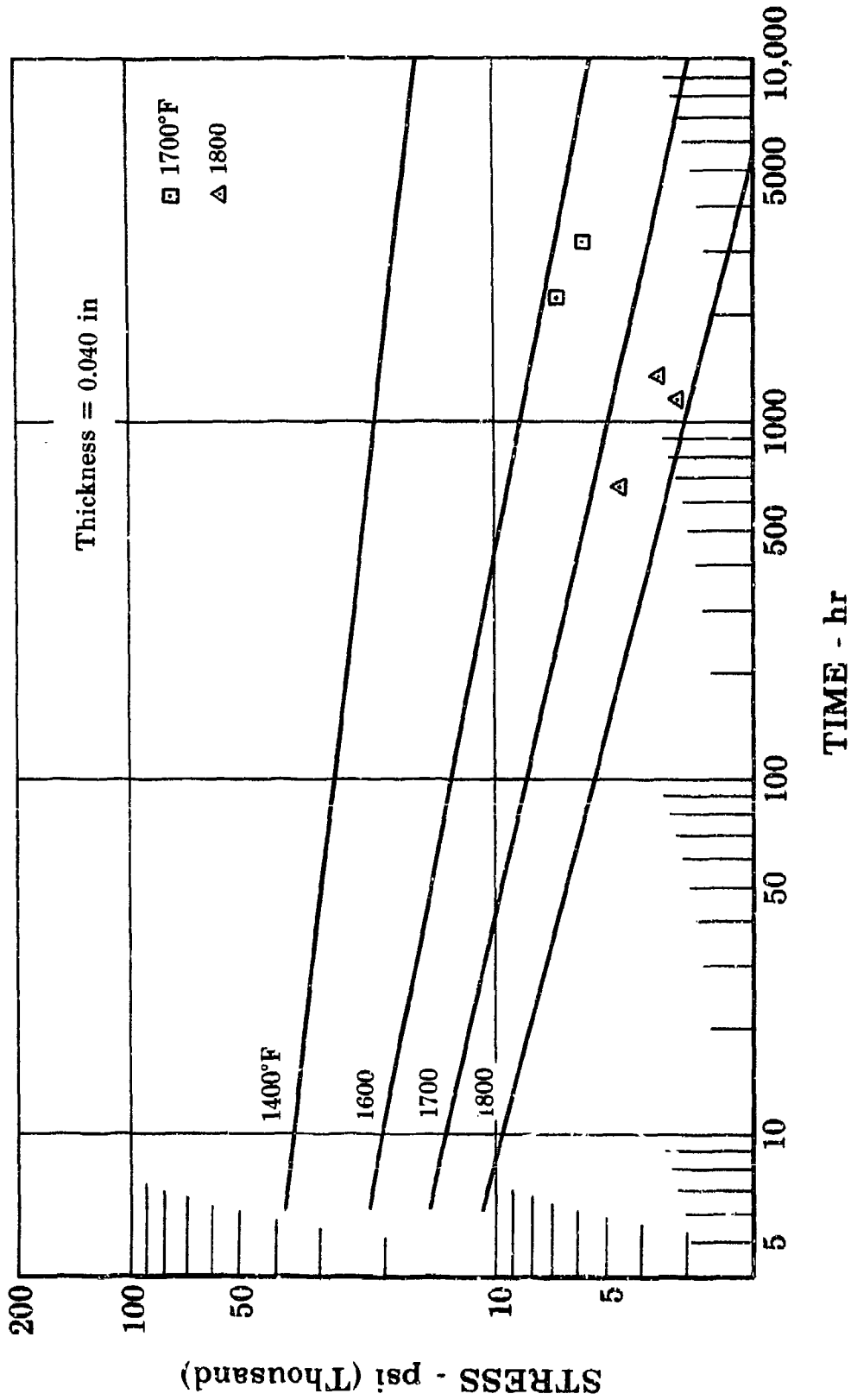
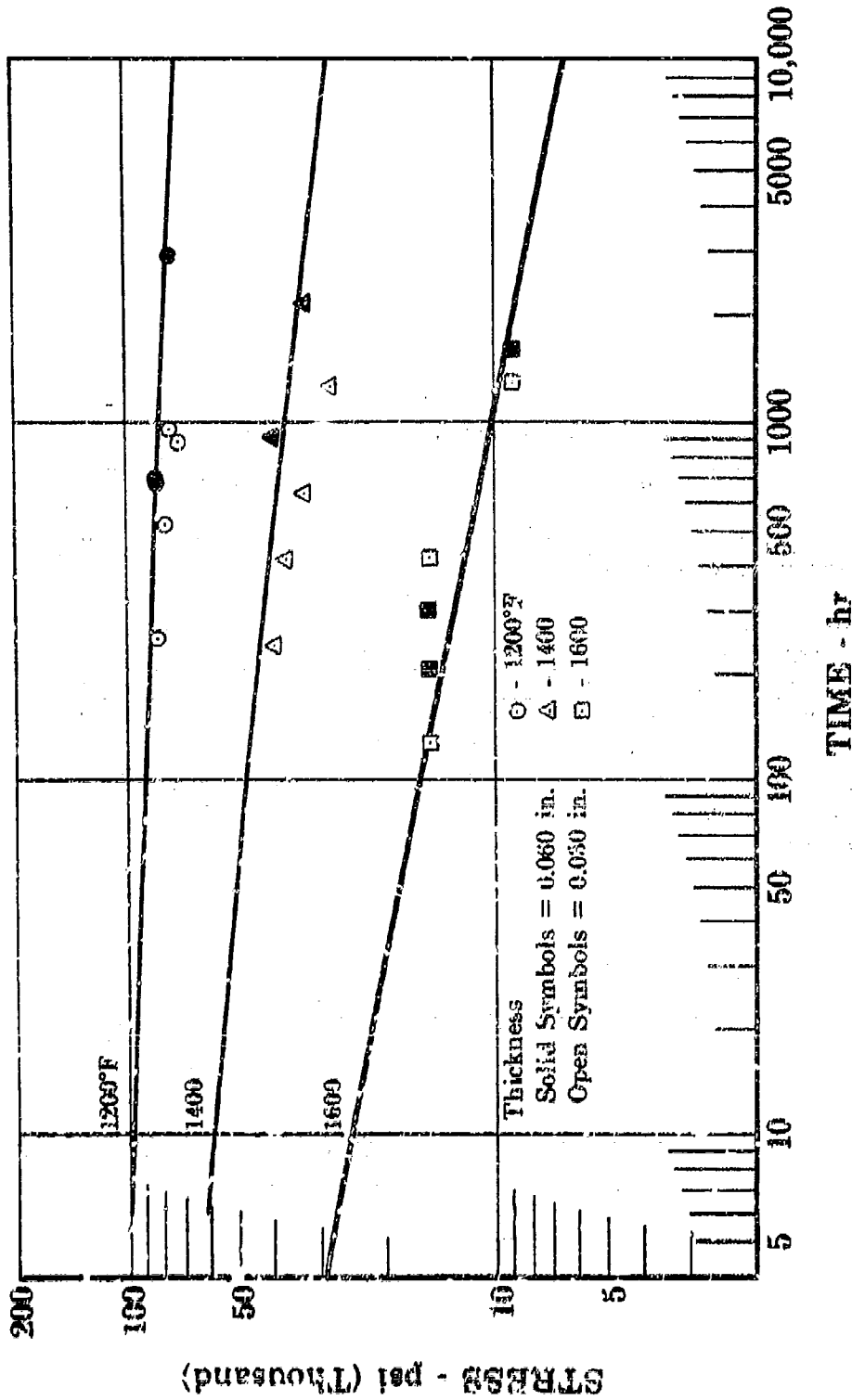


Figure III-B-29. L-605 Sheet (AMS 5537) Stress Rupture Test vs Design Curves

FD 15595



FD 15592

Figure III-E-30. Waspaloy Sheet (INA 1030) Stress Rupture Test vs Design Curves

III-E-30

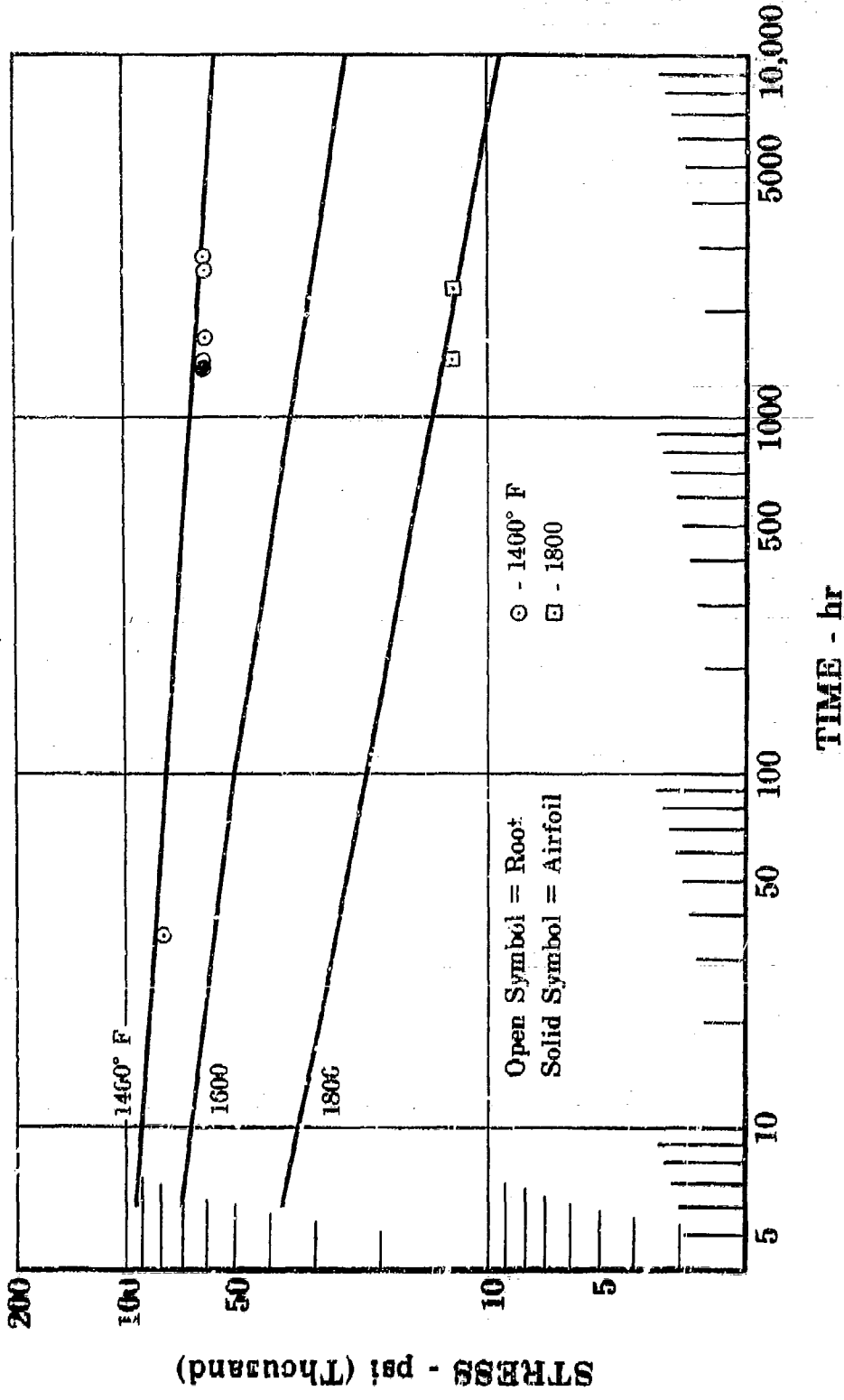


Figure III-B-31. IN-100 (PWA 658) Stress Rupture Test vs Design Curves

FD 15590

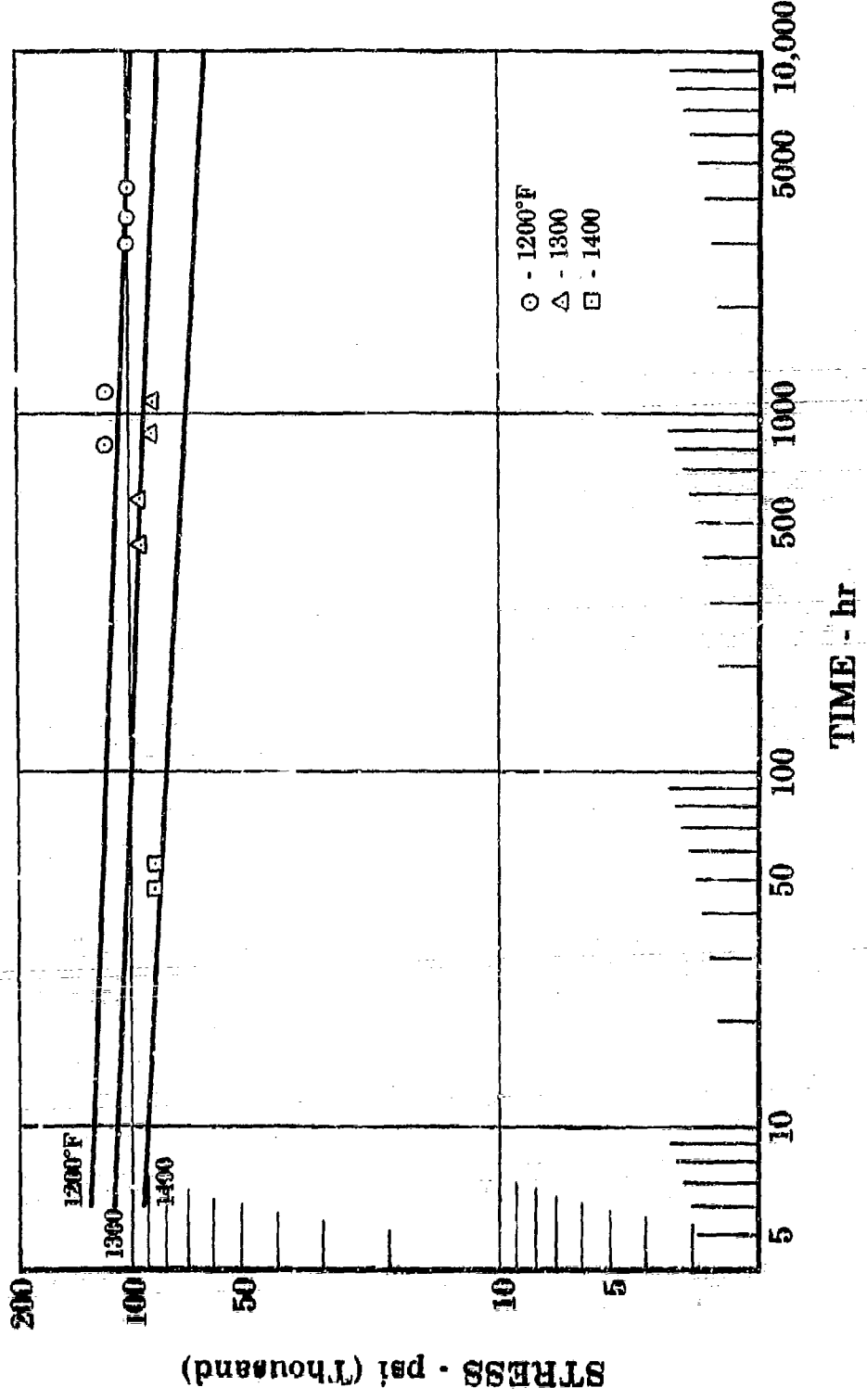


Figure III-E-32. Astroloy (PWA 1013C) Stress Rupture Test vs Design Curves

FD 15597

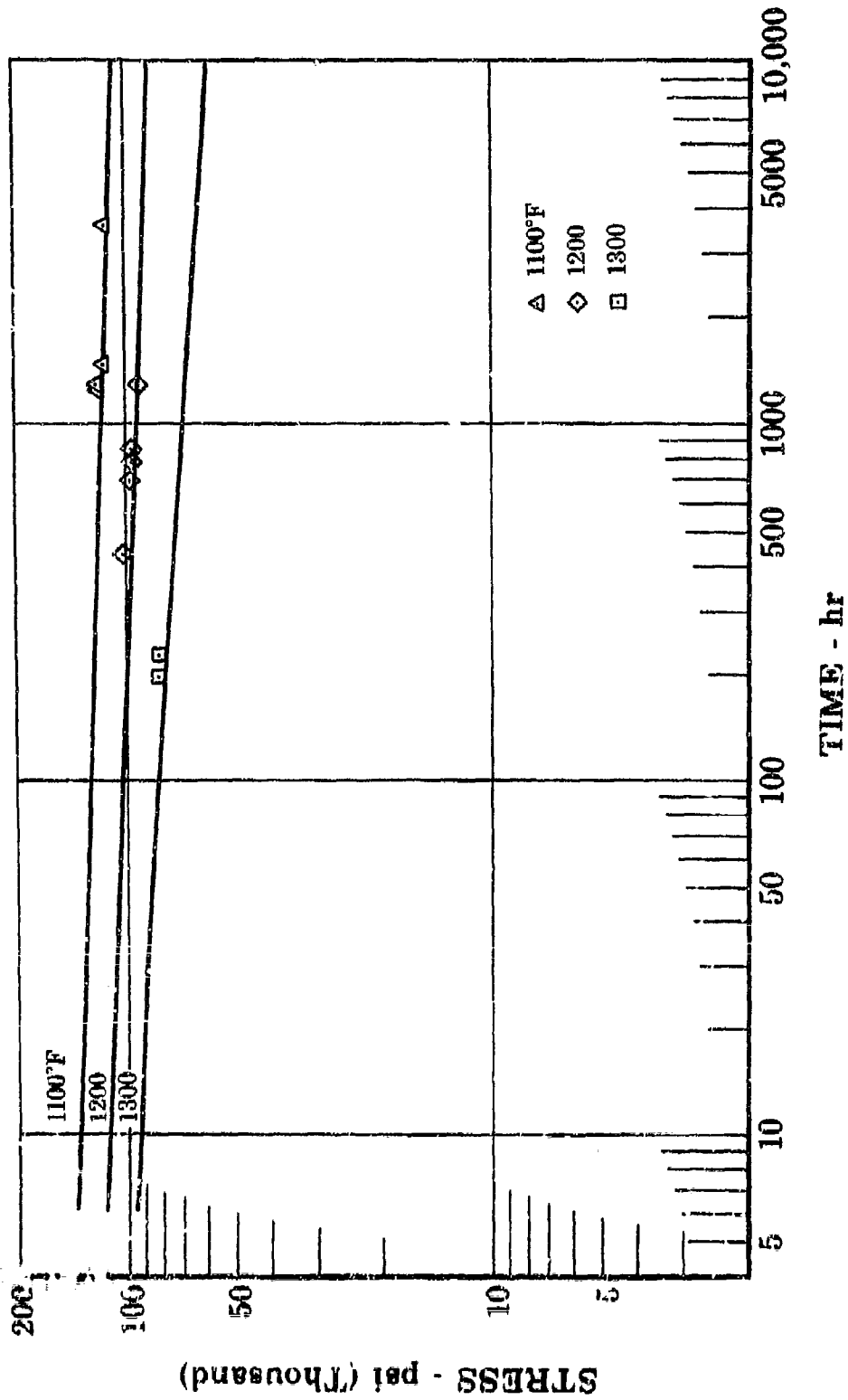
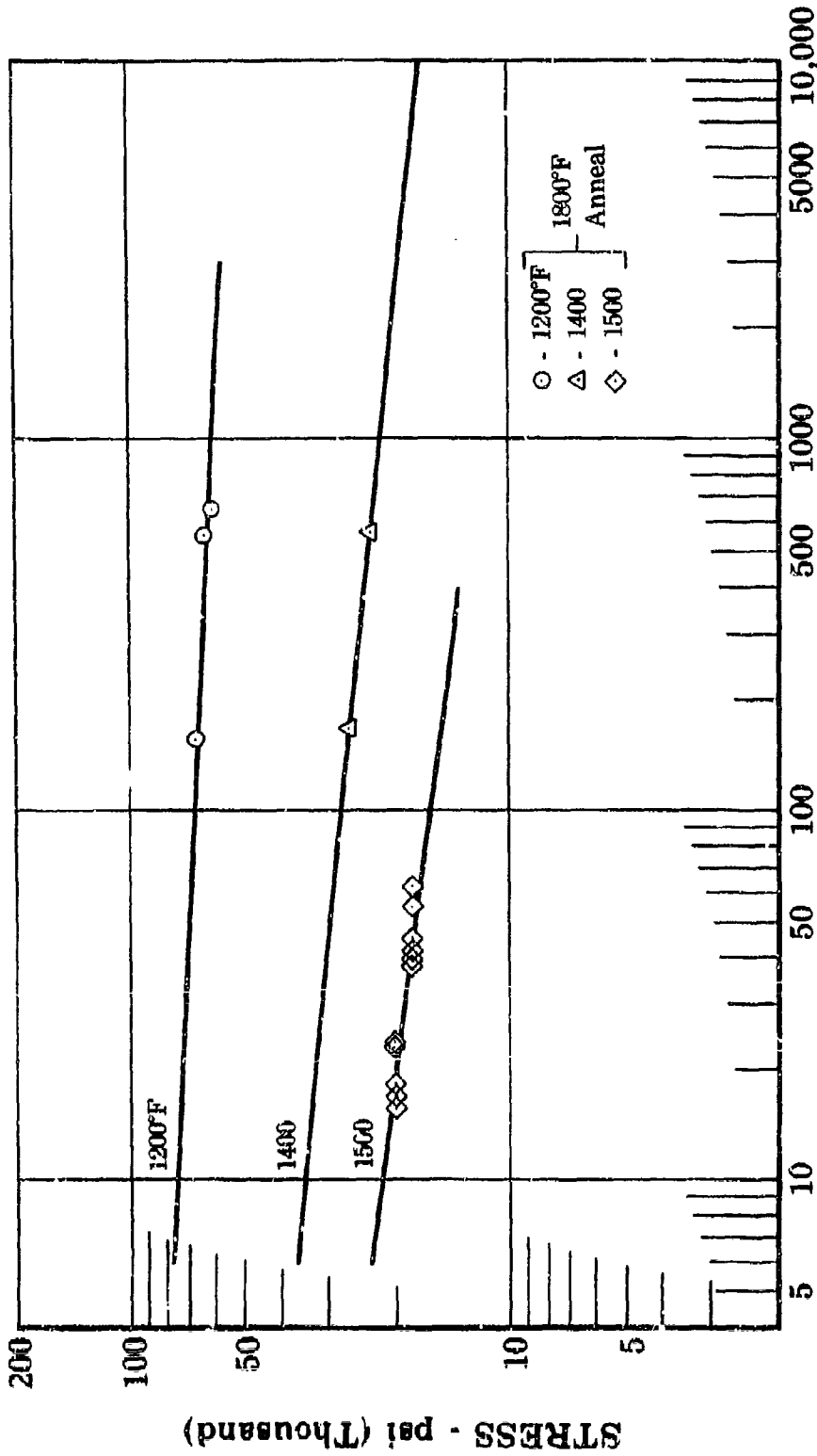


Figure III-B-33. Waspaloy Forging (FWA 1016) Stress Rupture Test vs Design Curves

FD 15594

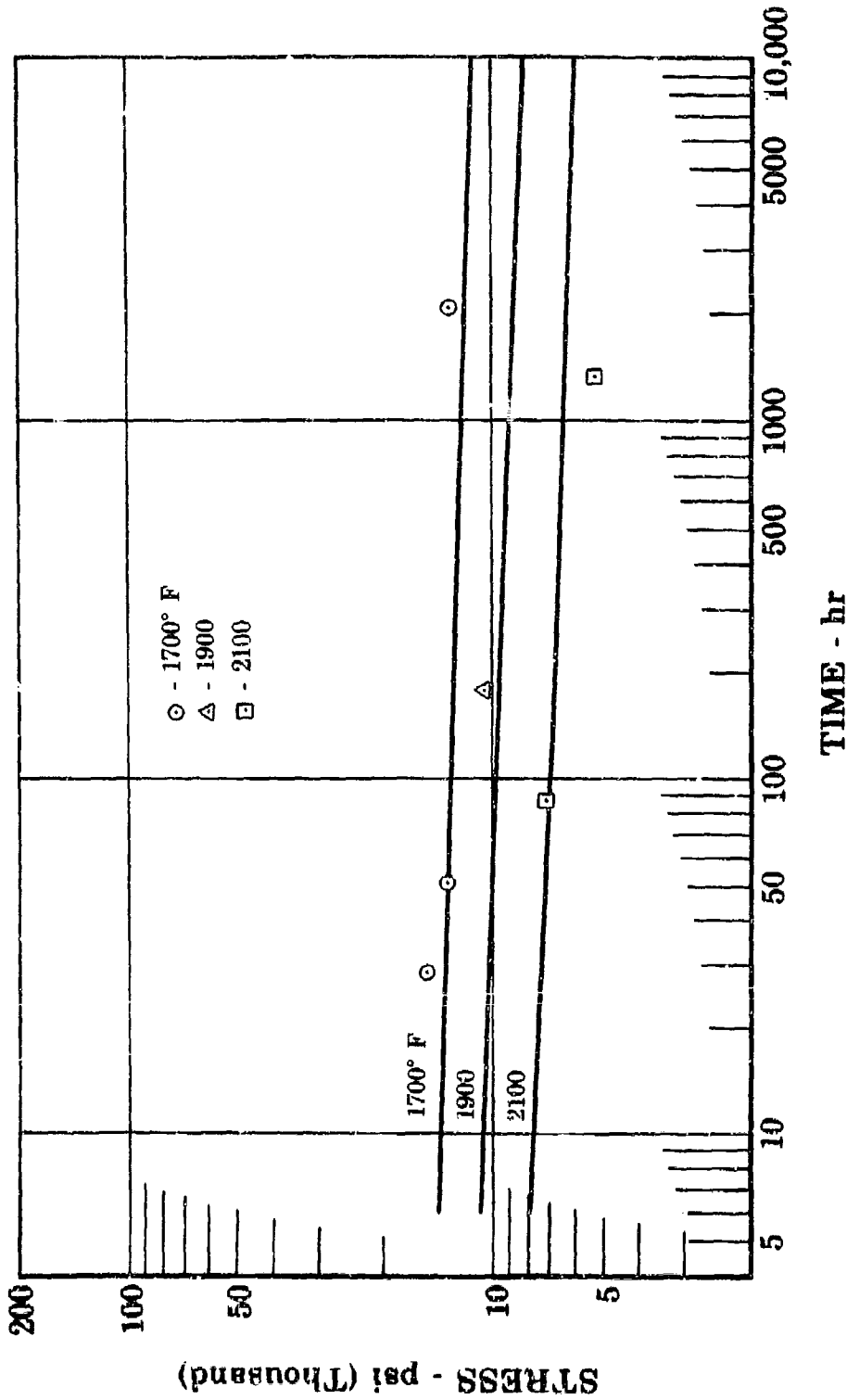




TIME - hr

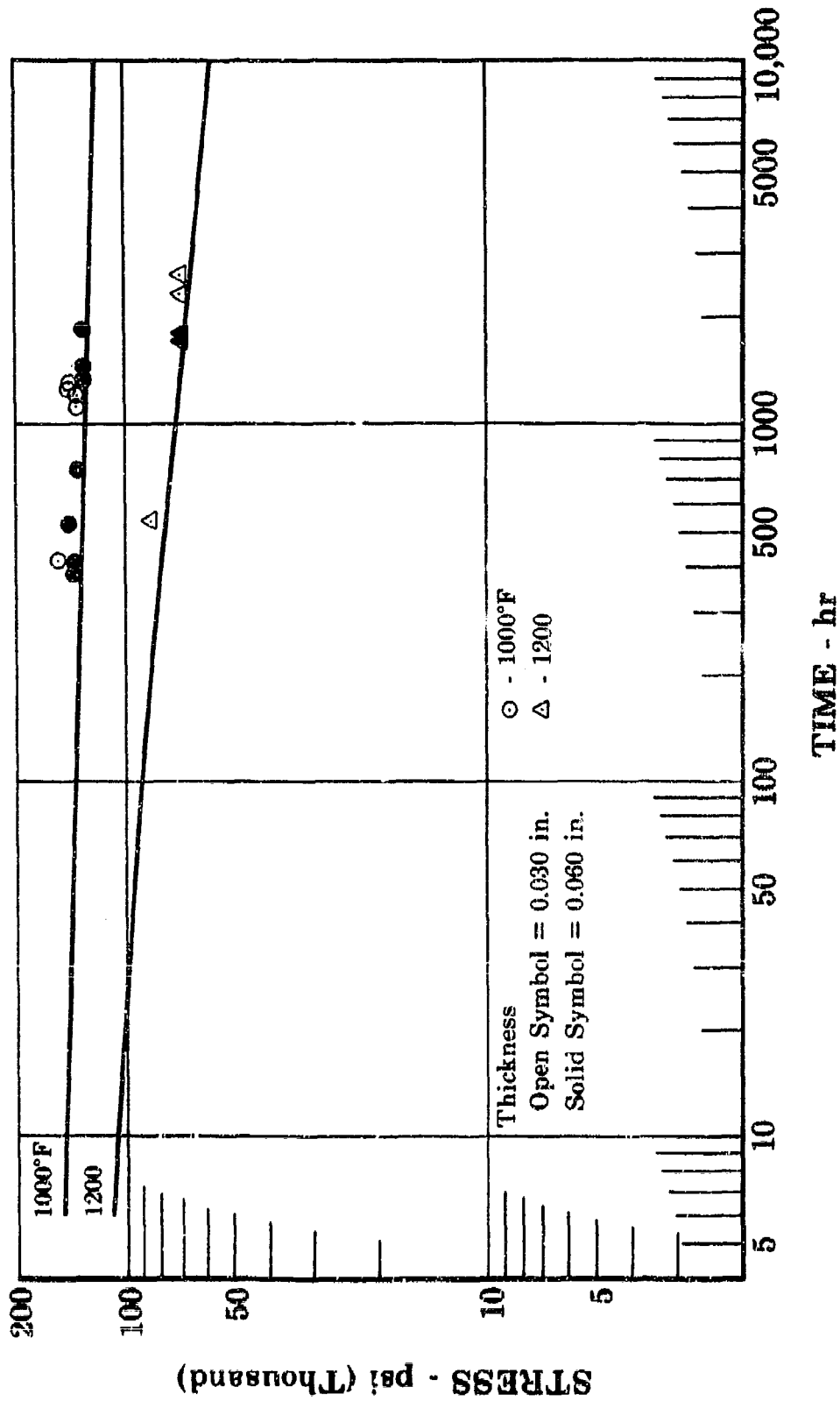
FD 15593

Figure III-B-34. Inco 625 Stress Rupture Test vs Design Curves



FD 15596

Figure III-B-35. TD Nickel (PWA 1035) Stress Rupture Test vs Design Curves



FD 15591

Figure III-B-36. I-718 Sheet (PWA 1033) Stress Rupture Test vs Design Curves

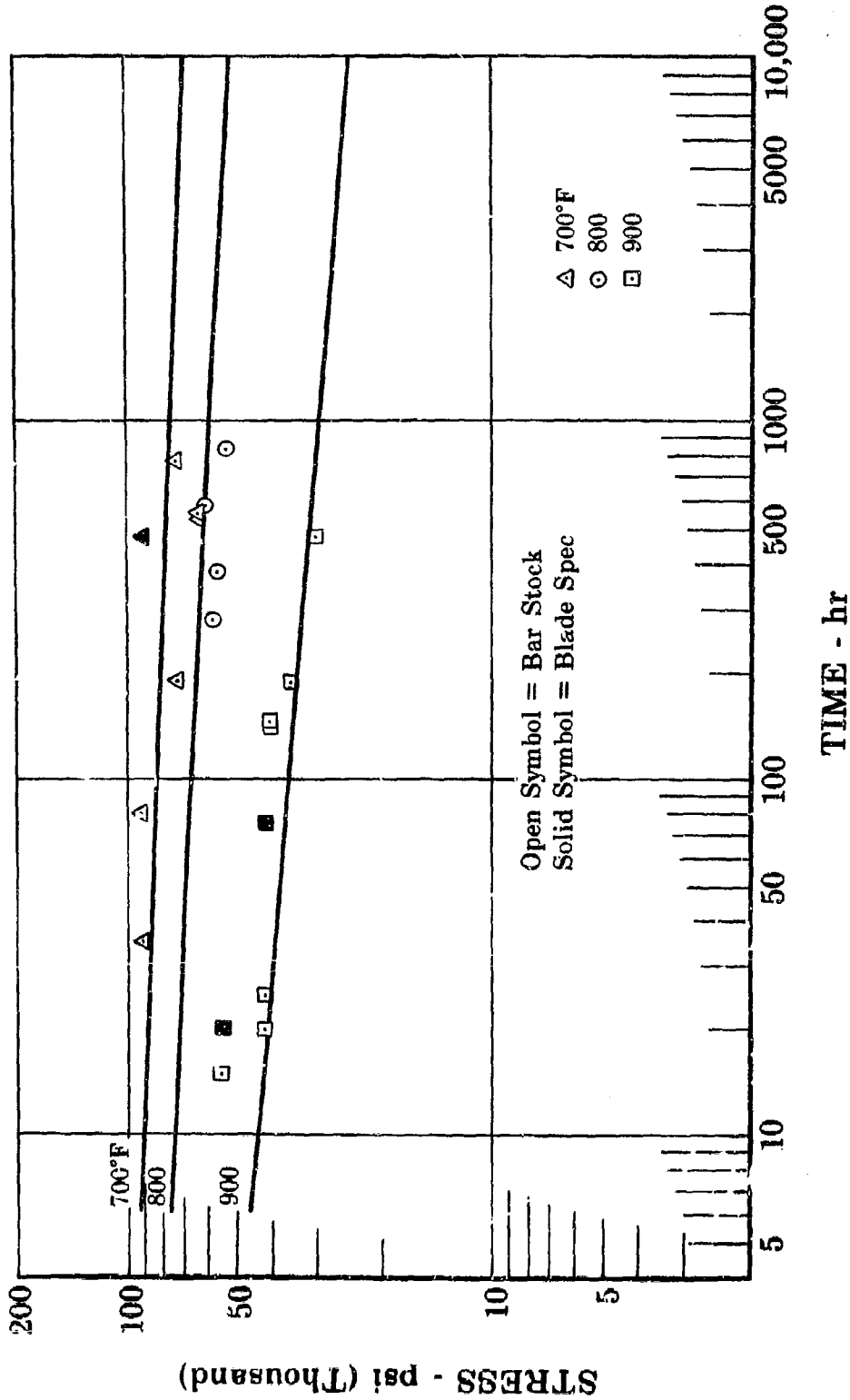
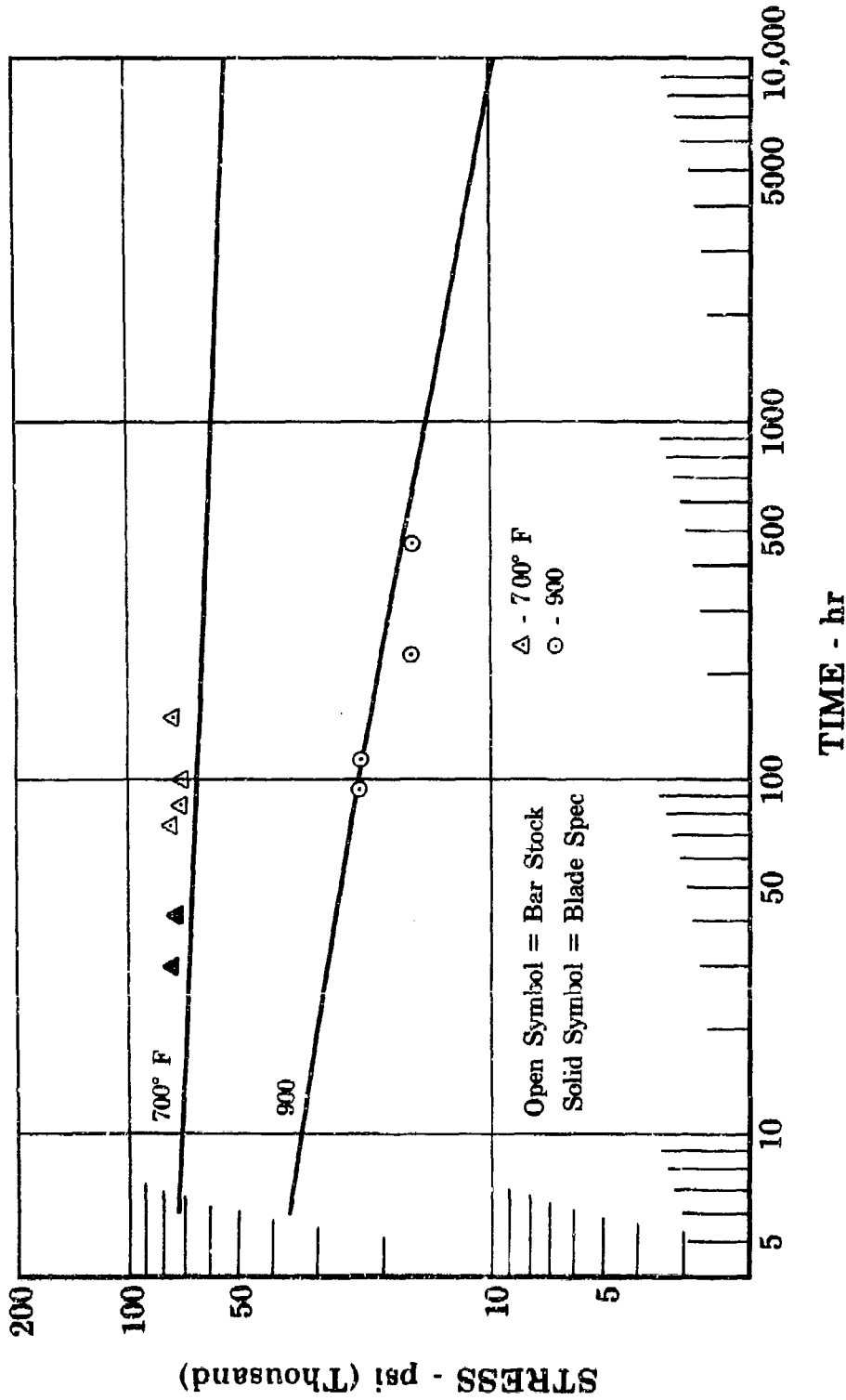


Figure III-B-37. Titanium (PWA 1205) 0.1% Creep vs Design Curves

FD 15647



FD 15566

Figure III-B-38. Titanium (PWA 1202) 0.1% Creep vs Design Curves

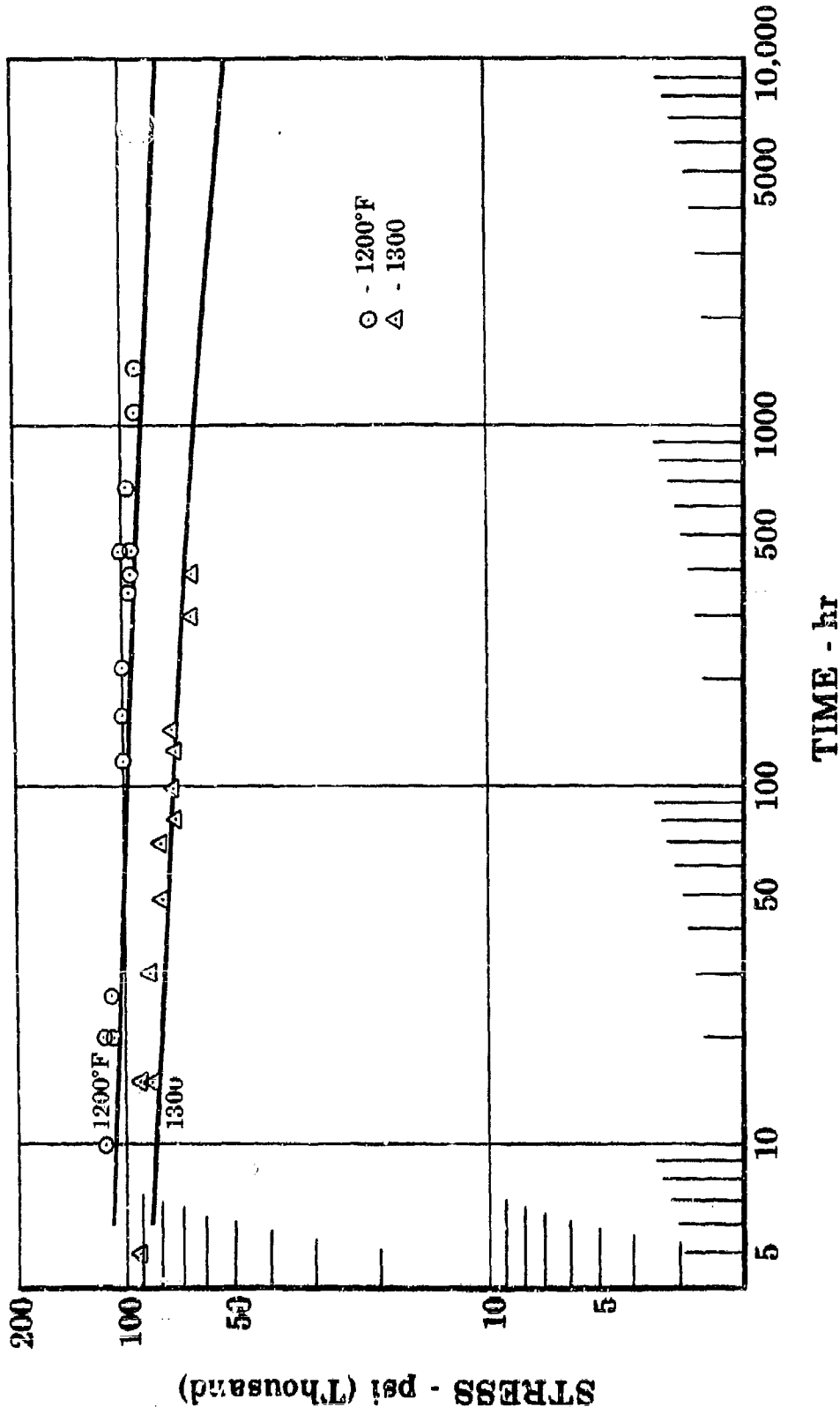


Figure III-B-39. Astroloy (PWA 1013) 0.1% Creep vs Design Curves

FD 15565

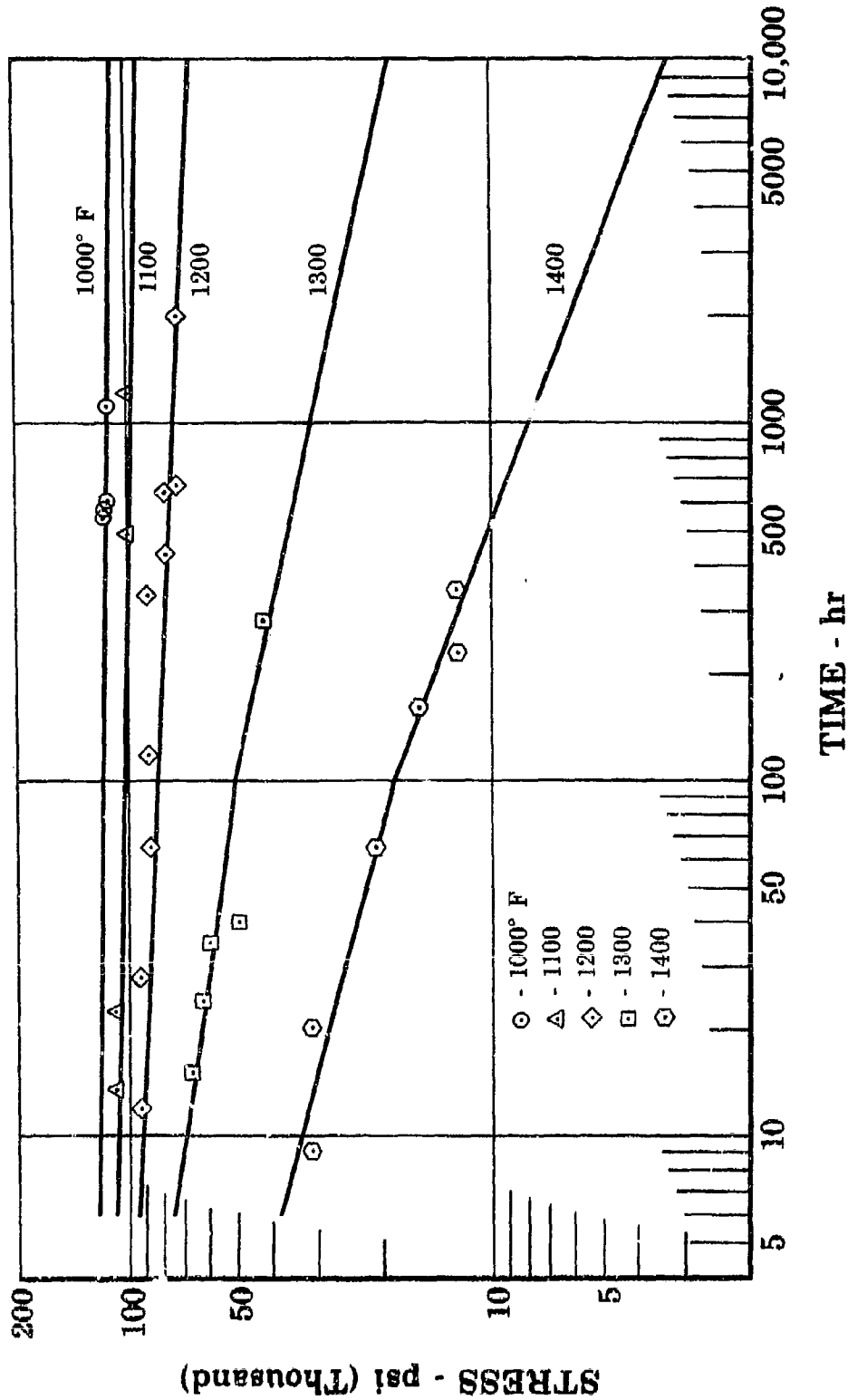


Figure III-B-40. Waspaloy Forging (PWA 1016) 0.1% Creep vs Design Curves

FD 15564

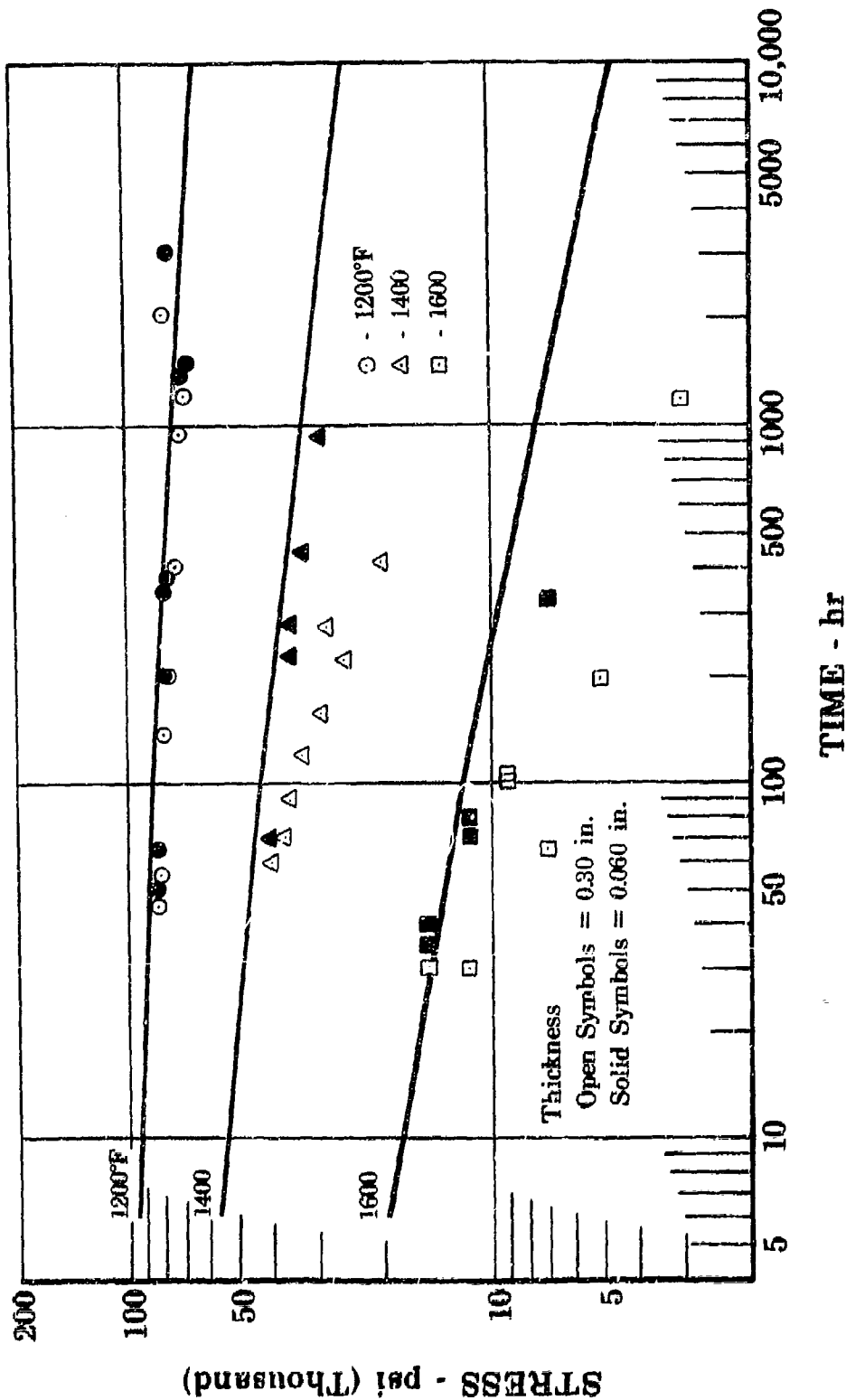
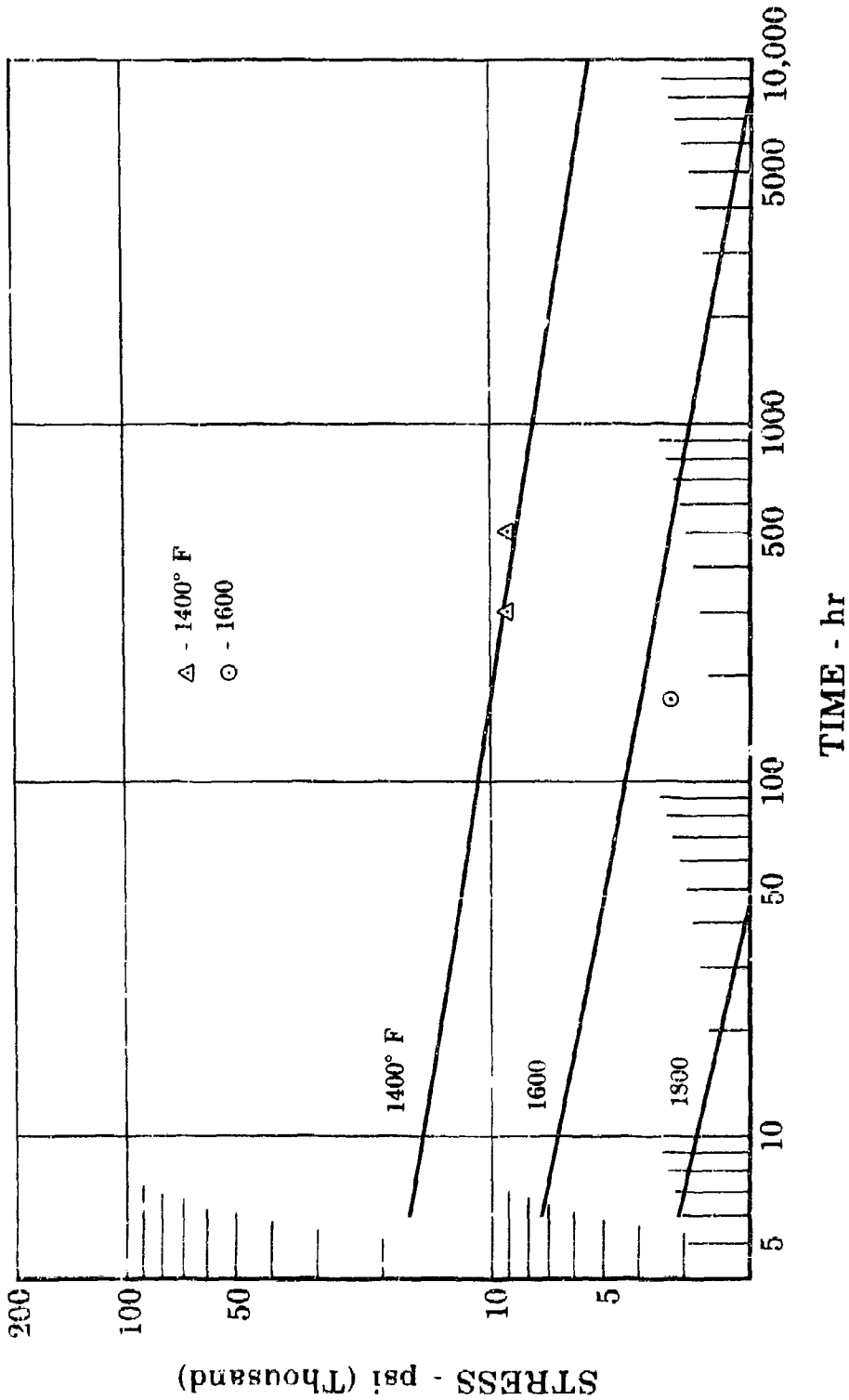


Figure III-B-41. Waspaloy Sheet (PWA 1030) 0.5% Creep vs Design Curves

FD 15563





FD 15562

Figure III-B-42. Hastelloy X Sheet (AMS 5536) 0.5% Creep vs Design Curves

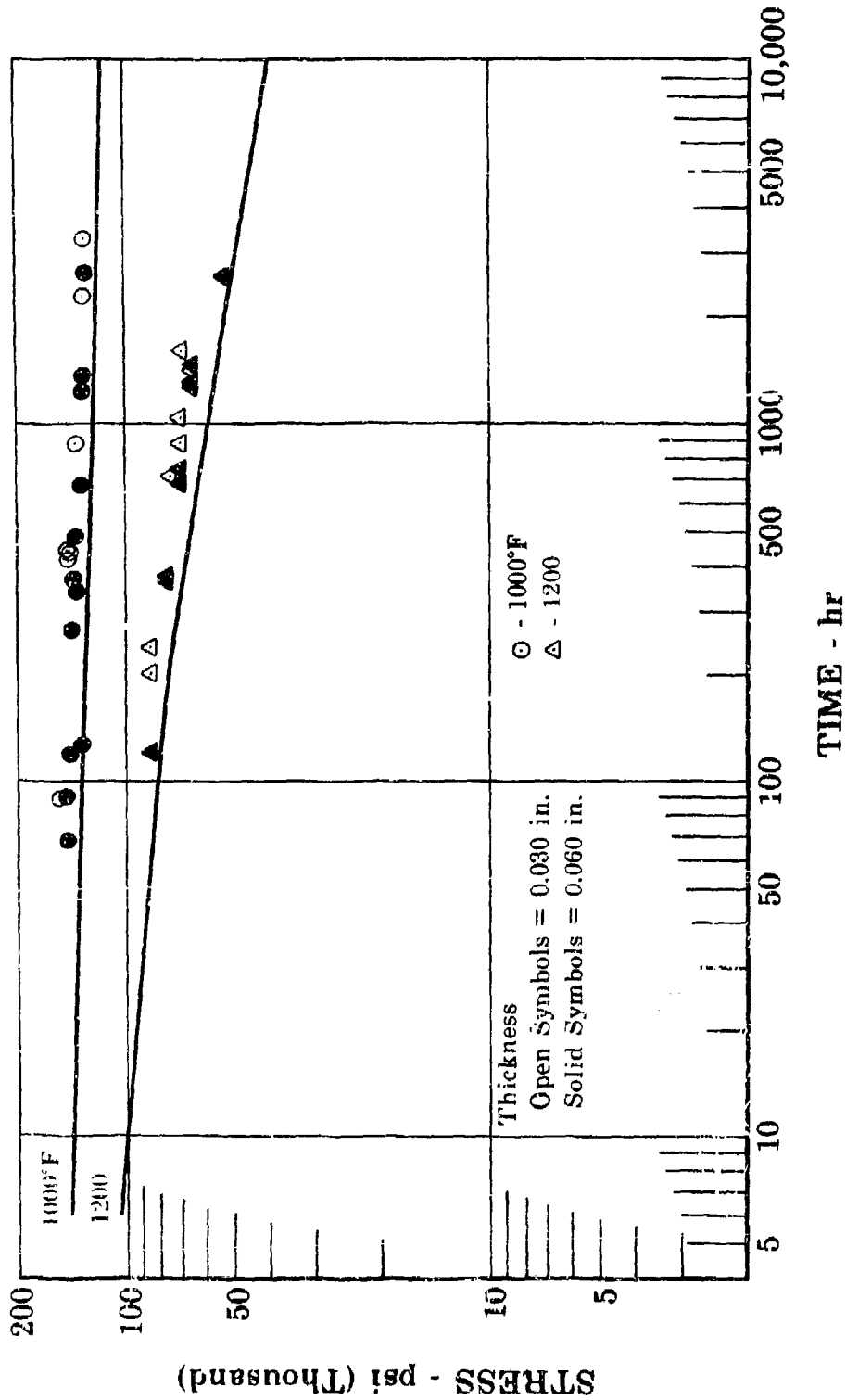


Figure III-B-43. I-718 Sheet (FR# 1033) 0.5% Creep vs Design Curves

FD 15561

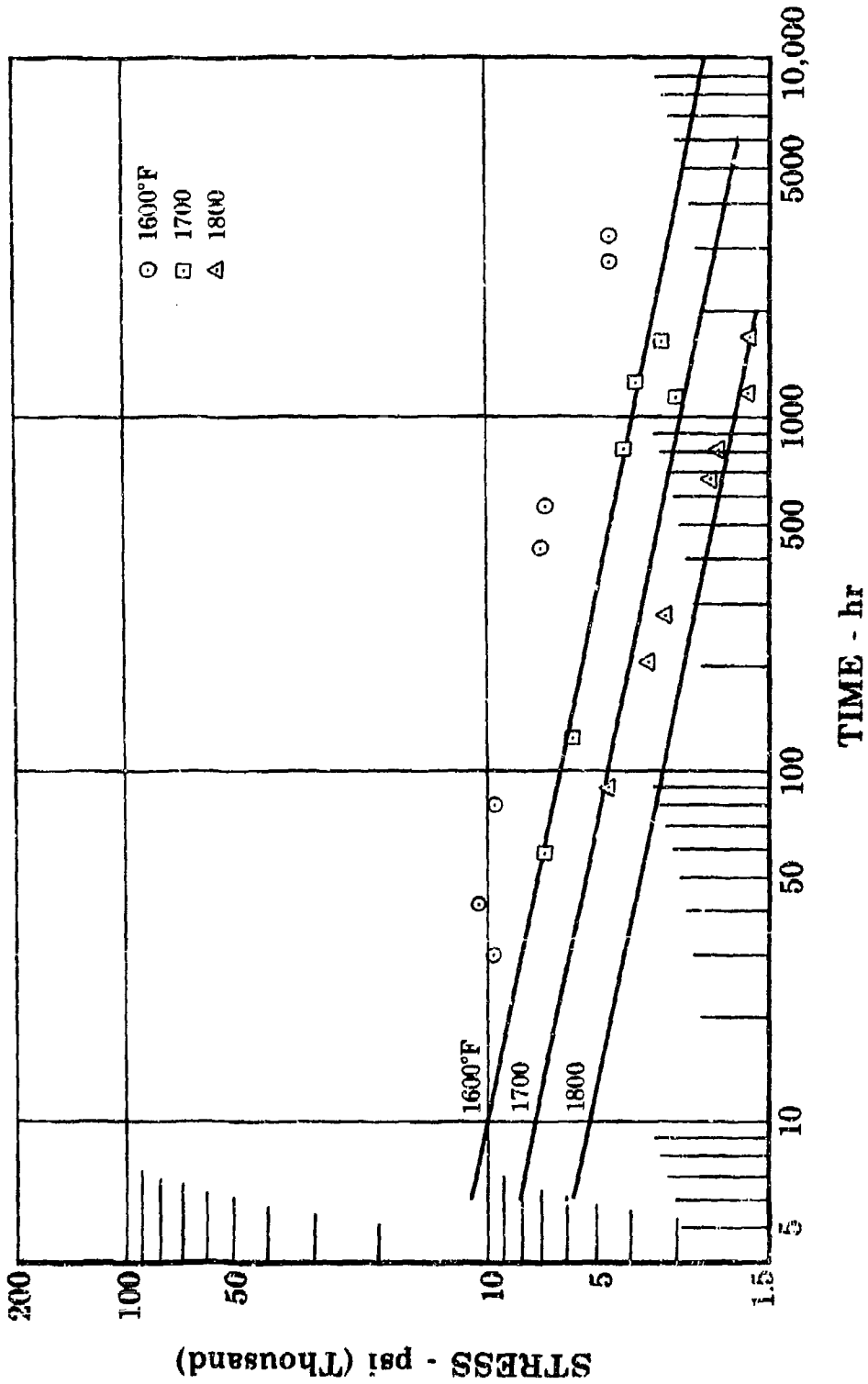
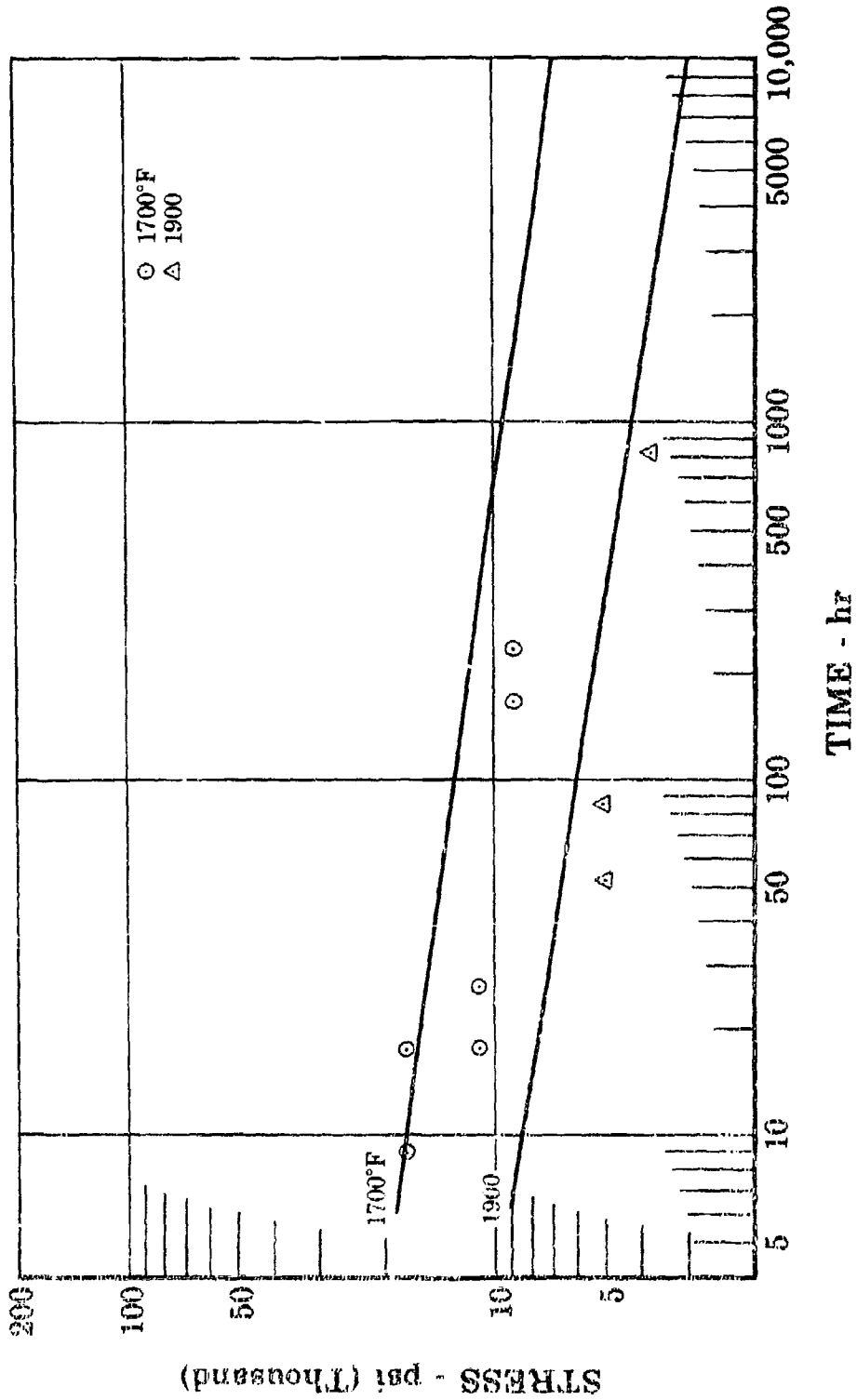


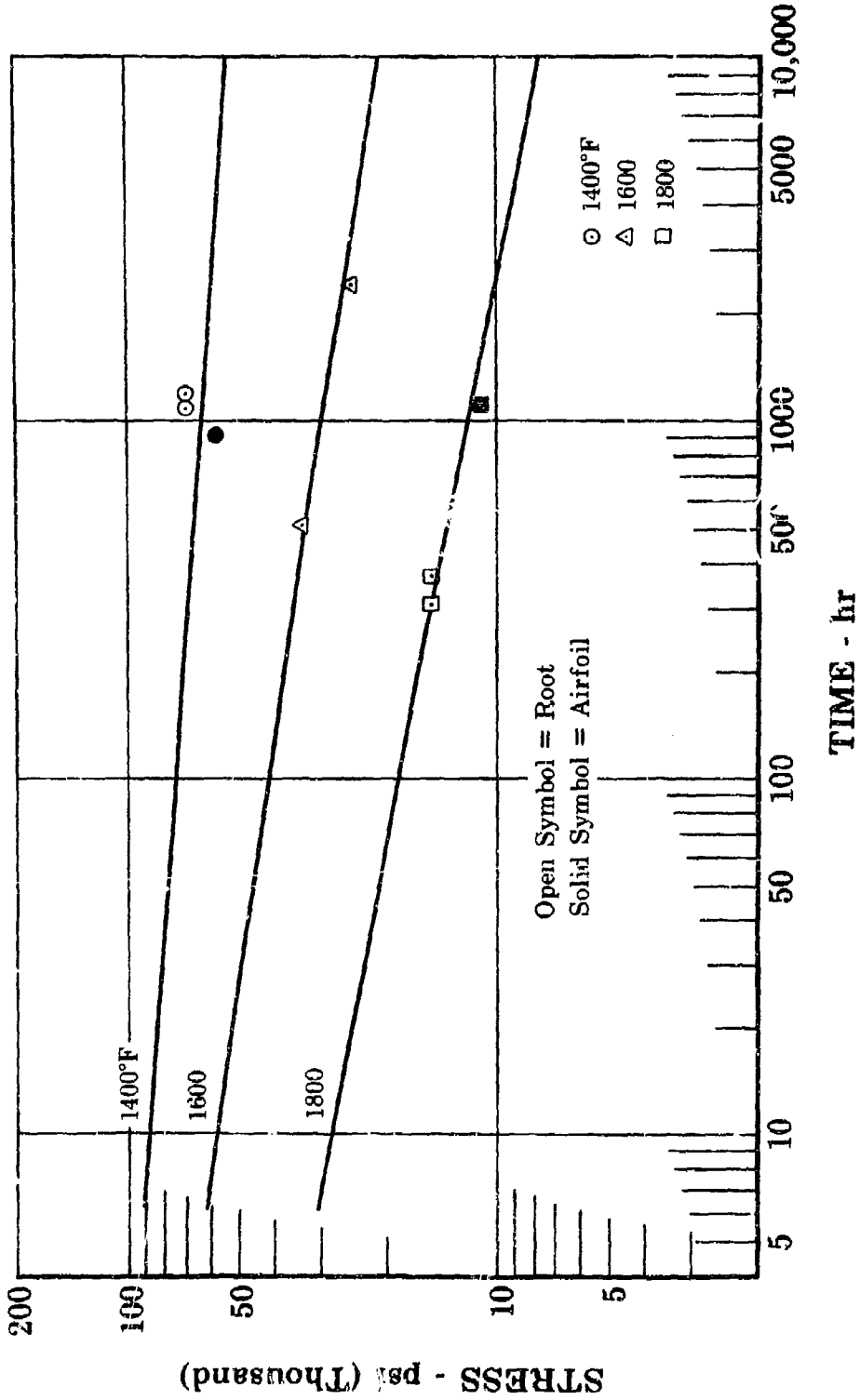
Figure III-B-44. L-605 Sheet (AMS 5537) 0.5% Creep vs Design Curves

FD 15643



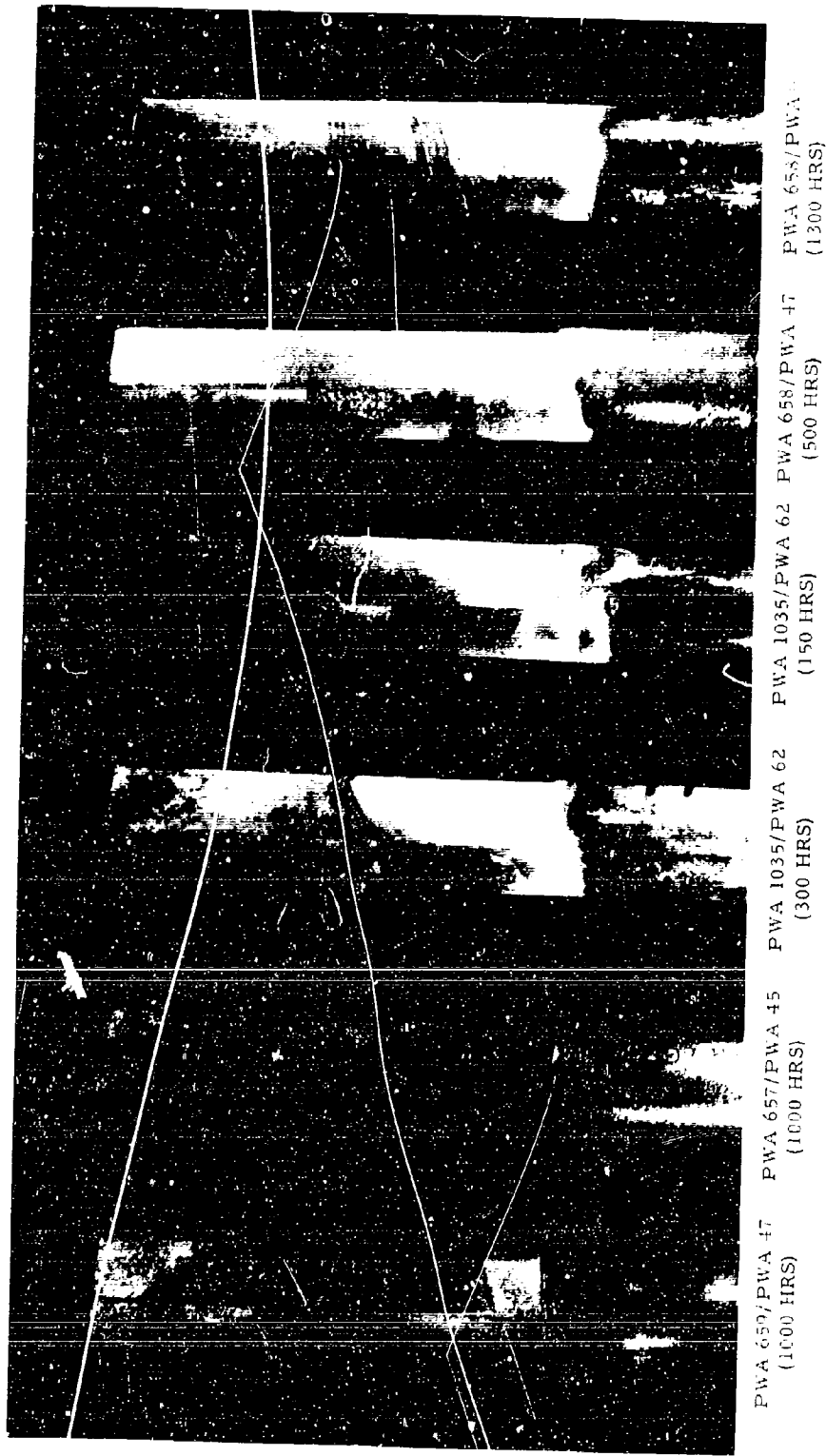
FD 15644

Figure III-B-45. SM 302 (EWA 657) 1.0% Creep vs Design Curves



FD 15645

Figure III-B-46. IN-100 (PWA 658) 1.0% Creep vs Design Curves



\*No. Not Assigned

Figure III-B-47. Specimens of SST Alloys Following Sulfidation Test

FD 15646

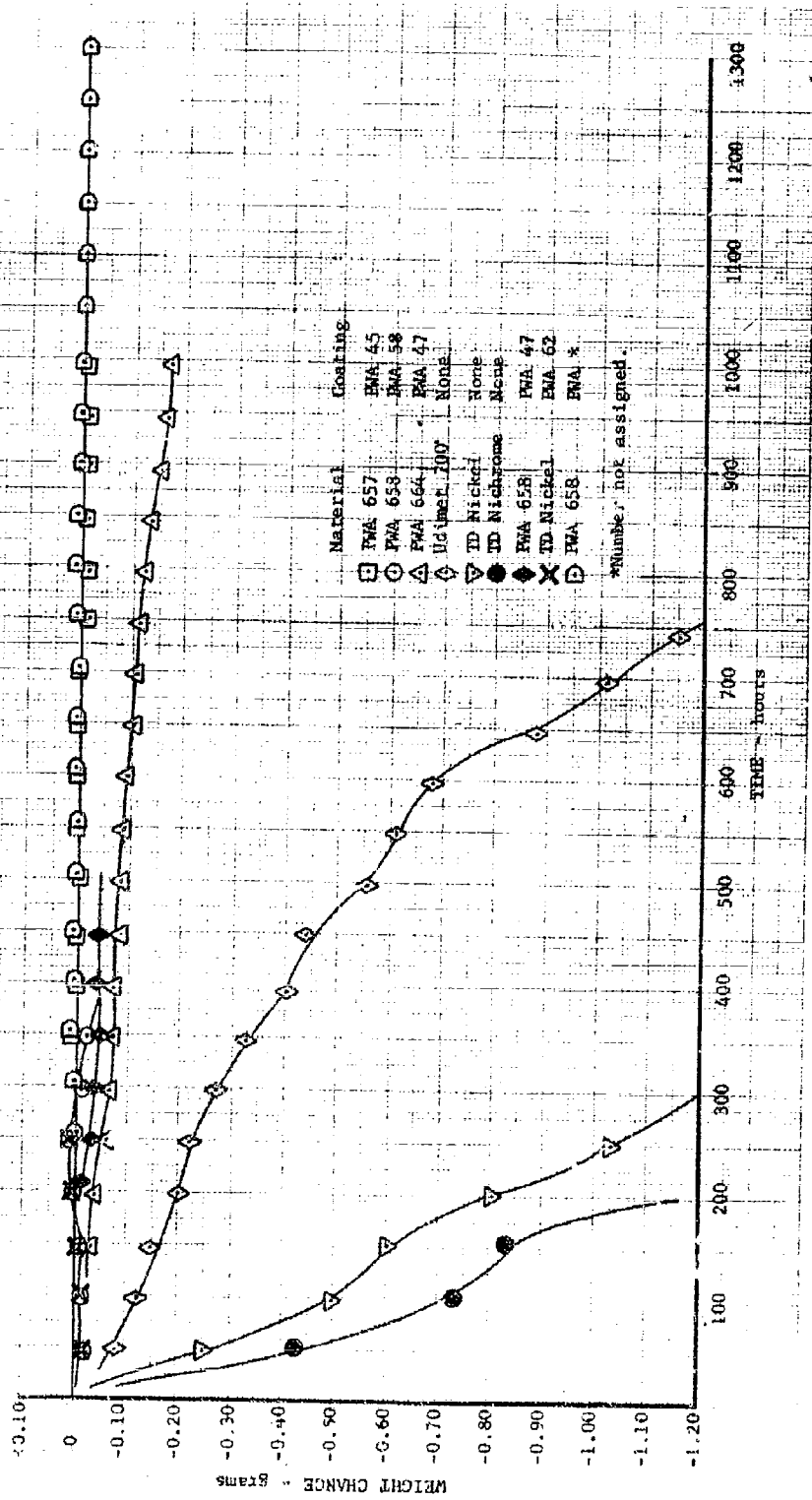


Figure III-B-48. Sulfidation Testing at 1800°F Using PWA 533 Fuel with Maximum Sulfur Content (0.3%) and 1.0 ppm Salt Content in the Air

DF 47360

C. COMPRESSOR

1. 0.6-Scale Fan Rig

	April	Phase II-C Total
Test time: 0.6-scale fan rig	29.56 hours	437.22 hours

The performance program for Build No. 8 of the scaled fan rig was completed during this period. This build was a test stand change from Build No. 7, and incorporated (1) the original design 1st-stage blades, (2) the Build No. 7 2nd-stage blades, and (3) the Build No. 5 "drooped" splitter. Included in the performance program were design speed and 111.2% of design speed with the 1st-stage vanes opened 4 degrees from nominal. During a design speed surge point at the end of the program, a 60-degree segment of the covering of the fiberglass bellmouth was ingested by the rig. Approximately 55% of the 1st-stage blades were damaged between the tip and the outboard shroud to an extent that they should not be used in the rig for performance; no other parts were damaged. Sufficient spare blades are available so that a complete set of these blades will be available for testing as required. Design of a sheet metal bellmouth to replace the fiberglass bellmouth has been completed as reported in paragraph III-A-2, and the part will be available for the next rig test.

Data from Build No. 8 testing are shown compared to build No. 5 data in figures III-C-1 and III-C-2. These results show the same reduction in total airflow that was shown in Build No. 7, but the "drooped" splitter caused an increase in bypass ratio and surge line in a manner similar to the results of Build No. 5. Peak efficiencies were not improved over Build No. 5 except at cruise speed, and were significantly lower than Build No. 7 at speeds below design speed. Build No. 8 has eliminated the question of what caused the total flow loss in Build No. 7. The 2nd-stage blades were the only parts different between Builds No. 5 and 8, and are severely limiting flow in the duct stream. Analysis of Builds No. 7 and 8 data indicates that the 2nd-stage blades are not performing as designed from approximately 40% span to the tip. The root of this blade is performing as designed, and is providing increased surge margin over the original design blade. Opening the 1st-stage vanes



4 degrees gave a slight increase in total flow, but on an overall basis there was little change. This change was made to see if the 1st-stage vanes might be limiting flow at high speed.

A detailed analysis is being made of Builds No. 7 and 8 data to make another redesign of the 2nd-stage blade that would eliminate the duct flow deficiency and improve the high speed efficiency, while maintaining or bettering the improved surge margin. The new 2nd-stage blade design that results from this analysis is scheduled for completion in May, and new parts will be scheduled for testing early in July.

## 2. Full-Scale High Compressor Rig

	April	Phase II-C Total
Test Time	4.28 hours	45.47 hours

Additional testing of the high compressor rig with simulated Build No. 5 fan discharge profiles at the high compressor inlet showed no adverse effect on overall compressor performance or stress level. Teardown of the rig revealed no discrepancies; all parts were accepted at magnaflux or zygl inspection.

Analysis of the data from Builds No. 2 and 3 revealed a lack of work capability near the roots of the front stage blades. This is believed responsible for the lower than desired surge pressure ratios noted in the March monthly progress report. To correct this flow deficiency, the 3rd-, 4th-, and 5th-stage blades are being redesigned by altering the root-to-tip ratio. This allows the stage to accomplish more work near the root of the blade. Hardware is being procured to incorporate this change into the rig for testing in June.

A second approach for improving the root flow is to recamber currently available stators. This can be accomplished in much less lead time, but possibly with a slight reduction in compressor efficiency. The front stators are recambered open at the flowpath ID to allow more airflow in this area. This results in uncambering the IGV and overcambering the 3rd- and 4th-stage stators at the ID trailing edge. The 5th- and 6th-stage stators are opened full span by overcambering the trailing edge to increase the work level of these stages

The compressor rig parts have been reoperated with these desired stator recambers for Build No. 4. This build is approximately 95% complete and it is expected that testing will be resumed early next month. Strain gages are incorporated in all stages of the compressor to monitor blade vibratory stresses. Additional interstage instrumentation is also incorporated for better data acquisition in the deficient areas.

CONFIDENTIAL

Pratt & Whitney Aircraft  
PWA FR-1855

FD 15369A

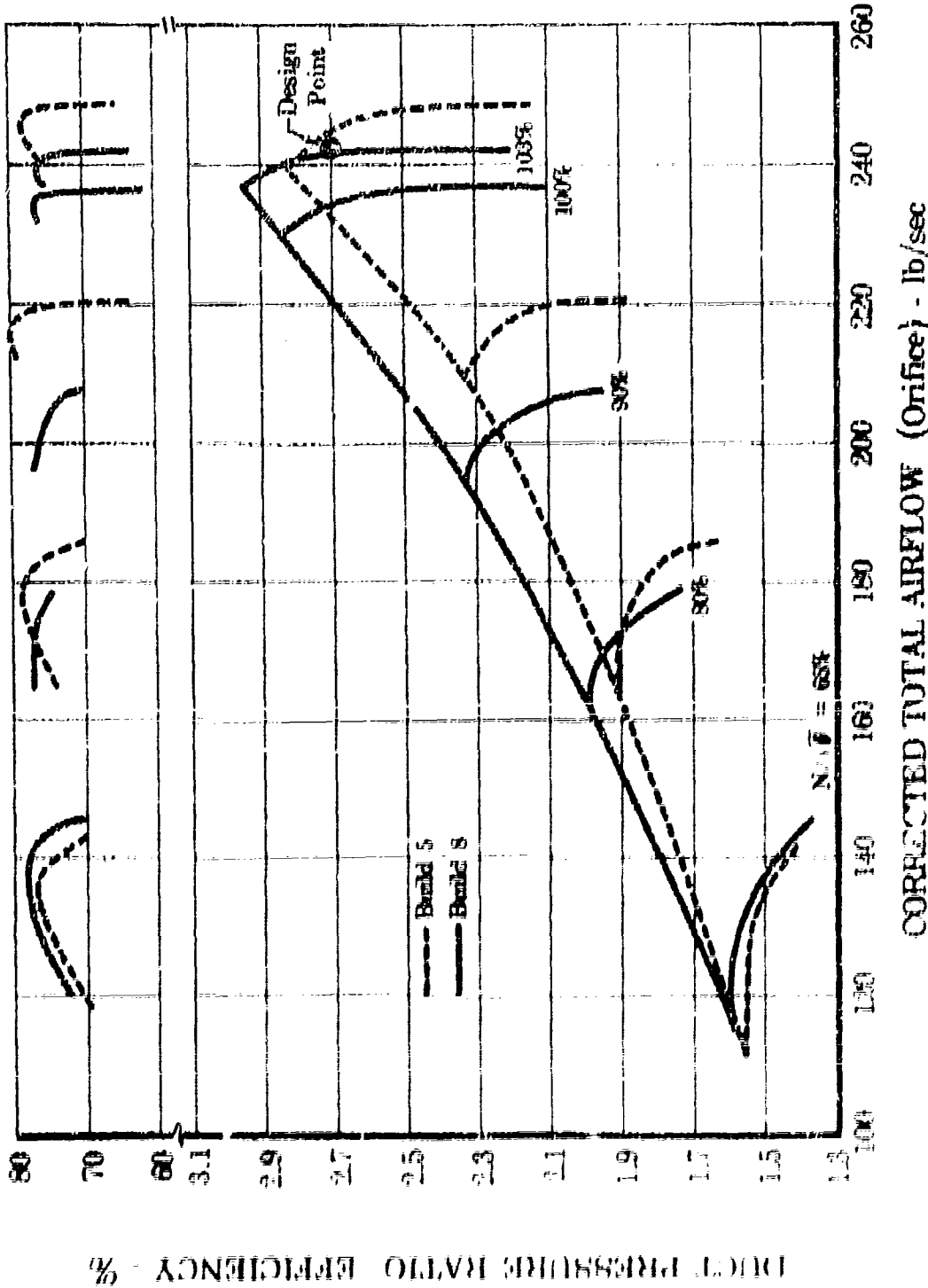
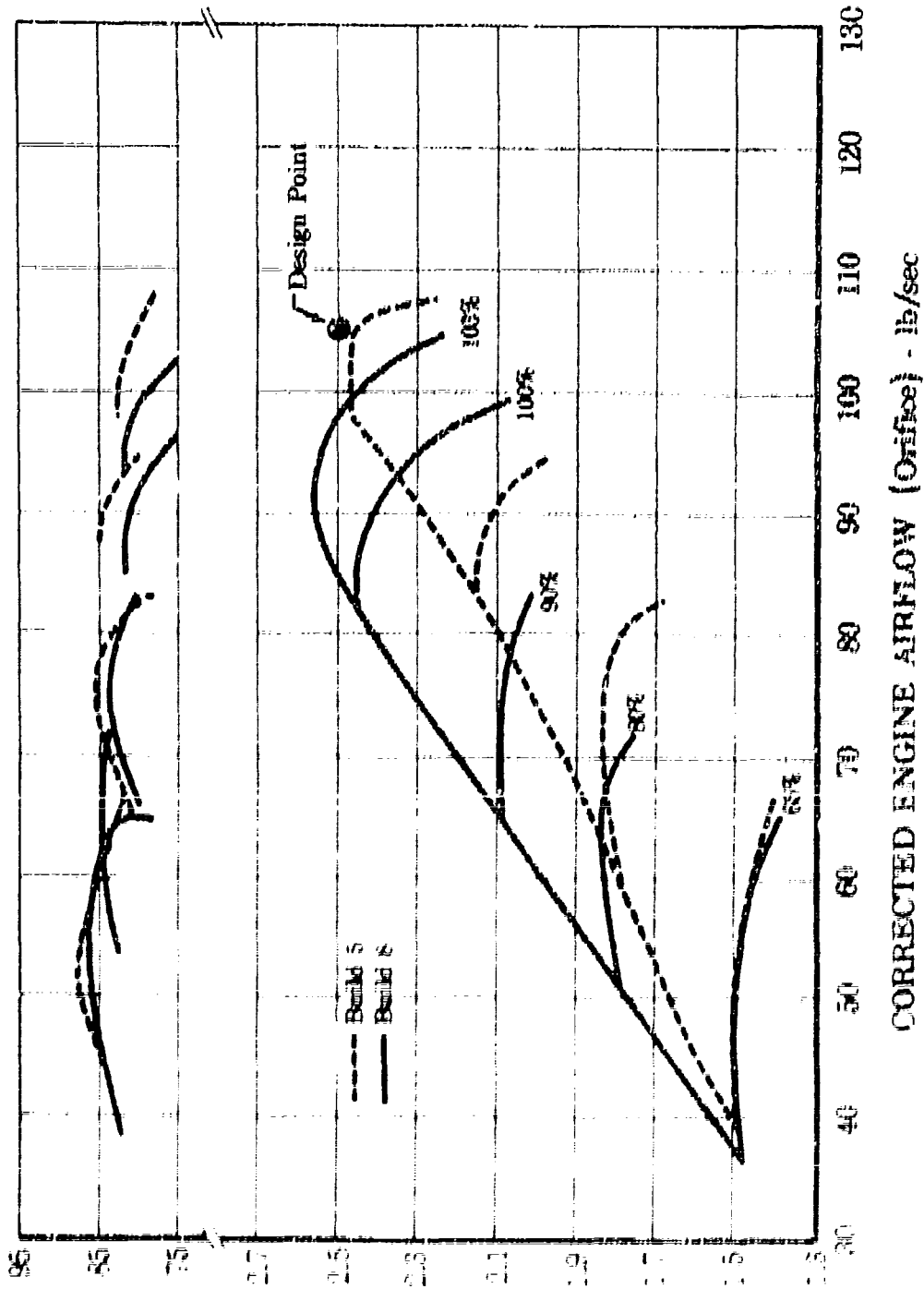


Fig. 11.10. Fan Stream Performance, Two-Stage Fan Compressor RIF

CONFIDENTIAL

CONFIDENTIAL

Pratt & Whitney Aircraft  
PWA PR-1855



FD 15368A

Pratt & Whitney Aircraft Engine Stream Performance, Three-Stage Fan Compressor Rig

ENGINE PRESSURE RATIO

CONFIDENTIAL

D. PRIMARY COMBUSTOR

	April	Phase II-C
Test time for the full annular combustor rig	0 hours	5.36 hours
	(See related technology also)	

1. Engine Combustor Testing

The full annular ram induction combustor successfully completed the first JTF17A-20 engine testing. Ignition characteristics, temperature distribution, and durability were satisfactory.

The combustor exhibited excellent ignition characteristics and rapid flame propagation throughout the full annulus on all starts. Selected 1st-stage turbine vane thermocouples were recorded in the transient mode with satisfactory distribution from ignition to idle.

Temperature distribution plots were taken on all steady-state points by recording all 1st-stage turbine vane thermocouples. The type of instrumentation used is shown in figure III-D-1. Calibration tests had been run previously in an air-cooled, instrumented turbine vane rig to establish a correction from indicated temperature to actual gas stream temperature.

The radial profile was relatively flat at idle. As the turbine inlet temperature was increased, the average radial temperature profile indicated a trend to the desired profile for 2100°F sea level takeoff. The radial profile at the maximum temperature condition tested is shown in figure III-D-2.

The  $\Delta T_{\max} / \Delta T_{\text{avg}}$  for the combustor steadily reduced as the turbine inlet temperature and combustor  $\Delta T$  were increased, to a value of 1.255 for the highest thrust condition. The trend of  $\Delta T_{\max} / \Delta T_{\text{avg}}$  is shown in figure III-D-3.

Temperature distribution for the highest turbine inlet temperature condition tested is presented in figures III-D-4 and III-D-5. Figure III-D-4 shows that the highest average temperature for any 1st-stage turbine vane is only 195°F above the overall average. Figure III-D-5 is the isothermal plot of the turbine inlet temperature distribution for the first engine test.

The combustor configuration tested was a Mod 5-1P, and included many changes developed from earlier runs in the JT4 rig. The condition after 11.63 hours was excellent. There was no carbon buildup similar to that occurring on the original ram induction combustors; only light soot was present. There was no burning or metal distress on any of the scoops or walls. Photographs of the combustor after testing are shown in figures III-D-6 through III-D-9.

2. Related Technology (Results of combustor testing conducted on other programs)

	April Related Program Time	Total Related Program Time
Annular combustor rig test time	4.09 hours	41.28 hours

Although the basic objectives of the JTF17A-20 combustor rig program have been met, limited testing is being conducted on ram induction combustors in both the annular rig and segment rigs, under a related program. The objective of this program is to define the design requirements necessary for simplified construction of a ram induction primary combustor.

Testing was continued with the ram induction combustor in the modified JT4 test rig. Tests were run with the Mod 5-1R (Modification of 5-1N, Ref PWA FR-1779, page III-D-2, with supports strengthened, dome edges cut back, primary cooling increased, and inner liner rotated so that similar scoops on the inner and outer liners are opposing) combustor, both with and without the diffuser deflector. At similar points, the  $\Delta T_{max} / \Delta T_{avg}$  increased from 1.27 to 1.61 when the deflector was removed. The JT4 rig has been disassembled and will be rebuilt with a ram induction combustor of simplified construction.

Six configurations of the ram induction combustor were tested in the 120-degree segment rig during the month. These were as follows:

- Mod 5-7B - Standard five-scoop combustor (Ref Mod 5-1Y, PWA FR-1825, page III-D-4) with portions of secondary scoops blocked.
- Mod 5-7C - Modification of the Mod 5-1Z (Ref PWA FR-1825, page III-D-4), single-row primary and single-row secondary with rear of secondary scoops blocked and cooling air at rear of secondary liner reduced.

- Mod 5-2D - Same as Mod 5-2C but with cooling air at rear of secondary further reduced.
- Mod 5-2E - Single-row primary (same as Mod 5-1Z) but with a double-row secondary.
- Mod 5-2F - Single-row primary and secondary (like Mod 5-1Z) but with row of secondary scoops moved to the rear of the liner.
- Mod 5-2G - Same as Mod 5-1Y (Three-scoop primary and two-scoop secondary) but with counter-rotational swirlers.

The effect of the scoop pattern and reduction of cooling air on the radial temperature profile can be seen in figure III-D-10. From these tests, it is concluded that the single-row primary has the performance potential to permit simplified combustor construction. A single-row secondary may have a high center peaked radial profile. The blocking of the secondary scoops and counter-rotational swirlers had no appreciable effect on combustor performance.

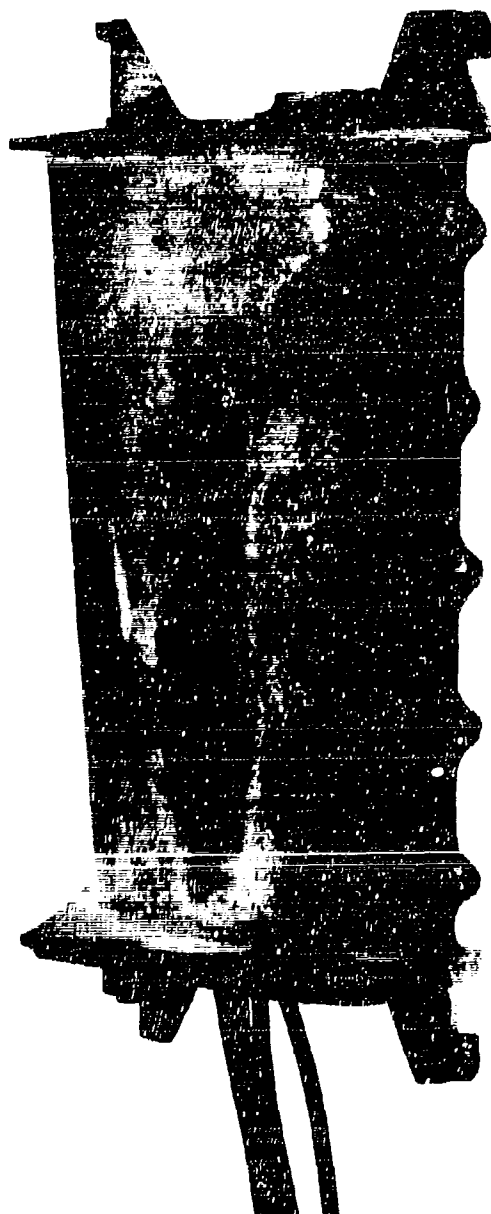
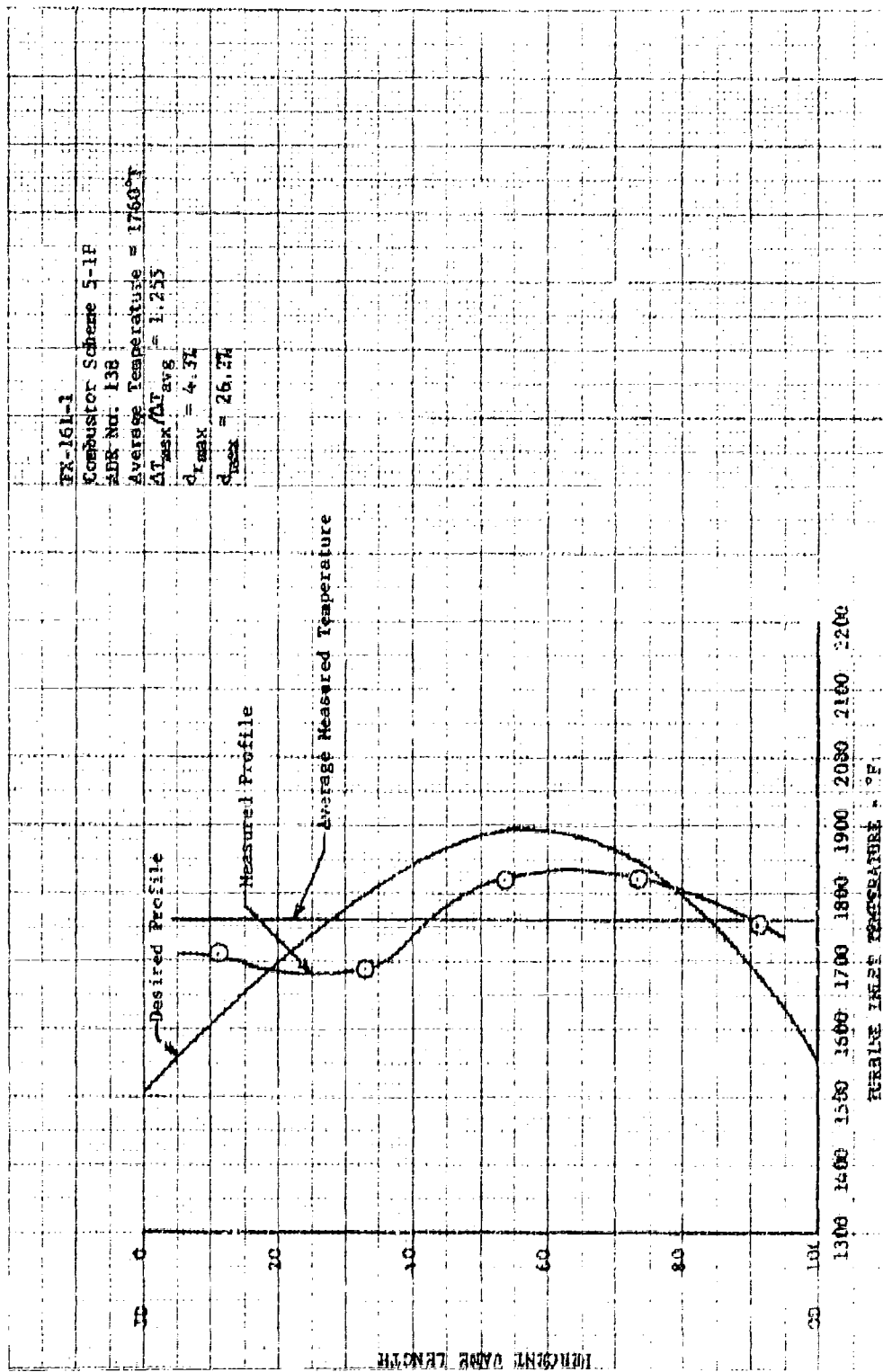


Figure 111-D-1. 1st-Stage Turbine Vane Showing  
Installation

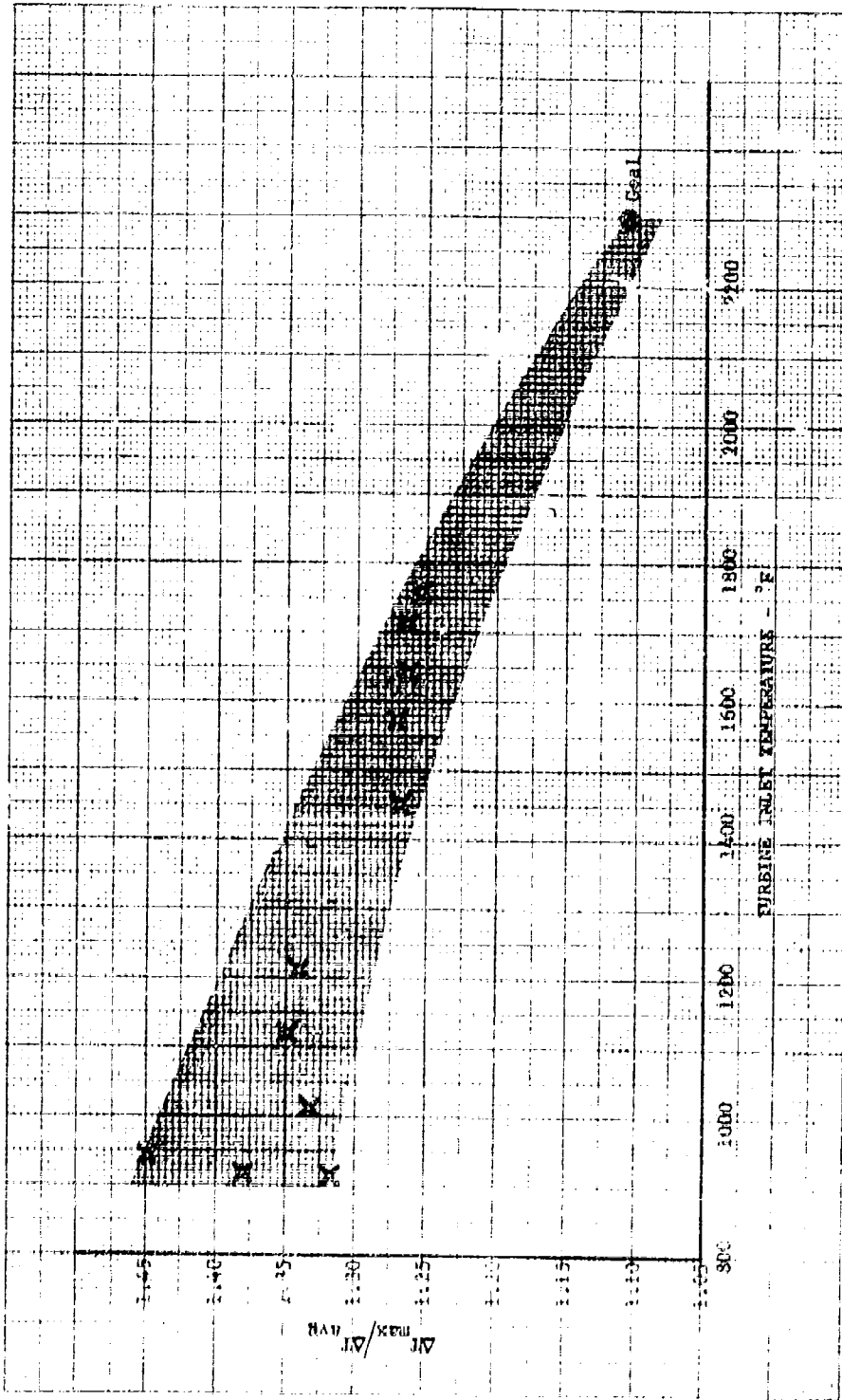
FF 57744





DF 47193

Figure III-D-2. Turbine Inlet Radial Temperature Profile



DF 47194

Figure III-D-3. Engine FX-161-G1 Combustor Scheme 5-1P

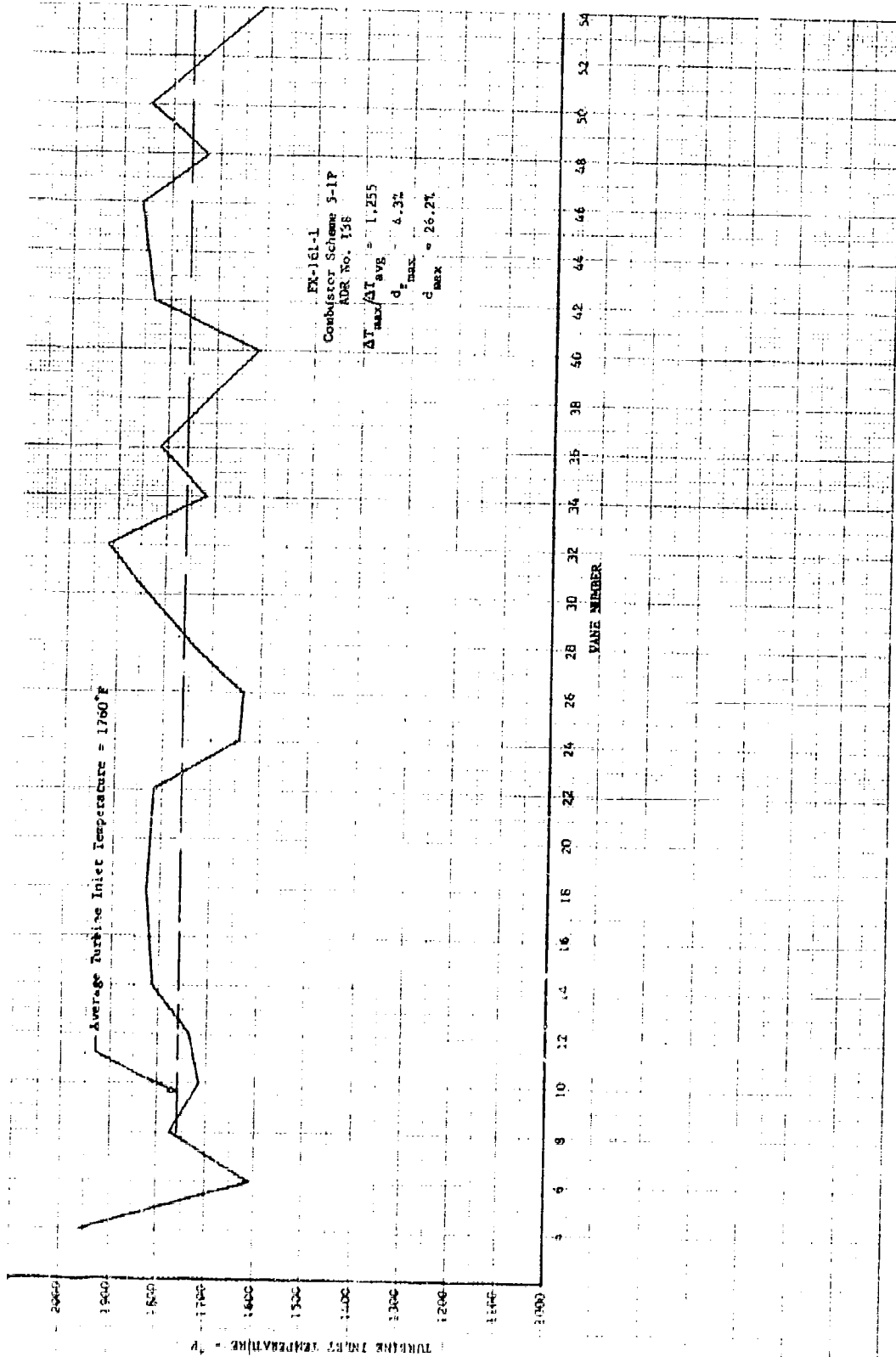


Figure III-D-4. Average Turbine Inlet Temperatures

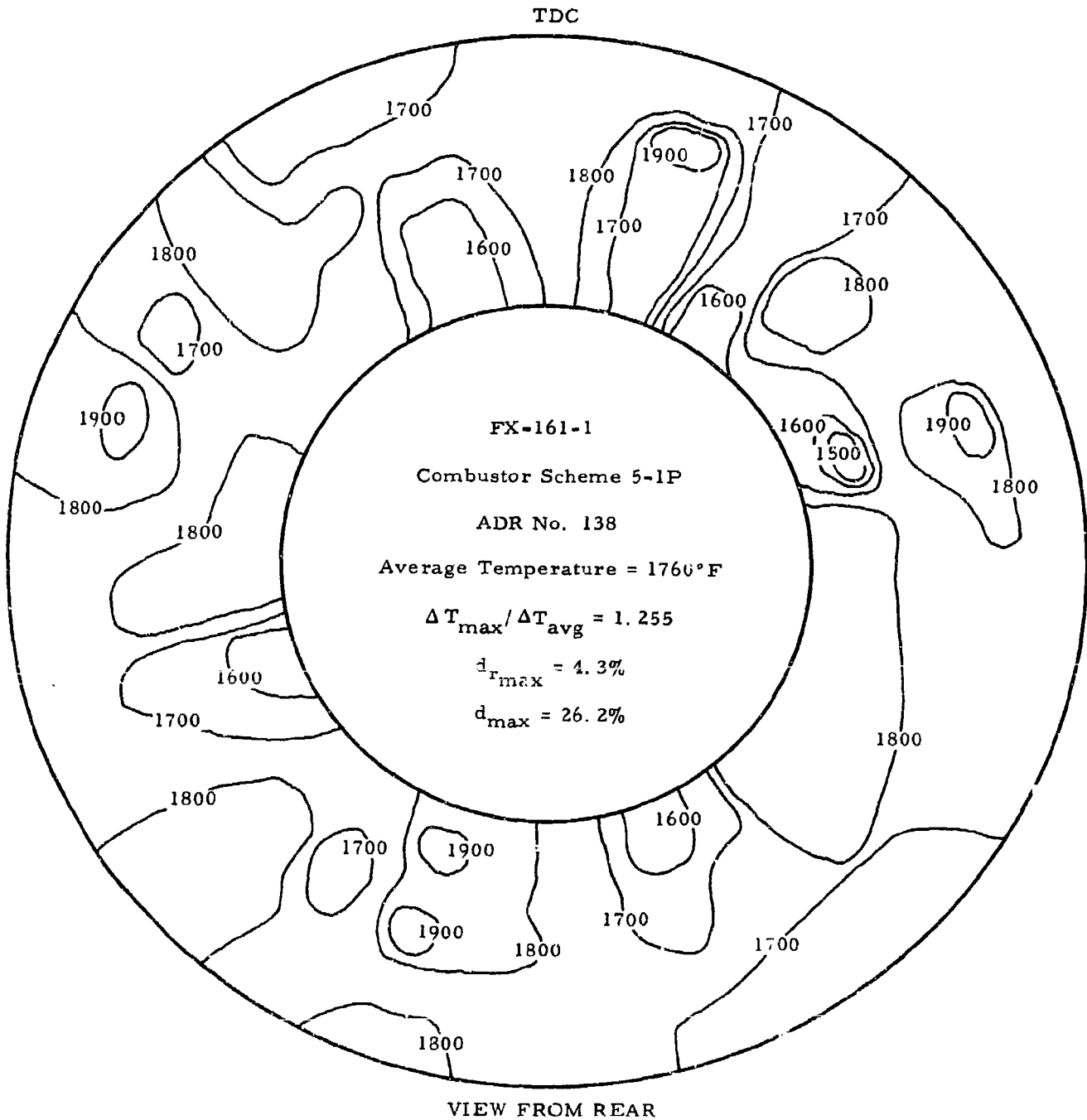


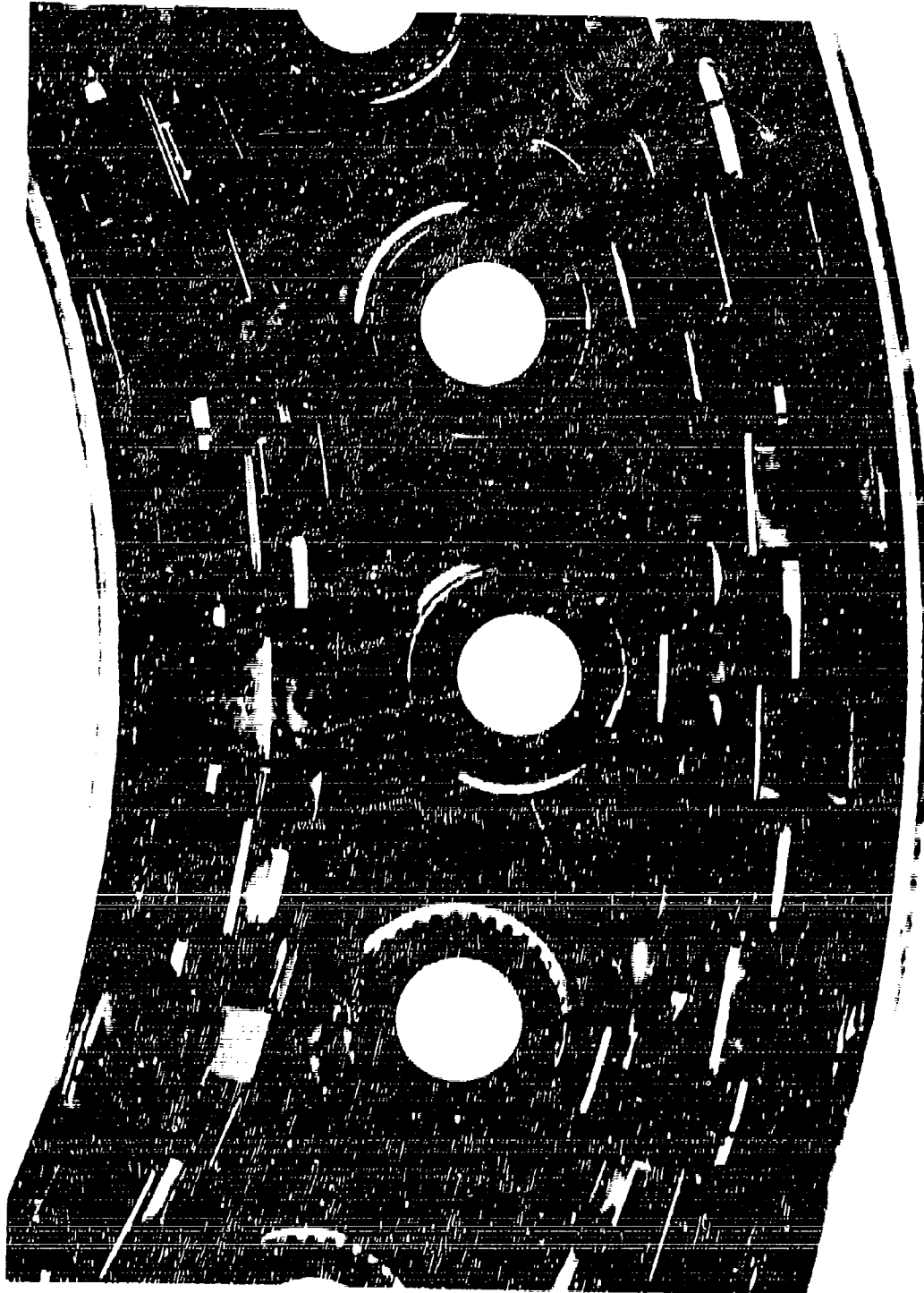
Figure III-D-5. Turbine Inlet Temperature Distribution

FD 15552

**CONFIDENTIAL**

Pratt & Whitney Aircraft  
TWA PR-1855

EE 57715



CONFIDENTIAL

**CONFIDENTIAL**

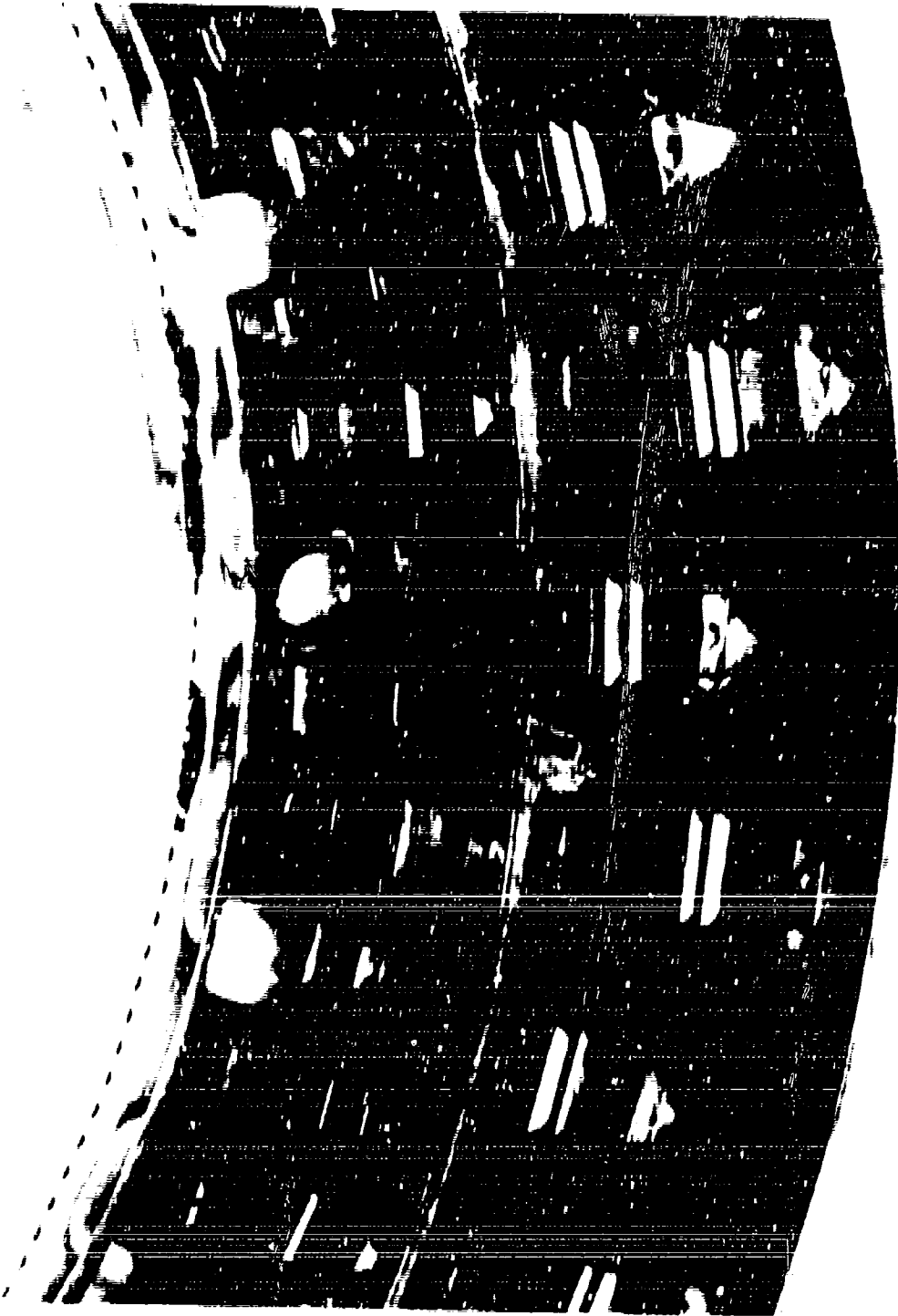
Pratt & Whitney Aircraft  
IWA 110-1075



**CONFIDENTIAL**

**CONFIDENTIAL**

Pratt & Whitney Aircraft  
PW-108



**CONFIDENTIAL**

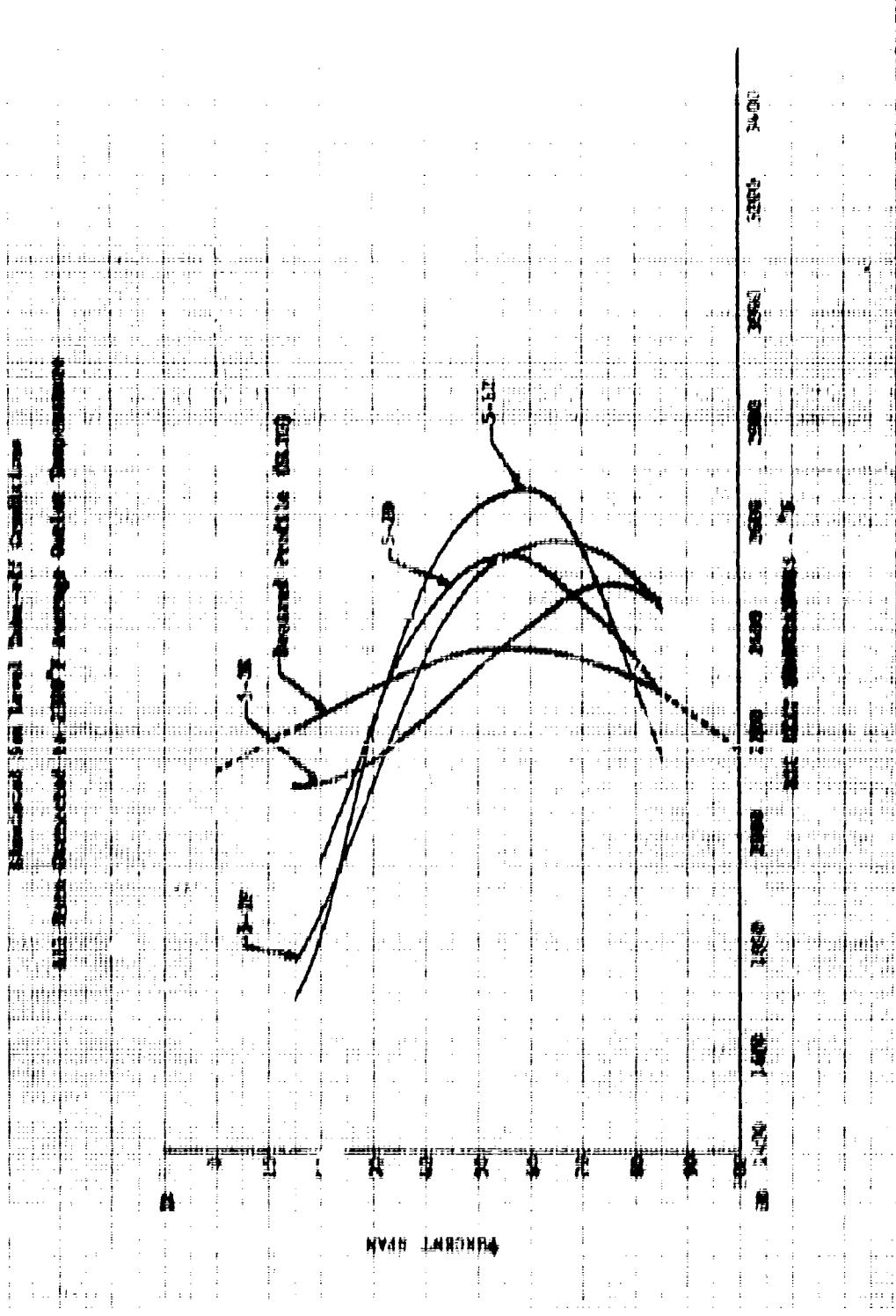


1  
2  
3  
4  
5  
6  
7  
8  
9  
10  
11  
12  
13  
14  
15  
16  
17  
18  
19  
20  
21  
22  
23  
24  
25  
26  
27  
28  
29  
30  
31  
32  
33  
34  
35  
36  
37  
38  
39  
40  
41  
42  
43  
44  
45  
46  
47  
48  
49  
50  
51  
52  
53  
54  
55  
56  
57  
58  
59  
60  
61  
62  
63  
64  
65  
66  
67  
68  
69  
70  
71  
72  
73  
74  
75  
76  
77  
78  
79  
80  
81  
82  
83  
84  
85  
86  
87  
88  
89  
90  
91  
92  
93  
94  
95  
96  
97  
98  
99  
100

Pratt & Whitney Aircraft



REV. 4-13-59



STANDARD DEVIATION vs. RPM

## E. TURBINE

## 1. Thermodynamic Cascade Rig

The results of the JTF17A-20 baffle blade test mentioned in the February progress report, PWA FR-1825, have been analyzed and the test data are shown in figure III-K-1. The initial tests have been completed on the JTF17A-20 4-wall, 1st-stage turbine blade (described in the February progress report, PWA FR-1779). A sketch of the part and preliminary test results are shown in figure III-K-2. This thermal skin cooling concept represents a major advancement in turbine blade cooling state-of-the-art.

The 4-wall blade exhibits superior cooling characteristics as compared to more conventional convective or film-cooled airfoils. An average midspan temperature of 1750°F was obtained with 2% cooling air at rig conditions, which simulated JTF17A-20 cruise condition (2200°F turbine inlet, 1100°F cooling air). This is an improvement of approximately 150°F over current operational convectively cooled airfoils as shown in figure III-K-3, and demonstrates that this airfoil will operate at metal temperatures significantly lower than those obtained previously.

A comparison of cooling effectiveness  $\left( \phi = \frac{T_{\text{gas}} - T_{\text{metal}}}{T_{\text{gas}} - T_{\text{cooling air}}} \right)$  of the 4-wall blade with the best previous convectively cooled scheme (3-wall blade) and film-cooled schemes is shown in figure III-K-4; this comparison indicates an improvement of approximately 23% at 2% cooling airflow. These results are corroborated by vane tests employing similar leading edge impingement cooling systems as shown in figure III-K-5.

The initial test in a program to evaluate radioactive kryptonation as a method for measuring surface metal temperature of JTF17A-20 turbine airfoils has been completed and the part has been sent to UAC Research Laboratories for analysis.

The rig is now being assembled with a JTF17A-20 1st-stage turbine vane to conduct the heat transfer test on the airfoil early in May.

## 2. Aerodynamic Cascade Rig

Only one rig checkout test was made during this report period because of facility air supply problems; however, it is anticipated that the overall aerodynamic performance program will be completed by 30 June 1966.

### 3. LCF Testing of Film Cooling Slots

The program for determining the LCF capabilities of various slot configurations has continued in the thermal shock rig (torch-type open-flame burner). The thermal cycle was modified to increase the temperature gradient across the airfoil, which results in an increased plastic strain. This was accomplished by installing a shield directly behind the cooling air slots in the airfoil which deflected the flame off the airfoil behind the shield. (See figure III-E-6.) The temperature gradient from the leading edge to behind the slots was increased from approximately 400°F (without the shields) to approximately 900°F (with the shields). A blade with a modified "S"-shaped slot in the airfoil was cycled at the revised conditions, and cracks were found in the leading edge after 1500 cycles. The blade was subjected to 1500 additional cycles; however, no cracks were generated at the slots during the entire 3000 cycles. Blades with "X"-shaped slots and "S"-shaped slots in the airfoils were each subjected to 3000 thermal cycles (revised conditions), but no cracks were generated at the leading edge or slots. Thermal cyclic test results to date verify analytical studies showing that airfoils with slots located a sufficient distance from the leading edge will generally crack in the leading edge before cracking in the stress concentration areas at the slots. Testing is continuing at an increased temperature gradient for further substantiation.

Thermal cycling of slotted airfoils in the induction heating rig has also been modified. The cyclic heating of the leading and trailing edge to 1800°F with a temperature gradient of 700°F and a 5000-lb pull applied resulted in cracks in the leading and trailing edges, as in the open-flame thermal shock rig. The induction heating coils are now placed directly over the slot locations in the airfoils. The temperature at the slot is stabilized at 1750°F, and 1400°F at the leading edge during the "heat-on" cycle. The temperature during the "heat-off" cycle is 1200°F at the slot and 1100°F at the leading edge. This will result in the highest thermal strain in the stress concentration area of the slots. Although the airfoils would not be subject to this temperature gradient during engine operation, this type of cycling is required to compare the various slot configurations.

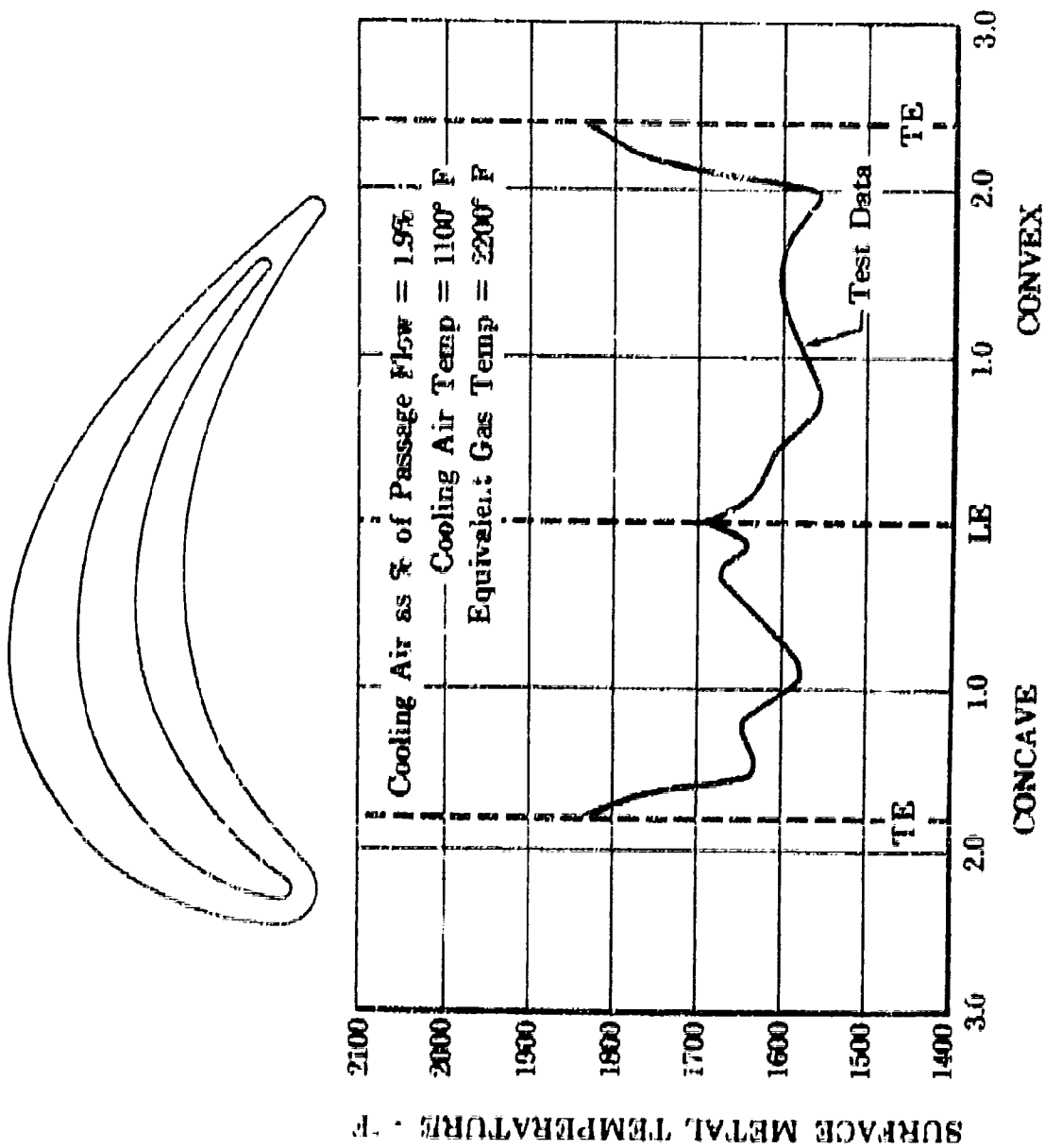
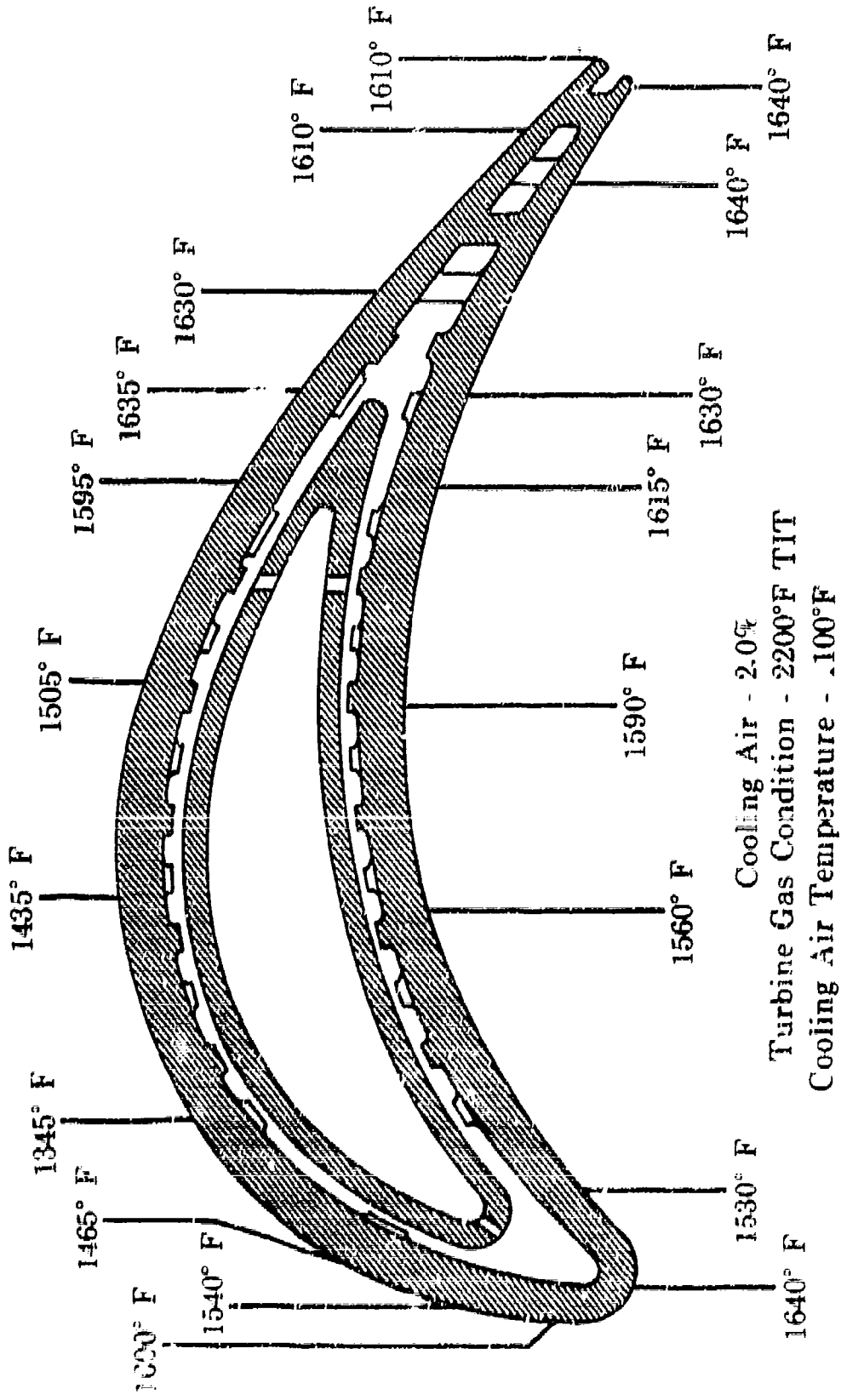


Figure III-E-1. JDE17A-20 1st-Stage Baffle Stadia and Test Data



FD 15608

Figure III-E-2. JT57A-20 1st-Stage 4-Wall Turbine Blade

FD 1564S

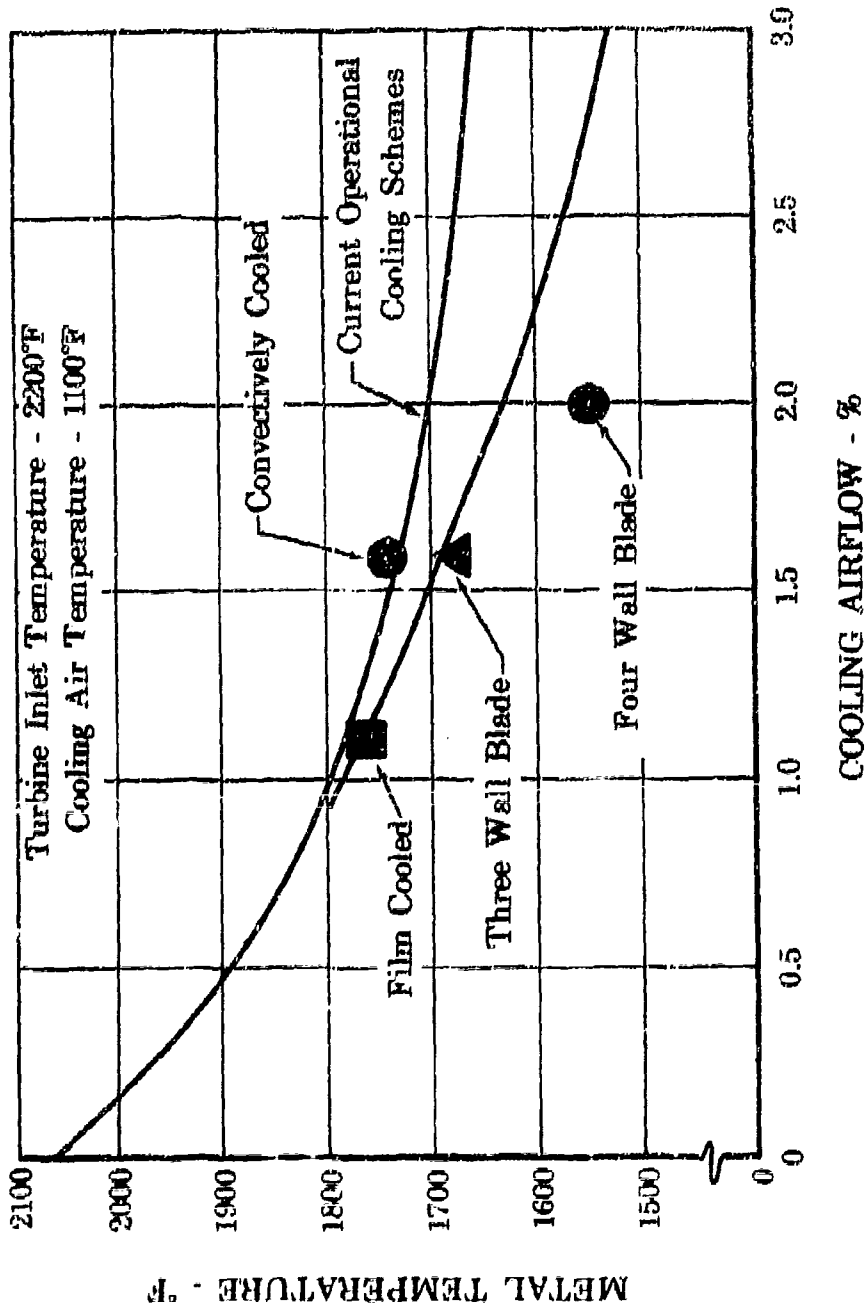


Figure III-E-3. JTF7A-20 First Blade Cooling

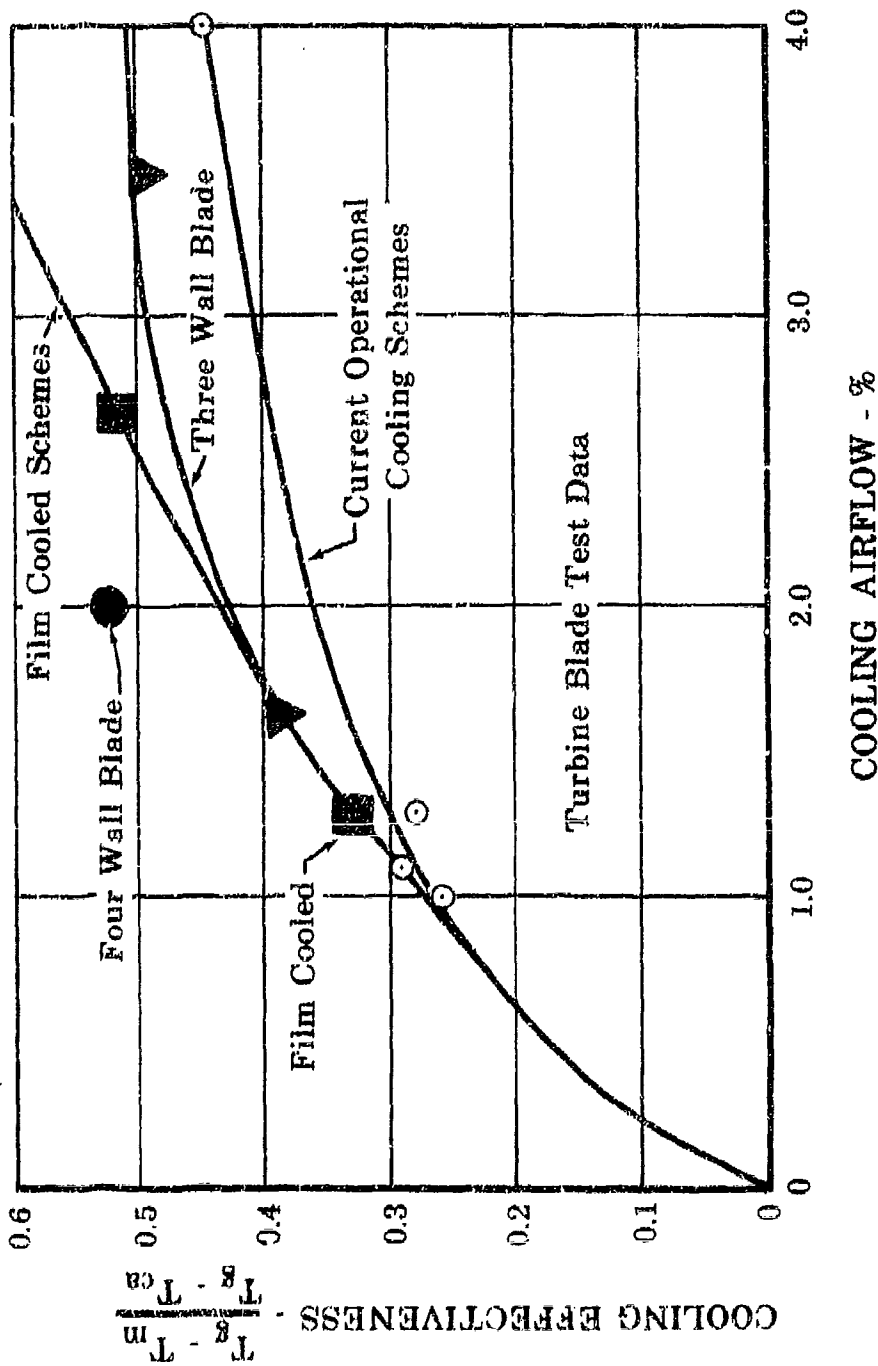


Figure III-E-4. Cooling Effectiveness vs Cooling Airflow (Blade)

FD 15649

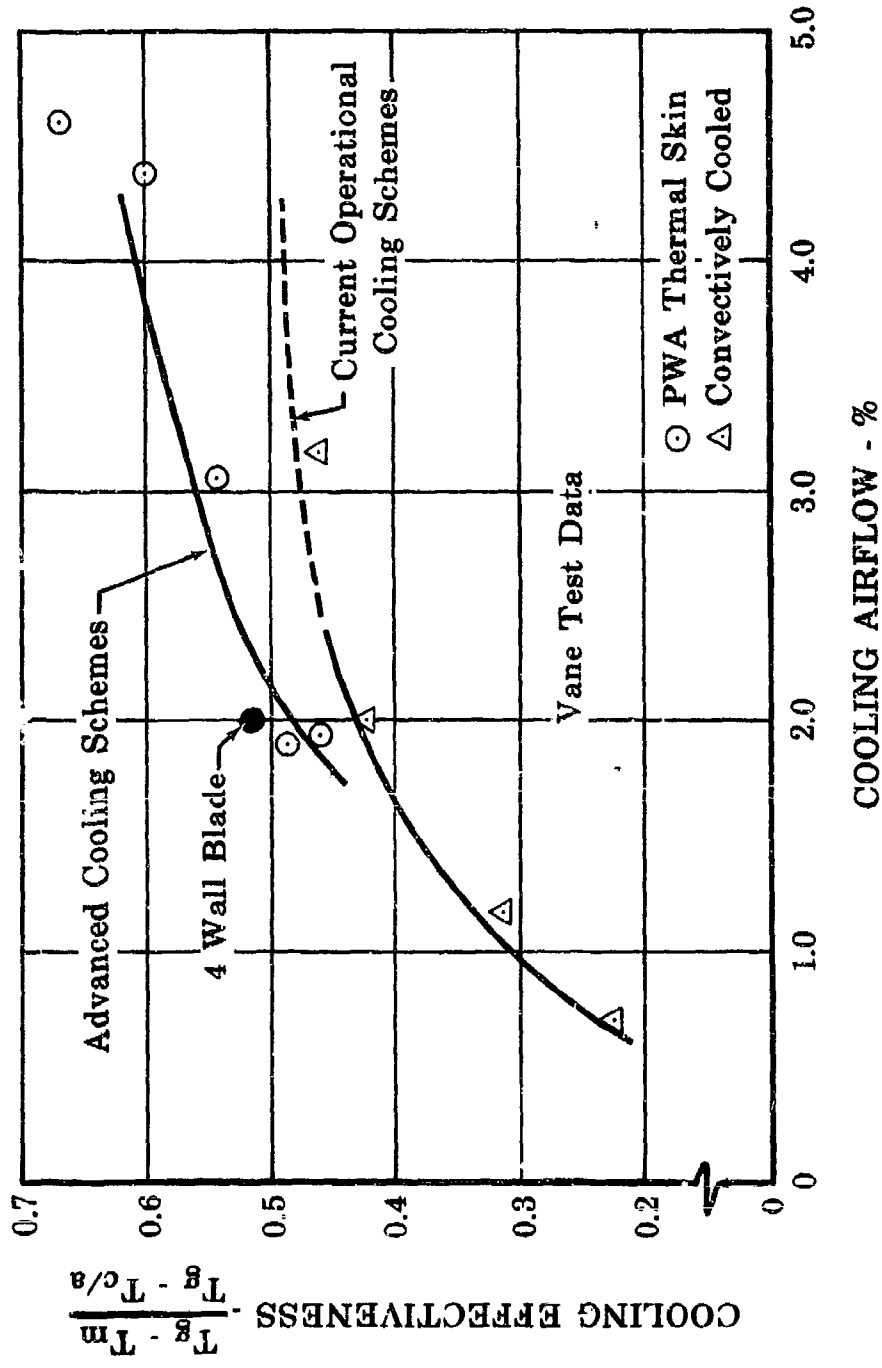


Figure III-E-5. Cooling Effectiveness vs Percent Cooling Air (Vane)



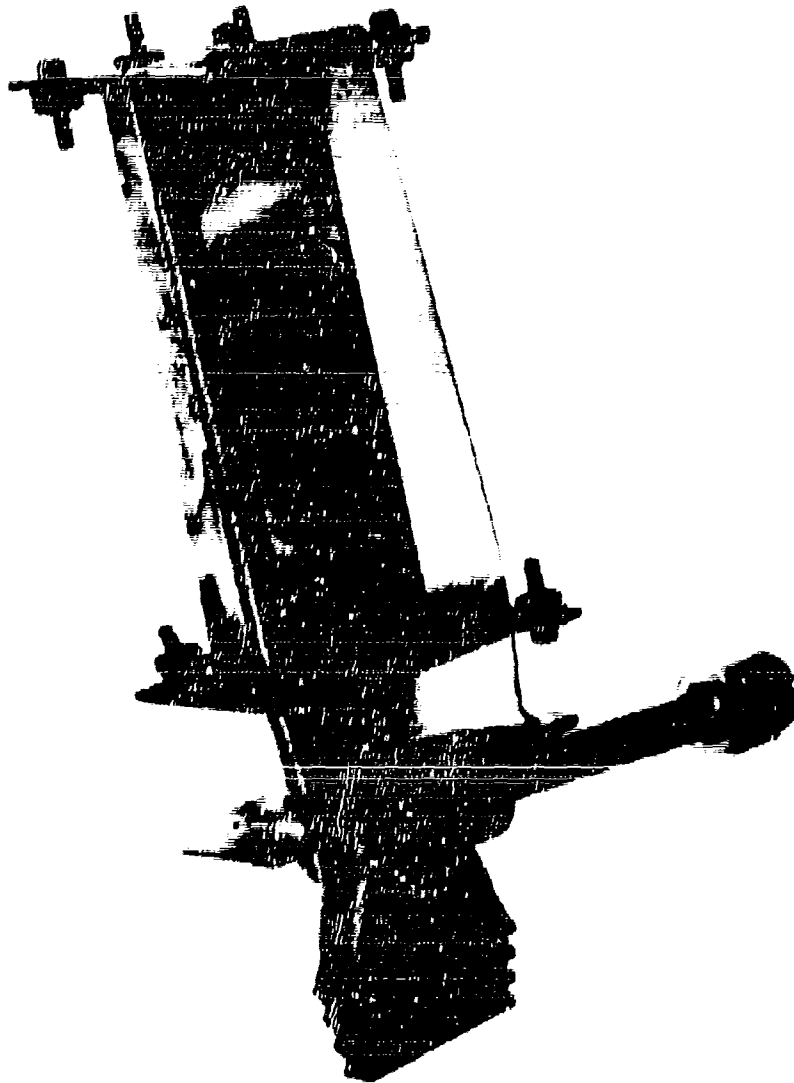


Figure III-2-6 A111-11 with Shrouding Installed  
Behind Cooling Air Inlets

FR 57750

III-2-6

F. AUGMENTOR

A summary of the augmentor development effort to date is presented in Appendix A of this report.

### G. EXHAUST SYSTEM

Cruise performance, optimization model tests were continued during April. Tests were conducted with variations of fan duct plug and shroud geometry, and the data were analyzed. The effect of plug base area, final plug angle, and shroud length on cruise performance was established by these tests. Results show that performance is sensitive to plug base area and final plug angle, but relatively insensitive to variations in shroud length. Optimum performance levels were obtained with small base areas and low final plug angles. The completion of optimization testing has been extended to 15 July to provide continued prototype design support, with some overlap for installation testing.

Drawings have been completed for the tertiary-door-open models that will be used for Mach 0.9 tests scheduled in June, and fabrication of parts has been started. These tests will investigate what effect clamshell, shroud, and tertiary door geometry have on model performance.

Design of a floating, trailing edge flap model has been initiated. Installation tests with this model are scheduled for August.

The lockheed wing model (figure III-6-1) is being instrumented and tunnel flow field instrumentation is being fabricated in preparation for the first phase of installation tests scheduled for June. These tests will investigate the wind tunnel flow field and the pressure distribution over the wing at Mach 0.6 and 0.9. Tests will be conducted with the wing at various angles of attack and located at several positions in the wind tunnel to determine the wing location that best simulates flight conditions. The boundary layer characteristics upstream of the tertiary air ducts, both above and below the wing, will also be investigated. The second phase of the installation tests, to determine wing-exhaust system performance, is scheduled for August. Initiation of the design of a Boeing installation model is being held pending a definition of wing geometry from Boeing. Start of the Boeing model design has been rescheduled for 15 June.

Fabrication continues on detail parts for both research supplement engine units.

Pratt & Whitney Aircraft  
PWA PR-1055

6  
2  
2  
B



## II. CONTROLS

### 1. Initial Experimental JT717A-20 Control System

#### a. Analytical Program

An analog computer investigation is being programmed for the Bendix CJ-Q1 main fuel control, H&D modified JFC-51 duct fuel control and H&D breadboard airflow control.

#### b. Main Control

The fourth CJ-Q1 control was delivered to PRDC from Bendix Products Aerospace Division. There are now four controls available for use at PRDC, two of which incorporate a fuel schedule in accordance with the initial performance estimates, and two of which have the revised fuel schedule as reported last month. Data from the initial engine run are being analyzed so that the best schedule can be chosen for future engine running.

#### c. Duct Airflow Computers

The second Hamilton Standard duct airflow computer has been returned to PRDC with the following improvements incorporated in the linkage:

1. A locating spring seat was added to the header of the  $\Delta P/P$  setting reference bellows.
2. Features were incorporated to limit the motion of the interconnecting link in the  $(P_L - P_M)/P_L$  setting servo to prevent disengagement.
3. The input linkage was allowed to minimize side play.

The data recorded on this unit prior to being returned to PRDC are shown in figure III-B-1.

The first unit will be returned to Hamilton Standard for incorporation of these fixes after they have been evaluated at PRDC.

#### d. Duct Fuel Controls

##### (1) JFC-51 Duct Fuel Control

The control assigned to the first experimental engine operated satisfactorily during the engine test, including operation of the duct heater.

A second control is being fitted with the parts required to remotely mount the duct fuel pump controller. This unit will be final leak-checked and delivered for installation on the second experimental engine.

(2) AA-M1 Duct Fuel Control

The first AA-M1 control "as received" calibration was discontinued when the second control, incorporating an improved fuel schedule, became available. This improvement was achieved by revising the fuel valve feedback cam contour; a revised cam is available for future installation in the first AA-M1 control.

The fuel flow schedule in the first AA-M1 control was shown in Figure III-II-13 of the February progress report. Figures III-II-2 through III-II-5 of this report show the Bendix "final data" schedules for the second control.

The AA-M1 test bench instrumentation has been improved during this period and the engine-type second loop duct exhaust nozzle actuator and feedback system has been installed. All of the AA-M1 calibration tooling has been received from Bendix.

e. Duct Manifold Quick-Fill System

Detail parts for the redesigned quick-fill breadboard system have been manufactured and will be assembled for bench evaluation. This repackaged system is intended for future engine test.

f. Ignition

Gas generator and duct heater lights were achieved without a mis-fire during the initial test of engine PX-161.

g. Initial Engine Test Results

The following control system components performed satisfactorily during the PX-161 engine test:

1. Gas generator fuel control
2. Gas generator fuel pump
3. Duct heater fuel pump
4. Duct heater fuel pump controller

5. Hydraulic pump
6. Duct heater variable exhaust nozzle area control
7. Duct heater fuel control.

One minor control discrepancy was detected during the PX-161 engine test.

An attenuator orifice in the hydraulic inlet to the compressor vane control was changed in order to provide full vane travel.

#### b. Modified Control System

Bench testing of the automatic modified control system is now scheduled for completion in August.

#### 1. Control System Component Experience Including "Hot" Testing (Related Technology)

Pratt & Whitney Aircraft has considerable experience from other engine programs on fuel system components using hot fuel and hot ambient temperatures. This experience is summarized in the following tabulation for the components being used in the JTP17A-20 experimental engine program.

Item	Total Engine Time, hr	Total Bench Time, hr	Hot Time, hr	Total Time, hr
Gas Generator Fuel Pump	18,200	32,700	6000	50,900
Duct Heater Fuel Pump	17,000	17,800	6700	35,400
Gas Generator Control	9,100	51,800	5100	60,900
Duct Heater Control (HBD)	17,600	54,400	9300	72,000
Duct Heater Control (BK)	5,000	15,700	400	20,700
Duct Pump Controller	17,600	54,400	9300	72,000
Hydraulic Pump	16,700	13,500	8300	30,200
Duct Nozzle Control	7,200	13,700	3800	22,900

The hot time tabulated includes (1) fuel inlet temperatures of 200°F and above, and/or (2) ambient temperatures of 400°F and above, (3) fuel temperatures up to 450°F, and (4) ambient temperatures up to 670°F. Except for the Bendix duct heater control testing, which was with aviation jet fuel, PWA 523 fuel was used in this testing. The PWA 523 fuel testing included 25,000 hours of testing with hot fuel which

includes 3300 hours of testing at greater than 200°F fuel inlet temperature; PWA 523 neat fuel has less lubricity than the PWA 533 aviation jet fuel.

The JTF17A-20 initial experimental engines in the Phase II-C program are being operated with existing developed components from other engine programs with minimum modification to expedite the development program. The various components selected provide flexibility in the mode of controlling the engine to aid in evaluating the control system concept being proposed.

## 2. Prototype JTF17A-20 Engine Control Systems

### a. Design Programs

Both control vendors have delivered a unitized fuel control mockup that incorporates a concept for rapid replacement of the control on the engine.

Environmental testing of the Hamilton Standard quick-disconnect seal plate concept has continued. To date, 100 hours of simulated SST environmental testing have been completed on parts that have aluminum bases incorporating steel rings for attachment integrity.

The unitized fuel control schematics are being updated to reflect the experience gained from the initial experimental engine tests.

### b. PIOC Computer Studies of JTF17A-20 Control System

As the result of the smooth duct heater ignition on the initial JTF17A-20 experimental engine tests, computer studies of the control system were conducted in an effort to reduce the time required to increase engine thrust from various levels to maximum augmentation. These studies resulted in the following control system configuration changes.

1. Duct heater authorization permission signal occurs at 80% high rotor speed.
2. Duct heater ignition is energized at the initiation of fast filling the Zone 1 manifold.



3. Duct fuel flow is maintained at the desired lightoff level for ignition purposes for approximately 1/4 second.
4. Zone II manifold filling is initiated whenever power lever position requests Zone II operation and Zone I fuel flow level is above lightoff flow.
5. Transfer from one-zone operation to two-zone operation occurs when Zone II manifold is full.

c. PRDC Computer Studies of HSD Control System

Computer studies of the HSD control system indicate that the above described control system changes result in an acceptable configuration for the conditions investigated, which are shown in figures III-II-6 through III-II-10. Figure III-II-6 shows that approximately 7.5 seconds are required from idle to maximum thrust at sea level conditions. Acceleration from a part-power condition representing approach power to maximum augmentation requires approximately 3 seconds at sea level conditions, as shown in figure III-II-7. A transient from maximum nonaugmented power to maximum augmentation at sea level conditions requires approximately 2.3 seconds, as shown in figure III-II-8. At cruise conditions, (Mach 2.7, 65,000 feet) approximately 3.5 seconds are required for the transient from idle to maximum augmentation, and 3.2 seconds from maximum nonaugmented power to maximum augmentation, as shown in figures III-II-9 and III-II-10, respectively. The similarity of the two transient times is primarily due to the fact that high rotor speed is within 100 rpm of duct heater authorization speed when operating at cruise idle conditions. As a result, duct heater initiation occurs within the first 0.3 second of the transient.

d. PRDC Analog Studies of Bendix Control System

The Bendix control system configuration has been revised in the same manner as the HSD system and investigated at engine cruise conditions. A transient from maximum nonaugmented power to maximum duct heat requires approximately 3.2 seconds, as shown in figure III-II-11. Figure III-II-12 shows the response of the engine to several types of power lever modulation in the augmentation range at cruise conditions. These data show

the variation in time during which total flow is held constant while the Zone II manifold is filled. The same response is expected from the HSD control system for these random power lever modulations.

e. Unitized Fuel System Pump

Preliminary requirements for the alternative unitized pump have been delivered to CECO, PESCO, TRW, AND HSD. CECO has advised that a preliminary proposal and layout will be delivered to PRDC early in May.

f. Review of Commercial Turbine Engine Control and Accessory Problems

A JTF17A-20 engine Controls Engineer visited the EAL Component Overhaul Facility at Miami, and the UAL Component Overhaul Facility at San Francisco, California, and attended the Turbine Engine Control and Accessory Maintenance Conference to review problems associated with current commercial engine controls and accessories. The 3-day Maintenance Conference was held at HSD and was attended by representatives of 15 domestic airlines, 19 overseas airlines, 3 overhaul corporations, SNECMA, United Aircraft Canada Ltd., United Aircraft International, P&WA, and HSD.

3. Advanced Control System Programs (Related Technology)

Installation coordination for the prototype hydraulic computer control for the J58 engine has been completed. Fabrication of plumbing and brackets for the J58 engine installation is approximately 90% complete, and the remaining parts are scheduled for delivery by mid May. Testing at HSD is continuing on schedule, with 1 June 1966 scheduled for control delivery.

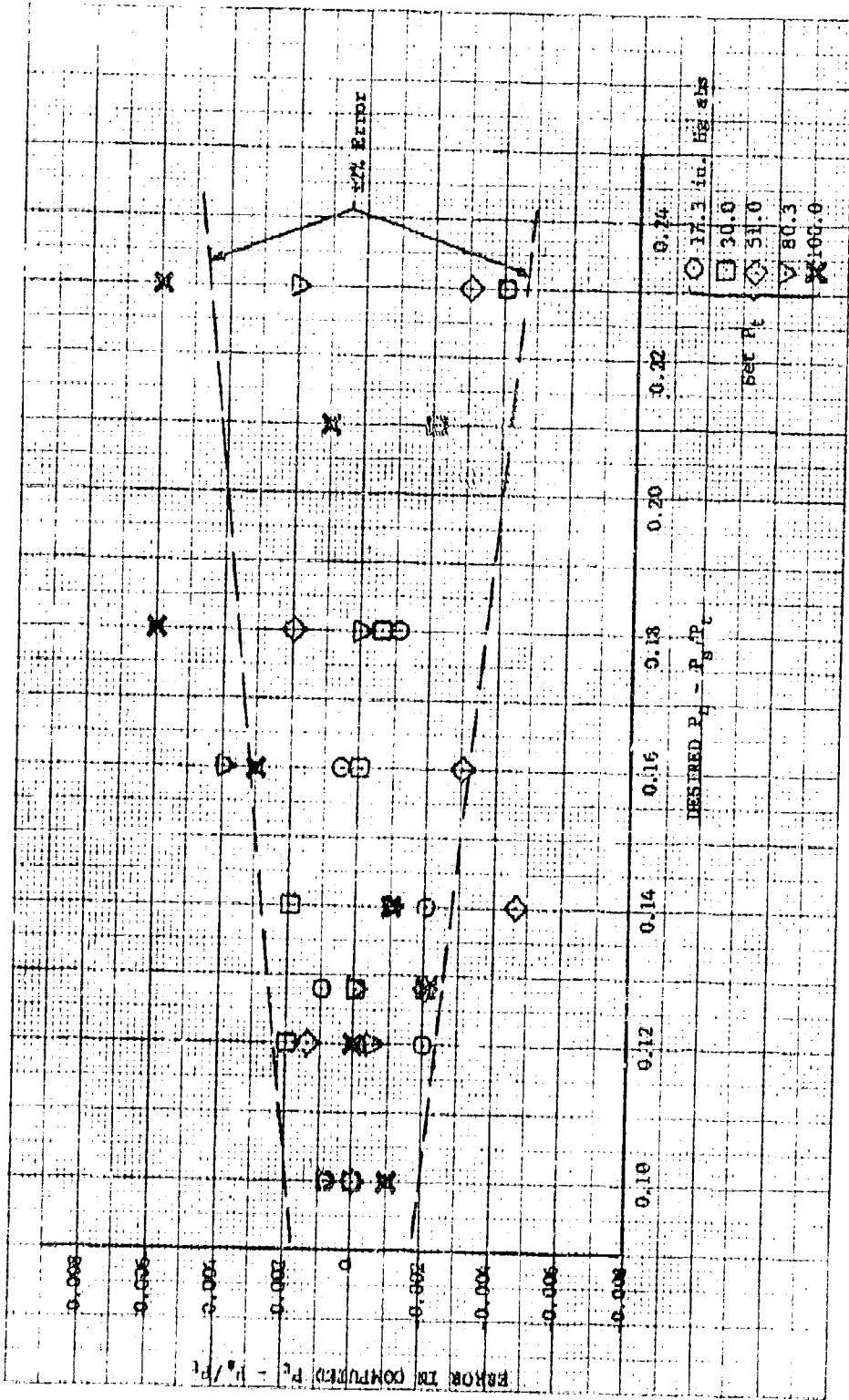


Figure III-H-1. HSD Nozzle Control Calibration Error in Computed  $(P_t - P_s)/P_t$  vs Desired  $(P_t - P_s)/P_t$  DF 47320

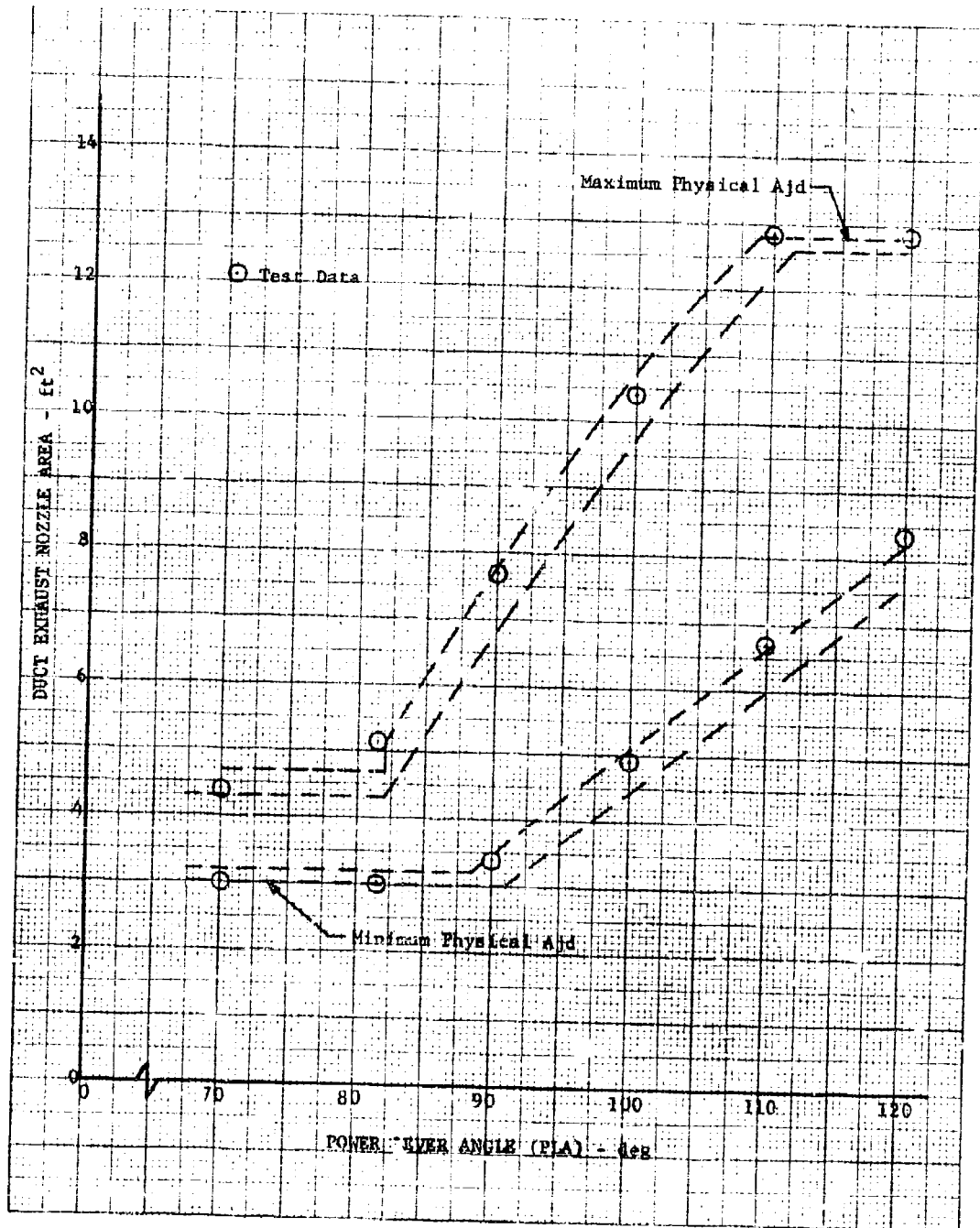


Figure III-H-2. S/N D07C002, AA-M1 Duct Fuel and Nozzle Control Calibration Duct Exhaust Nozzle Control Authority

DF 47321

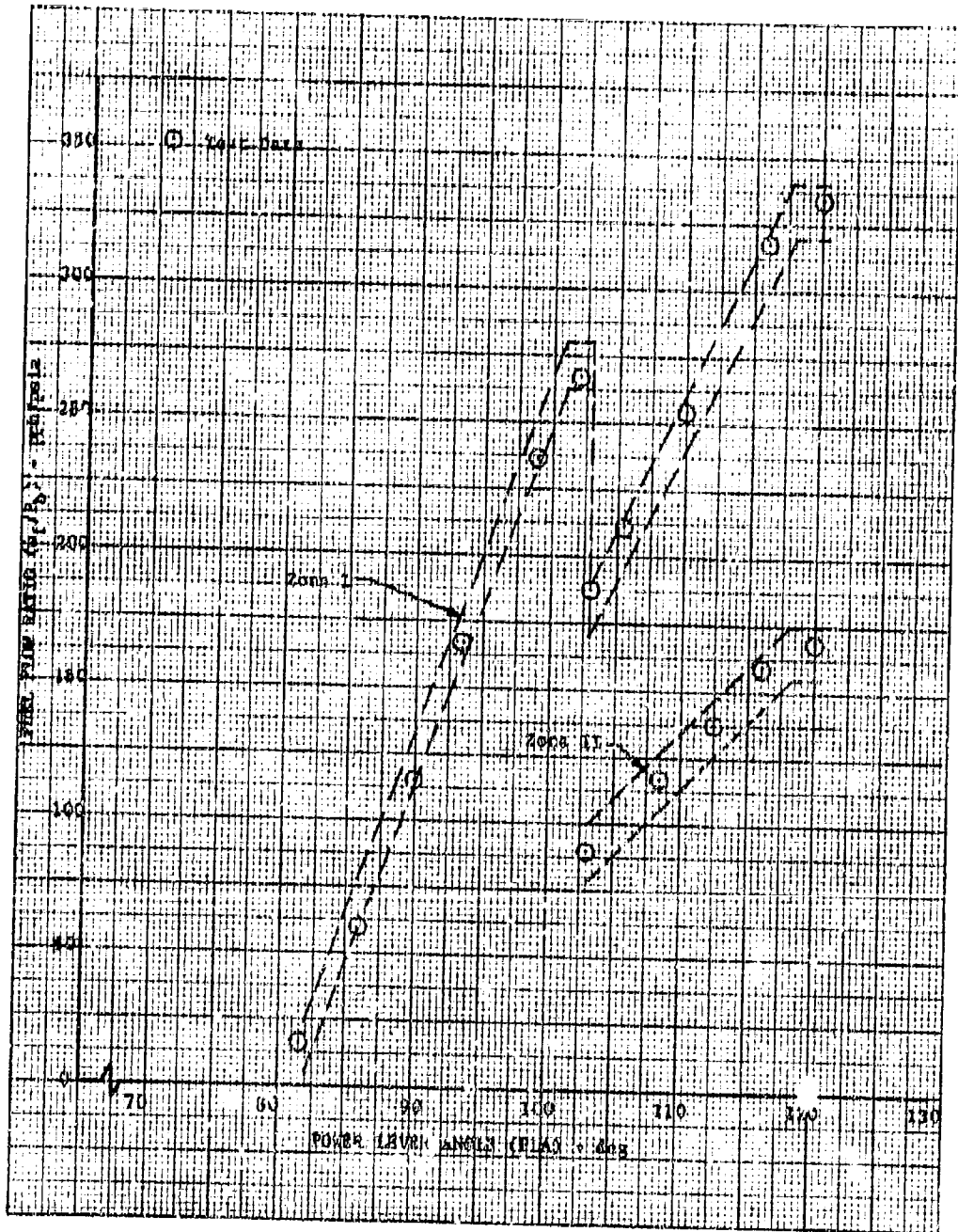


Figure III-H-3. S/N D07C002, AA-M1 Duct Fuel and Nozzle Control Calibration Duct Heater Fuel Flow DF 47322

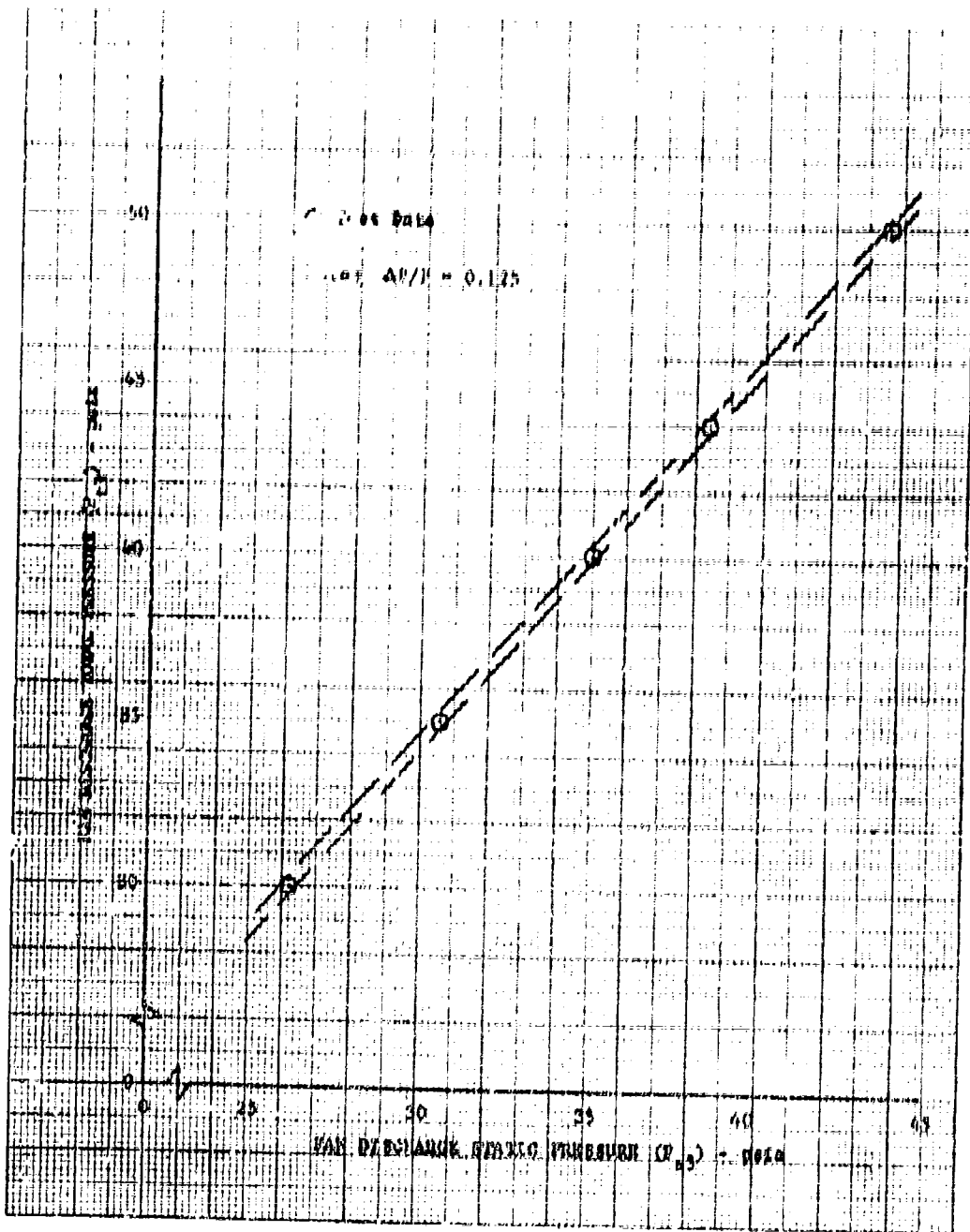


Figure III-H-4. S/N D07C002, AA-M1 Duct Fuel and Nozzle Control Calibration  $\Delta P/P$  Computer Schedule

WP 47323

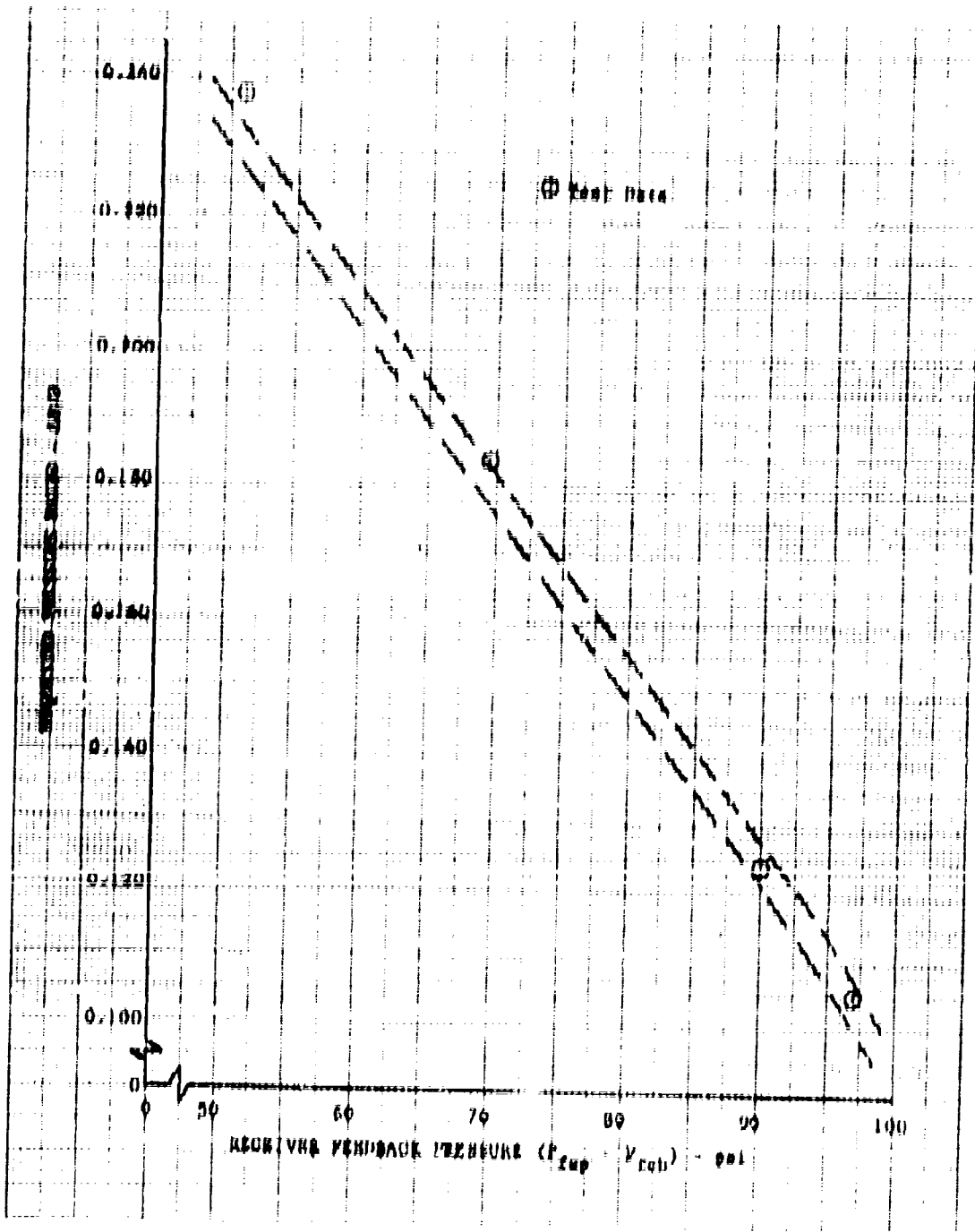


Figure III-II-5. S/N D07C002, AA-M1 Duct Fuel and Nozzle Control Calibration Pressure Ratio Schedule

DP 47324

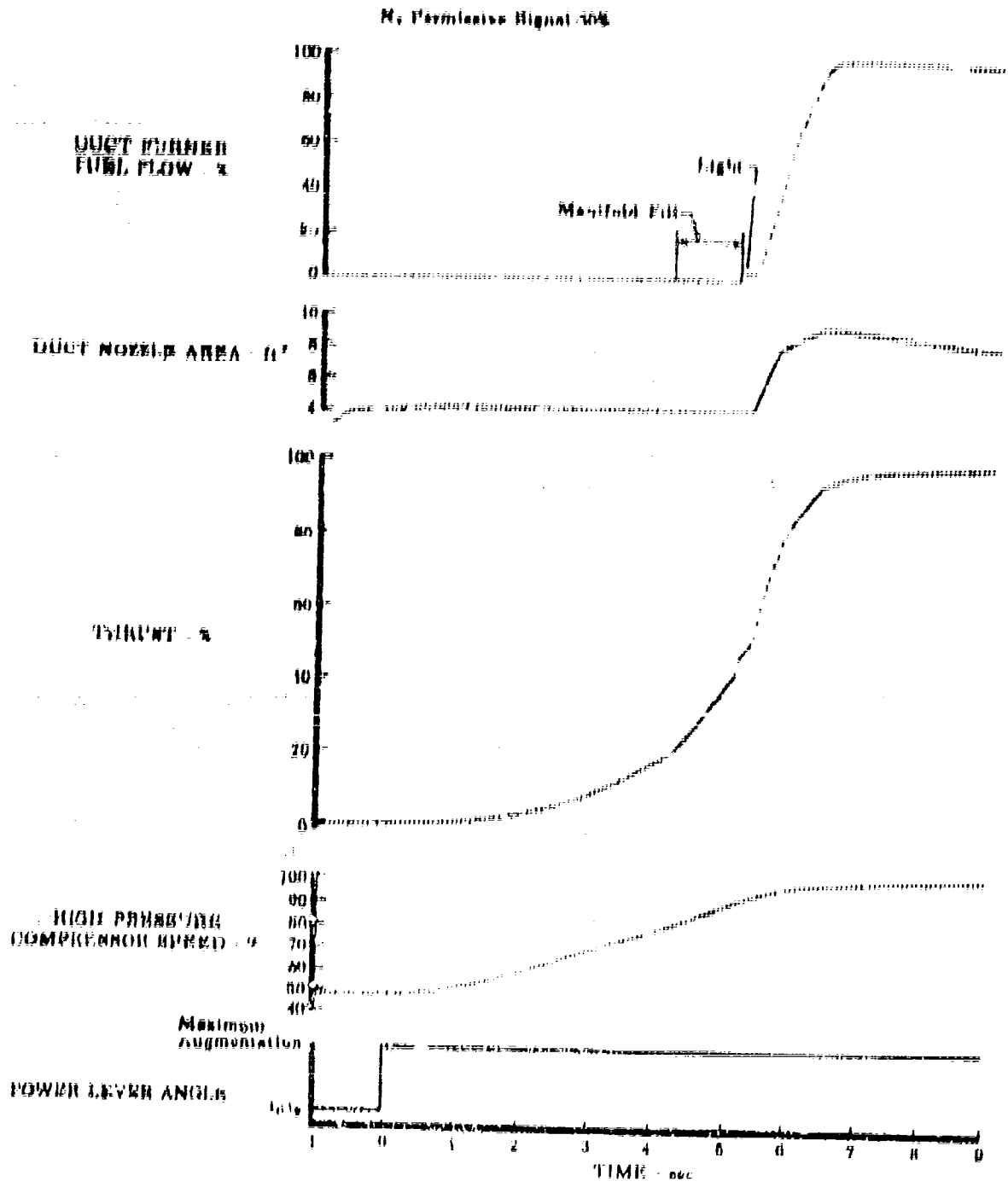


Figure 111-H-6. JTF17A-20 Response to PLA Modulation From FD 15623 Idle to Maximum Augmentation at Sea Level Conditions



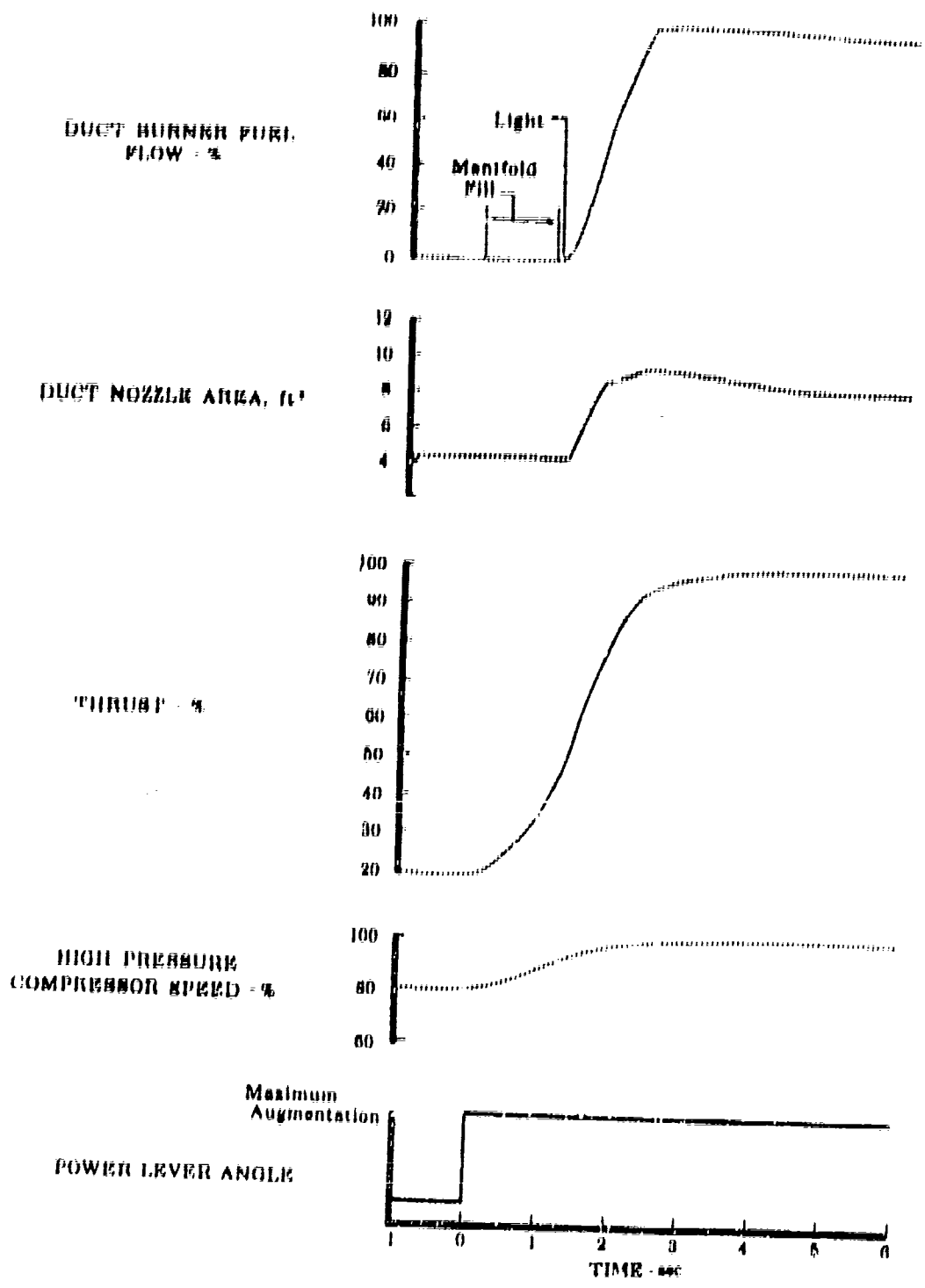


Figure III-H-7. JTF17A-20 Response to PLA Modulation from Part Power to Maximum Augmentation at Sea Level Conditions VD 15625

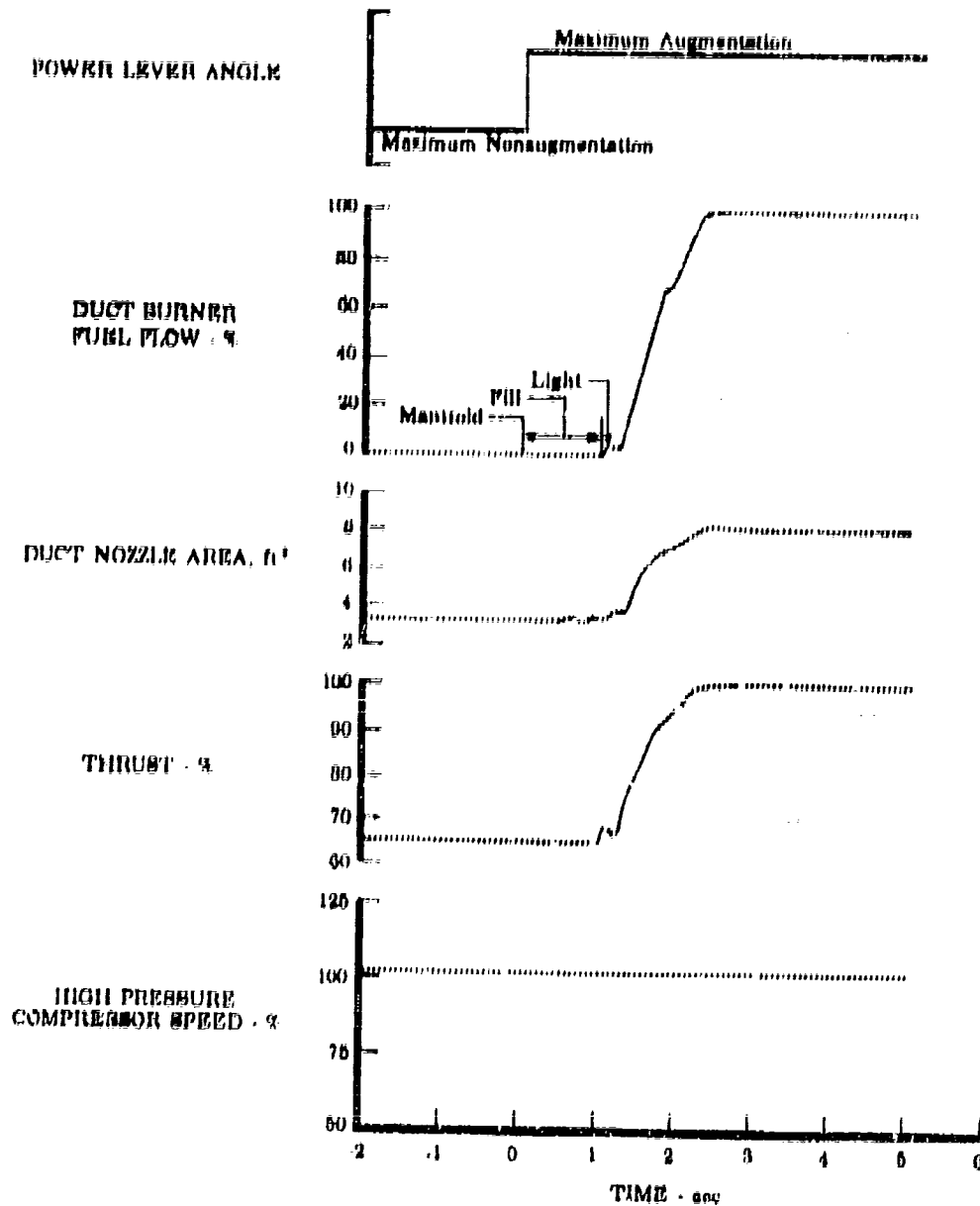


Figure III-H-8. JTF17A-20 Response to PLA Modulation from FD 15627  
 Maximum Nonaugmented to Maximum Augmentation  
 at Sea Level Conditions

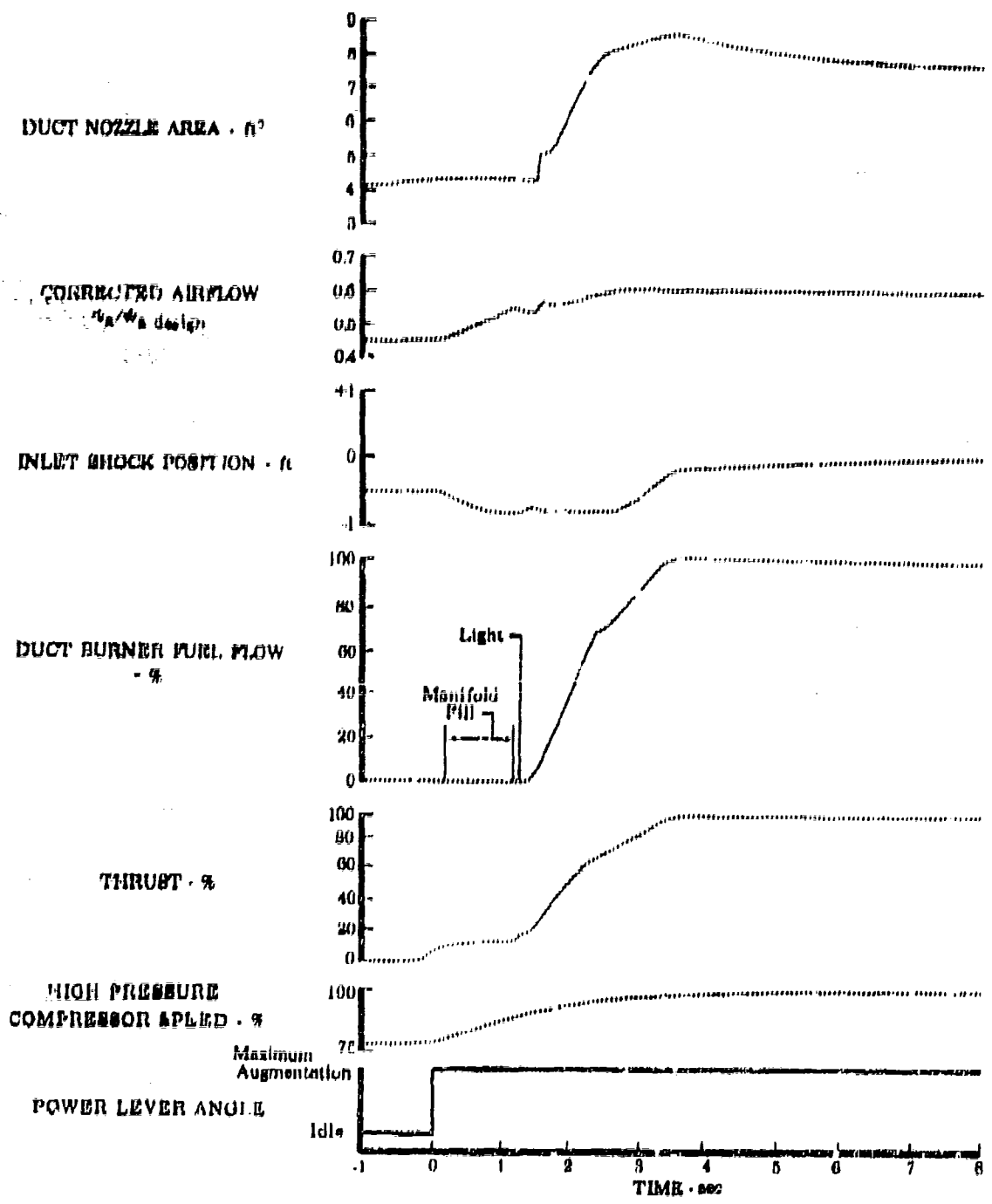


Figure III-H-9. JTF17A-20 Response to PLA Modulation from Idle to Maximum Augmentation at Cruise Conditions PD 15624

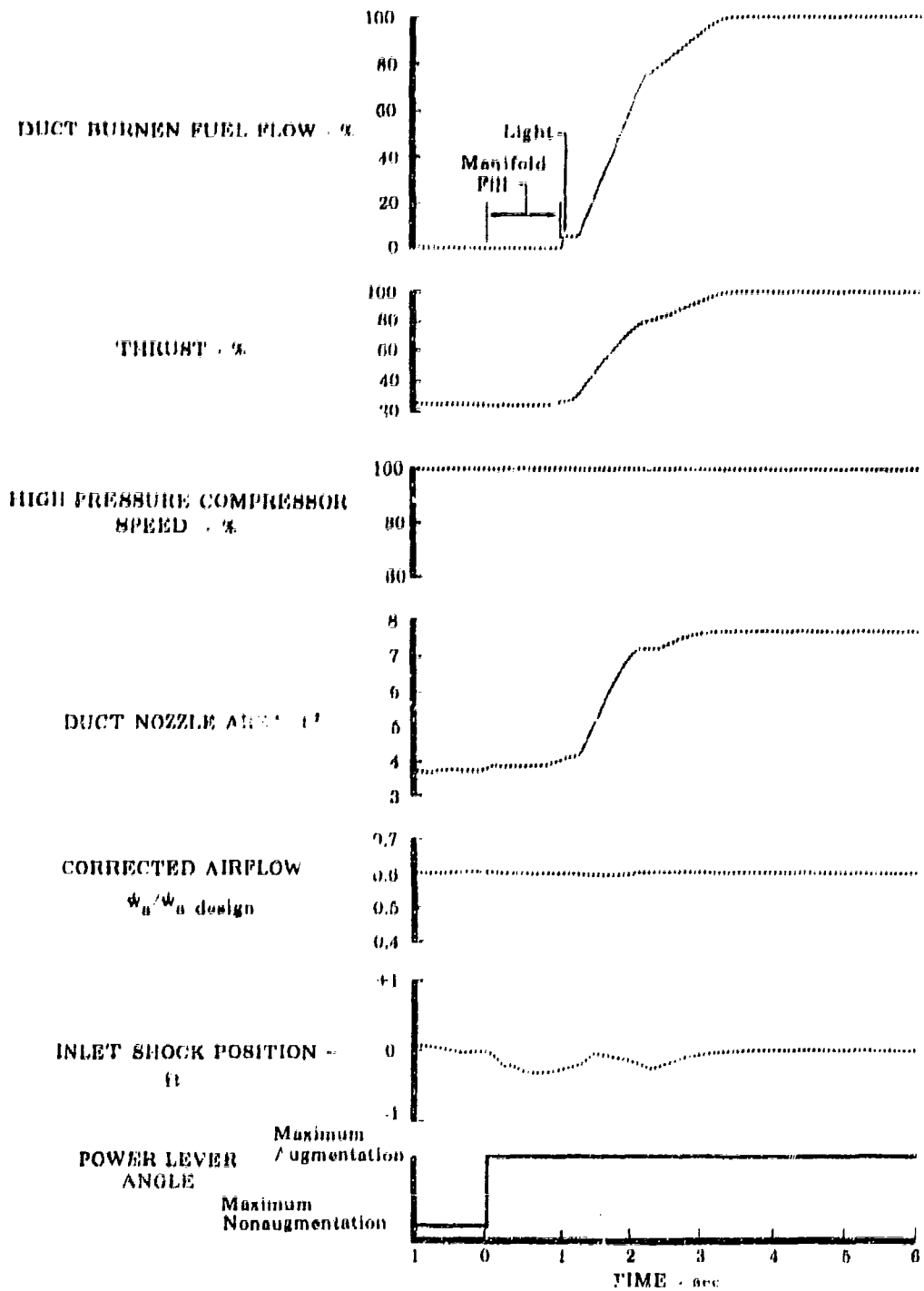


Figure III-H-10. JTF17A-20 Response to PLA Modulation from FD 15626  
Maximum Nonaugmented to Maximum Augmentation  
at Cruise Conditions

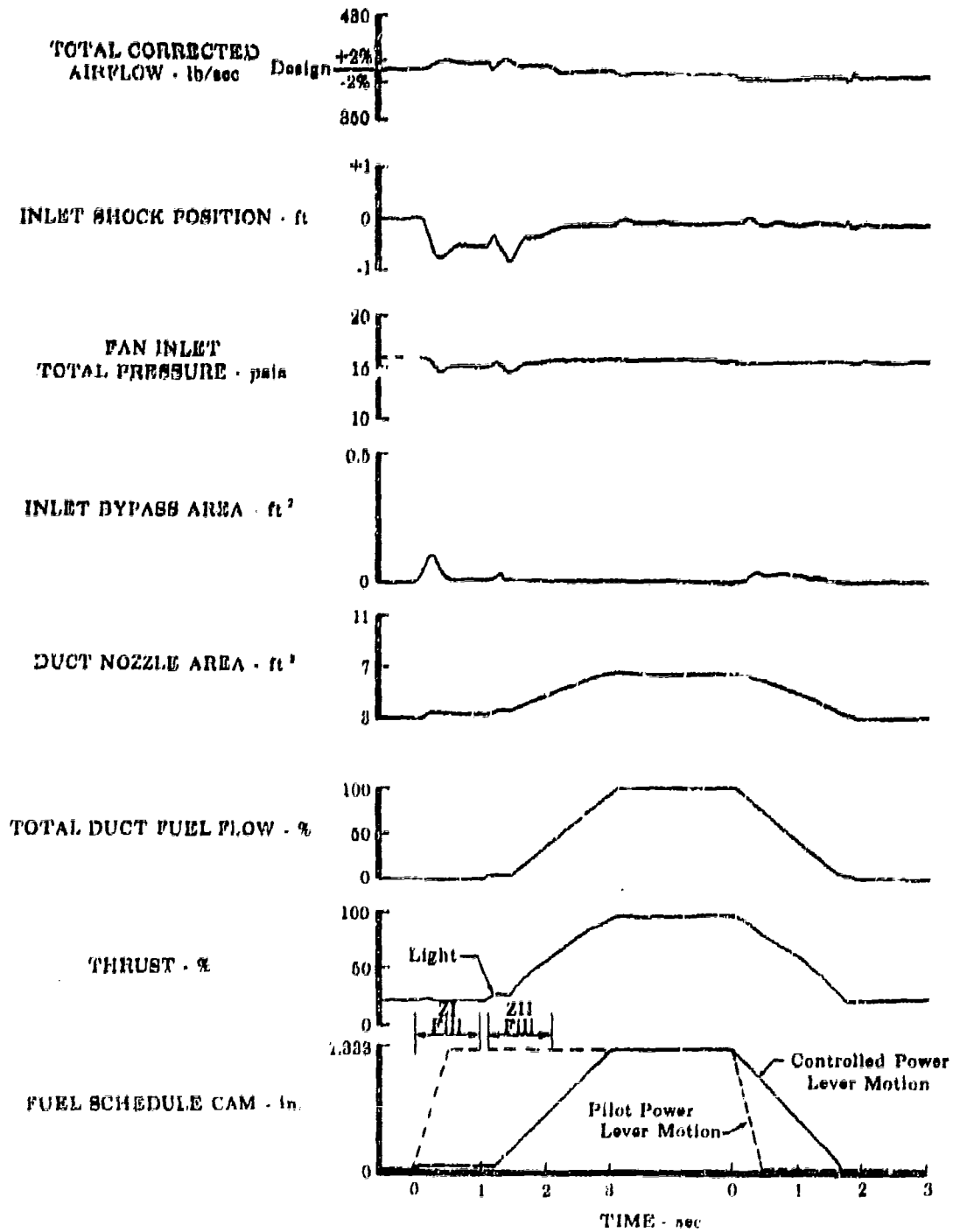


Figure III-H-11. JTF17A-20 Response to PLA Modulation from FD 15628  
Maximum Nonaugmented to Maximum Augmentation  
to Maximum Nonaugmented at Cruise Conditions

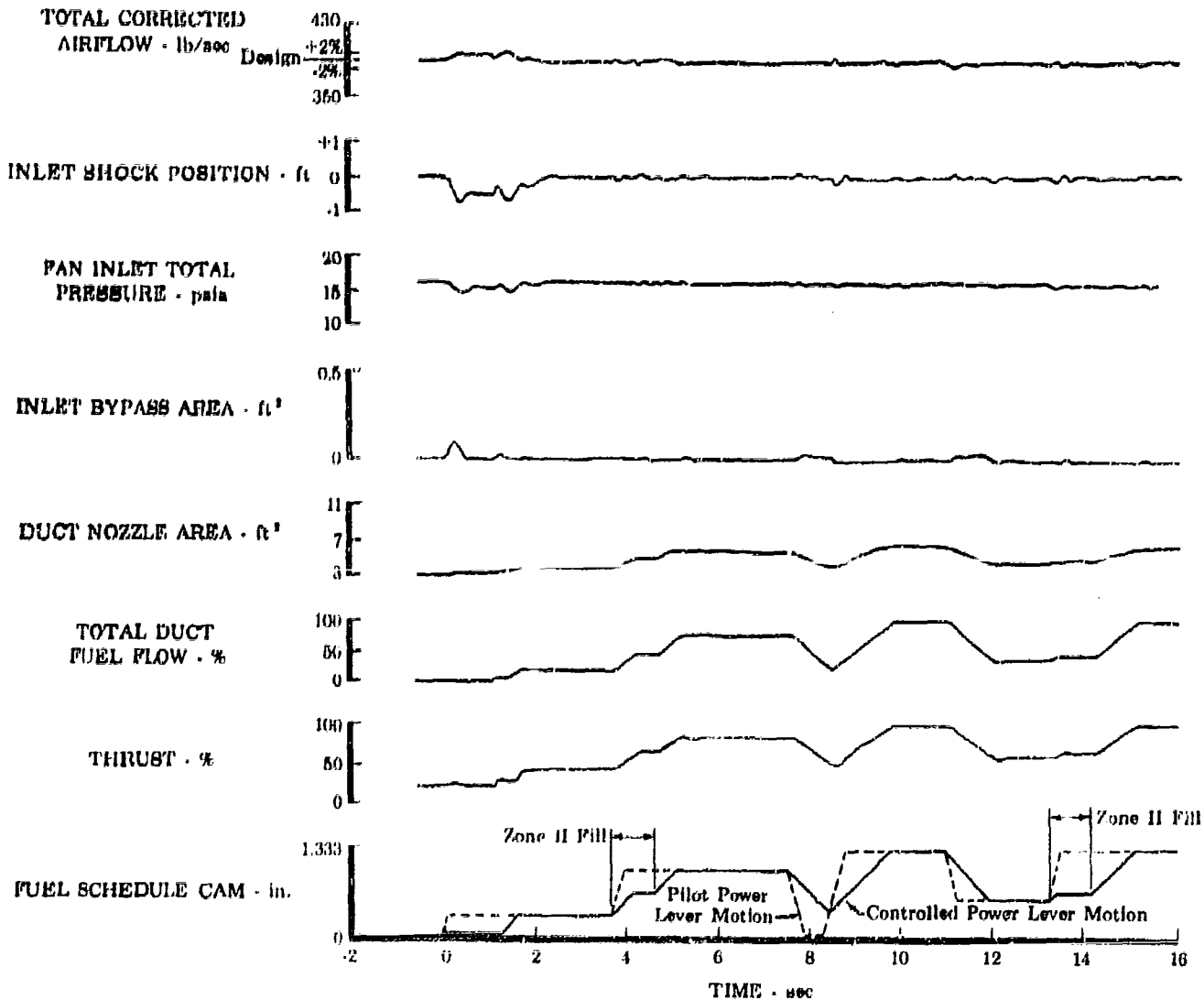


Figure III-H-12. JTF17A-20 Response to Random Power Lever Motion in the Augmentation Region at Cruise Conditions Including Duct Heater Ignition

FD 15629

## I. BEARINGS AND SEALS

The assembly and initial testing of the JTF17A-20 No. 1 and 2 compartment seal rig was completed during this report period. The primary purpose of this functional testing was to determine the compatibility of the compartment parts and to obtain compartment pressures and temperatures at test conditions duplicating the sea level operation on FX-161 engine. Figures III-I-1 through III-I-7 show the No. 1 and 2 compartment rig parts in various stages of assembly. A total of 11.61 hours of rig testing was completed. This testing was accomplished with complete compartment instrumentation and has demonstrated acceptable operation of the rig and engine compartment parts. Disassembly of the rig for inspection was in process at the end of the report period.

The JTF17A-20 No. 4 compartment seal rig was disassembled and inspected after completing 30.93 hours of room temperature and heated environment testing at rotor speeds up to 5800 rpm and simulated discharge pressurizing air temperatures up to 750°F. The disassembly inspection showed the rig engine parts to be in good condition as shown in figures III-I-8 through III-I-13. Oil leakage past the carbon seals and compartment front seal plate was noted and corrective action taken to eliminate possible leakage during engine testing. The oil leakage was primarily caused by inadequate scavenging of the seal liner cooling oil past the bearing support. To eliminate this condition, the flow passage area into the bearing support has been increased 300%. Static flow test of the compartment has demonstrated that the additional flow area is sufficient to properly scavenge the oil. Oil weepage was noted past the compartment front seal plate. The cause of this weepage is believed to have been a cocked labyrinth seal and loose stackup although there was no evidence of race turning. To eliminate future occurrence, a hydraulic tool has been made to seat the bearing and seal stackup during assembly. Rubbing of the inner labyrinth seal was also noted on its mating land. This wear, which is on the entire circumference, also indicates that the labyrinth seal was cocked in the stackup. All other parts showed little or no wear and no evidence of carbon deposits. The conclusion drawn from the No. 4 compartment rig test is that the engine parts and the design of the compartment pressurizing and vent system will function as intended for JTF17A-20 engine operation at both sea level static and Mach 2.7, 65,000 feet cruise conditions.

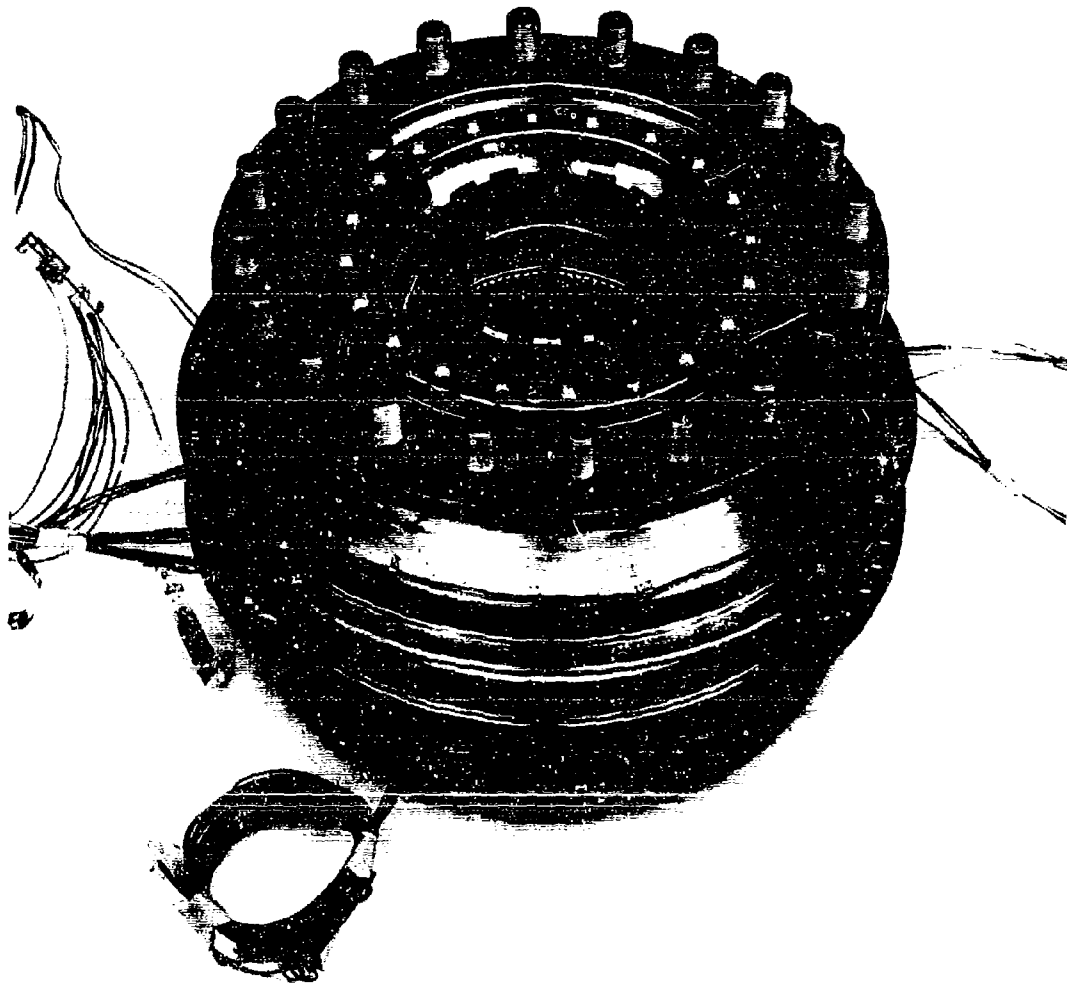


Figure III-I-1. No. 1 Hub and Support Assembly  
with Bearing and Seal  
(Front Side)

III-I-2

FE 57154



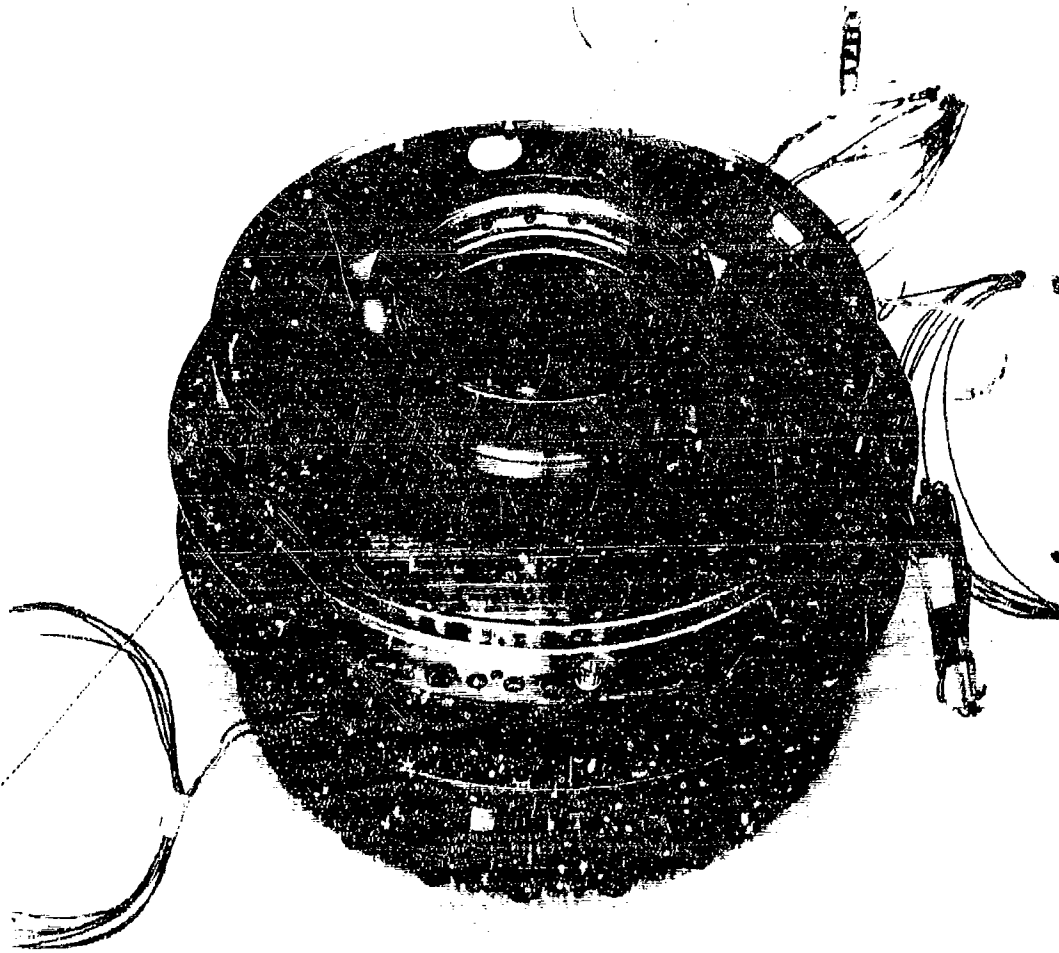


Figure III-1-2. No. 1 Hub and Support Assembly  
with Bearing and Seal  
(Rear View)

FE 5/152

III-1-3

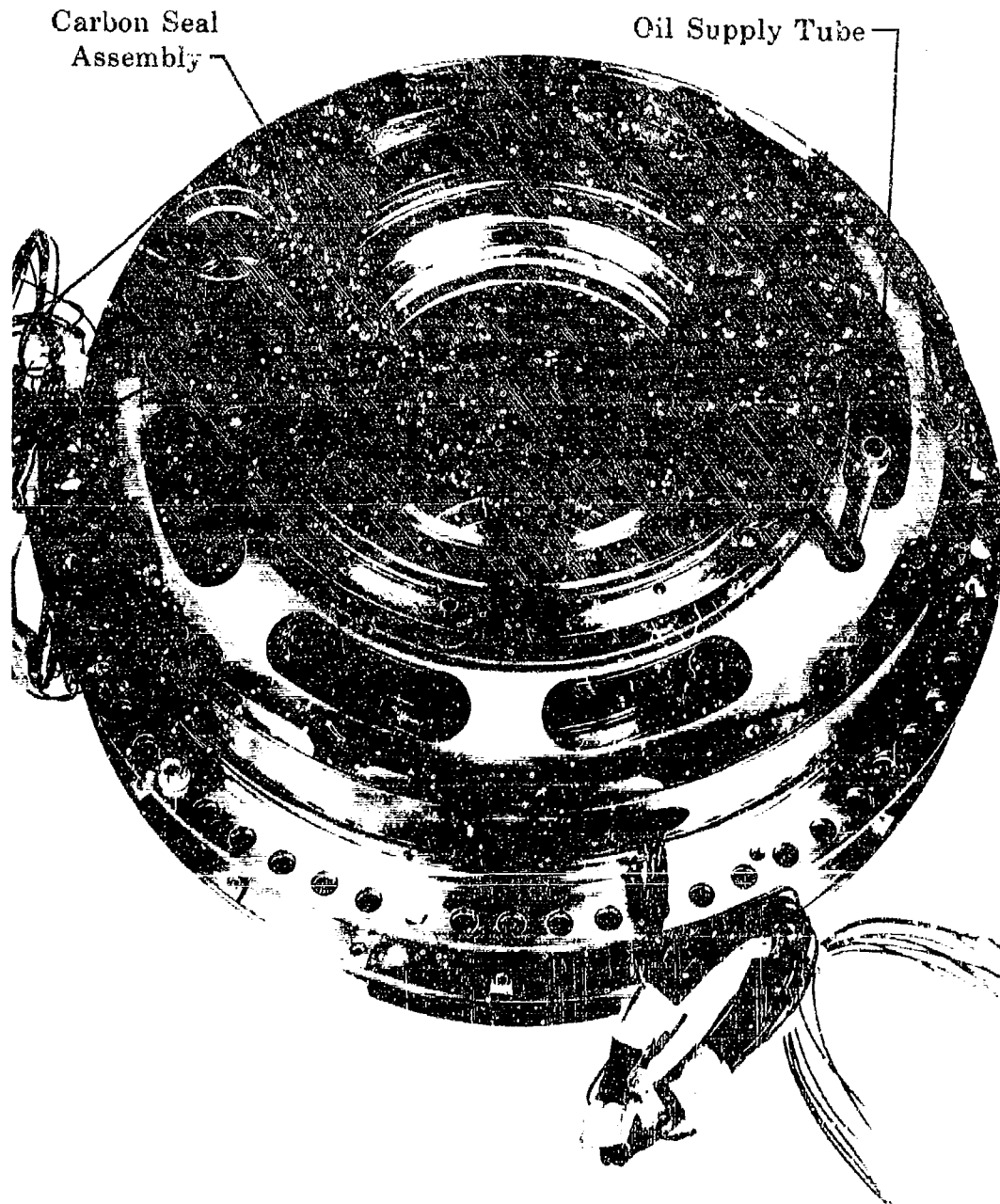


Figure III-I-3, No. 1 Hub and Support, Rear View  
with Middle Seal Assembly

FD 15612

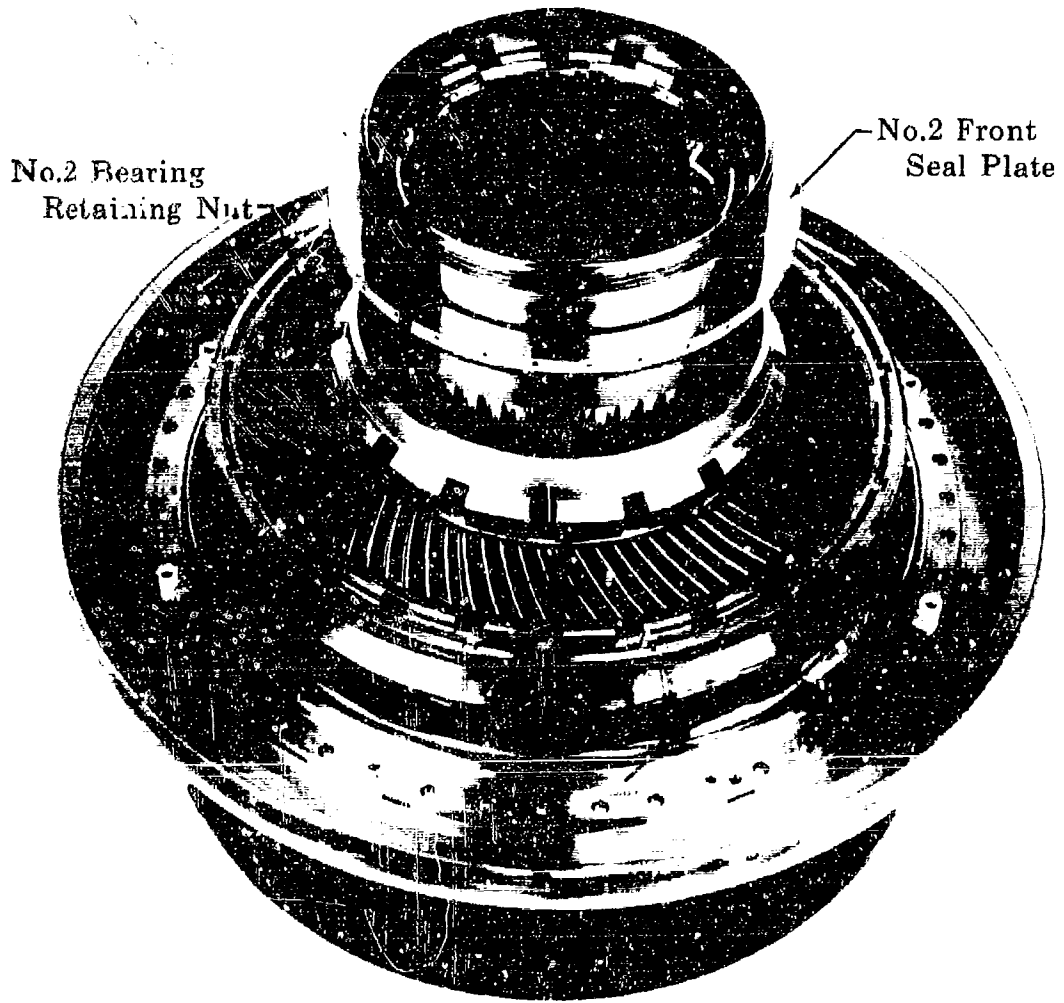


Figure III-I-4. No. 2 Hub, Seal, Bearing and Shaft Assembly

FD 15613



Figure III-I-5. No. 1 and 2 Seal Rig - Two-Speed Drive Gearbox Attached to Main Rig FE 57153

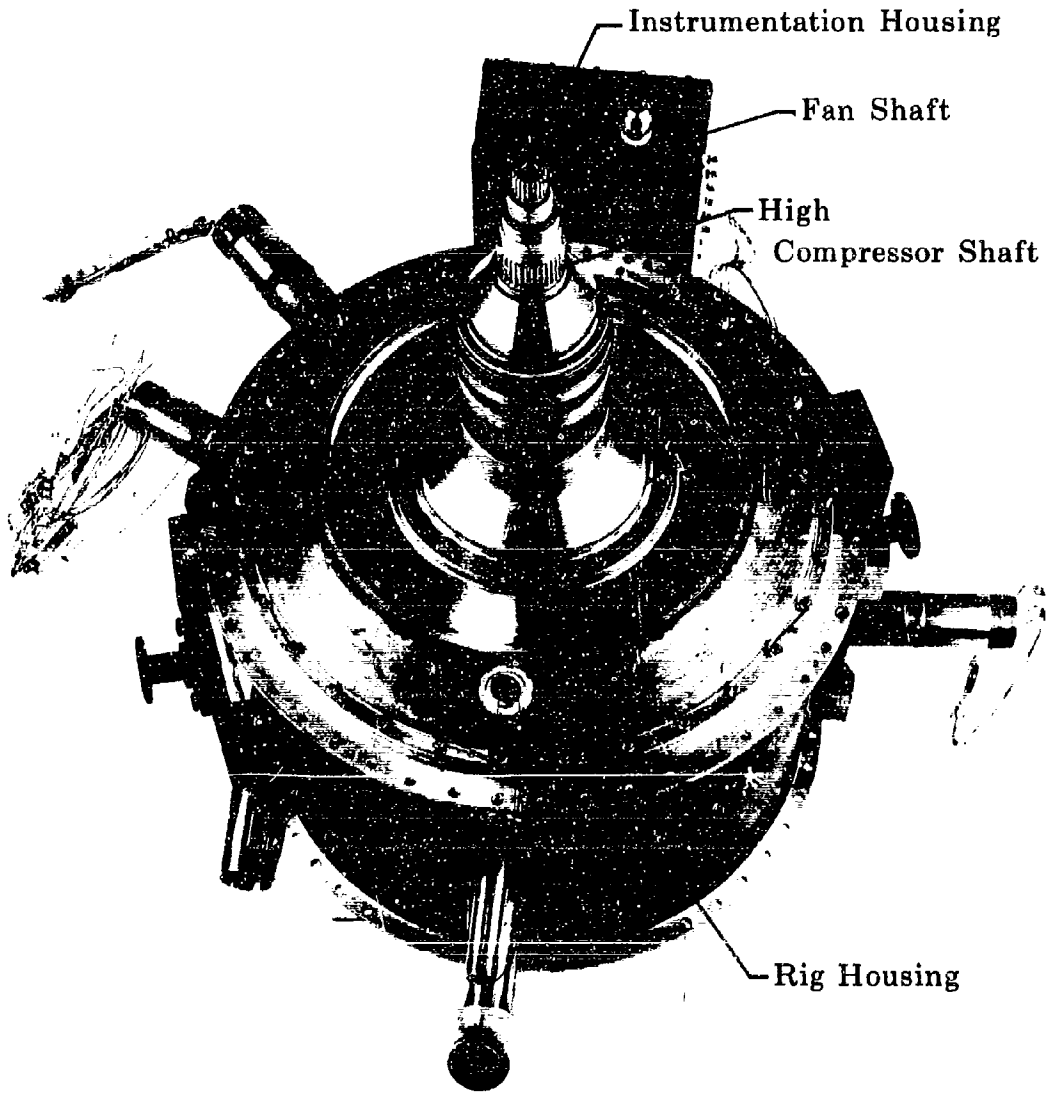


Figure 111-1-6. No. 1 and 2 Seal Rig, Rear  
Side - Inboard Cover Off

FD 15641

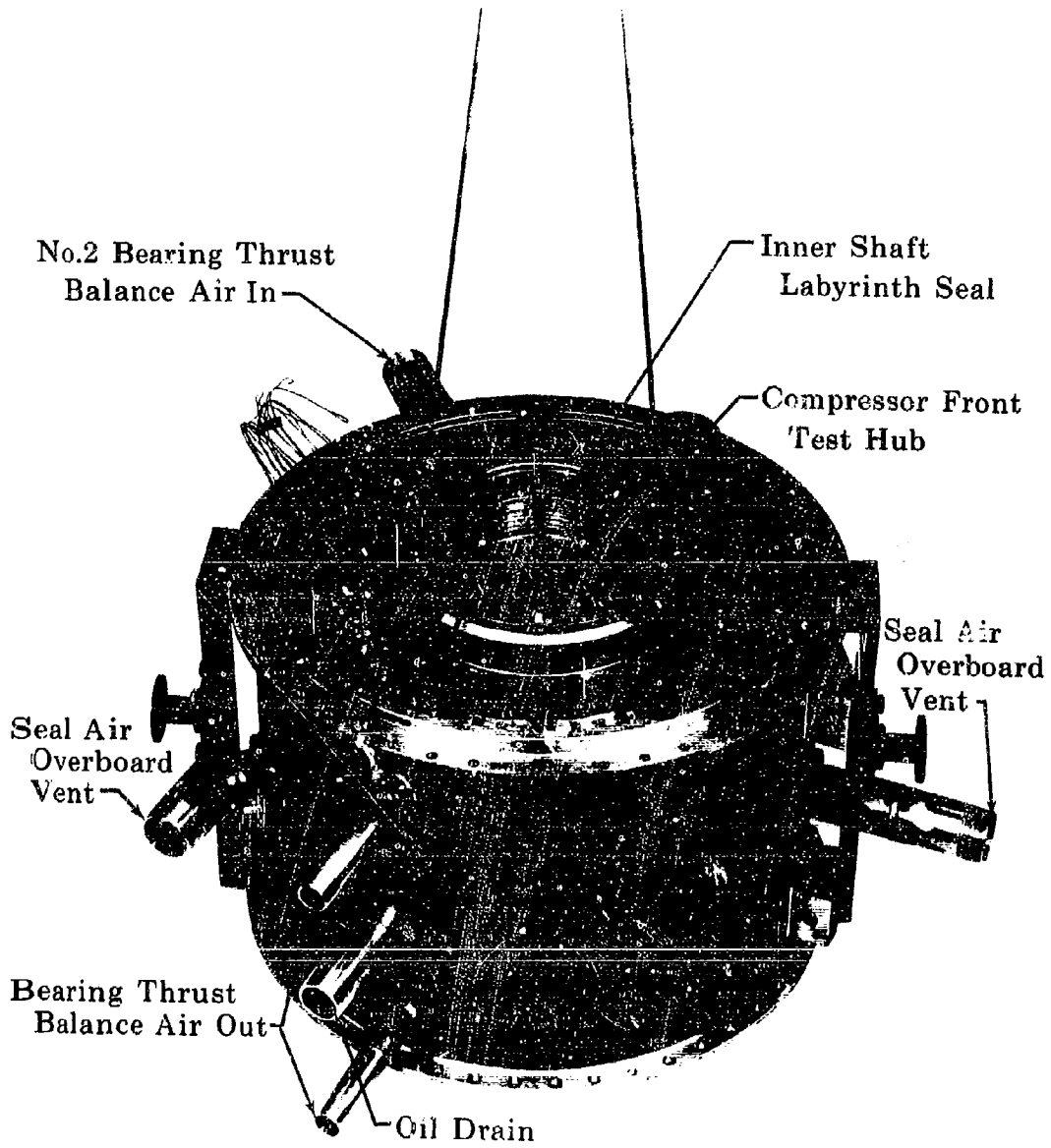


Figure III-1-7. No. 1 and 2 Seal Rig, No. 2 Hub and Support Assembly Installed in Rig Housing.

FD 15611

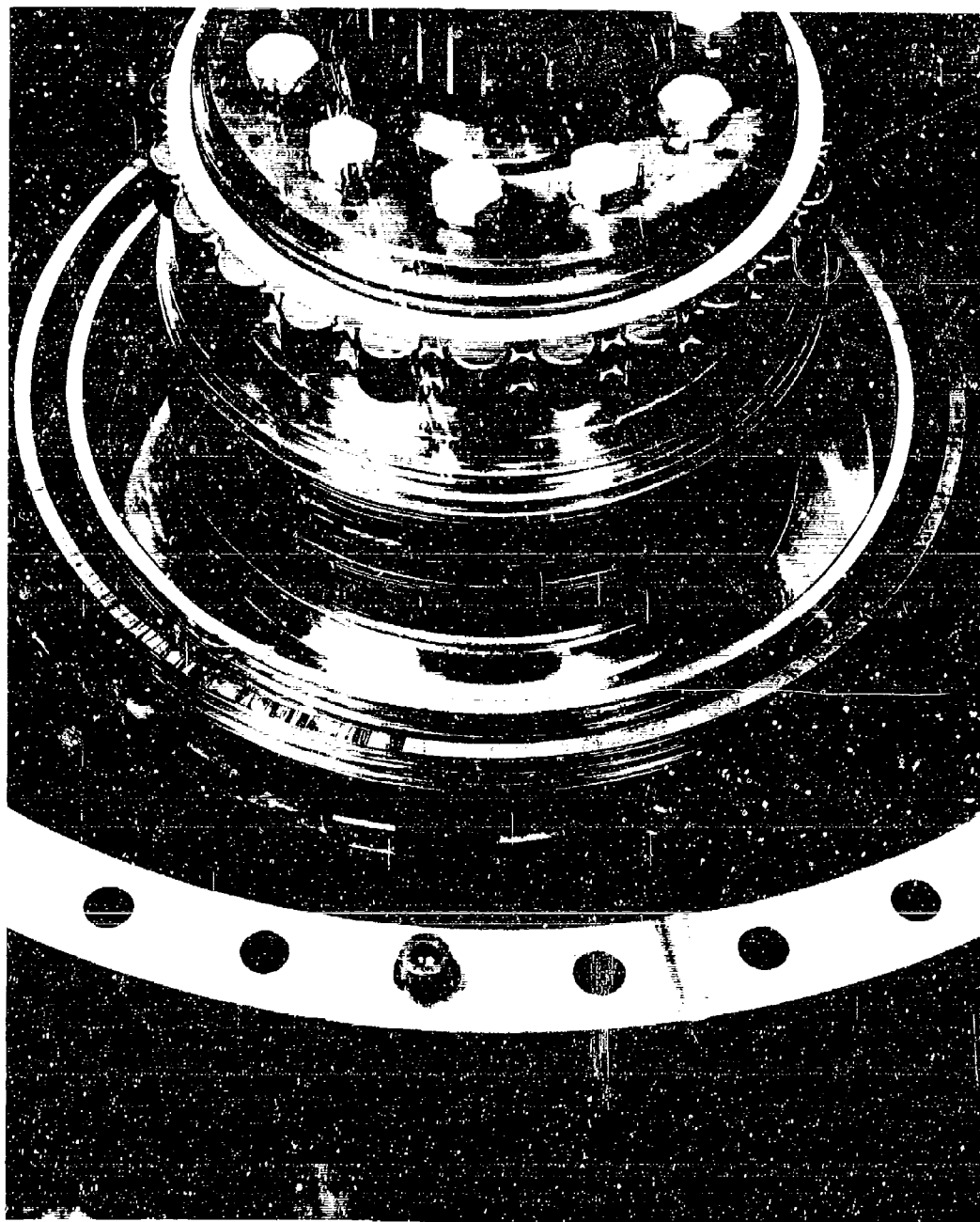


Figure T11-1-8. JTF17A-20 No. 4 Compartment Shaft FE 57094  
after Rig Test Showing Condition of  
Bearing, Carbon Seats and Labyrinth  
Seals



Figure III-I-9. JTF17A-20 No. 4 Compartment  
Roller Bearing After Rig Test  
Showing Condition of Cage, Inner  
Race, and Rollers

FE 57018

III-I-10



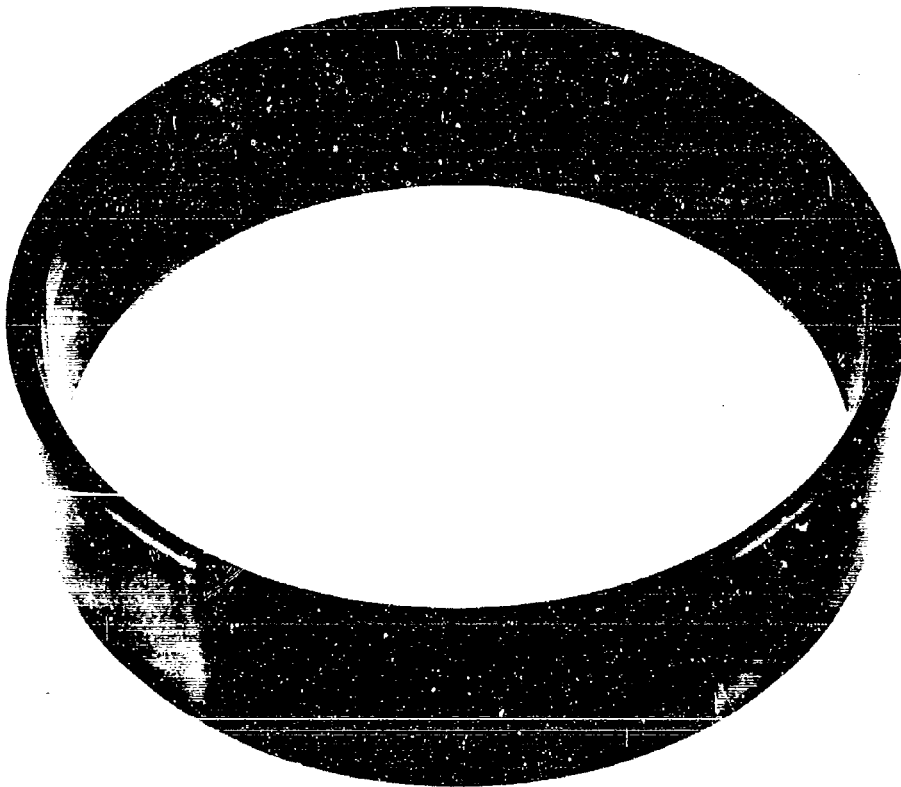


Figure III-I-10. JTF17A-20 No. 4 Compartment  
Roller Bearing Outer Race  
After Rig Test Showing Condition  
of the Race

FE 57019

III-I-11

FE 57095

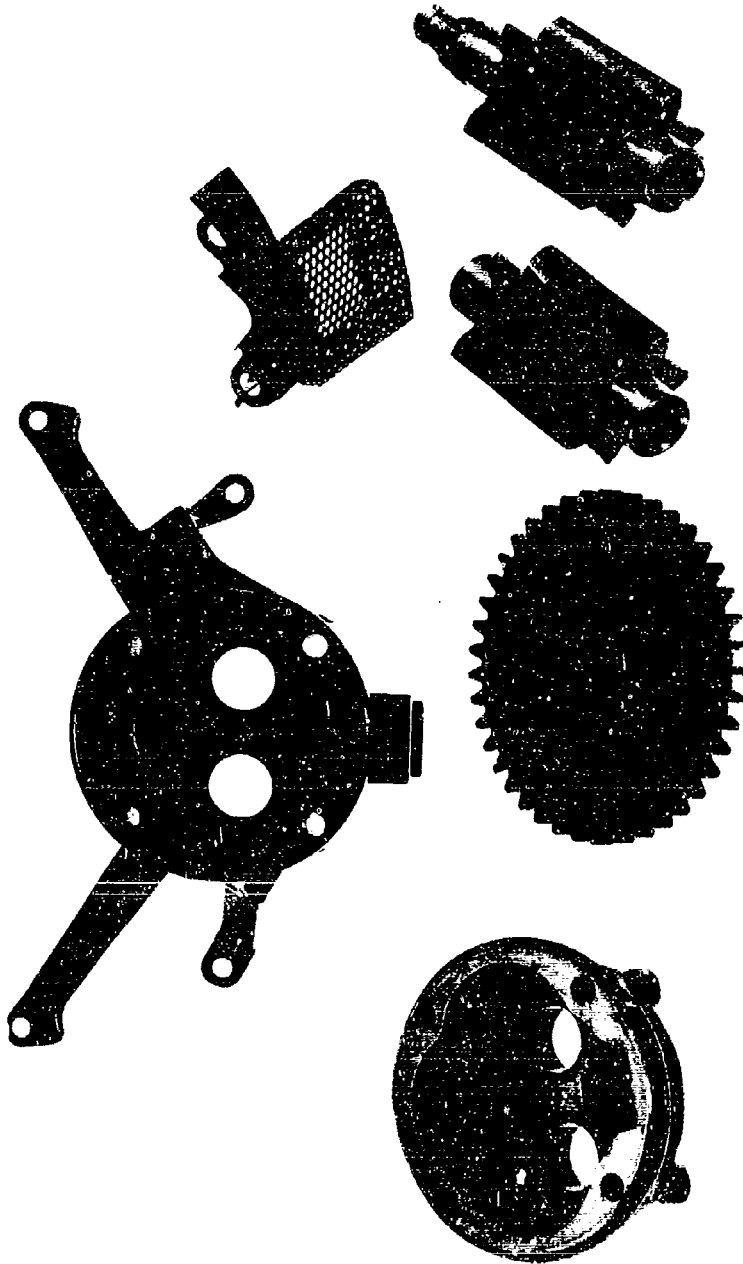


Figure III-I-11. JTF17A-20 No. 4 Compartment Scavenge Pump After Rig Test Showing Condition of the Scavenge Pump Gears and Housing

FE 57024

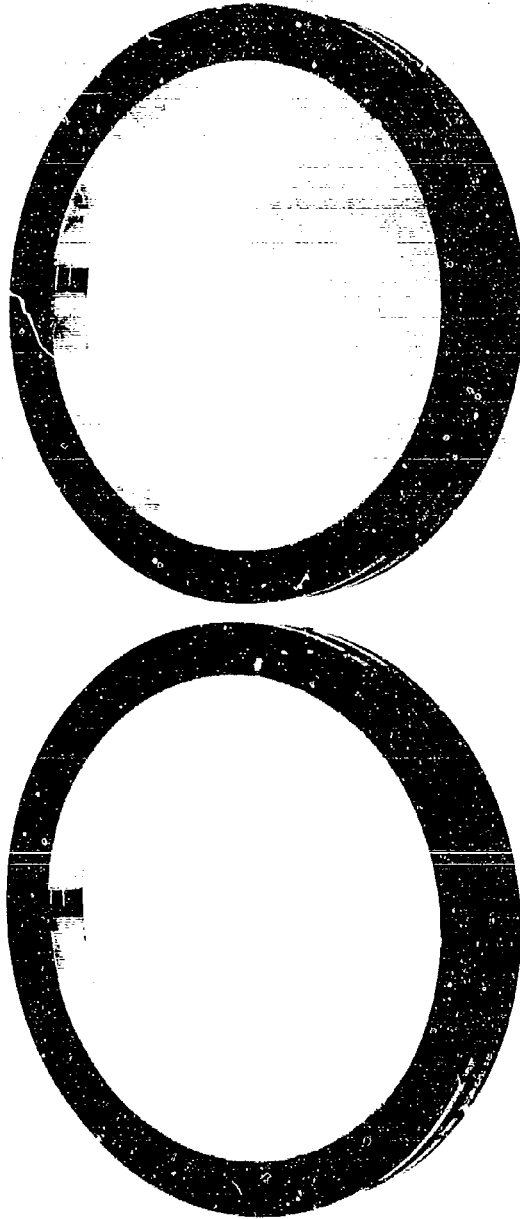


Figure III-I-12. JTF17A-20 No. 4 Compartment Carbon Seal Assemblies After Rig Test  
Showing Condition of the Carbons

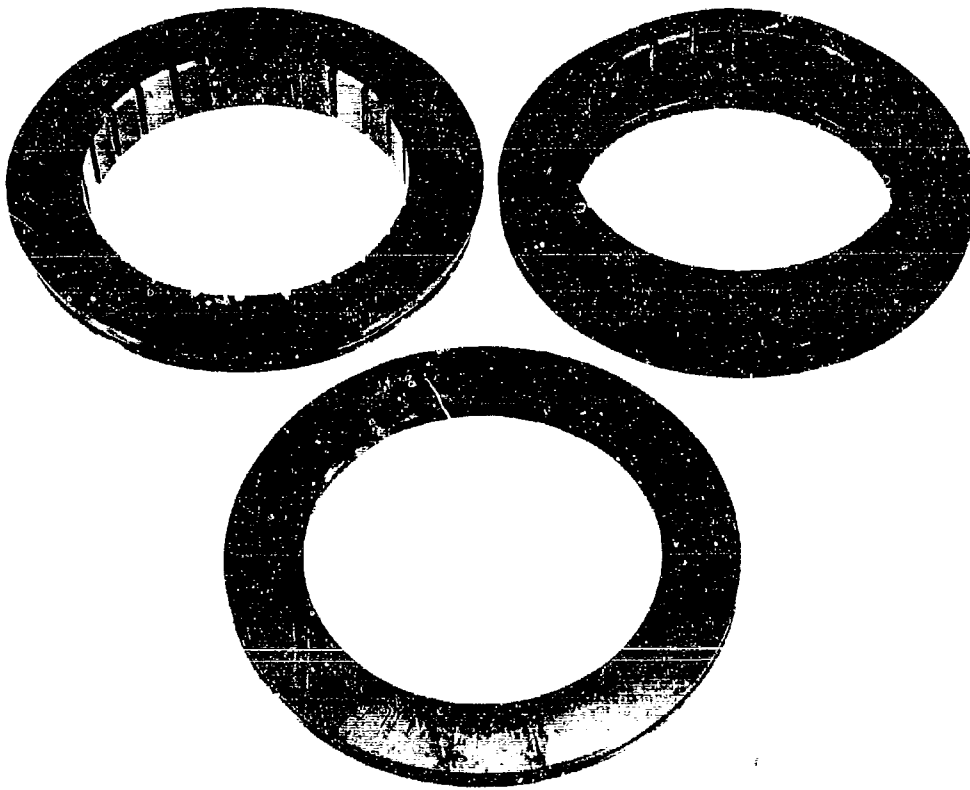


Figure III-I-13. JTFi7A-20 No. 4 Compartment Seal  
Plates After Rig Test Showing  
Condition of the Seal Plates

FE 57016

## J. FUELS AND LUBRICANTS

### 1. Fuels

Fuel coker tests have continued on aviation kerosene to confirm that the fuel is meeting the purchase specification requirements and to monitor its condition in storage. A series of coker tests have also established that the thermal stability breakpoint of the currently delivered fuel is 375°F/475°F. Another series of tests are now in process to establish the effect on thermal stability of releasing dissolved oxygen by exposing the fuel to a pressure of 1 psia.

Erosion and corrosion tests were continued with fuel that met the maximum sulfur allowable in the PWA 533 specification. This testing is discussed in paragraph III-B.

The fourth meeting of the SST Fuels Industry Advisory Committee was attended by project personnel on 20 and 21 April at FAA Headquarters in Washington, D.C. to present a progress review of the JTF17A-20 fuels activities. The material reviewed at this meeting is a summary of JTF17A-20 fuels activities to date and is presented in Appendix B of this report.

### 2. Lubricants

Laboratory tests were continued on candidate lubricants to determine conformance to specification requirements.

Oil samples were taken during the JTF17A-20 No. 4 compartment seal rig testing, as reported last month. During the 30.93 hours of testing with a maximum oil temperature of 385°F, the viscosity change of the Mobil Jet II test lubricant was 3.85% and the neutralization number change was 0.03. There was no evidence of oil coking on any of the compartment parts.

Oxidation-corrosion tendencies of the four candidate lubricants were determined in a series of tests using standard equipment and test procedures, except that more oil was used to facilitate intermediate sampling. The results of these tests, tabulated in table III-J-1, show that some lubricants are superior to others as evidenced by the weight loss of the metals, changes in viscosity and neutralization number, and sludge content.

Laboratory tests were continued to determine the foaming and evaporation loss characteristics of Mobil Jet II and Esso 2380 oil at varying temperatures and pressures.

Testing was initiated on the JTF17A-20 No. 1 and No. 2 compartment face seal rig with Mobil Jet II lubricant at conditions simulating the sea level operation on FX-16B engine. A total of 11.61 hours of rig testing was completed and disassembly of the rig was in process at the end of the report period.

Table III-J-1. Oxidation-Corrosion Data at Constant Airflow

Vendor Name	Mobil Jet II				Esso 2380				Haco 3211				Royco 899 (Royal C-915)			
	425		450		425		450		425		450		425		450	
Test Temperature, °F	1	2	1	2	1	2	1	2	1	2	1	2	1	2	1	2
Weight Loss, mg/cm <sup>2</sup>																
Silver	Nil	-0.01	+0.01	-0.05	-0.01	-0.01	+0.02	-0.02	Nil	-0.10	-0.05	+0.01	Nil	Nil	+0.02	-0.05
Copper	-0.09	-0.10	-0.09	-0.19	-0.05	-0.08	-0.15	-0.07	-1.19	-0.84	-1.84	-2.38	-0.28	-0.33	-0.63	-0.32
Steel	+0.02	+0.02	+0.02	-0.02	+0.01	+0.02	+0.02	+0.05	+0.02	+0.04	+0.04	-0.03	+0.02	+0.01	+0.05	+0.06
Titanium	+0.01	Nil	+0.04	+0.02	Nil	+0.02	+0.05	+0.04	Nil	Nil	+0.04	+0.03	Nil	Nil	+0.05	+0.05
Aluminum	+0.01	+0.01	+0.04	-0.03	+0.01	Nil	+0.03	+0.03	+0.01	+0.02	+0.03	+0.04	+0.01	+0.02	+0.05	+0.02
Magnesium	-4.34	-5.87	-5.98	-19.35	-0.52	-0.60	-19.00	-13.80	-2.10	-0.10	-24.1	-27.1	-0.02	Nil	-7.46	-2.07
Percent Visibility Increase at 100 F after																
12 hours	11.53	11.06	12.12	11.13	10.10	9.88	12.55	10.44	10.94	10.28	1.08	10.57	4.36	4.99	10.91	8.93
24 hours	15.91	15.47	21.24	18.72	14.90	15.30	22.16	19.11	15.70	15.84	19.73	20.46	7.51	8.48	11.77	12.47
36 hours	19.56	18.79	28.54	26.82	18.86	19.37	33.36	28.46	21.51	21.04	32.45	32.59	10.49	11.05	18.18	21.39
48 hours	23.94	22.95	40.66	40.80	23.63	24.12	54.62	39.77	28.89	26.78	102.94	114.83	11.81	13.27	31.93	36.47
Neutralization Number after																
12 hours	0.31	0.31	1.12	1.02	0.90	0.70	1.29	0.81	0.22	0.26	1.12	0.80	0.38	0.27	1.02	1.02
24 hours	1.29	1.29	1.76	2.35	1.90	1.70	3.32	2.52	0.89	0.64	2.56	1.98	0.64	0.64	1.98	2.08
36 hours	2.03	1.92	2.31	2.99	2.25	2.52	4.12	2.20	2.46	1.39	2.99	2.88	1.12	1.18	3.04	4.70
48 hours	3.99	2.49	6.45	6.19	3.50	3.00	6.41	5.52	3.59	3.59	6.21	5.97	2.35	3.20	5.28	8.80
Sudge, % Wet.			Trace	Trace			0.04	0.04			0.04	0.04			2.50	1.25

## K. INLET SYSTEM COMATIBILITY

### i. Inlet Distortion

The computer program for calculation of single blade row transient response data has been completed and partially checked out. The effect of the size of the mesh used in the numerical integration is being investigated in an effort to reduce the time needed to complete a calculation.

The feasibility of writing a computer program to estimate the off-design matching of a multistage compressor under the influence of inlet distortion is being considered. The complexity of such a program necessitates the employment of simplified representations of the performance of each stage when compared with those currently used in compressor performance estimation. Similarly, the transient response calculation must be simplified to hold the program running time within manageable levels. Data from four of the 0.6-scale fan tests are being examined to determine if the simplified representations will be sufficiently accurate to provide reliable estimates. No fundamental faults have been uncovered to date, and the examination is proceeding toward a better definition of the way the boundary limitations between stages may be handled.

### 2. Engine/Inlet Compatibility

A detailed engine and control dynamic simulation is being prepared for use by The Boeing Company and by Lockheed California Company in engine/inlet compatibility studies. The simulation will consist of a digital computer calculation deck. Performance will be calculated for discrete time intervals, and output of selected parameters as a function of time will be available. The simulation will have the capability of accepting time varying input of power lever angle, flight condition, and inlet condition.

Data for an inlet dynamic simulation have been received from Lockheed California Company. The simulation is being reviewed and will be used for engine/inlet compatibility studies.



L. NOISE

Modifications to engine test stand A-3 that will improve conditions for JTF17A-20 sound recordings were completed this month. Far field microphone locations were installed on a 300-foot radius aft of the engine. Preliminary data have been obtained at these locations with both J57 and J58 engines, and shows good repeatability and agreement with the SAE prediction method. The effects of reflecting surfaces around the stand have been minimized through alterations to the stand and the addition of sound-absorption material.

The analysis of sound recordings is currently performed using an octave band analysis system that provides a plot of the octave band sound pressure levels. Several faster methods of analysis are under review. These methods would be fully automatic and would provide inputs for a computer program that would provide values of perceived noise.

Analytical evaluations are being performed for acoustical liners of the Helmholtz resonator type. Maximum absorption of the energy incident on resonant liners compares favorably with the absorption of nonresonant types. Resonant liners also offer the potential of light weight and eliminate the possibility of fire hazard due to oil and fuel absorption into the materials used in the nonresonant type. Measurement of the sound pressure level within the duct, as well as other pertinent parameters necessary for liner design, are now in process.

M. MOCKUPS

Duplication of the Lockheed configuration on the engineering mockup has been completed.

The JTF17A-20 engine installation mockup for the Boeing Company is still awaiting further definition from Boeing. The estimated delivery date for the mockup is now 26 July 1966.

Mockups demonstrating the control "quick-disconnect" concept were received from Bendix Products Aerospace Division and Hamilton Standard, and are discussed in paragraph III-H.

N. COORDINATION

1. General

Revised JTF17A-20 Engine Specification 2681B (Boeing) and 2682B (Lockheed), dated 15 March 1966, were transmitted to Boeing, Lockheed, and other authorized recipients during this report period. The revision included performance deck changes, minor changes to Lockheed specification weight, and an engine operating envelope change for Lockheed.

FRDC fuels group personnel visited Boeing, Lockheed, aviation jet fuel suppliers, and major airlines to discuss the proposed SST fuel requirements. P&WA personnel made a presentation before the SST Fuels Industry Advisory Committee Meeting at FAA Headquarters, Washington, D.C., 20 and 21 April.

Boeing SST Program Engineering and Research personnel visited FRDC 29 March to discuss current tubing technology and P&WA experience with mechanical plumbing connectors.

Mr. F. Howard of SST Propulsion Branch, visited FRDC 31 March and 1 April for JTF17A-20 engine program discussions.

On 12 April, Mr. R. N. Torell, Chief Engineer, FRDC, Mr. G. A. Titcomb, SST Program Manager, and other staff personnel briefed FAA Headquarters personnel on the JTF17A-20 engine design details, development program, growth studies, and latest noise attenuation studies.

Boeing SST program personnel headed by Mr. H. W. Withington, Director of Engineering, and Mr. F. A. Maxam, Chief Engineer, visited FRDC on 14 and 15 April and were briefed on J58 engine; the SST program and JTF17A-20 engine were also discussed.

Personnel from Booz-Allen Applied Research, Inc., and Research Analysis Corporation visited FRDC on 18 April to obtain necessary information required for their FAA subcontracts on SST economics.

Delta and National Airlines personnel visited FRDC on 19 and 20 April for general JTF17A-20 engine and SST program discussions.

Mr. Harold Luskin, Lockheed California Company Assistant Program Manager for Propulsion and Mr. Charles Kammann, SST Program Contracts, visited FRDC on 20 April to discuss engine/airframe interface activities for the Phase III proposal; they also received a general JTF17A-20 engine briefing.

After SST Fuels Industry Advisory Committee Meeting, Boeing fuels engineer, Mr. G. Hays, and Mr. E. Petesch, Chief, Mechanical Equipment Staff, visited FRDC on 22 April, for follow-on fuels discussions and general familiarization with JTF17A-20 engine program.

FRDC continued to exchange comments with Boeing and Lockheed on analytical methods for calculating JTF17A-20 noise data. JTF17A-20 design information on the fan duct system was provided to Boeing for their study of a simulated duct noise test rig.

General J. Maxwell and Dr. R. Blisphinghoff of the FAA visited FRDC on 21 April for SST program discussions.

## 2. JTF17A-20 (B) Engine

Installation coordination activity continued during this report period. The more significant installation items covered were:

1. Additional preliminary engine heat rejection estimates based on the latest Boeing estimated fuel temperature profile for a typical mission were transmitted to Boeing.
2. The Boeing preliminary engine ground handling concept was reviewed and is considered acceptable.
3. FRDC submitted a preliminary engine electrical installation drawing, which represented our response to a review of the Boeing wiring diagram depicting engine-supplied electrical items, connection interfaces and wiring requirements.
4. Boeing approved FRDC proposed location of the main and duct heater igniters to the lower quadrants of the engine to improve the removal envelopment.

5. Activity on the Boeing mockup engine is currently at a very low level as a result of a further delay in definition of the Boeing configuration.

Boeing has indicated primary interest in the JTF17A-21 study engine. We are currently studying their requirements.

The Boeing Inlet-Engine Compatibility Test Plan was reviewed by FRDC. Comments and necessary changes to arrive at a currently acceptable coordinated plan have been forwarded to Boeing during this report period. These changes will require revising the test plan already submitted.

Secondary airflow systems were reviewed and our recommendations were transmitted to Boeing. The ducting/control valves system utilizing air from the engine inlet periphery was recommended at this time. However, a more detailed analysis is being prepared for transmittal to Boeing.

### 3. JTF17A-20 (L) Engine

Lockheed has advised that they desire an accelerated program of inlet/engine compatibility tests using early boilerplate hardware. Meetings were scheduled at Tullahoma for 27 April with both AEDC and Lockheed personnel for test program discussion. The Lockheed group visited FRDC prior to these meetings.

Coordination is continuing with respect to Lockheed's request for the increased performance (JTF17A-21L) study engine. Performance decks in both IBM 360 and 7090 form were requested by 1 May, in addition to a new engine model specification.

Lockheed is continuing to study relocation of the engine on the wing. A feasibility study drawing of an elliptical reverser-suppressor designed to eliminate or minimize problems associated with lowering the engine relative to the wing was forwarded to LCC for use in their review.

Lockheed has verbally informed us that they now intend to use an electrical power lever control system; they are now studying two or three possible systems. Upon completion of their studies, Lockheed will submit formal proposals for our review and comment. We are now supplying them information to enable them to complete these studies.

## 0. MAINTAINABILITY

### 1. Design Review

Tradeoff design analyses, directed toward further improvement of the maintainability of the JT17A-20, are in process in the following areas.

1. A study of commercial overhaul and maintenance errors for period of operation 1 January 1962 through 31 January 1966 is being made to determine engine areas where errors could be eliminated by incorporation of foolproofing features, which would reduce maintenance time for reoperation and the level of required maintenance skills.
2. A design of the fan rotor is being evaluated that makes the 1st-stage fan disk an integral part of the fan hub, thus eliminating the long tiebolts and disk holes.

Elimination of the disk holes will improve the durability of the fan assembly by removing the possibility of wear of the bolts and bolt holes as well as facilitating installation and removal of the assembly.

3. A review is being made of the recommendations made by Trans World Airlines in their report "BTT Design Goals and Guide Lines for Power Plant Maintenance." A comparison of these recommendations versus maintainability features of the JT17A-20 engine will indicate the extent of the PWA maintenance concept with specific airline philosophy.
4. Further design studies are being made on the split intermediate case configuration to determine feasibility of disconnecting power takeoff and accessory drive shafts for removal of the No. 2 bearing from the inlet.
5. An analysis is in process to establish all of the maintainability features required with the engine installed in the aircraft. Features incorporated will reflect airline, airframe, and field service requests.

Pratt & Whitney Aircraft

PWA FR-1855

6. Additional chip detector provisions are being reviewed. Locations of additional provisions will be at the main oil pump and No. 1 and No. 2 compartment pump. Present chip detector provisions are located at the accessory drive overboard drain, main gearbox, oil tank, and oil pump gearbox.
7. Borescope inspection provisions for the 2nd-stage turbine blades are being incorporated. This would complete the inspection provisions for all turbine stages.
8. The use of bearings incorporating antirotation features throughout the engine and accessories is being evaluated. This would provide added insurance against bearing race splining, eliminate bearing race retaining nuts (with their attendant high torque provisions), and eliminate special spanner nut wrenches.
9. An airline request to remove the oil pressure regulating valve from the engine oil system has precipitated review of the advantages and disadvantages of the pressure regulating valve in the oil system.
10. The analysis of weight tradeoff versus number of bolts in a given flange has been continued to determine the percentage saving in man-hours for a given component removal compared to a resulting weight increase. The results will be reported in a later report.

P. VALUE ENGINEERING

Value Engineering proposals for cost reduction changes being analyzed for incorporation in the engine design have reached a total of \$78,000 per engine.

Recent engine design changes involving cost reduction include:

Redesigned high compressor rotor	- \$13,800
Redesigned burner inlet fairing	- \$ 2,000
Shortened duct heater	- \$ 6,900

Cost comparisons made to support design decisions have been completed on:

- Main burner design changes
- Compressor shroud design
- Compressor chord choice

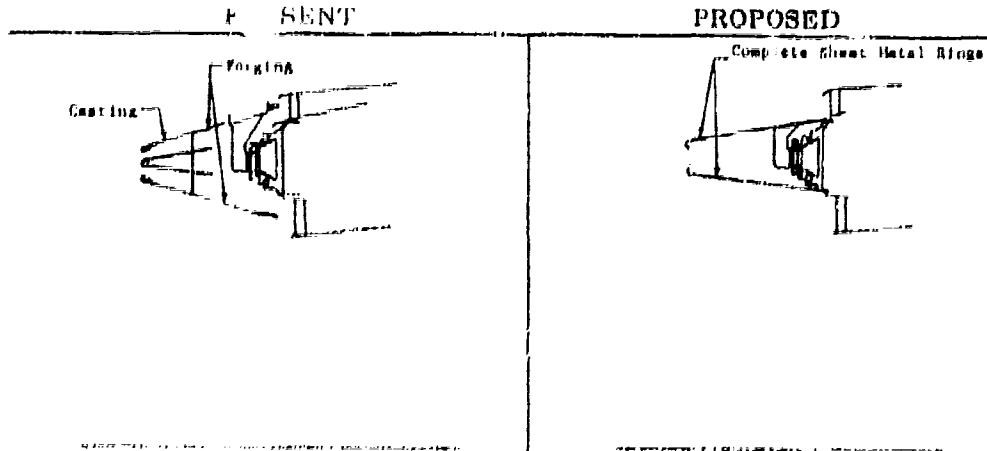
Typical Value Engineering proposals completed during this period are shown in figure III-P-1 and III-P-2.





**VALUE ENGINEERING PROPOSAL #** 4.01

Proposed by J. Chamberlain Date 1-6-66  
 Part No. 2114761 Name Inlet Guide, Main Combustion Chamber  
 Primary Function Guide Inlet Air To Main Burner  
 Secondary Function \_\_\_\_\_  
 Environment \_\_\_\_\_



Material	Material				
	P	M	L	O	T
Present Cost	1645	219	790	1199	3000
Proposed Cost	9	15	189	672	210

Δ Cost/Part = 92000

Δ Cost/Engine = 57000

Proposal	Comments
Design the cast and forging deflection into a sheet metal ring that is an integral part of the burner.	Change will save 60 %

**Feasibility**

Structures

Vibration

Heat Transfer

Fluid Flow

Maintainability

Performance

Weights

Reliability

**CONFIDENTIAL**

Pratt & Whitney Aircraft  
PWA FR-1855



**VALUE ENGINEERING PROPOSAL # 6.05**

Proposed by Project Engineering Date 3-9-66

Part No. 2119967-1 Name Duct Heater

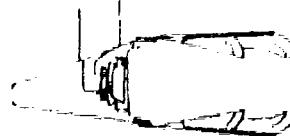
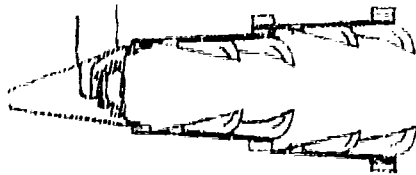
Primary Function Retain Flame In Duct Heater

Secondary Function \_\_\_\_\_

Environment \_\_\_\_\_

**PRESENT**

**PROPOSED**



Material

Material

	P	M	L	O	T
Present Cost	--	375	1299	4590	6999
Proposal Cost	--	0	0	0	0

$\Delta$  Cost/Part -- \$6999

$\Delta$  Cost/Engine -- \$6,000

Proposal

Remove aft section of duct heater

Comments

Removal of aft section will save 65lb

Feasibility

Structures

Vibrations

PWA 10494B

Heat Transfer

Fluid Flow

Maintainability

Performance

Weights

Reliability

Figure 111-P-2. Value Engineering Proposal #6.05

111-P-2

**CONFIDENTIAL**

## Q. CONFIGURATION MANAGEMENT

Coordination has continued on those items that cannot be shown on the installation drawings or mockups until definition has been agreed upon by P&WA and the airframe contractors. The JTF17A-20 engine installation mockup at Lockheed California Company is static pending completion of the airframe mockup to a point where the engine can be mounted. The JTF17A-20 engine installation mockup for The Boeing Company is still delayed pending further definition from Boeing. The estimated delivery date is now 26 July 1966. The effort on the engineering mockup is discussed in paragraph III-M. Table III-Q-1 shows the status of the engine configuration.

Table III-Q-1. Status of Airframe/Engine Coordination

Airframe Contractor	Item	Status
TBC	Engine Mount	Boeing has possible nacelle shape pending configuration decision and mounting concept with the inlet supported separate from the engine. P&WA studying while awaiting better definition and configuration decision.
TBC	Ground handling	P&WA advised Boeing that the scheme submitted by them is feasible.
LCC	Control inputs	LCC is now planning to use an electrical power lever. They are studying several schemes which they will submit to P&WA.
TBC	Control inputs	Awaiting definition from Boeing.
LCC & TBC	Flowmeters	P&WA has received no comment from either airframe contractor concerning the flowmeter experience and recommendations that were submitted. P&WA is studying the incorporation of Boeing's mass flowmeter configuration.

Table III-Q-1. Status of Airframe/Engine Coordination (Continued)

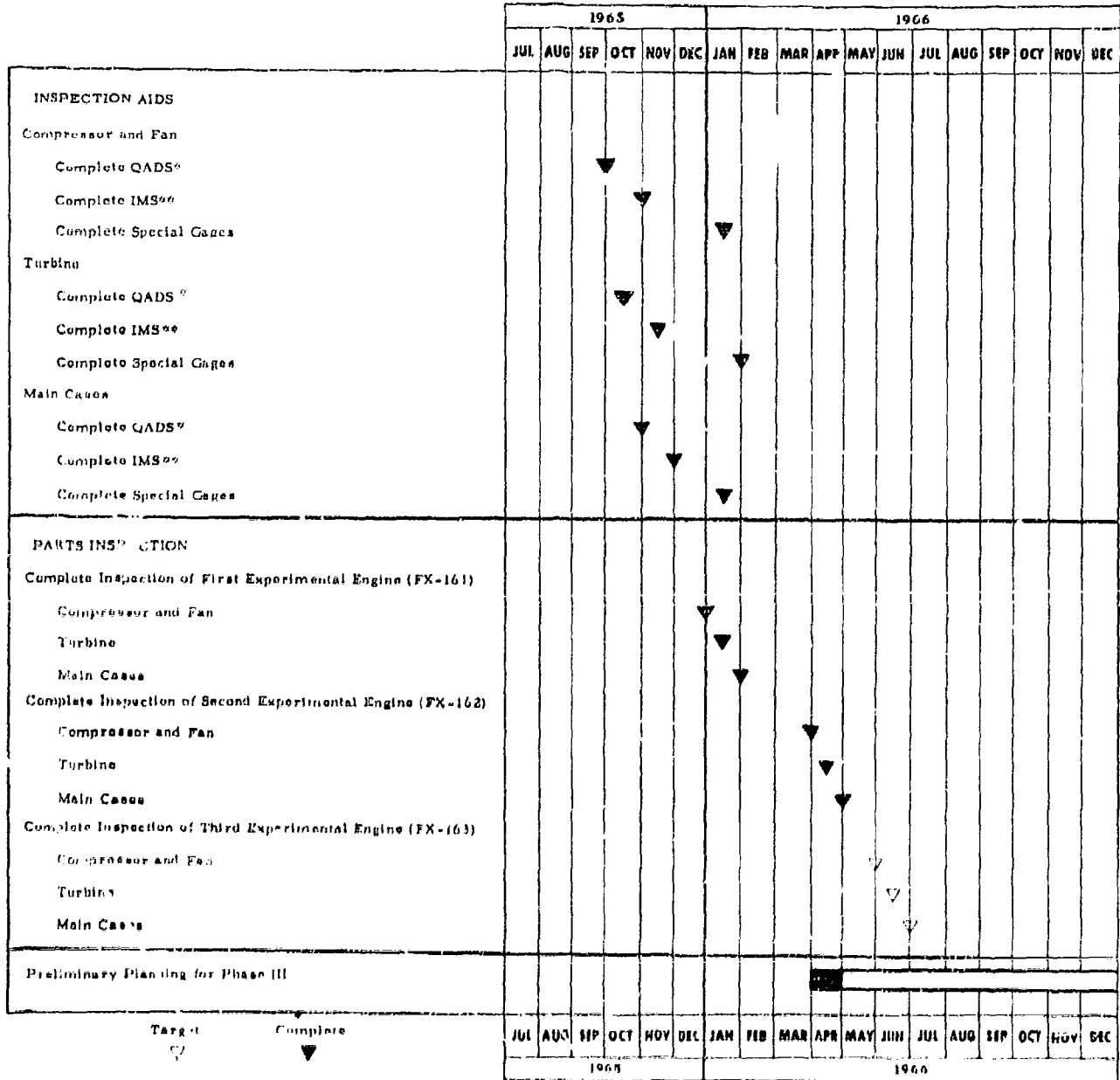
Airframe Contractor	Item	Status
TBC	Overboard drains	P&WA is awaiting comment from Boeing concerning the attachment configuration.
LCC & TBC	Fuel supply & return	Awaiting definition.
LCC & TBC	Labyrinth seal vents	Vent configuration and locations are being established by P&WA design.
TBC	Secondary air	P&WA recommended continuation of the ducted system with air from the engine inlet periphery. P&WA is preparing for transmittal a comparative analysis of sources for secondary air.
TBC	Component Arrangement	P&WA is continuing design work to establish an external component arrangement to satisfy Boeing's desire that all major fuel lines and components be 1 foot above the bottom of the mount rings.

At the request of the Lockheed California Company, Pratt & Whitney Aircraft has provided data on several improved versions of the JTF17 engine for their analysis and aircraft studies. As the result of their studies, Lockheed has chosen one of these versions as the best configuration of our engine and has requested that we prepare a preliminary specification for the study engine selected. This engine has been designated the JTF17A-21L, and a copy of the Preliminary Engine Specification No. 2698, dated April 29, 1966, for this engine was issued.

R. QUALITY ASSURANCE

The inspection aids including Quality Assurance Data Sheets (QADS), Inspection Method Sheets (IMS), and special gages are current, requiring changes only in response to recent experimental changes. Inspection of parts for the second experimental engine (EX-162) has been completed. Preliminary Quality Assurance planning for Phase III has been started. Quality Assurance schedule milestones for Phase II-C are shown in figure III-R-1.

Pratt & Whitney Aircraft  
PWA FR-1855



\* Quality Assurance Data Sheets  
\*\* Inspection Methods Sheets

Figure III-R-1. Quality Assurance Schedule Milestones

FD 15642

## S. RELIABILITY AND SAFETY

### 1. JTF17A-20 Mathematical Model

A mathematical reliability apportionment model is used to identify functional interdependencies between engine components so that the effects of a functional failure may be traced through the engine. A failure mode and effect analysis (FMEA) is conducted for each "block" in the mathematical model. Both the mathematical model and the FMEA are being extended to subassembly and part levels; however, as we progress downward through the mathematical pyramid from the overall reliability estimate the successive partitions of the reliability estimates have less and less precision. Therefore, reliability estimates will not be made below the level of components except in a relative sense to compare one design to another.

Separate models trace failure effects resulting in premature engine removal and inflight shutdown. Predicted failure rates per 1000 hours for each engine section are noted on the diagrams.

For the engine to operate in all modes, all subsystems on the top horizontal line must function. For one of these subsystems to operate in all modes the components connected to it by a vertical line must all operate. The failure of one or more components may limit the subsystem capabilities and require an inflight shutdown. The failure of one or more components will require unscheduled maintenance and may require a premature engine removal.

The mathematical model is shown in figures III-S-1 through III-S-13.

### 2. Fire Hazard Analysis

#### (a) General

The JTF17A-20 engine is designed to operate at engine inlet temperatures up to 520°F at steady state (600°F transient), as opposed to 120°F for present commercial subsonic engines. This analysis, which considers the possibility of ignition by spontaneous combustion, by high energy sparks, and by engine case burnthroughs, shows that the likelihood of nacelle fires in the JTF17A-20 is less probable than in subsonic airplanes.

Although engine inlet temperatures are higher for the JTF17A-20 engine, the maximum engine case temperatures, as shown in figure III-S-14, are no higher than for the JT3C-7 engine presently in service in the Boeing 720 airplanes.

The comparable cruise conditions as shown in figure III-S-14 are 35,000 feet at Mach 0.8 for the JT3C-7, and 55,000 feet at Mach 2.7 for the JTF17A-20B (lowest altitude for supersonic cruise). At the respective cruise conditions, the maximum external case temperatures are 1050°F for the JT3C-7 and 850°F for the JTF17A-20. The JTF17A-20 maximum case temperatures are lower than those for the JT3C-7 because of the cooler fan air enveloping the gas generator.

A review of all P&WA engine experience in commercial service has shown no instances of external, engine-caused, nacelle fires.

(b) Engine Case Burnthrough

A review of engine case burnthrough experience shows fifty-two (52) instances of engine burnthroughs (of which approximately 1/3 caused nacelle burnthroughs) during 27 million hours of operation. These are tabulated in table III-S-1, page III-S-3. Engine burnthroughs were confined to two causes in the engine.

The first cause was burner can disengagement from the fuel nozzle cluster resulting in burnthrough of the outer combustion duct. The JT3-JT3C-7 burner can design is shown in figure III-S-15. In this design the burner can is restrained from moving axially by lugs at the front end of the can and is restrained from moving radially at the rear end of the can by band clamps attaching the can to the transition duct. If the band clamp fails, the burner can becomes disengaged from the fuel nozzle cluster, thus causing burnthroughs of the outer case. The SST annular burner design, as shown in figure III-S-16, allows the installation of the fuel nozzles after the burner is installed in the transition duct, thus eliminating the need for a clamp. The front end of the annular combustor is retained (to the diffuser case) by 12 radial pins of which six are redundant, which means that any six of these pins can fail without affecting the axial position of the burner, thus precluding disengagement from the fuel nozzles.



The second area causing burnthrough involved failures in the tubing between fuel nozzle housings, which are exposed to gas path, aerodynamic, and vibratory loads. Some load is also imposed by the burner can that is supported by the fuel nozzle body. In the case of the JT8D the three-piece fuel nozzle support configuration resulted in seal leakage at two parting surfaces with consequent burnthroughs. (Refer to figure III-S-17.) This problem was readily corrected by a seal change.

Table III-S-1. Commercial Engine Case Burnthroughs From Start of Operation Through June, 1965

	Total Operating Hours - 27,974,064			
	Total Burnthroughs - 52			
	Reliability Factors - 0.00186 Failures Per 1000 hours			
Cause	JT3	JT3D	JT4	JT8D
Can Disengagement	10	7	2	1
Manifold or Nozzle Cluster Failure	20	7	3	2

The JTP17A-20 engine has each nozzle, for the main combustor and the Zone I of the duct heater, installed in a one-piece nozzle holder and does not support the annular burner. This eliminates any parting face seals that are potential leak points inside the engine and removes loads which might otherwise be imposed on the nozzle.

More recently, but not included in the time period shown in table III-S-1, there has been a burnthrough due to burner can segment separation in the overlap seam welds. Seam welds have built-up stress concentrations and are more susceptible to cracking. This problem is also aggravated by burner can crossover tubes and tangency hot spots. The JTP17A-20 engine has an annular, high reference velocity burner that eliminates this hot spot problem. The burner construction does not use seam welds.

The duct heater combustor is similar in design to the primary combustor. Eight radial pins, four of which are redundant, preclude disengagement from the nozzles; therefore, the same analysis is applicable.

It has also been determined that if the duct heater Zone II internal fuel injector manifold should rupture, the mixture is too rich locally to support combustion so that no hot spot is created and no damage results. This has been experimentally confirmed by actual test on the duct heater rig.

(c) Spark Ignition Sources

To ignite a fuel-air mixture at temperatures below the spontaneous ignition temperature, a very high energy ignition source must be provided. The only engine-supplied electrical system that fits this description is the dual-igniter system.

Service experience indicates that failures of ignition systems have not caused arcing or external sparking. The reasons for this excellent record are (1) proper shielding of leads and (2) the necessity for a close gap to ground to exist to produce a spark. Actual test results of required gap versus ambient pressure, as shown in figure III-9-18, show that a gap of more than 0.060 inch will not result in sparking at any pressure level. Tests were made using the proposed JTV17A-20 ignition system.

Based on present commercial experience, fire hazards with respect to inadvertent arcing of engine-supplied electrical circuitry in the SST engine are less than with the present commercial engines because case temperatures are no higher and velocities are greater.

(d) Engine Nacelle Fire Hazards As a Function of Plumbing Integrity

Another possible source for nacelle-engine fires is leaks at plumbing joints or broken lines. There have been no fires in PWA commercial engine experience attributable to fuel leaks. In addition, there have been only rare instances of fuel plumbing failures.

During development of the J58 engine for sustained high supersonic operation, a major development effort was expended on improved plumbing connections and establishing more elaborate and exacting design criteria for plumbing and plumbing supports. To minimize the overall plumbing design time and increase engine reliability, computer programs incorporating these design criteria for tubing were developed. The computer program provides a quick and accurate means to route tubes for the best compromise of length, weight, and flexibility to keep static stresses low and uniform. The computer program calculates the stress at any point in the tube with any desired combination of support points. It also

calculates the relative displacement of the tube to the bracket attachment to permit the bracket to be properly designed to accommodate thermal expansion in a direction to minimize stresses. Fixed brackets are positioned at points where no movement due to thermal growth is required to eliminate resonant vibrations.

This development experience and design technique is being used in the JTV17A-20 design, and will ensure reliable plumbing.

Actual experience on the J58 engine installation has shown that three fuel leaks and four oil leaks have occurred at high Mach numbers, and no fires resulted (even though case temperatures are significantly higher). This experience substantiates the laboratory data that velocities, stay times, and engine case temperatures will not permit spontaneous ignition.

During the initial J58 engine development, completely brazed plumbing connections were used and were entirely unsatisfactory. The problem with these connections was nonuniform brass coverage in the joints. In addition to this, the accessibility and maintenance, and overhaul times were unacceptable.

Mechanical joints with conical metal seals were a vast improvement. However, leakage problems were still evident through the brazed ferrule. The latest design for plumbing uses an integral ferrule and tube configuration that eliminates all brazing or welding in the plumbing.

By using integral fittings that have proven consistently reliable, and by the proper routing and bracketing of plumbing based on service proven design criteria, the possibilities of leakage on the JTV17A-20 engine due to failure of seals or plumbing is negligible.

#### (a) Fire Hazard Due to Supersonic Operation

Although the service record is excellent, if leaks should develop, spontaneous ignition of the resulting fuel-air mixture is not possible, even during supersonic operation. Spontaneous ignition is a function of nacelle air velocity, pressure, and temperature. Experimental data have been prepared by Pulling of the British National Gas Turbine Establishment showing the required stay time for spontaneous ignition versus air temperature and pressure, as shown in Figure III-5-19.

### (f) Nacelle-Engine Cavity

Because the JT17A-20 engine case temperatures are no higher than present commercial subsonic engines at any condition of flight, only the supersonic flight regime, where the environmental temperatures are higher, is considered. Three points were selected along the flight path, as shown in figure III-8-26. Point A is the point at which the case temperature at the rear mount equals the JT3C-7 engine case temperature at the corresponding location on the engine. Point B is the minimum altitude, maximum Mach number cruise condition for the SST engine, and point C is the maximum altitude, maximum Mach number cruise condition.

Point A was selected because above this point the SST engine case temperature increases above the JT3C-7 case temperature at the corresponding location on the engine. Point B was selected because it represents the maximum nacelle temperature and pressure point. Point C was selected because it represents the maximum nacelle temperature and minimum pressure point and a slightly higher case temperature.

The calculated values of engine nacelle cavity pressures, temperatures, and velocities for the three points on the maximum Q side of the operating envelope are shown in table III-8-2. This table shows that for the worst case of pressure, temperature and velocity, a residence time of 150 seconds is required for spontaneous ignition.

The stay time for the given fuel-air mixture is less than 0.008 of the time required for spontaneous ignition. This assumes that the fuel-air mixture is at case temperature. Note that the table presents two concepts of engine-nacelle design: (1) a pressurized nacelle with secondary airflow through the nacelle; and (2) a nonpressurized configuration that has a bulkhead in the vicinity of the rear engine mount, with the area upstream of the bulkhead vented to atmosphere.

If the pressurized nacelle concept is used, the residence time is much less than in the above analysis. For example, at the cruise condition the stay time is 0.001 of that required for spontaneous ignition.

Table III-1-2. Residence Time Required for Spontaneous Ignition versus Anticipated Residence Time

Motor No.	Altitude, ft	Nozzle Pressure, psia	Nozzle Velocity, fps	Case Temperature, °F	Residence Time Required to Ignite, sec	Actual Residence Time, sec
Pressurized Nozzle	55,000	7	400	800	30	0.030
	60,000	1.4	290	820	50	0.061
	65,000	12	310	850	100	0.092
Vented Nozzle	55,000	1.35	10	800	150	1.2
	60,000	0.4	10	820	100	1.2
	65,000	6	10	850	150	1.2

(g) Duct Heater - Gas Generator Cavity

Temperatures in the fan cavity area, gas generator case and the fan ID case are shown in figure III-8-14. Velocities for this area are shown on figure III-8-21 and table III-8-3. This area is swept by fan discharge air with a minimum velocity at sea level takeoff of 160 fps. The maximum fan case temperature is 1500°F at sea level takeoff. At this temperature the required stay time is 0.007 second, or a distance of 1.1 feet must be traveled after the fuel-air mixture is heated to 1500°F to spontaneously ignite. It is concluded that by the time this distance is traveled, the hot layer of fuel-air mixture will have been directed into the cooling louvers and into the combustion zone of the duct heater.

It should be noted that in order for a fuel-air mixture to spontaneously ignite, the mixture must be at the required spontaneous ignition temperature for a finite period of time.

Table III-8-3. JTF17A-20 Cavity Residence Time Required for Spontaneous Ignition Versus Anticipated Residence

Moeh No.	Altitude, ft	Cavity Pressure, psia	Cavity Velocity, fps	Maximum Case Temperature, °F	Residence Time Req. to Ignite, sec	Actual Time, sec
9LTO	---	36	160	1310	0.0500	0.0120
2.7	55,000	37	320	1500	0.0070	0.0062
2.7	80,000	9.5	320	1520	0.0300	0.0062

Because the bulk of the cavity air at cruise is at a temperature of 600°F, only the film of air scrubbing the duct heater ID wall approaches the temperature of the case; therefore, it is estimated that the average film temperature will be on the order of 1000°F when the case temperature is at 1500°F. Applying this temperature to the Mullins Stay Time Curve yields a stay time of 4.5 seconds, which is 0.13 of the time required for spontaneous ignition. If the air velocity is 320 ft/sec as shown in table III-8-3 in the area of the hot case, the actual stay time is 0.0062 second. If a fire did occur in the engine cavity, it is certain to occur at the back end of the cavity where case temperatures are maximum.

Since the distance between cooling louvers in the duct heater inner liner is approximately 12 inches, it is calculated that by the time the film of cavity air scrubbing the inner wall has reached the spontaneous ignition temperature and remains at that temperature for the required time, the film of air will have re-entered the duct heater through the cooling louvers, possibly causing a hot spot or burning on the inside wall of the duct heater liner. This is not considered to be a disastrous type failure or a type failure that would make the engine inoperative or affect the mission completion.

To further substantiate these conclusions, tests are planned, during engine development, to simulate fuel leaks in both the nacelle and engine cavity compartments.

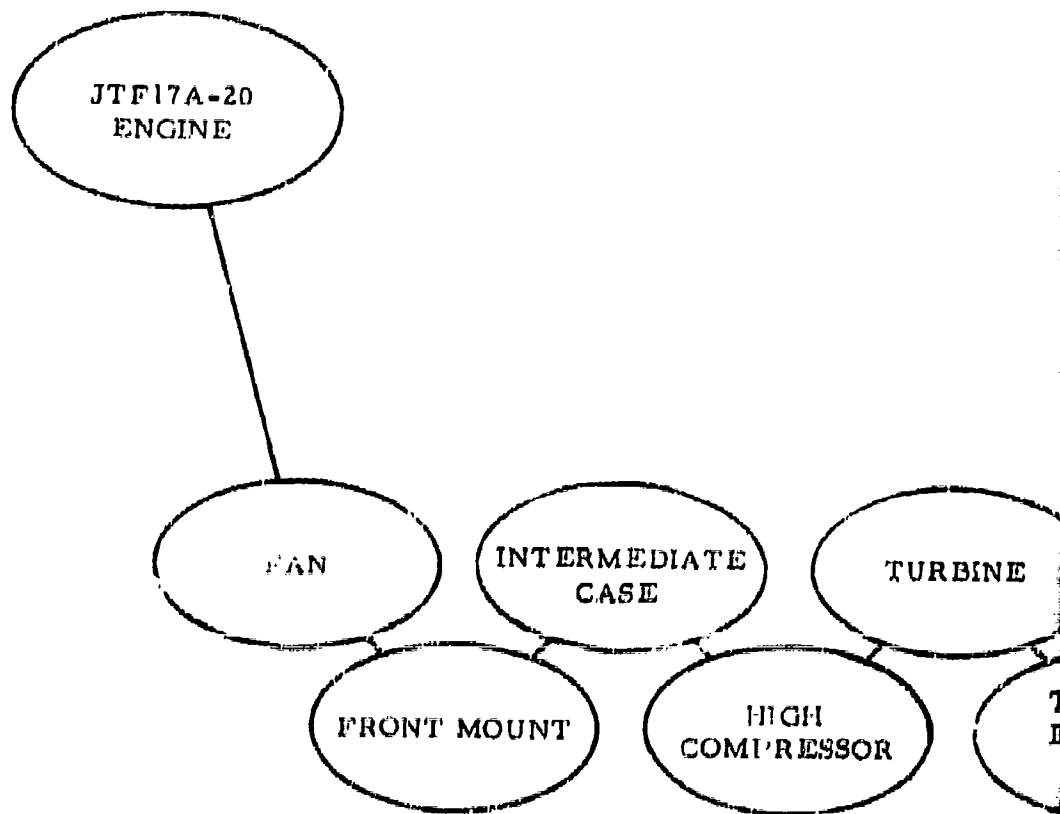
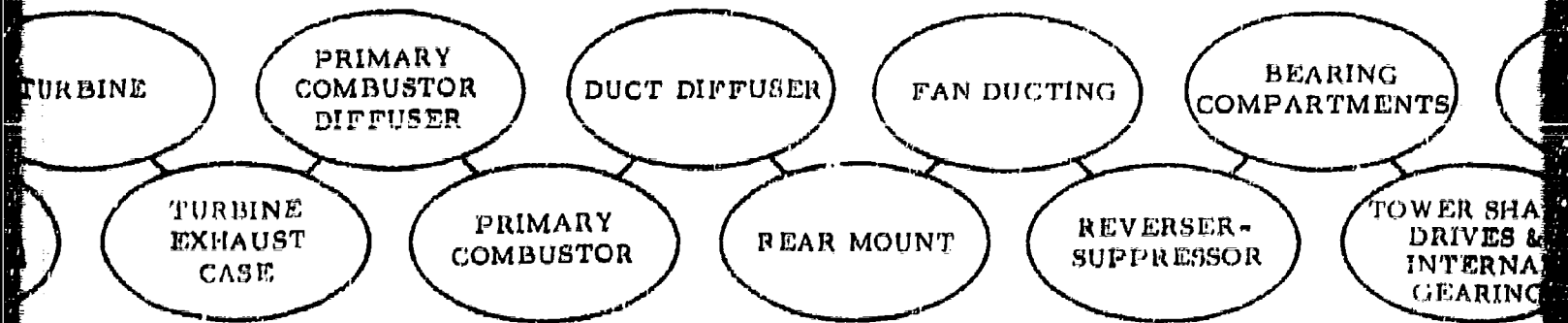
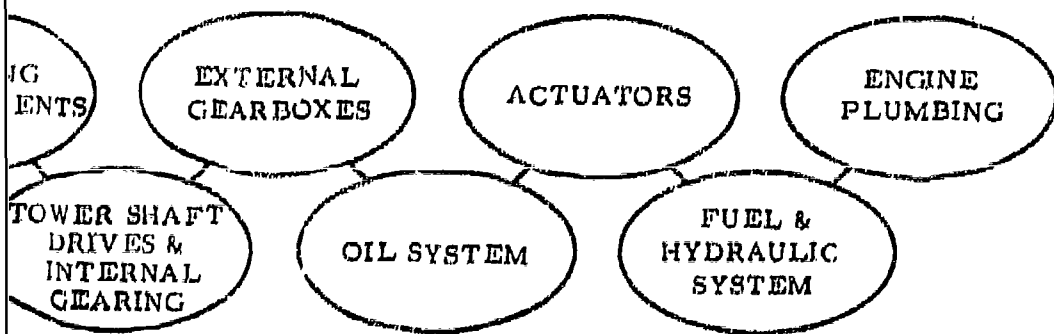


Figure III-9-1. JTF17A-20 Engine Reliability Mathematical Model, First Level Block Diagram, In-Flight Shutdown







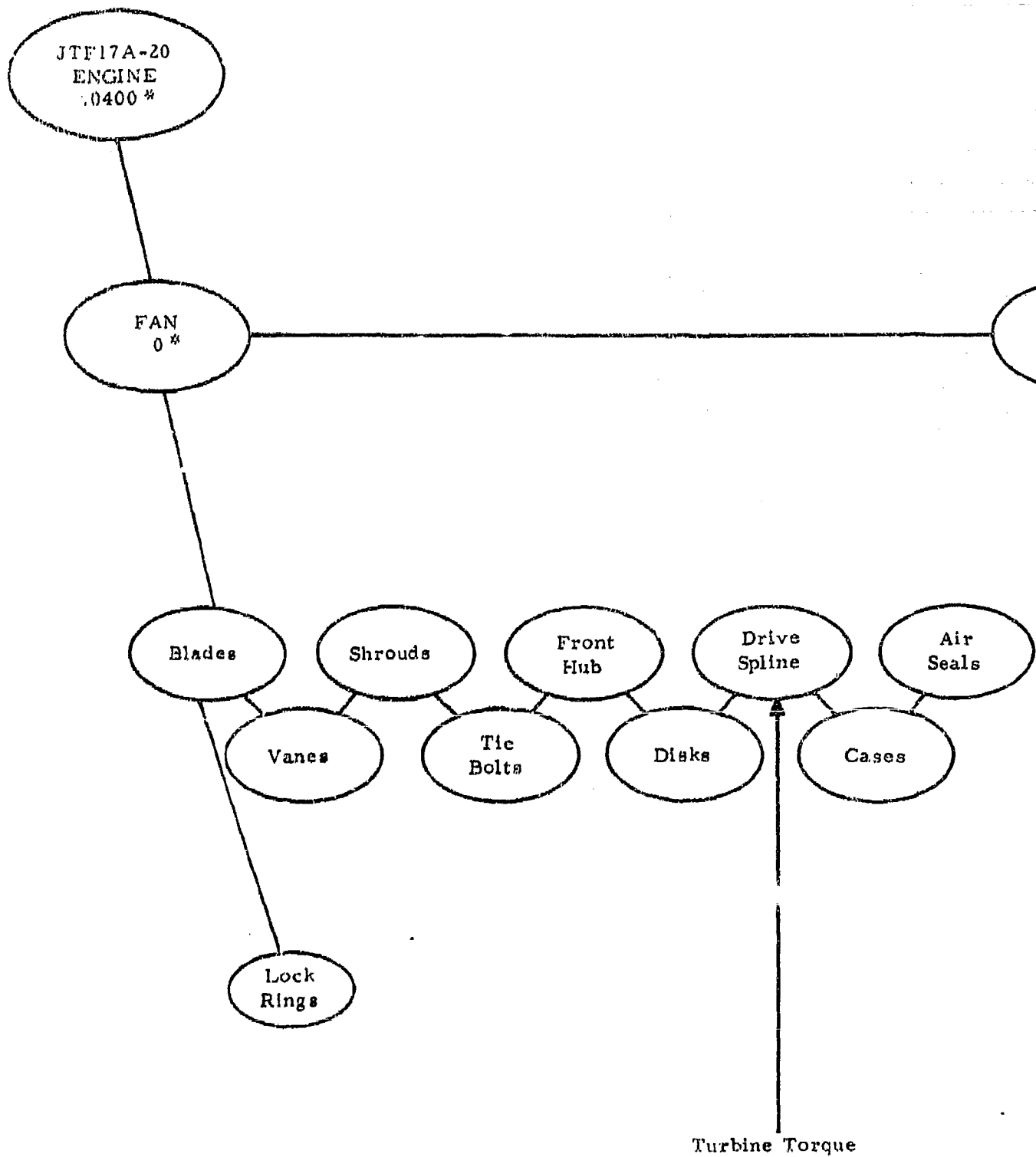
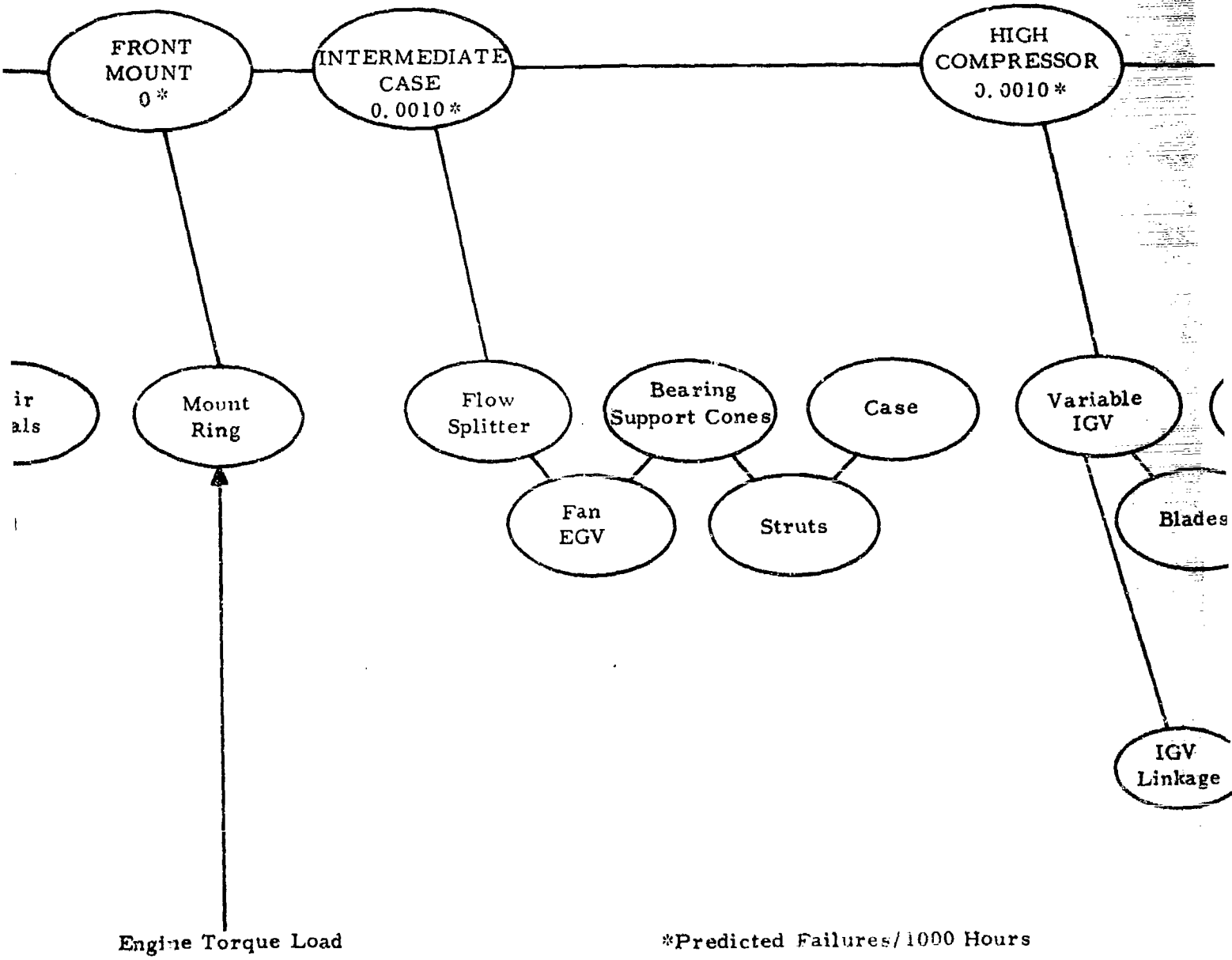
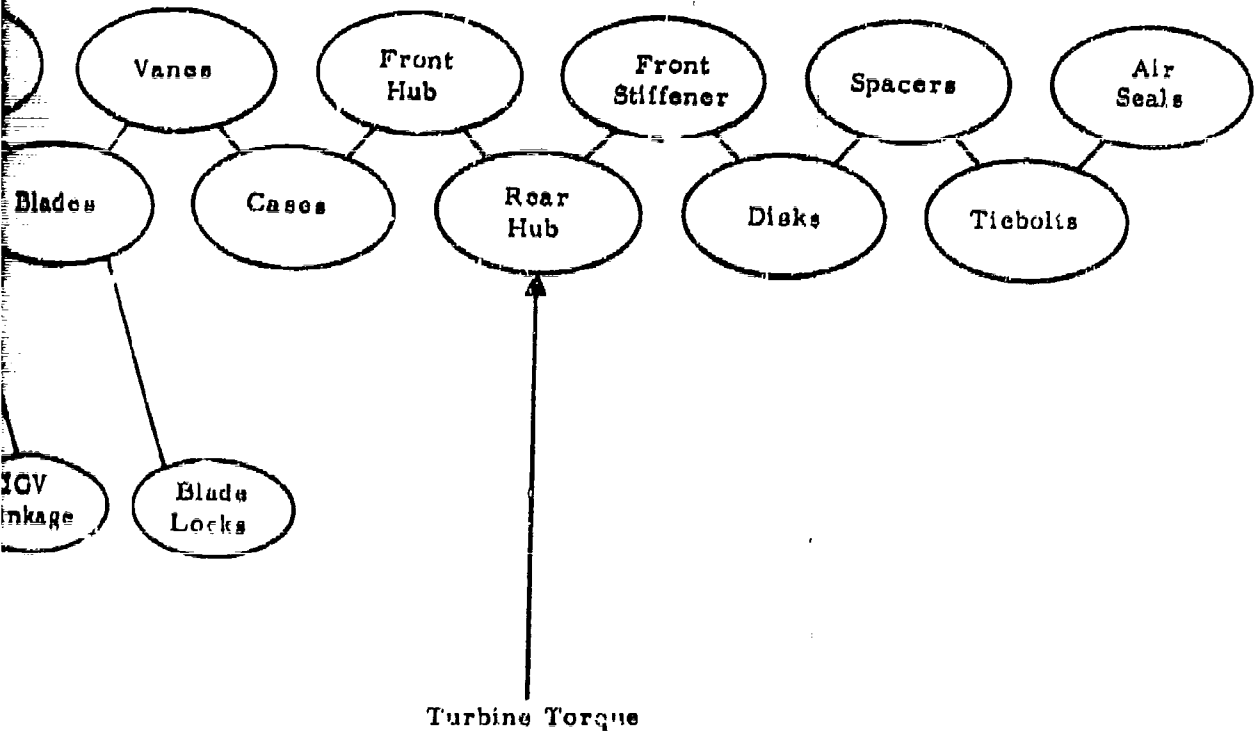


Figure III-S-2. JTF17A-20 Engine Reliability Mathematical Model,  
In-Flight Shutdown (Sheet 1)



*Handwritten mark*



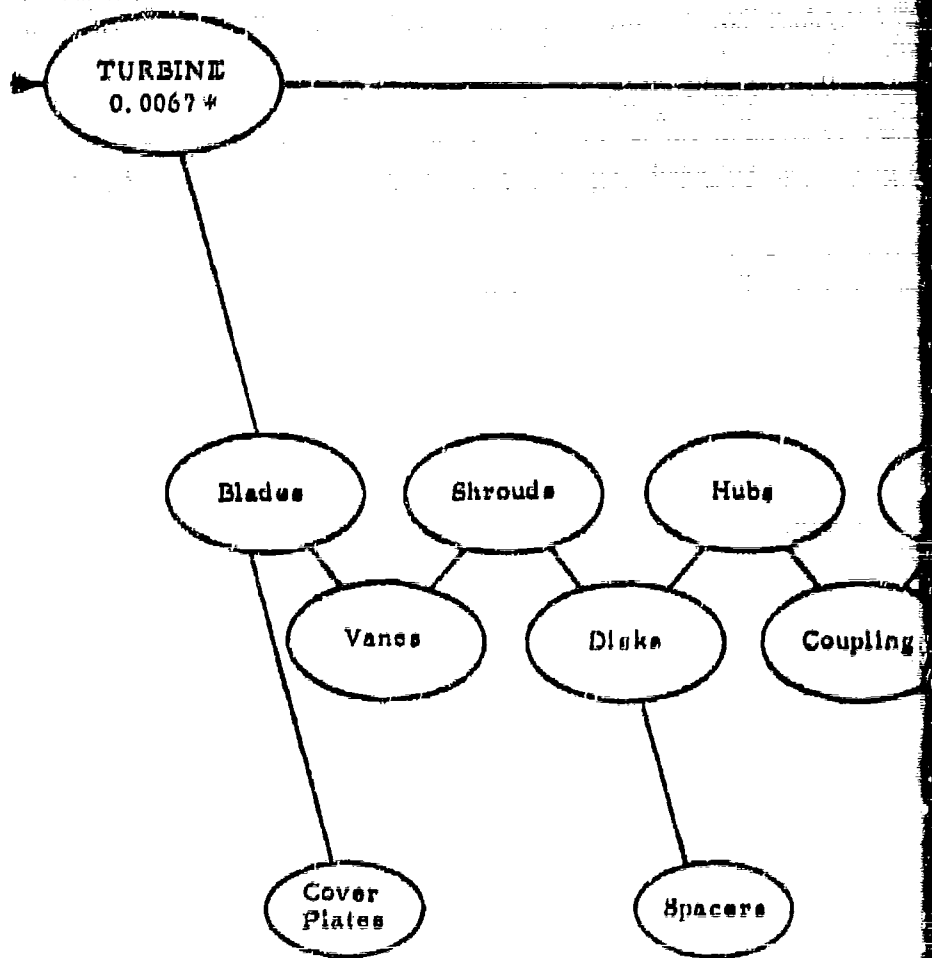
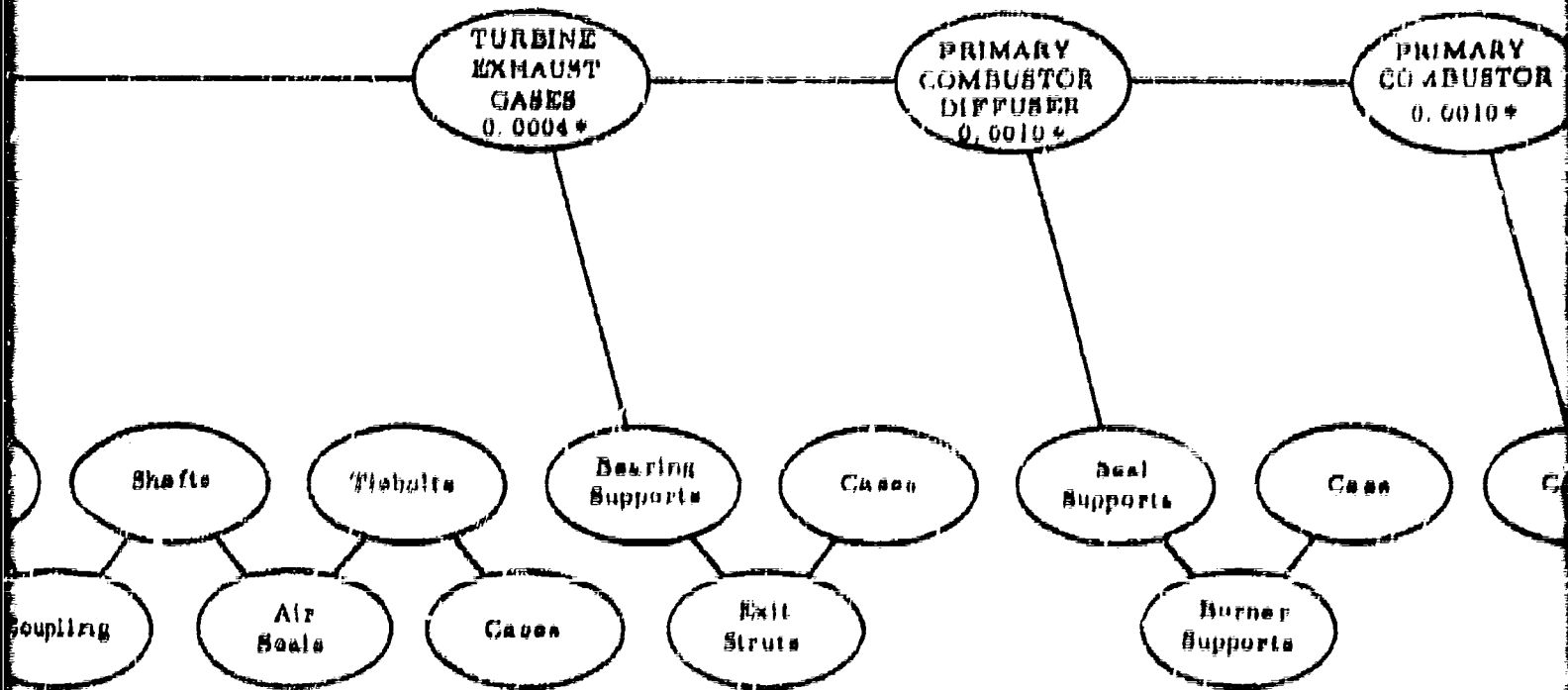
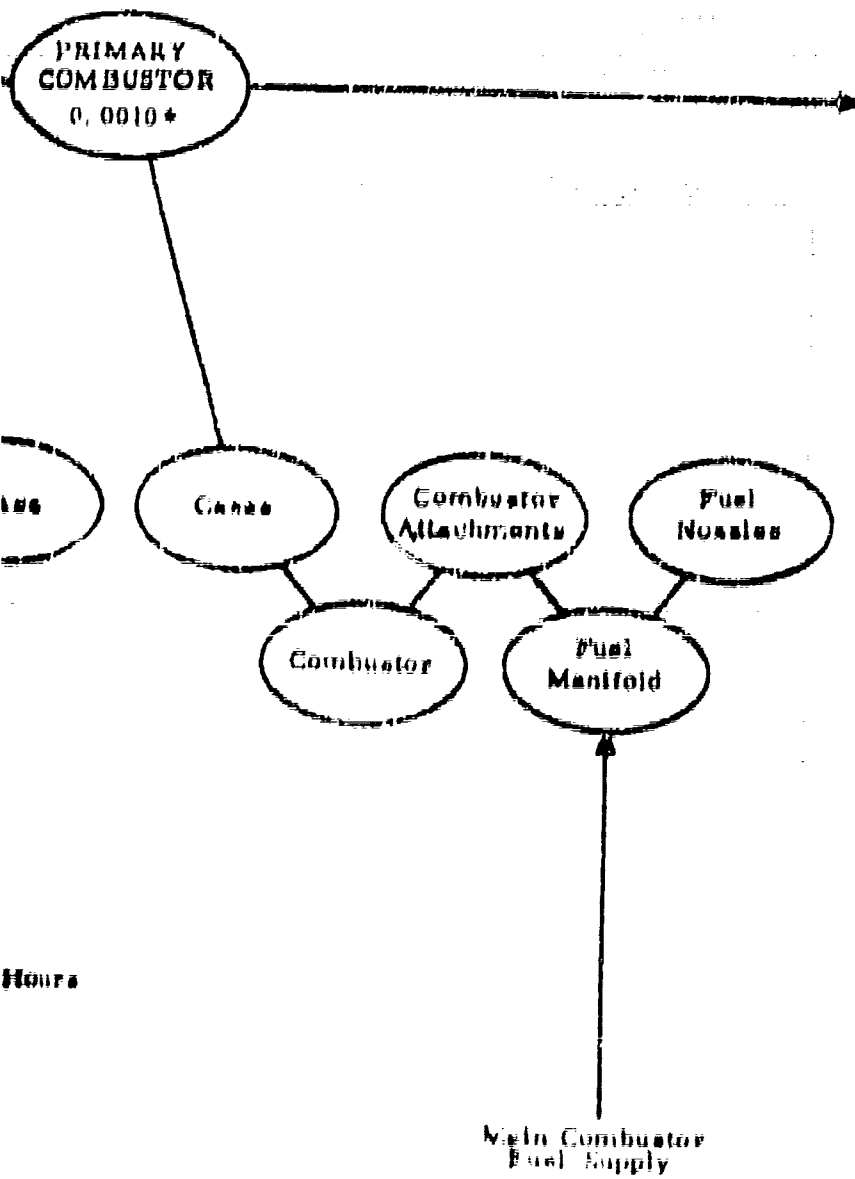


Figure III-S-3. JTF17A-20 Engine Reliability Mathematical Model,  
In-Flight Shutdown (Sheet 2)



\*Predicted Failures/1000 Hours





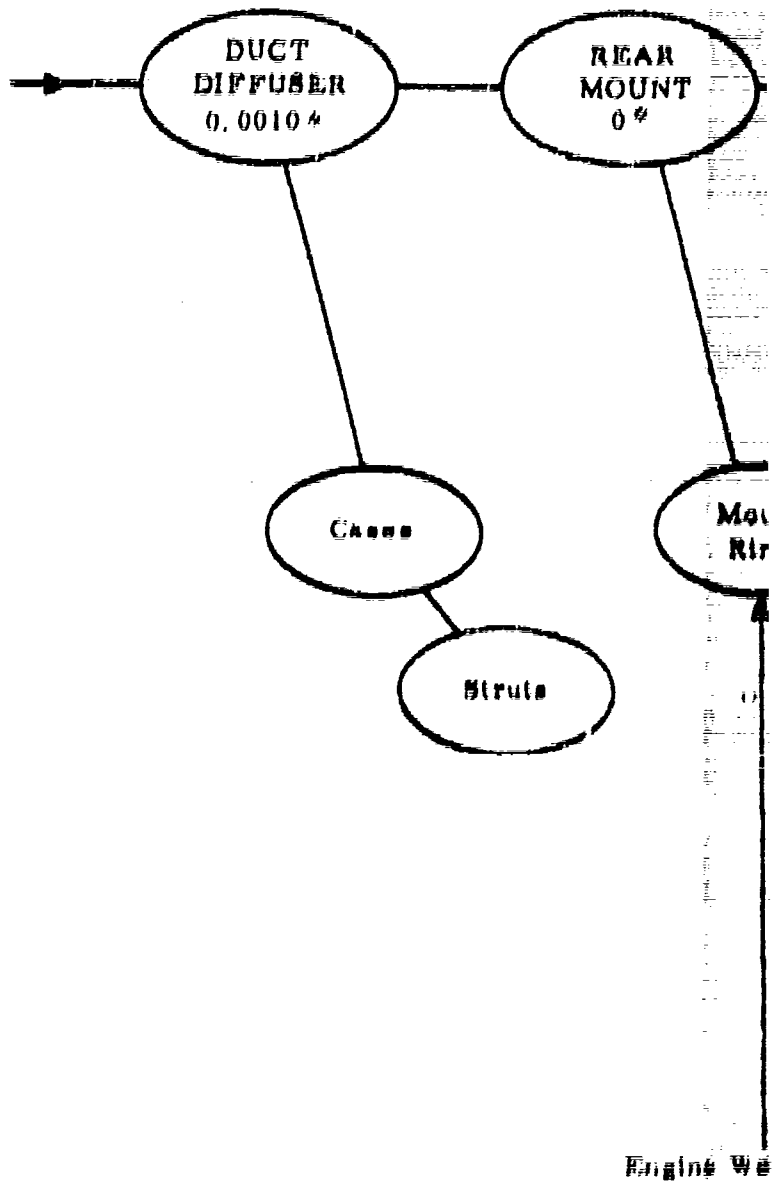
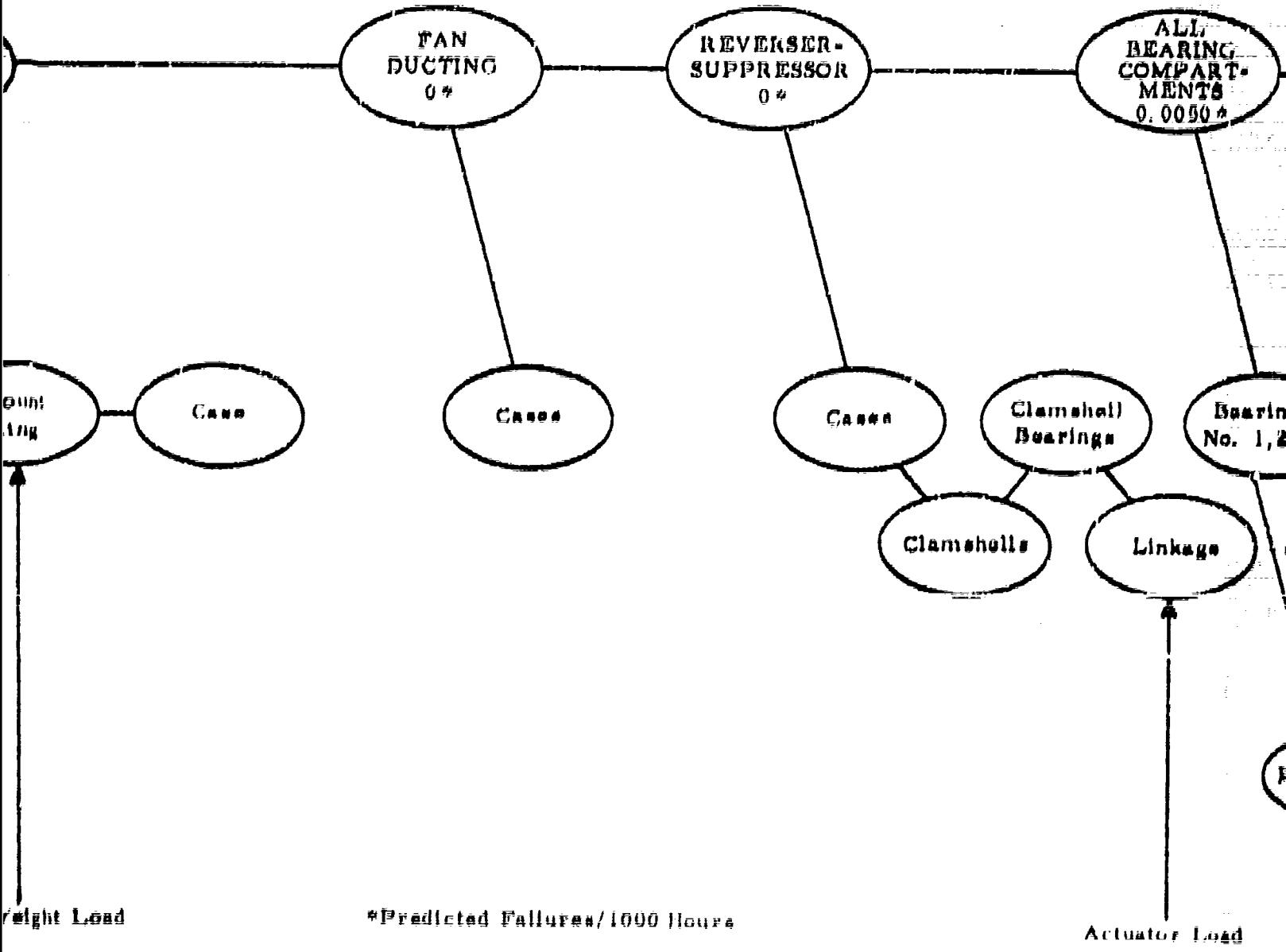
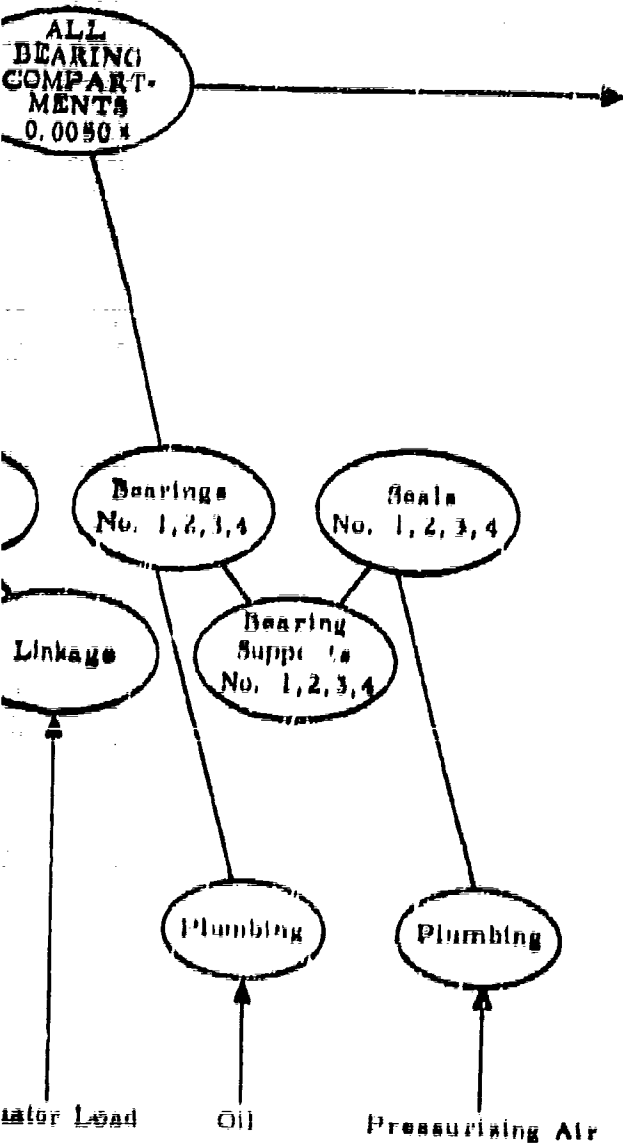


Figure 111-8-6, JTF17A-20 Engine Reliability Marking Model, In-Flight Shutdown (Sheet 3)





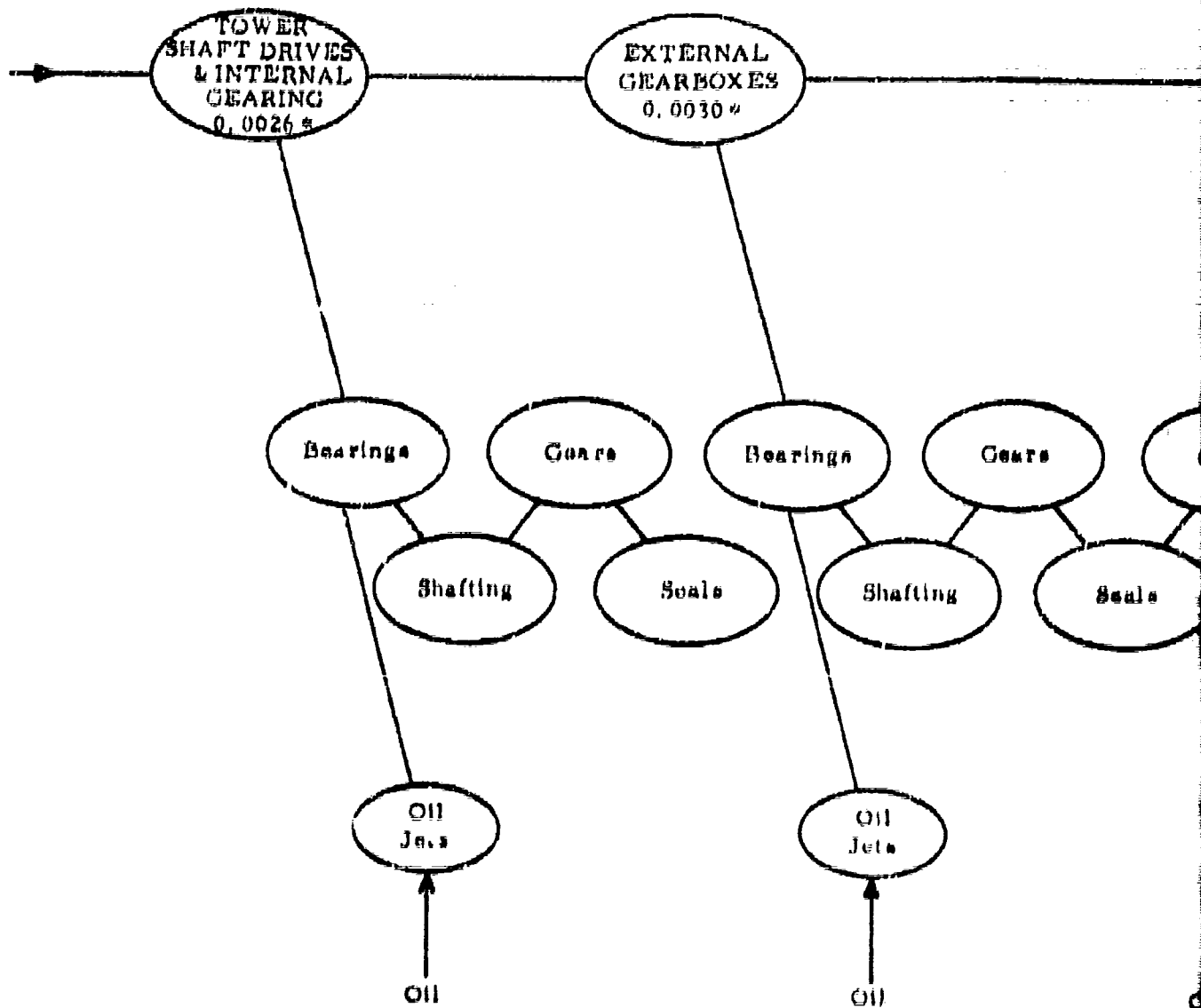
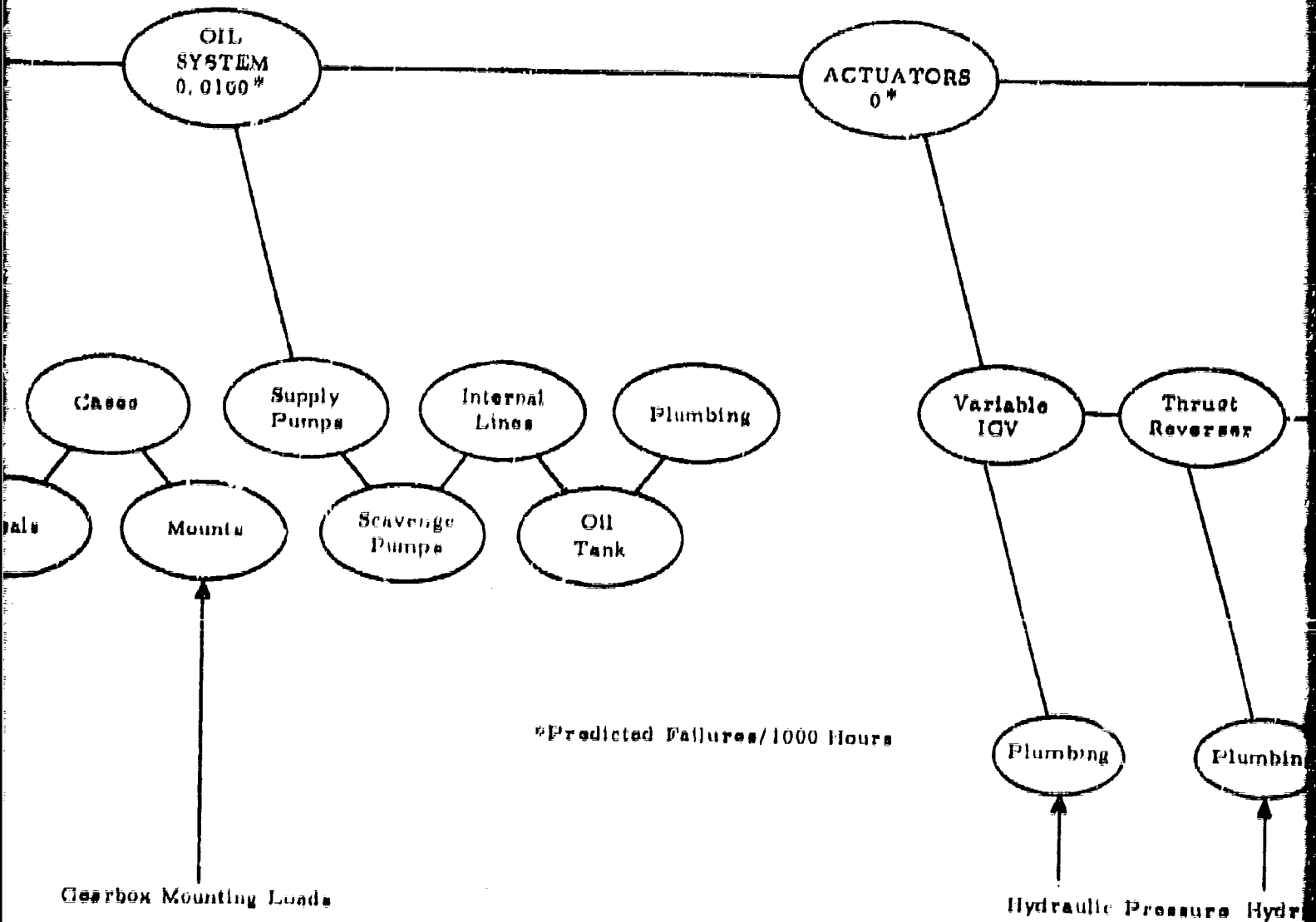
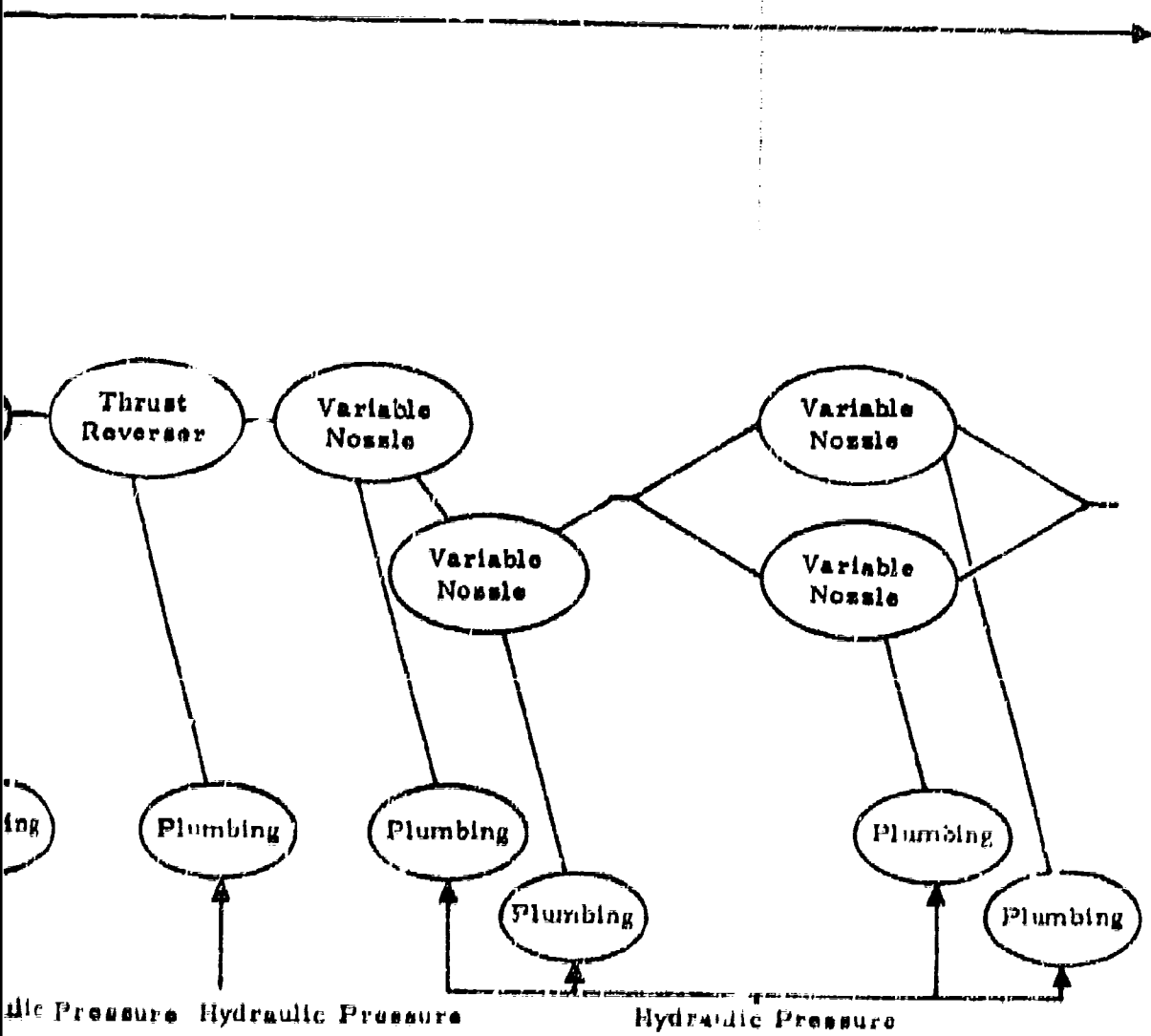


Figure III 5-5. JT17A-20 Engine Reliability Mathematical Model, In-Flight Shutdown (Sheet 4)

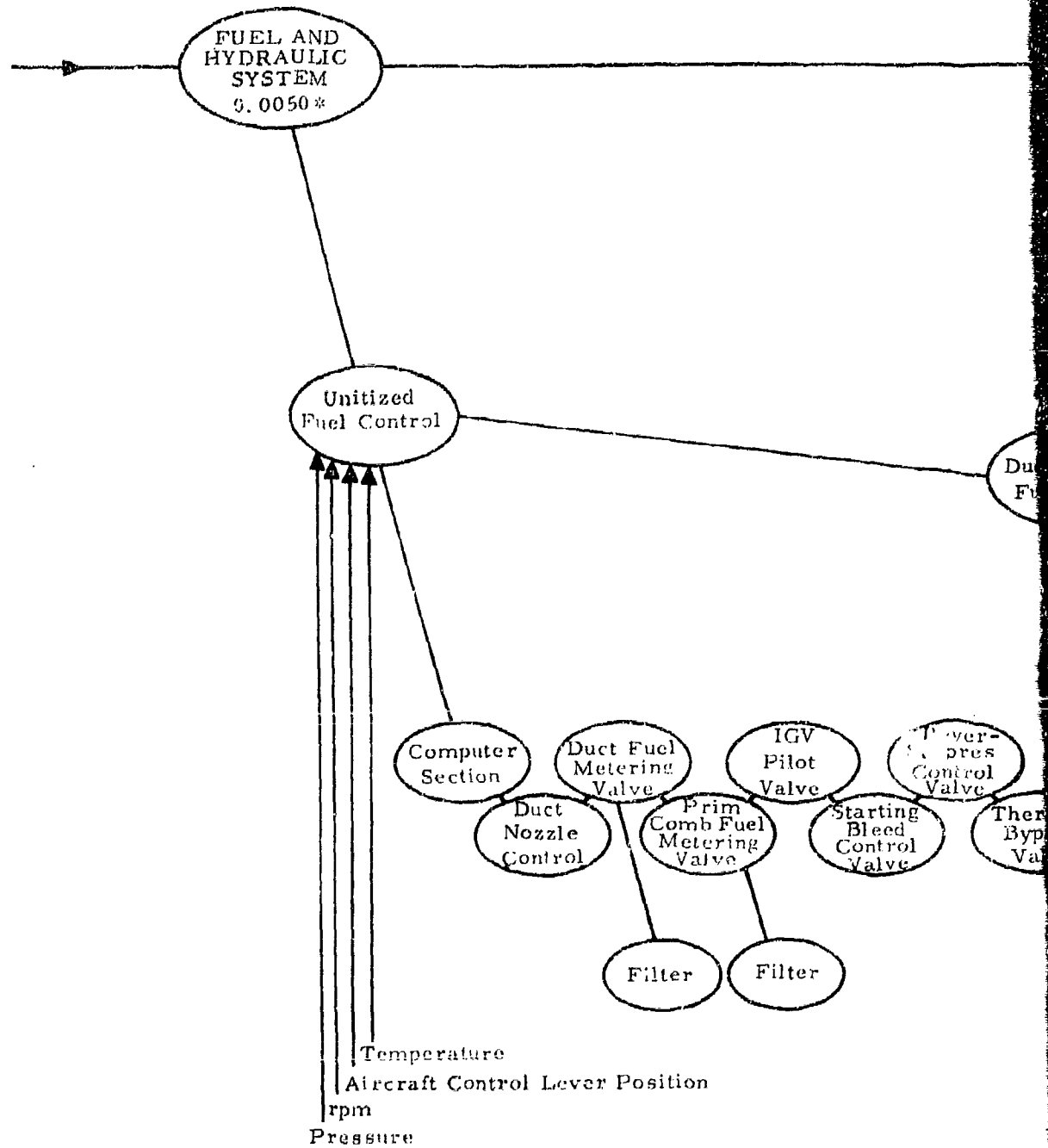




FD 15509

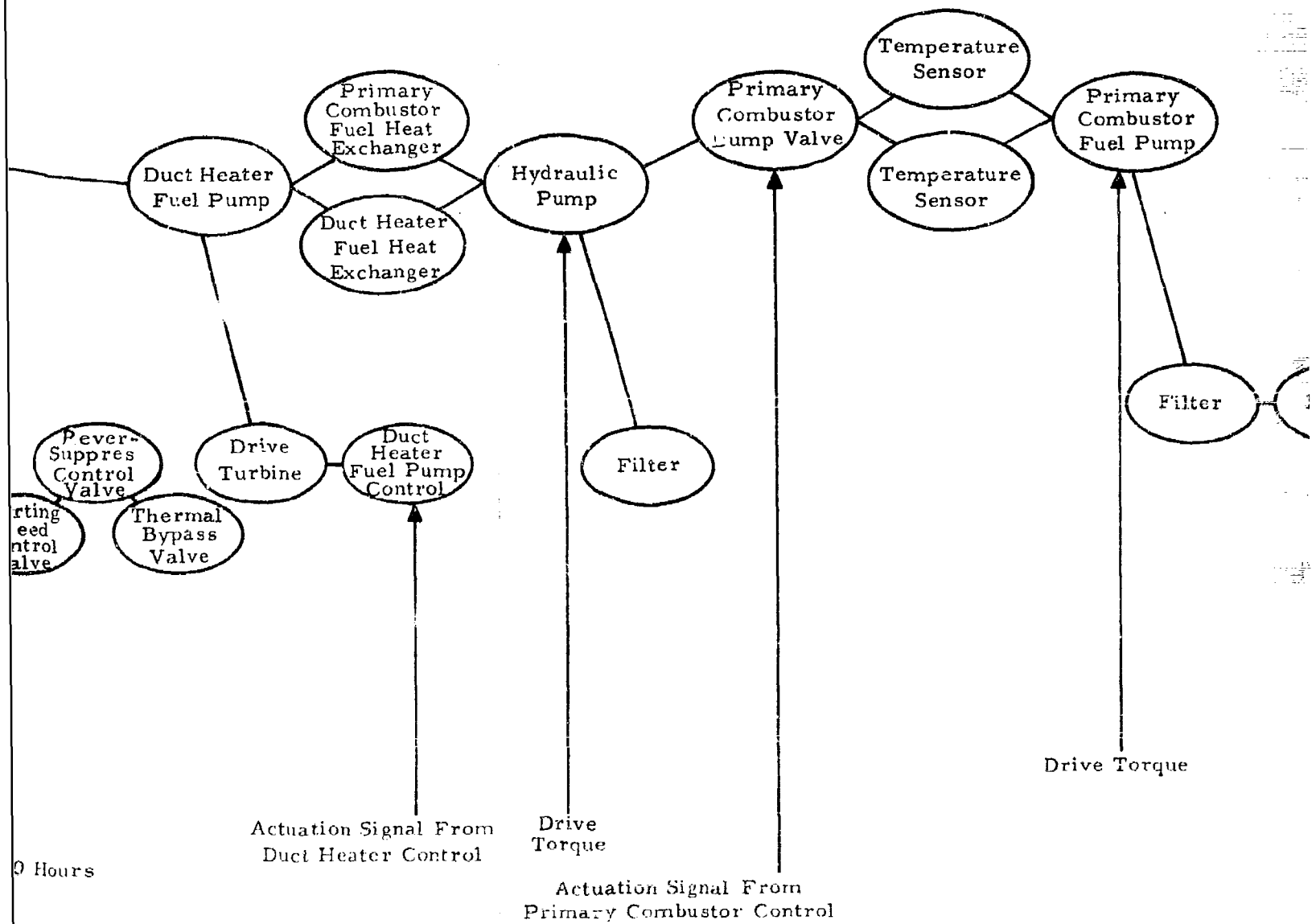
11-5-14

3



\*Predicted Failures/1000 Hours

Figure III-B-6. JT17A-20 Engine Reliability Mathematical Model,  
In-Flight Shutdown (Sheet 5)





ENGINE  
PLUMBING  
0.0003\*

Primary  
Combustor  
Fuel Pump

Filter

Filter

Torque

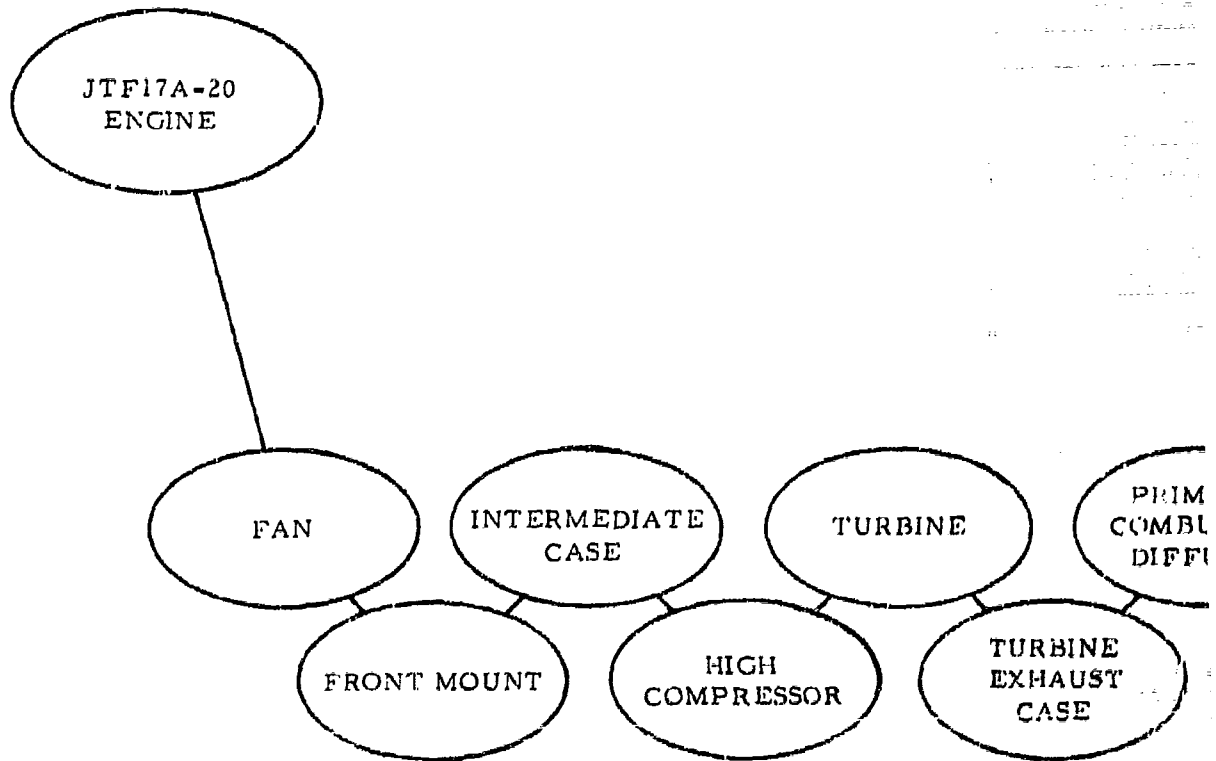
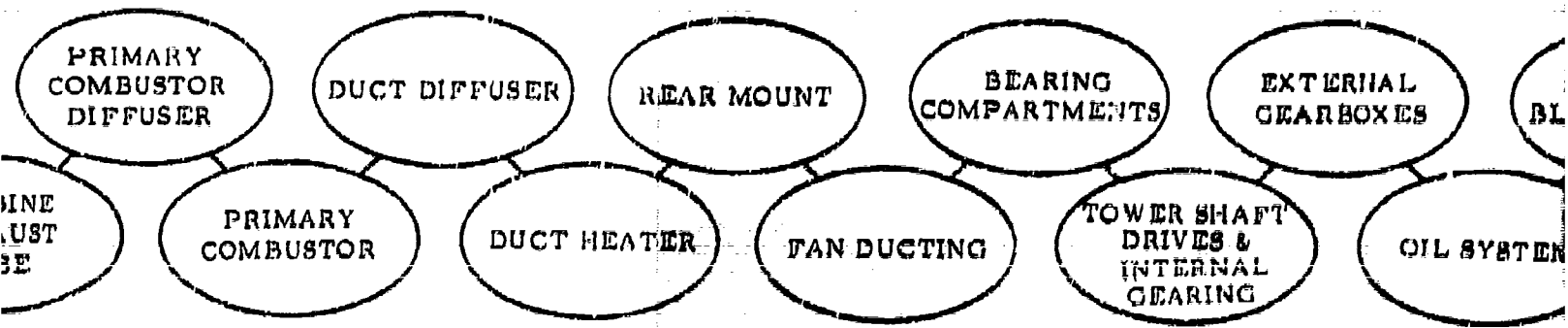
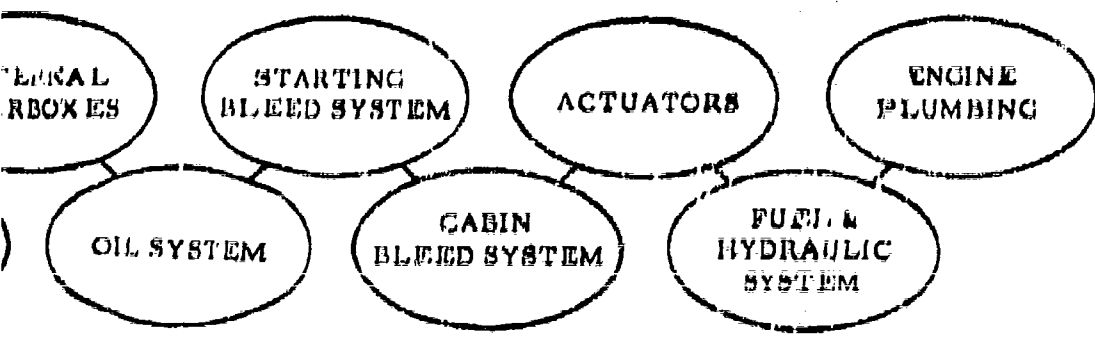


Figure III-S-7. JTF17A-20 Engine Reliability Mathematical Model, First Level Block Diagram (Premature Engine Removal)





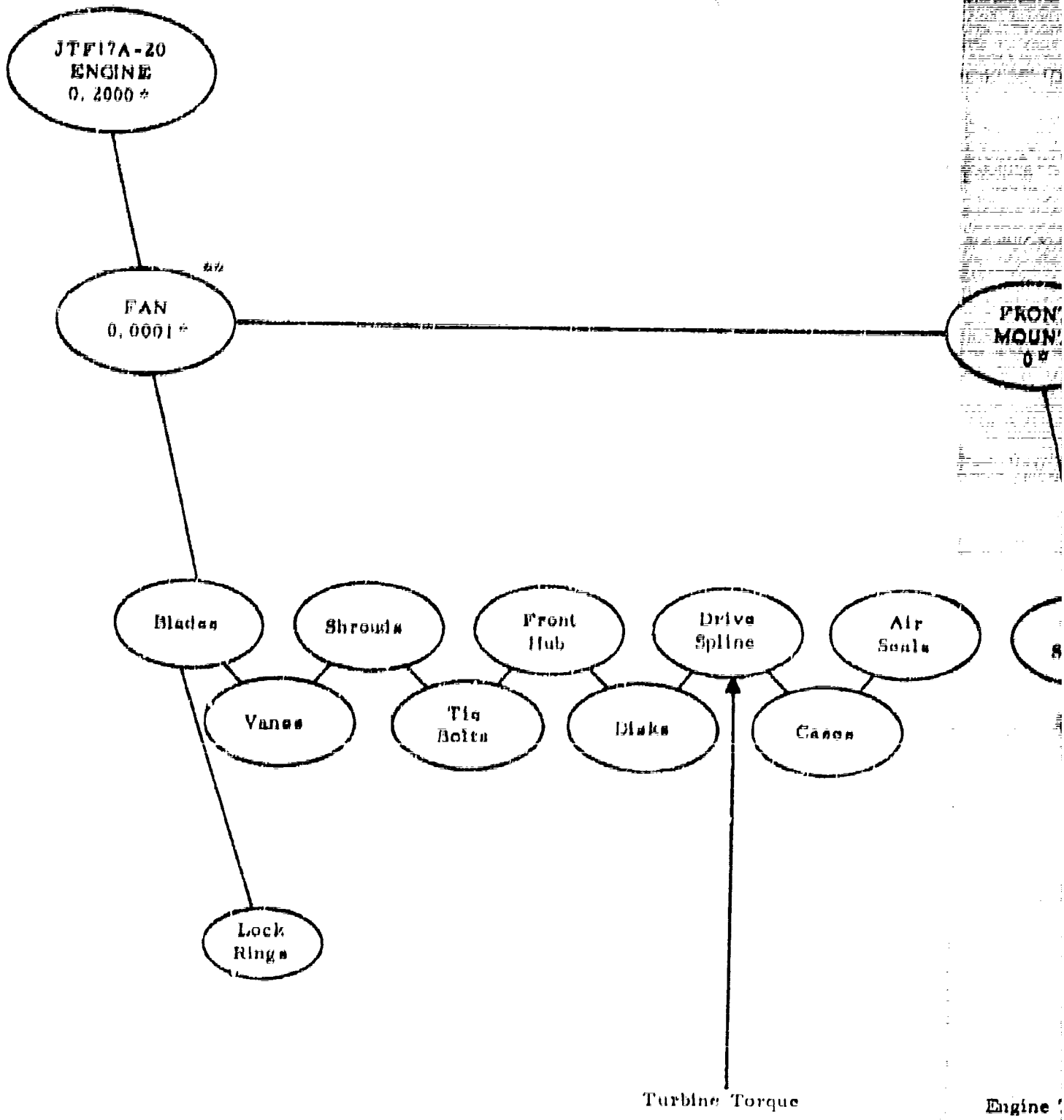
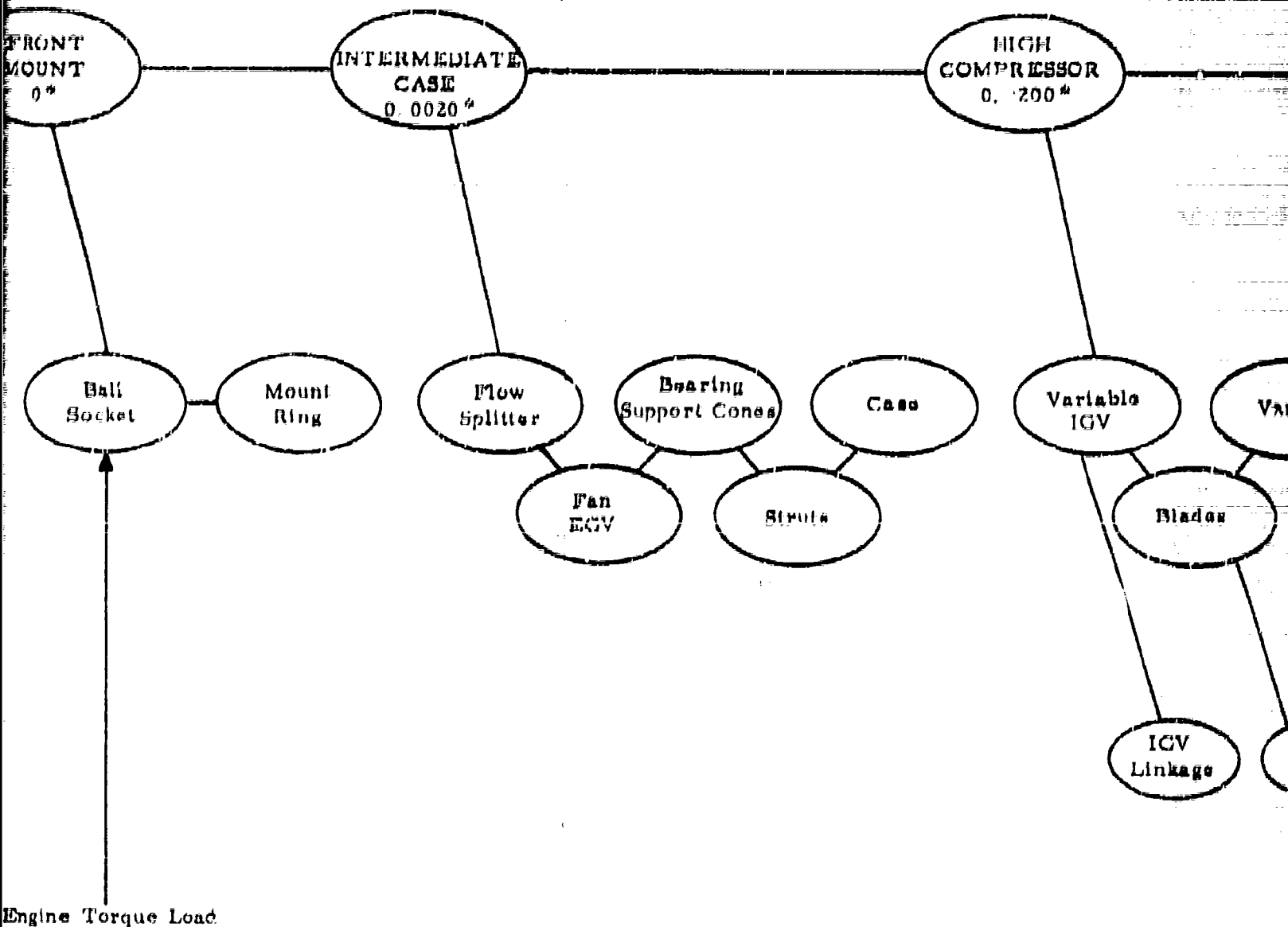
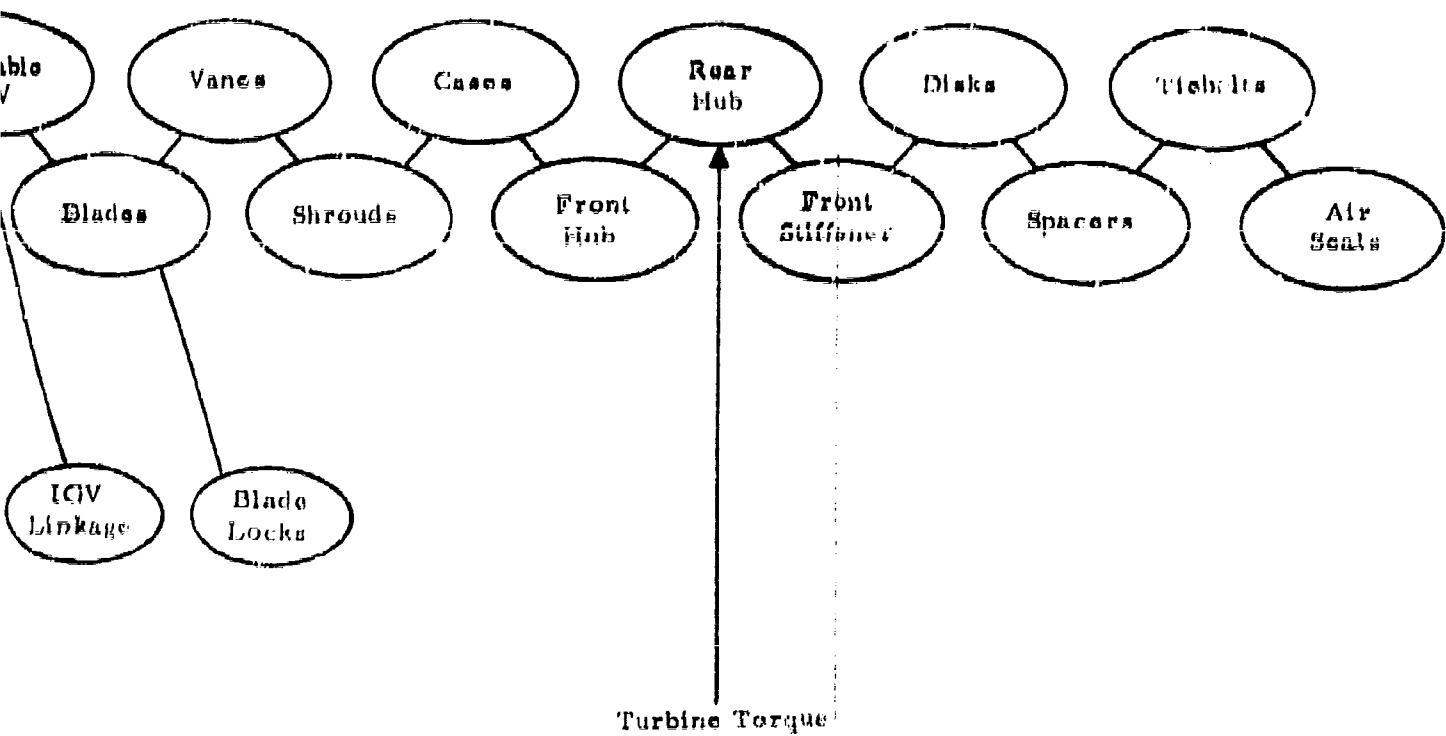


Figure III-9-8. JTF17A-20 Engine Reliability Mathematical Model,  
Premature Engine Removal (Sheet 1)



\*Predicted Failures/1000 Hours

\*\* Subsystem Components are Replaceable with Engine Removal



ours  
Replaceable

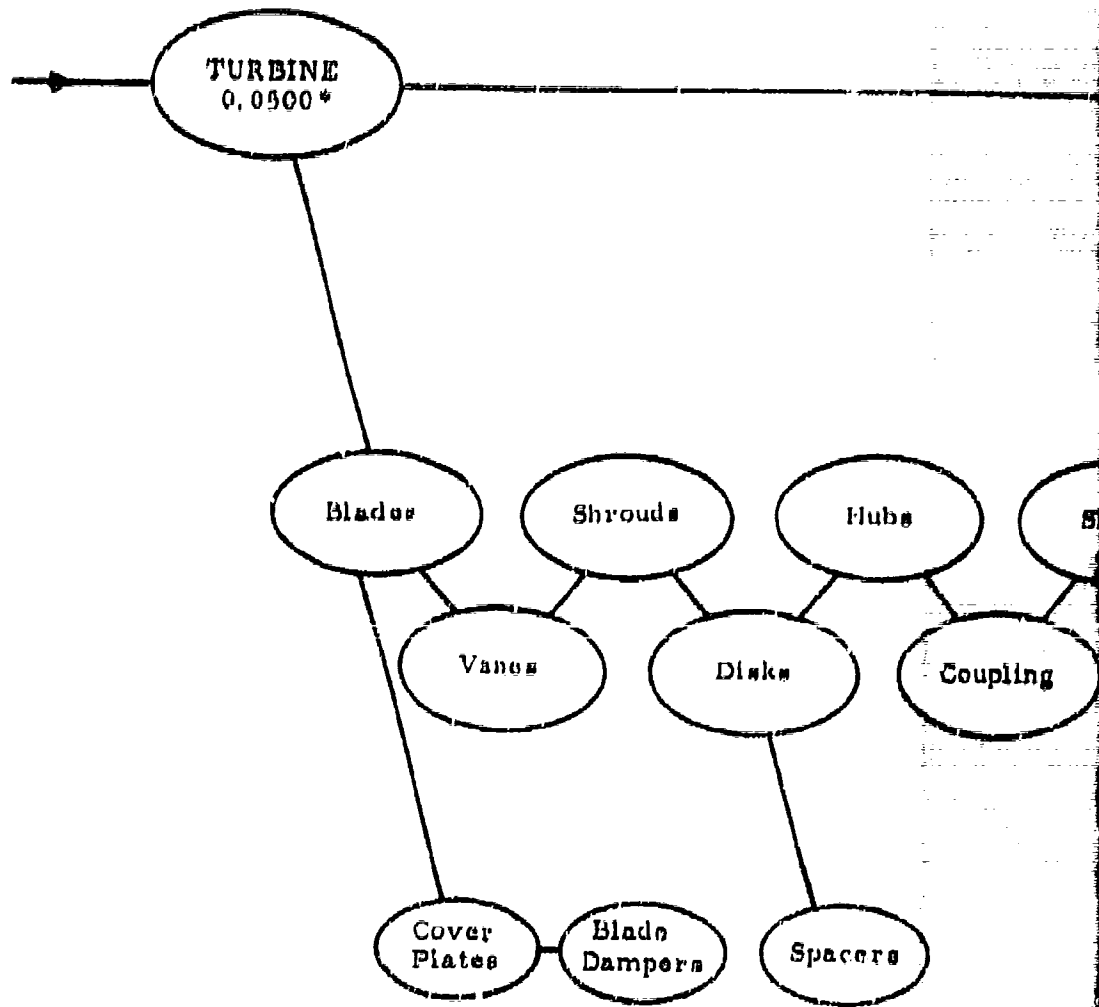
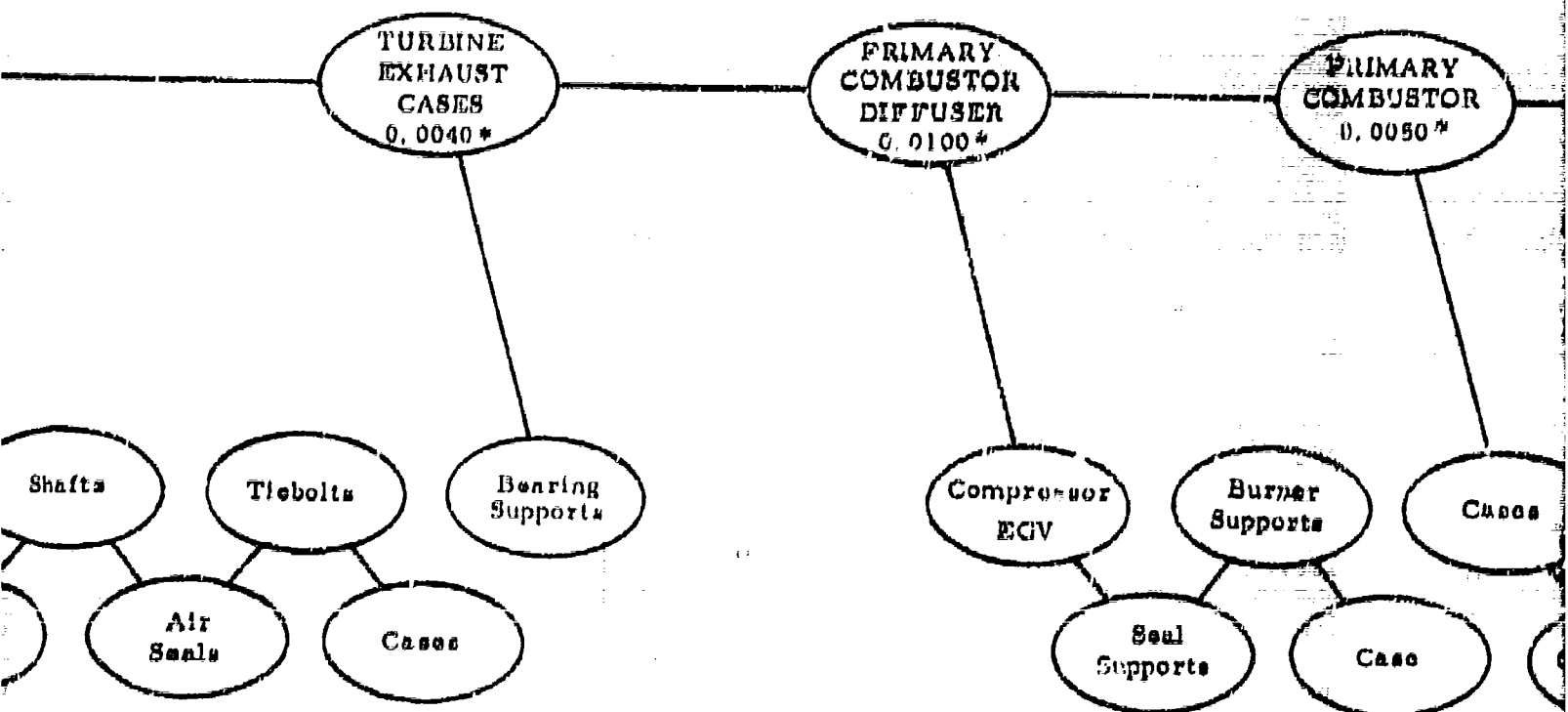
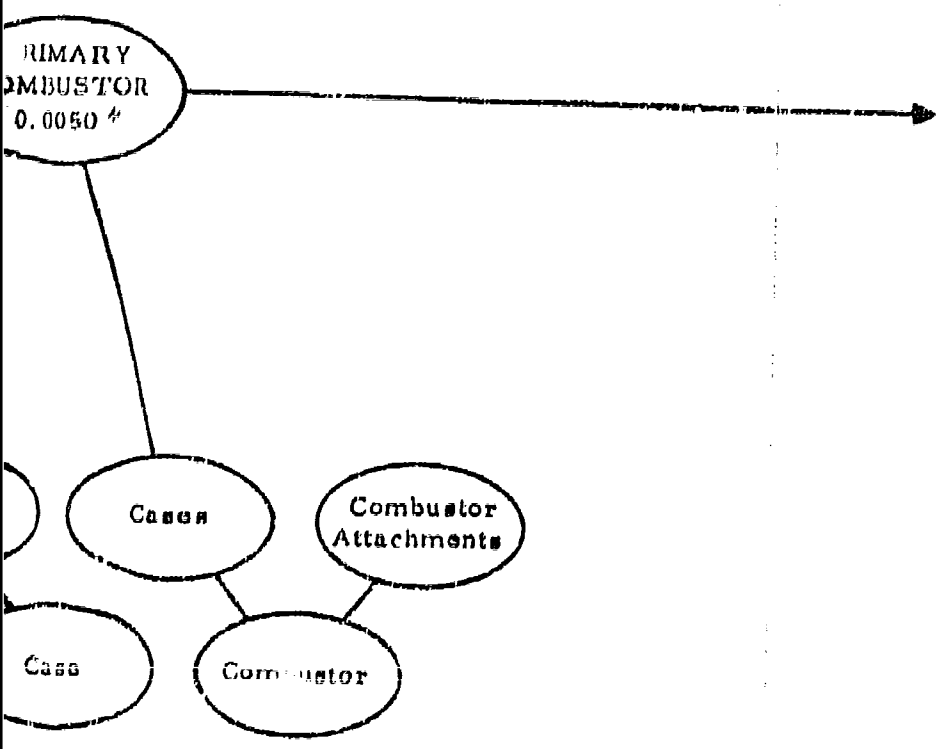


Figure VII-8-9. JTF17A-20 Engine Reliability Mathematical Model,  
Premature Engine Removal (Sheet 2)





\*Predicted Failures/1000 Hours



FD 15529

III-S-18

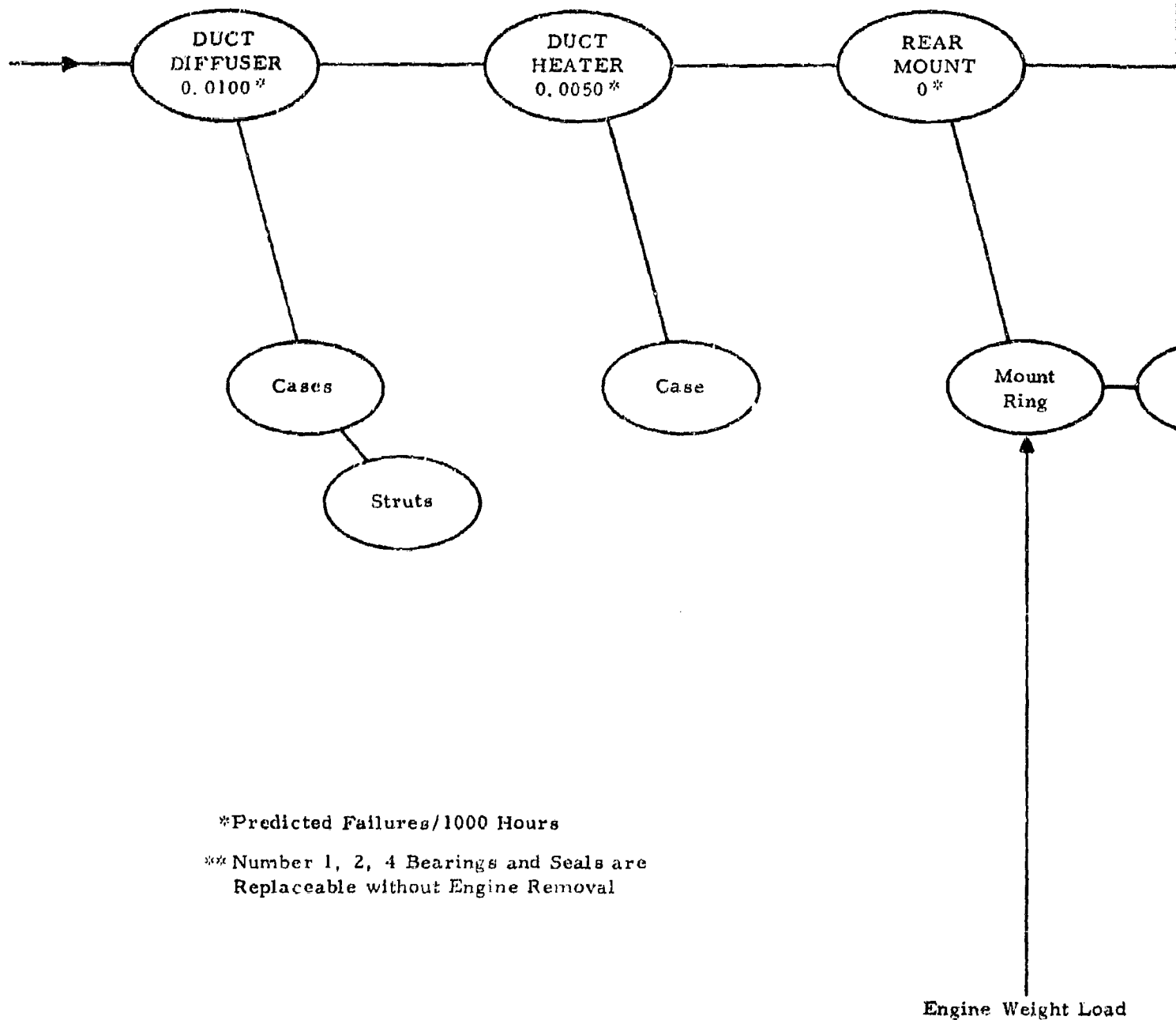
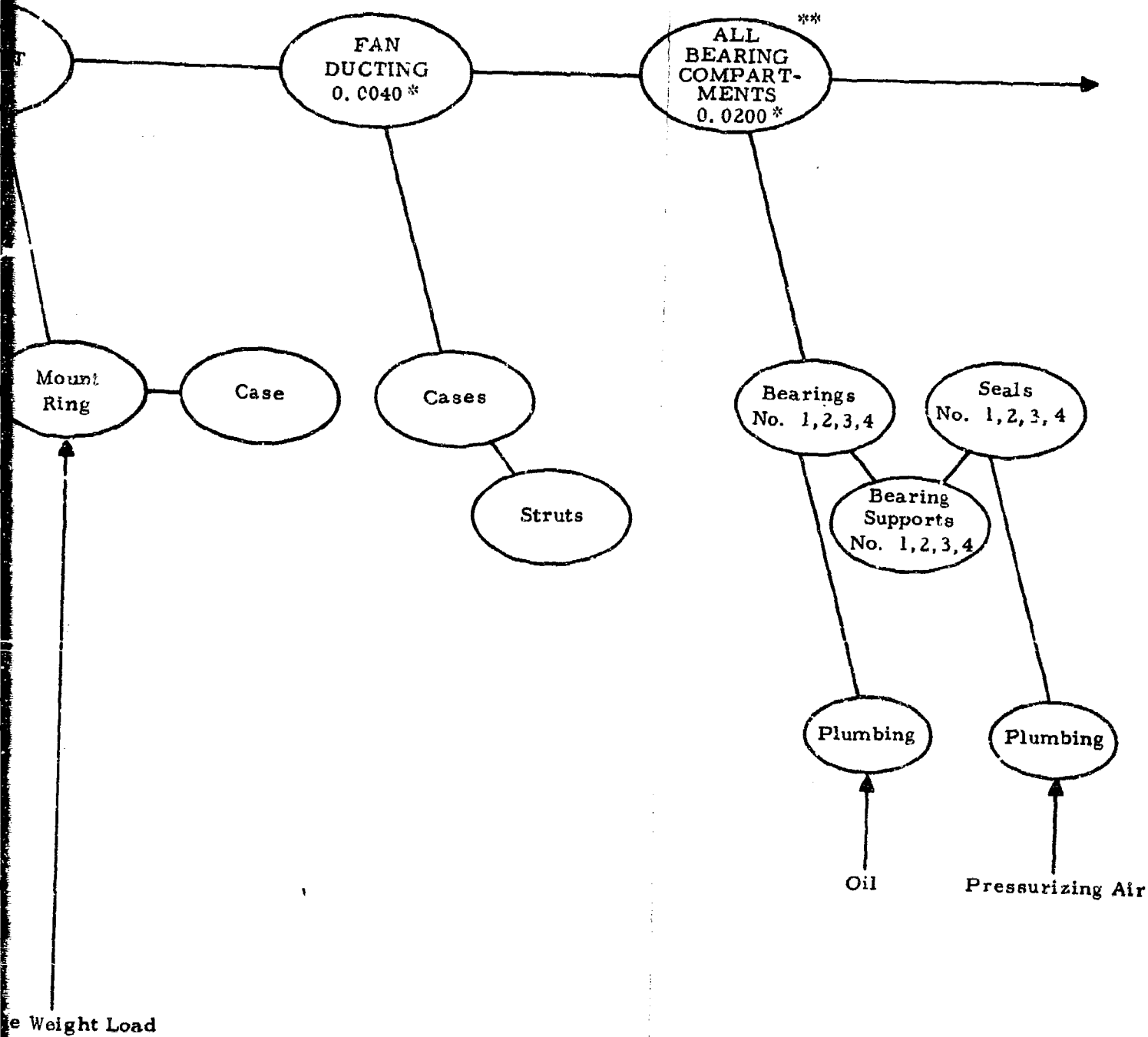


Figure III-S-10. JTF17A-20 Engine Reliability Mathematical Model,  
Premature Engine Removal (Sheet 3)



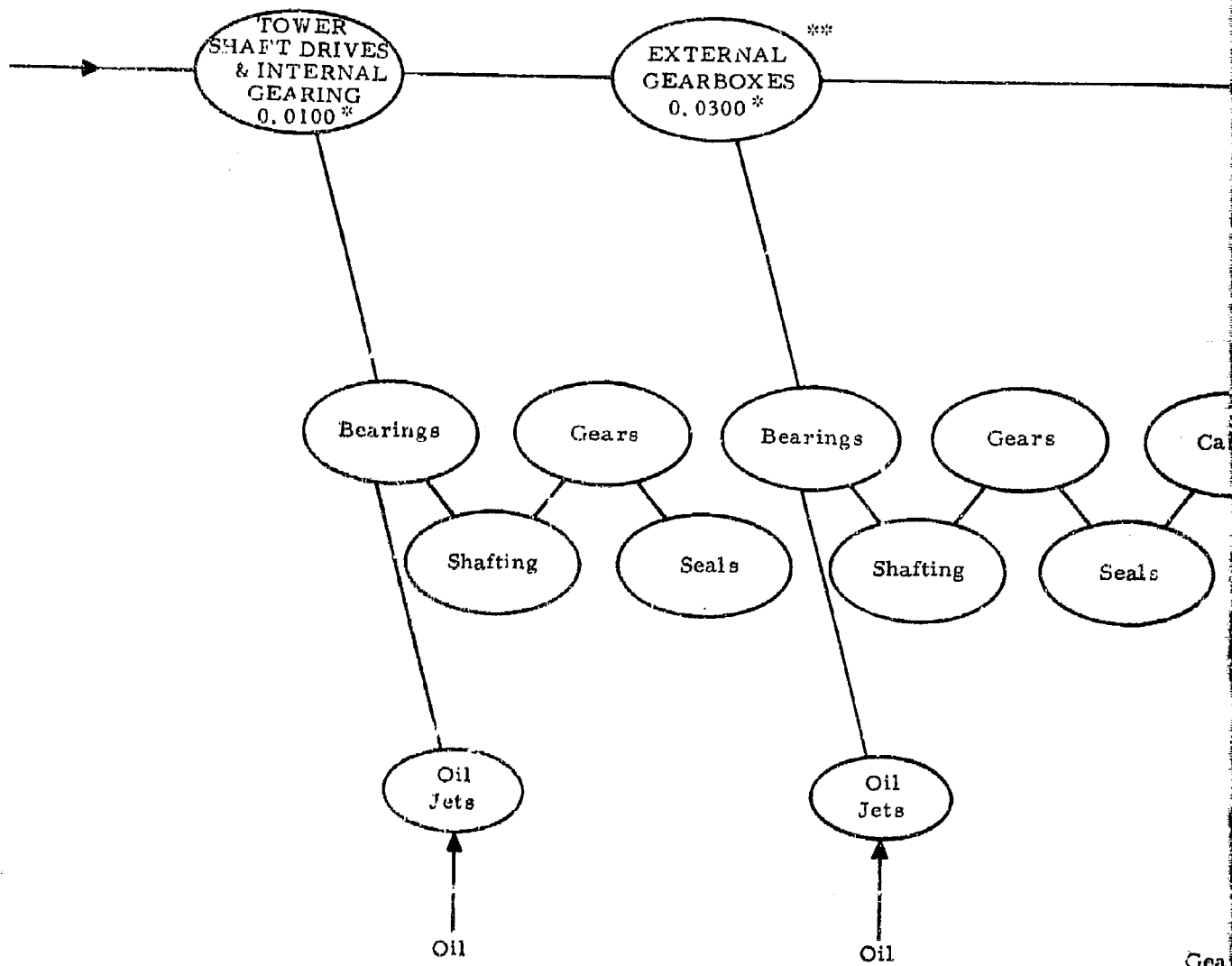
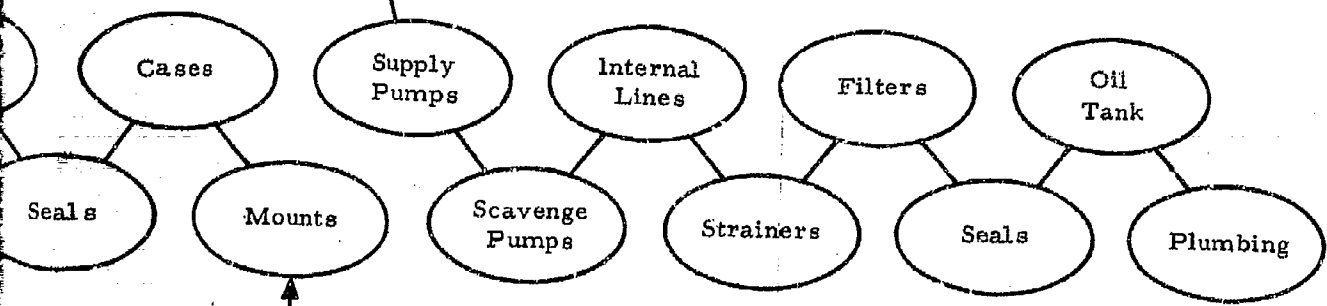
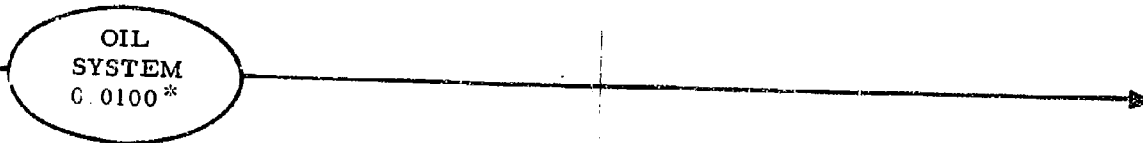


Figure III-8-11. JTF17A-20 Engine Reliability Mathematical Model, Premature Engine Removal (Sheet 4)



\*Predicted Failures/1000 Hours  
\*\*Subsystem Components are Replaceable  
without Engine Removal

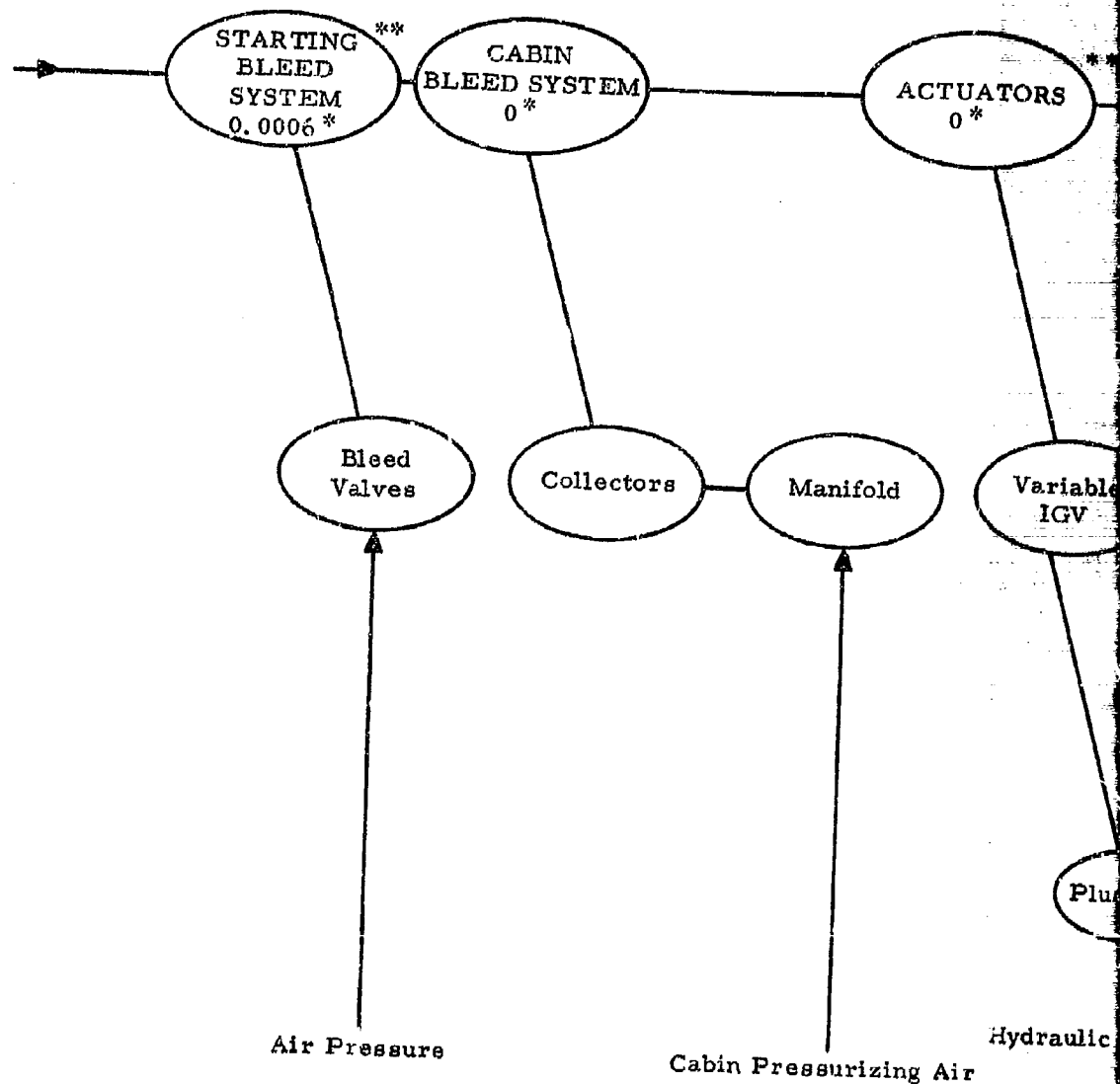
Gearbox Mounting Loads

An arrow points from this text up to the 'Mounts' node in the diagram.

FD 15532

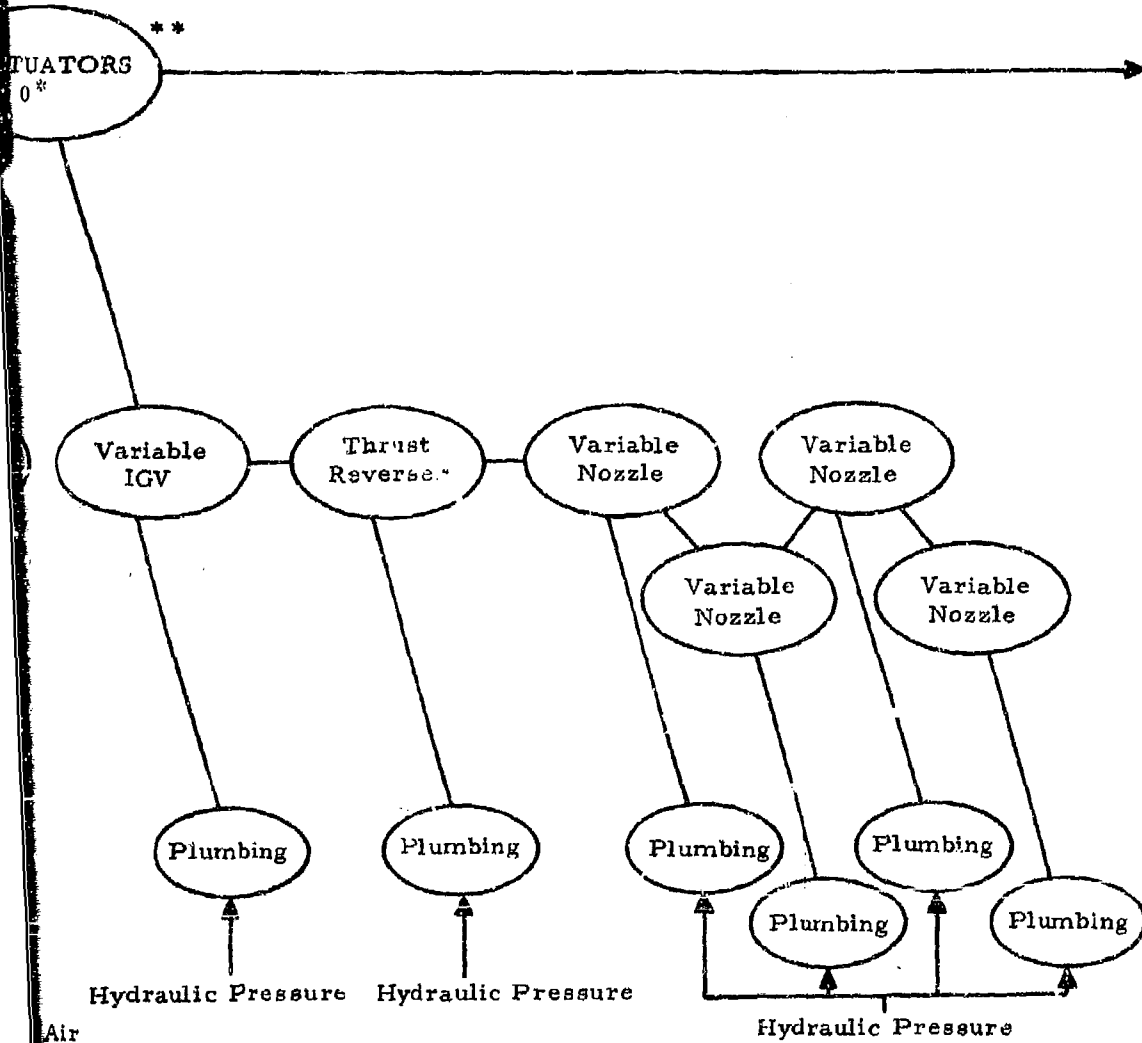
111-8-20

2



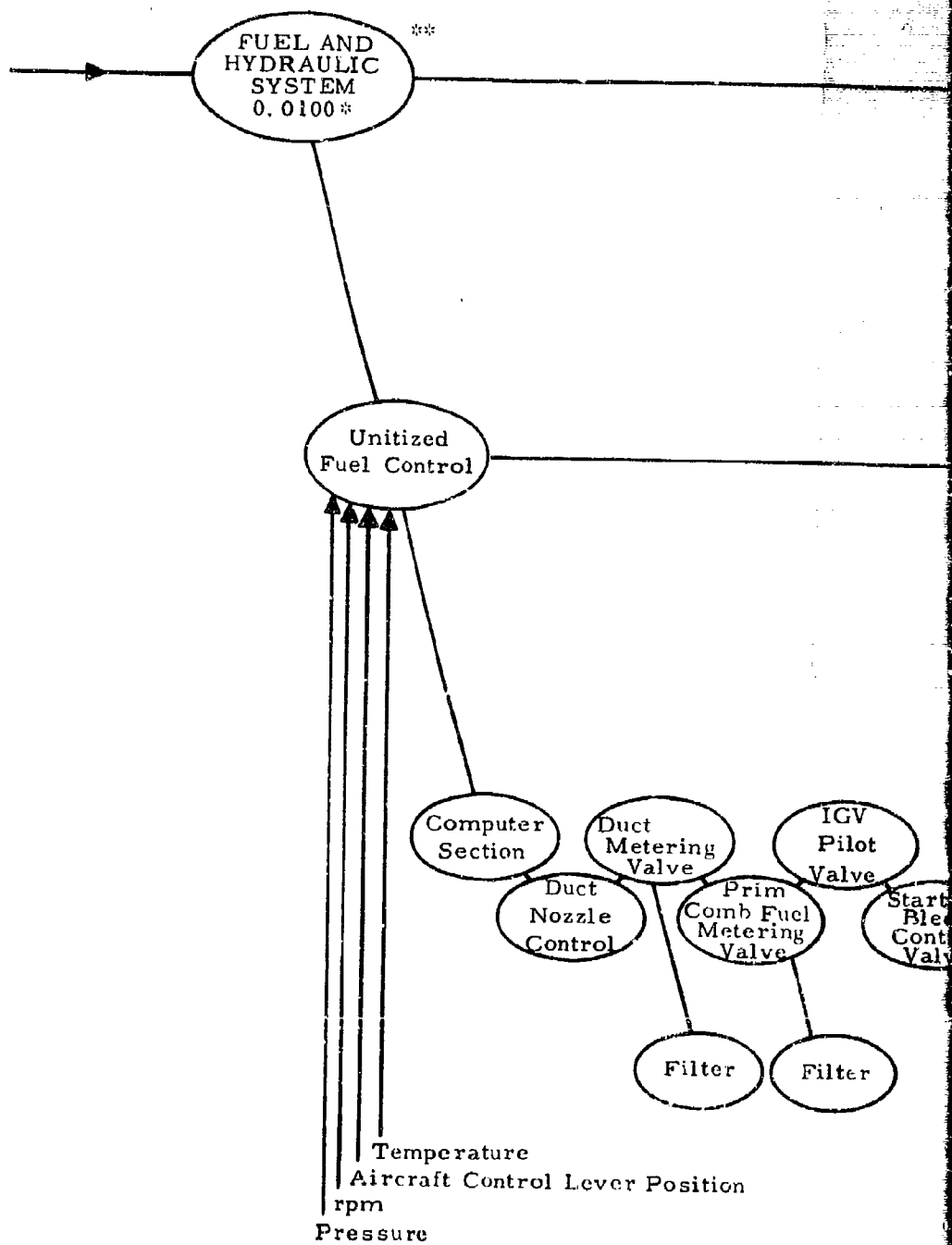
\* Predicted Failures/1000 Hours  
 \*\* Subsystem Components are Replaced without Engine Removal

Figure III-S-12. JTF17A-20 Engine Reliability Mathematical Model, Premature Engine Removal (Sheet 5)



Air  
1000 Hours  
Parts are Replaceable  
Level





\* Predicted Failures/1000 Hours  
 \*\* Sub System Components Are Rated Without Engine Removal

Figure III-S-13. JTF17A-20 Engine Reliability Mathematical Model, Premature Engine Removal (Sheet 6)

ENGINE  
PLUMBING  
0.0003 \*

Primary  
Combustor  
Fuel Pump

Filter

IGV  
Pilot  
Valve

Rever-  
Suppres  
Control  
Valve

Starting  
Bleed  
Control  
Valve

Thermal  
Bypass  
Valve

im  
Fuel  
ring  
Valve

Filter

Drive  
Torque

ures/1000 Hours  
omponents Are Replaceable  
he Removal

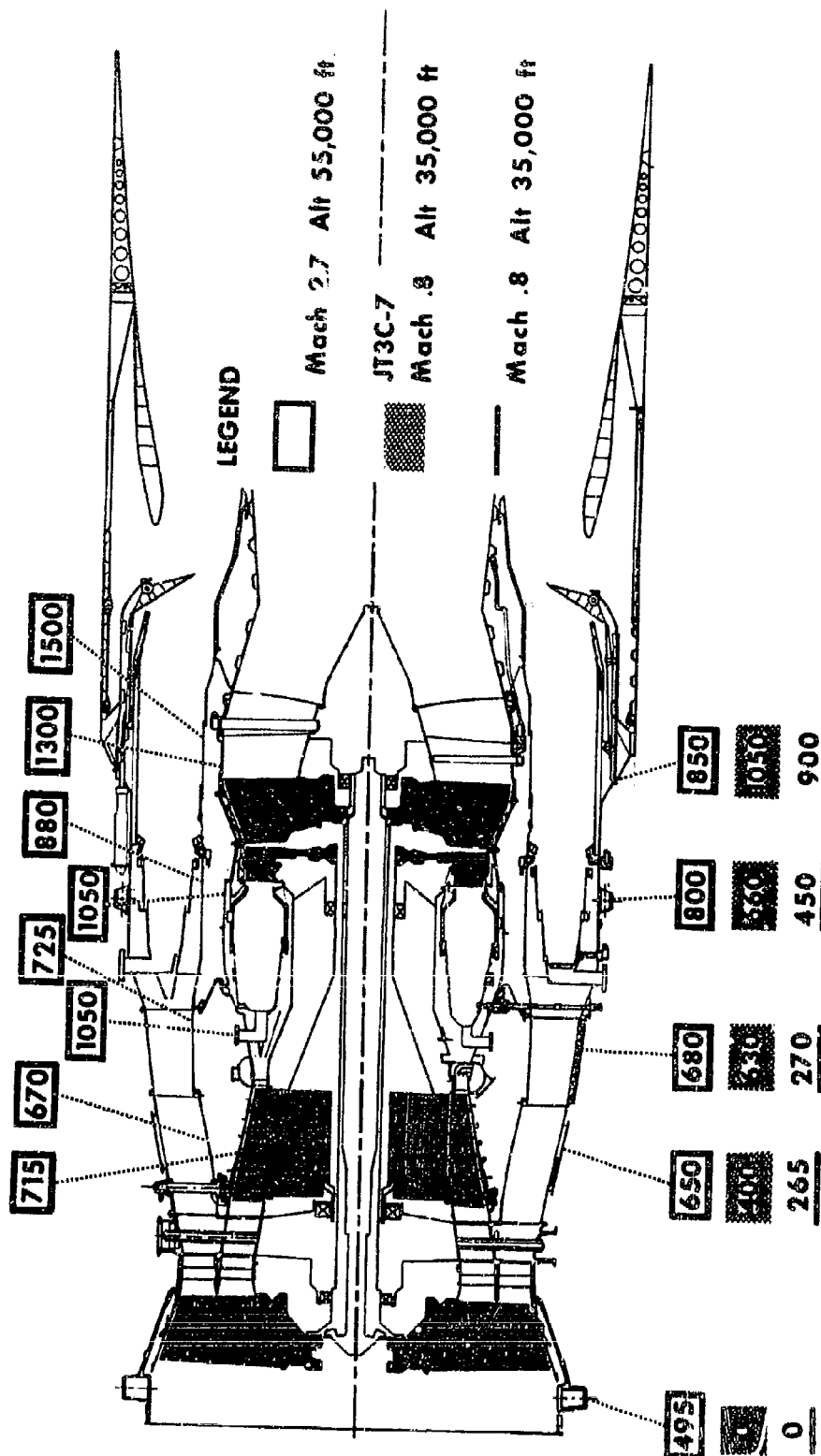
FD 15567

111-S-22

2

CONFIDENTIAL

Pratt & Whitney Aircraft  
PWA FR-1855



111-S-23

CONFIDENTIAL

Figure 111-S-14. JT3C-7 Engine Case Temperatures

GS 2301

FD 15607

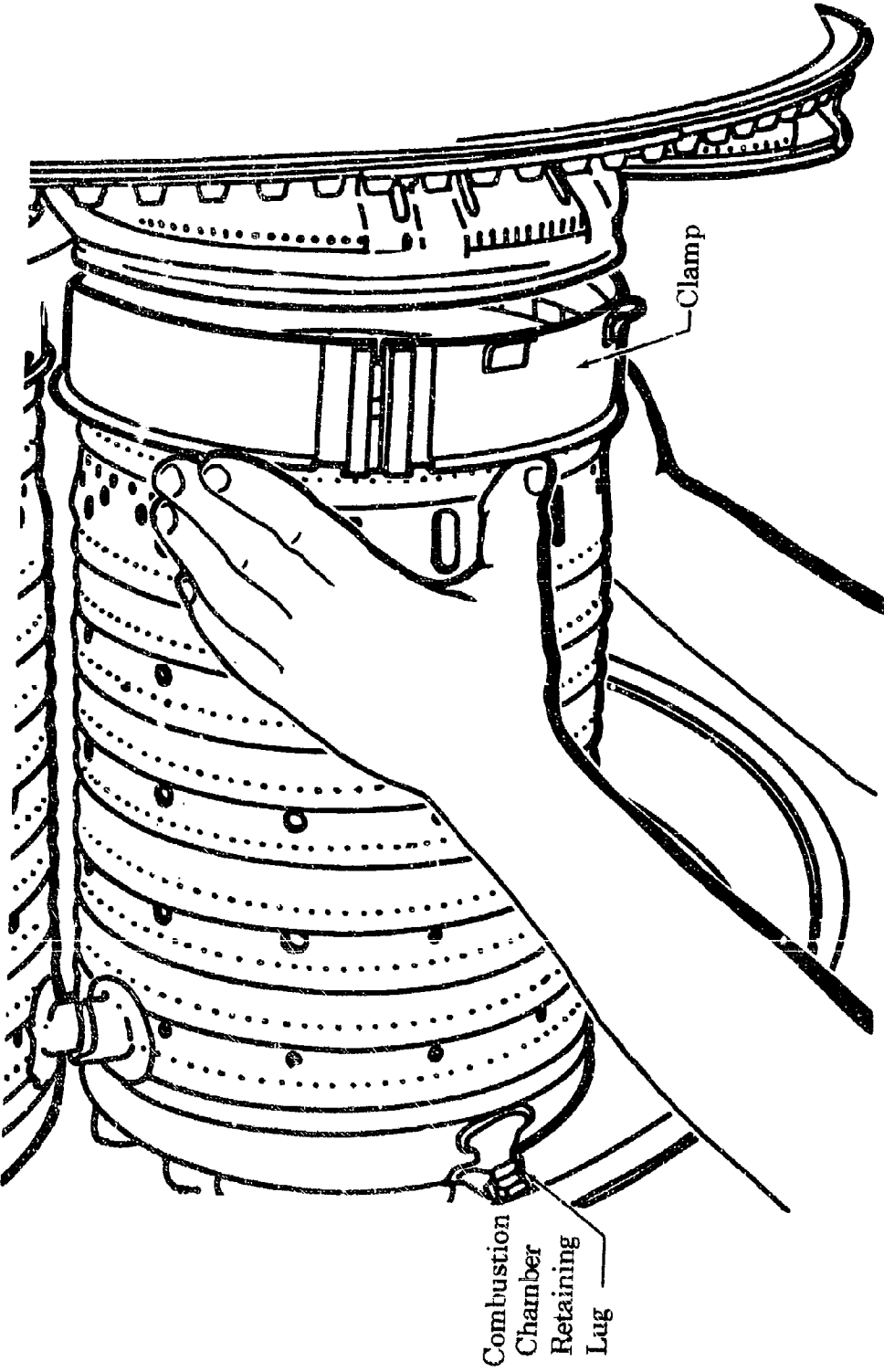
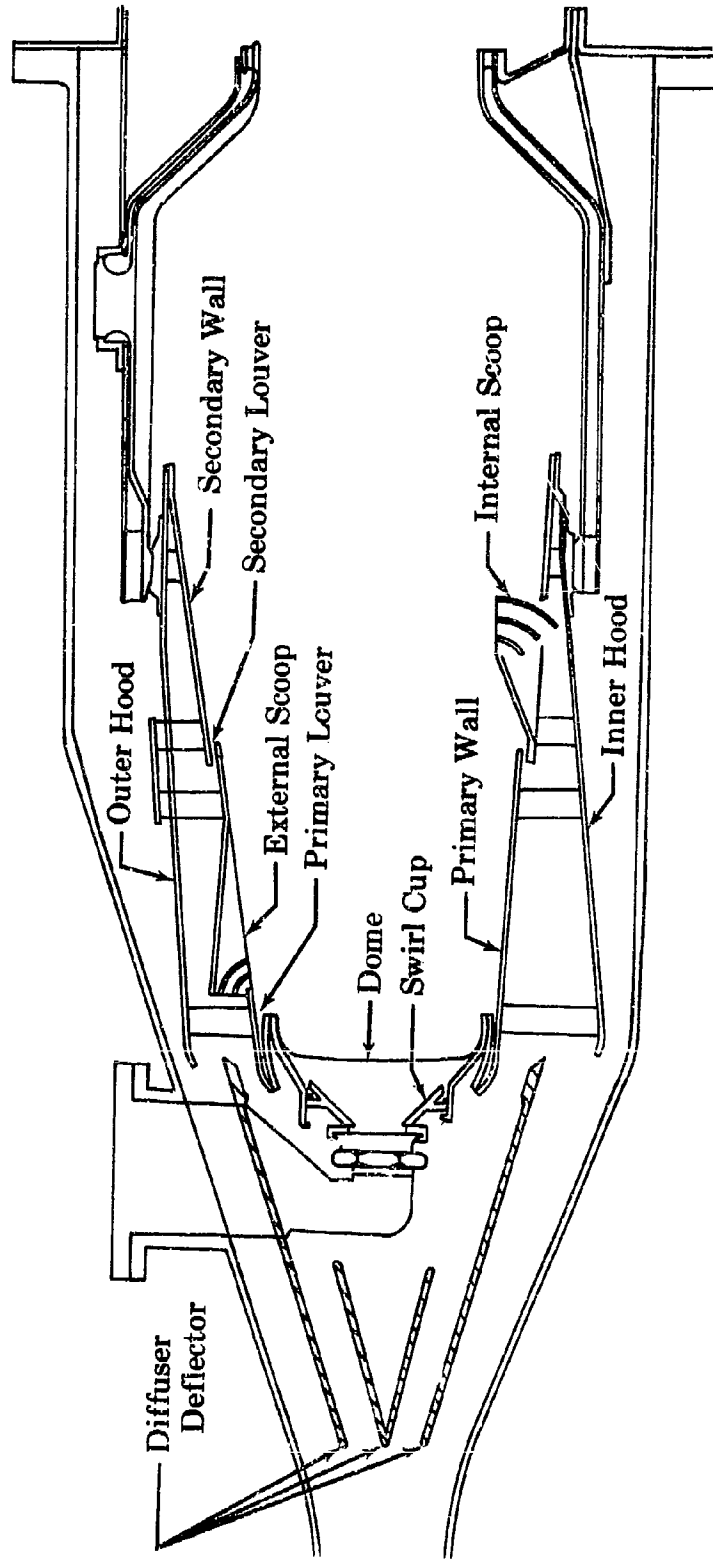


Figure III-S-15. JT3C-7 Installation of Burner Cans

CONFIDENTIAL

Pratt & Whitney Aircraft  
FWA FR-1855



III-S-25

CONFIDENTIAL

Figure III-S-16. JTF17A-20 Primary Combustor

FD 14833

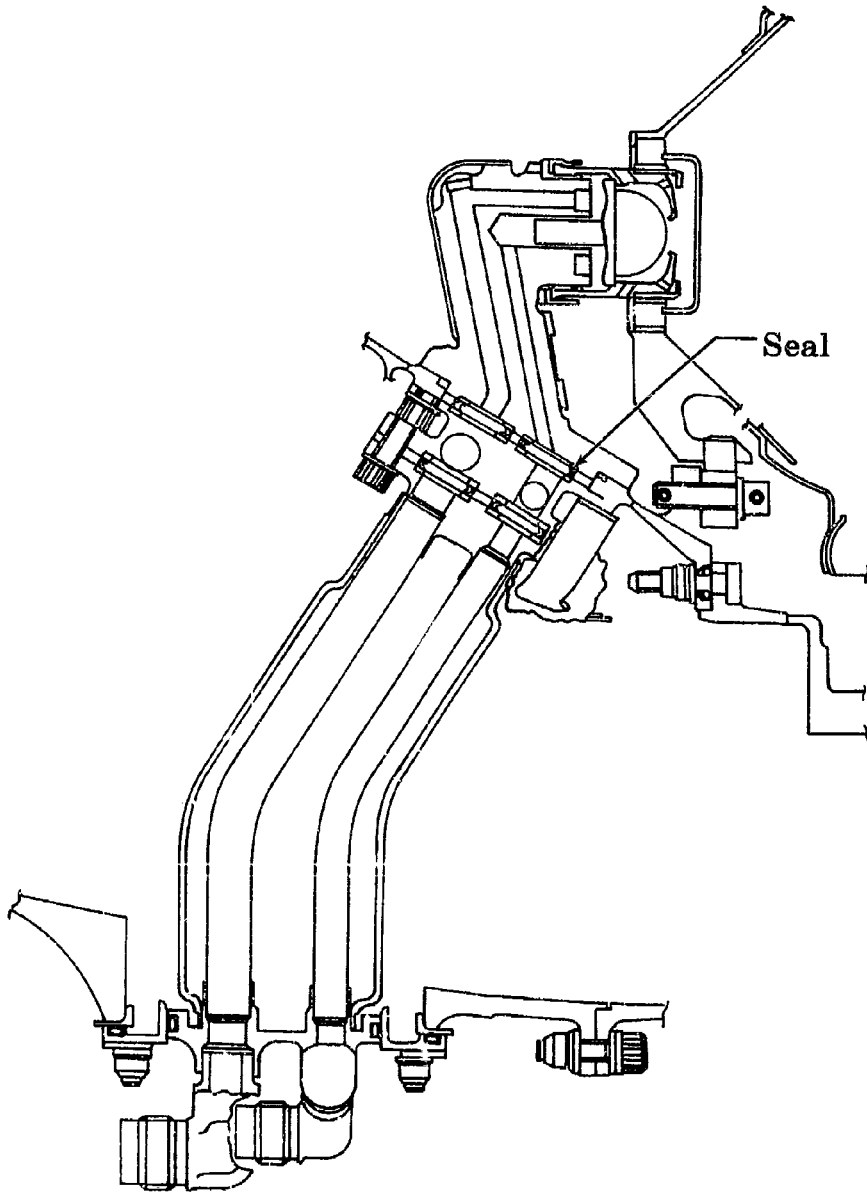


Figure III-S-17. JT8D Nozzle Assembly

FD 15606

III-S-26

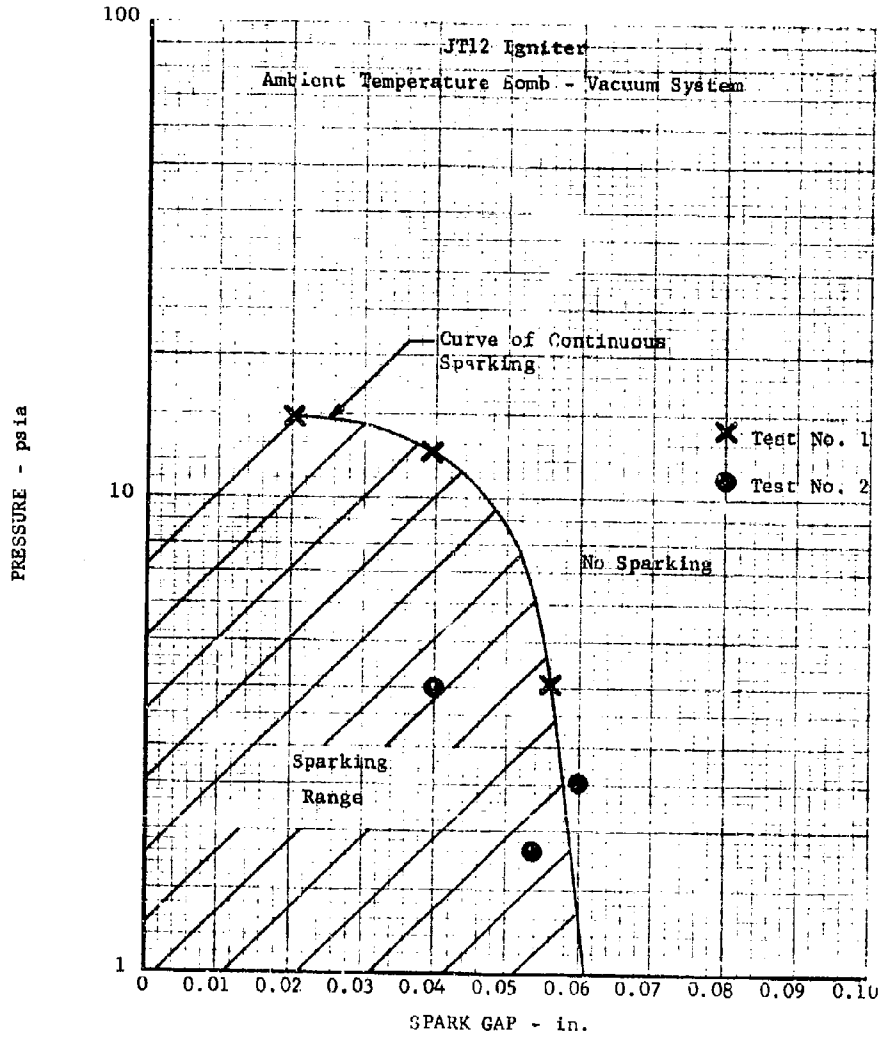


Figure III-S-18. Spark Ignition Point

DF 47186

III-S-27

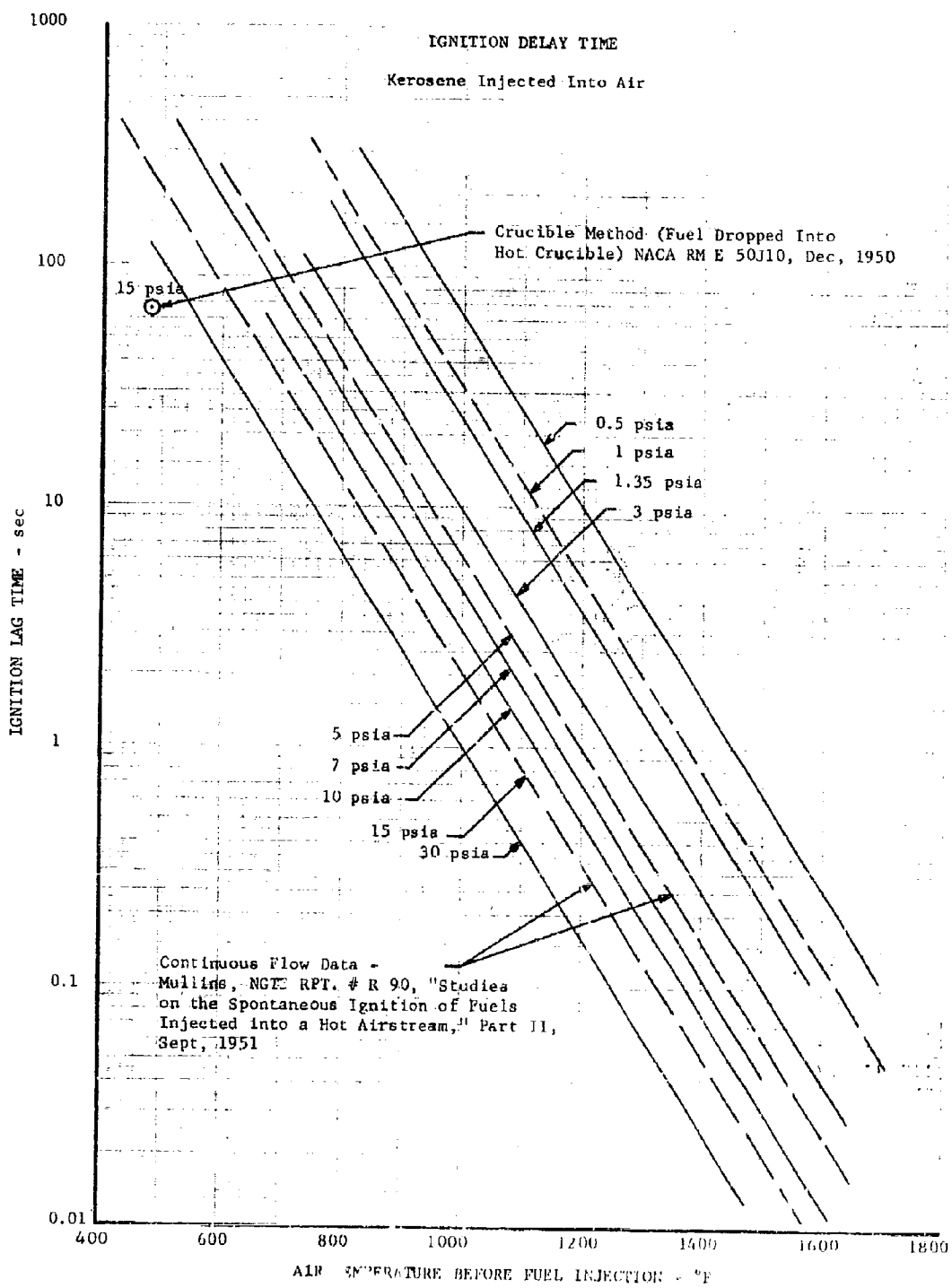


Figure III-S-19. Ignition Delay Time

DF 47187



CONFIDENTIAL

Pratt & Whitney Aircraft  
PWA FR-1855

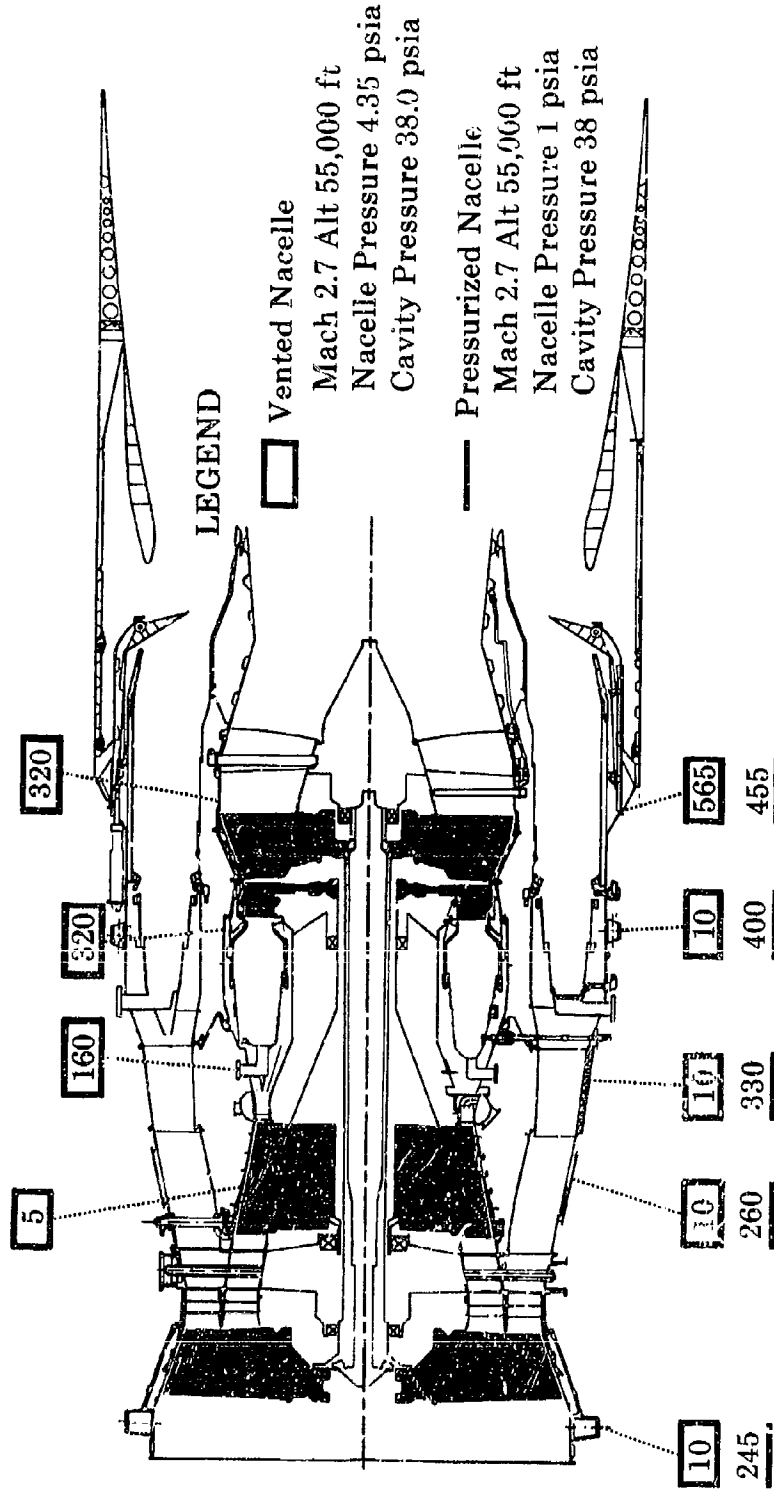


Figure III-S-21. JTF17A-20 Engine Nacelle Cavity Velocities

FD 15632

III-S-30

CONFIDENTIAL

SECTION IV  
AIRLINE COMMENTS

Trips to the maintenance facilities of Eastern Airlines, Miami, Florida and United Airlines, San Francisco, California, were made by Mr. R. E. Gordon from P&WA's SST Controls Engineering to obtain information concerning:

1. A review of the fuel and ignition system overhaul standards such as testing procedures, test limits, leakage limits, physical condition of detail parts acceptable for reassembly of the component, etc., as established by P&WA and our Component Vendor manuals and by the airlines.
2. A review with the airline's engineering department with respect to the authorization of reoperation limits in detail parts and assemblies, and allowable wear on parts prior to replacement.
3. Information on their record-keeping system relative to TBO's, premature removals, etc.
4. The problems the airlines have had with fuel and ignition system components which caused in-flight shutdowns, premature engine removals, premature component removals, plus problems found during component overhauls.
5. Information on spark igniter type used and their operating life.
6. Experience with piston-type hydraulic pumps.

Information gained on these trips will be used as a guide during the SST component design and development phases toward providing components that do not have these same problems.

SECTION V  
STATE-OF-THE-ART

A review of a Grumman Aircraft report, "An Aircraft Fatigue Monitoring System," was completed by the Reliability and Maintainability groups for possible application in the JTF17A-20 development program. The system outlined in the report is applicable to static airframe sections in temperature environments of  $-65^{\circ}\text{F}$  to  $+165^{\circ}\text{F}$ . The temperature range over which the monitoring strip adhesive bonding material is effective is too low for SST engine application. This system is not considered applicable to the JTF17A-20 development program in its present stage of development. When this system reaches the stage of development in which the monitor strips and adhesives will withstand the SST temperature environments, it will again be considered.

APPENDIX A

Augmentor Development Review

SECTION I  
INTRODUCTION

This appendix presents the results of the duct heater experimental program to date for the Phase II-C contract period. This experimental rig program was conducted to provide the necessary design and performance information to support the engine program.

SECTION II  
BACKGROUND

The ram induction principle utilized in the JTF17A-20 augmentation system is a new approach to combustor design. In this concept the dynamic pressure of the air flowing past the combustor liner is used in addition to the static pressure differential across the liner as a driving force for the air entering the combustor. This allows the combustor to operate in high velocity flow fields or at high burner "reference velocities", thus reducing the requirements for diffusion of compressor or fan discharge air with the attendant total pressure losses to the cycle. The ram induction principle also provides high levels of turbulence with high heat release rate potential for a given burner pressure loss.

The ram-induction principle was selected for the augmentor for the JTF17A-20 engine because it possesses the advantages of wide operating range, high combustion efficiency, exceptional ignition characteristics, simplicity and inherent reliability, and low total pressure loss to the fan stream.

A significant amount of testing had been conducted on a 7 x 11-inch sector rig to develop the ram-induction combustor prior to its selection for the SST application. These tests proved that the potential of the principle could be realized from a system suitable for use in a supersonic engine.

The sequence of events in the design and development of the JTF17A-20 augmentor system is as follows:

1. Testing of full-scale sectors of the duct heater system
2. Preliminary design of the engine flow path and augmentor
3. Evaluation of the flow path and augmentor on a water table
4. Design of the augmentor
5. Evaluation of the duct diffuser in a 0.6-scale annular diffuser rig
6. Fabrication of major engine cases
7. Evaluation of the augmentor in a full-scale annular duct heater rig
8. Assembly and testing of an experimental JTF17A-20 engine with duct heater.

**Pratt & Whitney Aircraft**

FWA FR-1855

Appendix A

In each case, information from the preceding task was fed logically into the performance of the task at hand. The organization of this report represents the chronological sequence of the development of the combustor, and is presented in the following order:

1. Full-scale sector duct heater rig results
2. Water table and diffuser rig tests
3. Full-scale annular duct heater rig results.

SECTION III  
FULL-SCALE SECTOR DUCT HEATER TESTS

## A. RIG DESCRIPTION

The full-scale sector duct heat heater test rig consisted of the following components, which are shown schematically in figure A-III-1:

1. Air inlet section
2. Venturi section
3. Transition section
4. Duct heater support section
5. Tailpipe section
6. Variable area nozzle
7. Diffuser section.

The air inlet section straightened the airflow and provided a near-stagnation region where accurate total pressure and total temperature measurements could be made upstream of the venturi section. The air inlet section was fabricated from a 24-in. length of 12-in. pipe, which provided an air inlet Mach number of approximately 0.02. Inlet flow was straightened by a bank of 1.5-in. diameter 12-in. long tubes. Station 1 total temperature taps were located 6 in. upstream of the venturi inlet; total pressure taps were just upstream of the total temperature taps. Stainless steel (type 347) was used throughout.

A venturi, which was used for an accurate low pressure loss airflow metering device, was sized to provide proper airflow when choked. The venturi was made from type 347 stainless steel and was constructed in two sections consisting of a 4.0-in. diameter throat with a contoured flow nozzle inlet and a 10-degree included angle diffuser section. The throat diameter was measured at 70°F. A coefficient of linear expansion of  $12 \times 10^{-6}$  in./in. °F was used to correct the throat diameter for higher temperature airflow. The venturi meter was made as part of the rig to minimize the effect of air leakage on the accuracy of the measurement of combustion efficiency.

The transition section connected the 12-in. diameter outlet of a heater burner, utilized to provide elevated inlet temperature, to the rectangular 7 x 11-in. duct test section. The length of the transition section enabled the heater burner products to be completely mixed prior



Pratt & Whitney Aircraft

PWA FR-1855

Appendix A

to entering the test section. The transition section was built in two parts: an 18-in. long transition from round to rectangular, and an 18-in. long 7-in. wide by 11-in. high rectangular duct.

The duct heater support frames provided a constant-area, 7-in. wide by 11-in. high, rectangular duct 30 inches long. (See figure A-III-2.)

The water-cooled tailpipe was a straight duct that provided the same burning length as the engine augmentor. The tailpipe was 36 inches long and was made primarily of 1/4-in. stainless steel plate. A 0.50-in. gap between the inner and outer duct walls provided a cooling water passage.

A variable-area nozzle (figure A-III-3) provided sufficient area variation to operate at choked conditions for duct reference Mach numbers from 0.12 to 0.20 and fuel-air ratios from 0.005 to 0.067 (stoichiometric). The nozzle was water-cooled in the same manner as the tailpipe section. Two circular, water-cooled rods were used to vary the exit area. The rods were constructed from a 2.50-in. diameter tube welded to a 1.00-in. diameter tube, with the 45-degree conical section connecting the tubes. The area was varied by regulating the immersion of the large diameter portion of the rod. The rods were actuated by a small hydraulic cylinder, and a locking device was provided to keep the rods from rotating. A total pressure rake with a total pressure tap located every 1.375 inches was incorporated in each rod. The nozzle area could be varied from a maximum of 53.0 in.<sup>2</sup> (when both probes had their 1.0-in. diameters fully extended into the duct) to a minimum of 22.0 in.<sup>2</sup> (when the 2.5-in. diameter portions are fully extended into the duct). The probes were sealed to the duct by a pressurized labyrinth seal.

The water-cooled diffuser provided smooth transition from the rectangular exhaust nozzle to the round ejector. The diffuser was 65 inches long and was made primarily of 1/8-in. type 307 stainless steel plate. The small rectangular end is a 7 x 11 in. inner wall area, and the large round end has a 17.25-in. inside diameter. The diffuser included angle is 3 degrees. Spray water tubes are used for retreating the inner wall, as well as for providing the necessary spray water for cooling the exhaust gases.

## B. TEST STAND DESCRIPTION

Sector rig duct heater tests were conducted in B-2 test stand. Figure A-III-4 shows the installation of the rig in the test stand. As shown in figure A-III-5, a J75 turbojet was used as an air supply for the rig and a two-stage ejector. The air temperature is related to the engine pressure ratio, but was normally approximately 450°F for duct heater testing at simulated sea level conditions; at these test conditions, the J75 engine is capable of supplying up to 20 lb/sec of bleed air at a pressure of 100 psia. When using the ejector for altitude testing, inlet temperature was controlled by mixing engine bleed air with ambient air at the rig inlet.

The fuel system is shown schematically in figure A-III-6. Flow was controlled manually through needle valves upstream of flowrators. Three independent fuel zones were provided; the flow to each of the three zones was independently measured by flowrators. Fuel temperature was measured by 0.25-in. sheathed chromel-almel thermocouples, and read on a Brown 0-800°F temperature indicator; each zone was measured separately. Fuel pressure for each zone was read on an 8-in. Heise gage.

Cooling water was supplied through three separate manifolds and is regulated by gate valves. The discharge also consisted of three manifolds and separate gate valves, which enabled regulation of pressure and flow. Spray water was discharged into the diffuser section downstream of the variable nozzle.

Water flow was measured in the discharge manifold of the catalytic and variable nozzle section by a 3-in. turbine meter with electronic counter readout. Water pressure was measured at the inlet of each manifold by 0 to 100 psi gages.

To calculate the heat losses, the water temperature rise was measured. Each inlet and exit manifold was provided with 0.25 in. sheathed chromel-almel thermocouples. The temperatures were recorded by a 0 to 800°F Brown Temperature Indicator and on a differential potentiometer.

## C. INSTRUMENTATION

Station 1 was located 6 inches upstream of the venturi inlet. Total pressure and temperature at Station 1 were used to calculate the airflow through the venturi. Total pressure was sensed with a Kiel probe, and temperature was measured with a five-ring shielded chromel-alumel thermocouple. Total pressure was read on either an 80-in. Hg manometer or a 14-in. 0-100 psi Heico gage. Temperature was read on a 0 to 300°F Brown temperature indicator.

Station 2 was located in an' immediately downstream of the venturi throat. Two static taps were located in this area; one tap was in the throat and the other tap was 3.5 inches downstream of the throat. These were used only to determine if a choked condition existed in the venturi throat. If the throat was choked, the static pressure would be decreasing down the length of the venturi diffuser to the position of the shock wave. The taps were connected to a U-tube Hg manometer that would show a positive reading during the choked condition.

Station 3 was located immediately forward of the duct heater. Total pressure was measured with Kiel probes and static pressure was measured with 0.030-in. diameter wall taps. These pressures were read on 80-in. Hg manometers. Temperature was measured with 5-ring, shielded chromel-alumel thermocouples, and read on a 0 to 300°F Brown temperature indicator.

Station 4 consisted of the discharge nozzle section of the rig; the rig exhaust area and total pressure were measured at this station. Total pressure was measured by pressure ports on the upstream side of the movable nozzle rods and read on 80-in. Hg manometers. There were 32 pressure ports, 16 on each nozzle rod. The nozzle area was determined by measuring the position of the movable nozzle rods. One rod was locked in position before the test and measured manually. The adjustable rod position was measured utilizing an electrically driven traverse position indicator.

Station 5 was located at the front of the diffuser section. Static pressure was measured with 0.030-in. diameter wall taps and read on 80-in. Hg manometers. This static pressure was used with the total pressure at station 4 to determine when the discharge nozzle was choked.

#### D. ANALYSIS OF DATA

The exhaust temperature of the duct heater was determined by solving the continuity equation at the plane of the variable area nozzle. By knowing the airflow rate (W), the total pressure (P), and area (A) of a choked nozzle, the total temperature (T) can be solved using the following equation:

$$T = \left( \frac{\text{Const} \times P \times A}{W} \right)^2$$

The airflow rate was measured by the choked venturi, and the pressure was measured by the pressure rake in the exhaust nozzle rods. The area of the variable area nozzle was determined from the potentiometer indication of the rod position. An assessment of the exhaust nozzle discharge coefficient was made by comparing airflow measurements with the choked venturi upstream under cold flow conditions.

Corrections to this temperature were made by calculating the heat transferred to the tailpipe and nozzle cooling water. The actual temperature rise was then compared with a theoretical temperature rise calculated with a theoretical combustion IBM deck to determine the combustion efficiency.

#### E. TEST RESULTS

A total of 643 hours test time was accumulated on the full-scale sector rig test from 1 July 1965 to 21 March 1966 on eight basic duct heater designs. For continuity, duct heater models tested as part of PWA's Independent Research Program are reported herein. These designs are shown in Figures A-III-7 through A-III-15.

The Mod K duct heater design (Figure A-III-15), utilized for the JT1A-70 engine, evolved from the Mod E (Figure A-III-11). This version showed the highest efficiency at cruise conditions. Figure A-III-16 shows the efficiency of the Mod K compared to previous duct heaters tested at simulated cruise conditions.

Although the Mod F exhibited excellent performance at high pressures associated with sea level and cruise conditions, the operating range at low pressures and temperatures encountered during transonic flight was less than desired. Like the Mod D (Figure A-III-10) showed somewhat

wider operation (although lower cruise efficiencies), due to the increased dome height which resulted in lower velocities inside the combustor, this feature was incorporated into the Mod K. The rich blowout fuel-air ratio increased from 0.005 to 0.015 at 9-psia burner inlet pressure.

Thus, development of the augmentor has been concentrated on increasing the operating range and efficiency at transonic flight conditions without suffering any performance penalties at sea level and cruise pressures.

The Mod H (figure A-III-12) was a modification of the Mod D (figure A-III-10). The secondary liner assembly was replaced by a new configuration having external scoops and integral turbulators. This design was the first to operate over the entire operating range, utilizing two fuel zones at 9-psia inlet pressure and 200°F inlet temperatures at a duct reference Mach number of 0.15. Efficiencies at cruise (figure A-III-7) and transonic (figure A-III-18) conditions were lower than the augmentors previously tested.

The Mod J (figure A-III-15) was conceived as a low-cost research tool to investigate air distribution, scoop size, turning angle and the utilization of tubular scoops. Through the use of these tubes it was found that small, staggered scoops were effective in increasing efficiency. In addition, by overturning the rear scoops, the gas recirculation within the combustor was strengthened, thereby increasing the operational limits of the duct heater. A refinement of the Mod J to decrease pressure loss is shown in figure A-III-14. This combustor utilized formed circular scoops with air flow distribution patterned after the tubular scoop design. Performance of the duct heater with the formed circular tube scoop was comparable to the tubular scoop. The Mod J had high efficiency at cruise conditions (figure A-III-17) and operated over a wide range at low pressure (figure A-III-13).

A shortened version of the Mod E, also modified by incorporating a wide (9-inch) dome with two toroidal or in-flow swirlers, was tested. The secondary liners were removed, effectively decreasing combustor length by one diaphragm and causing the scoops to discharge air upstream at a 40-degree angle toward the dome. Ninety-degree turning angle turbulators were used

## Pratt & Whitney Aircraft

PWA FR-1855

Appendix A

upstream of the Zone II fuel injectors. Performance of this shortened Mod E showed that it had a wide operating range and possessed a somewhat higher efficiency than the other mods at high fuel-air ratios. However, the efficiency at fuel-air ratios below 0.025 is somewhat lower. Figure A-III-19 shows a Mod K modified to this configuration.

### F. CONCLUSIONS

1. The Mod K duct heater that was selected for the initial JTF17A-20 engine design was derived from the Mod D and E heaters and exhibited excellent performance characteristics at simulated SLTO and cruise conditions.
2. The operating range of the Mod K duct heater at very low pressures and temperatures (upper left hand limit of the engine flight envelope) was less than desired.
3. Duct heaters have been developed (later modifications to the Mod H) that have greater operating range capability at low pressures and temperatures.
4. Significant weight reduction can be achieved by eliminating rear panels and scoops without seriously affecting duct heater performance.

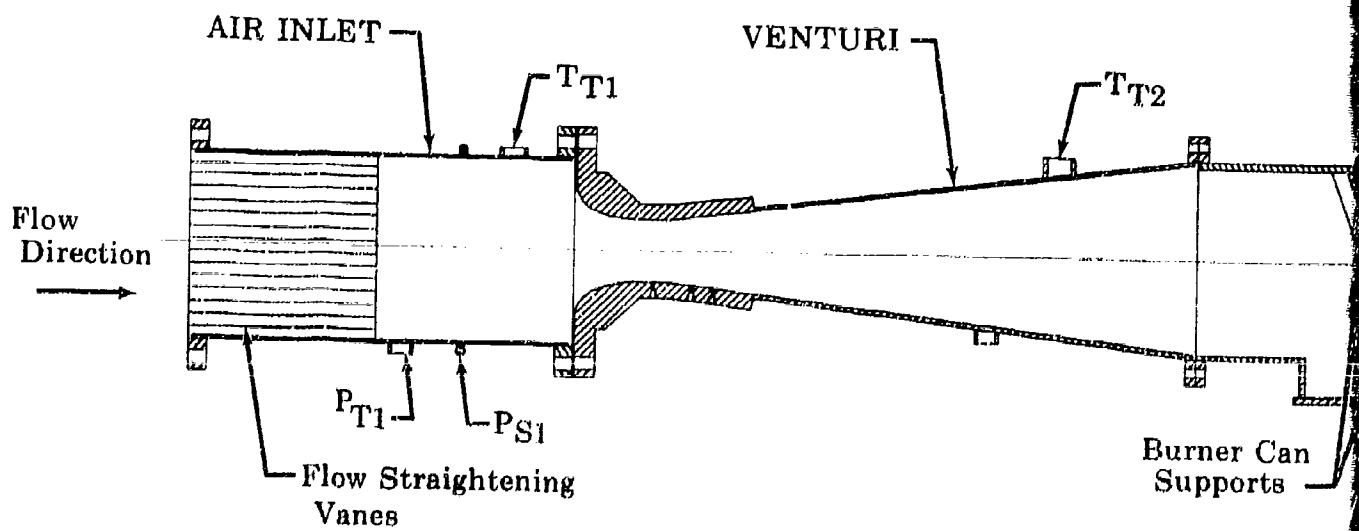
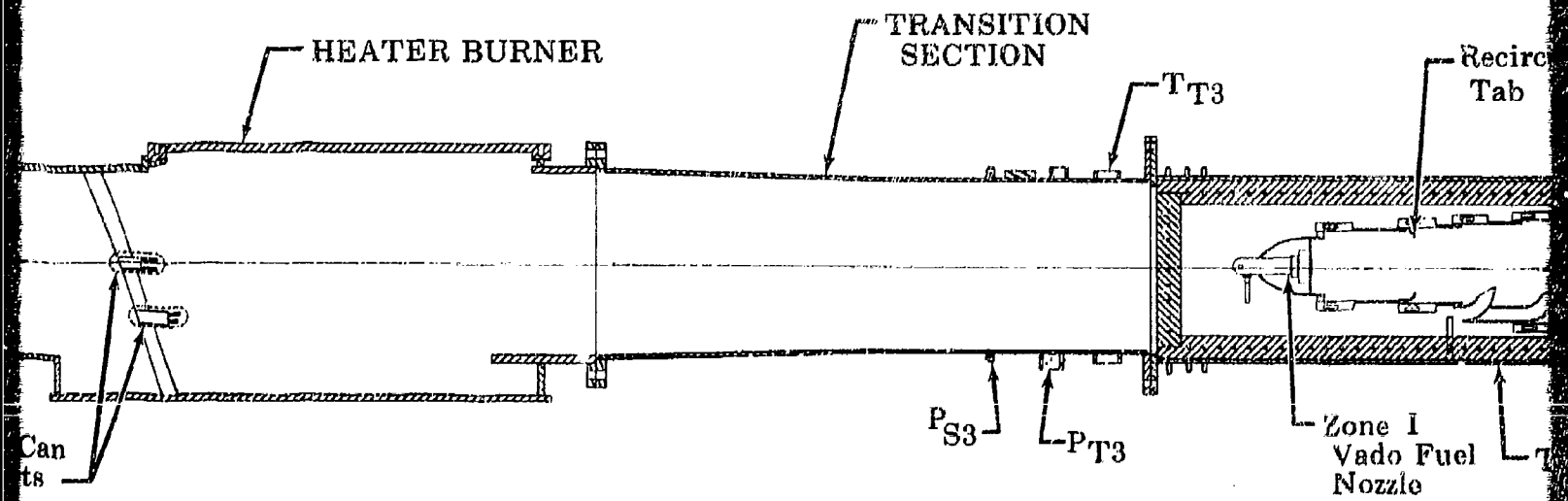


Figure A-III-1. Schematic of Duct Heater Test Section



HEATER BURNER

TRANSITION SECTION

$T_{T3}$

Recirc Tab

Can  
ts

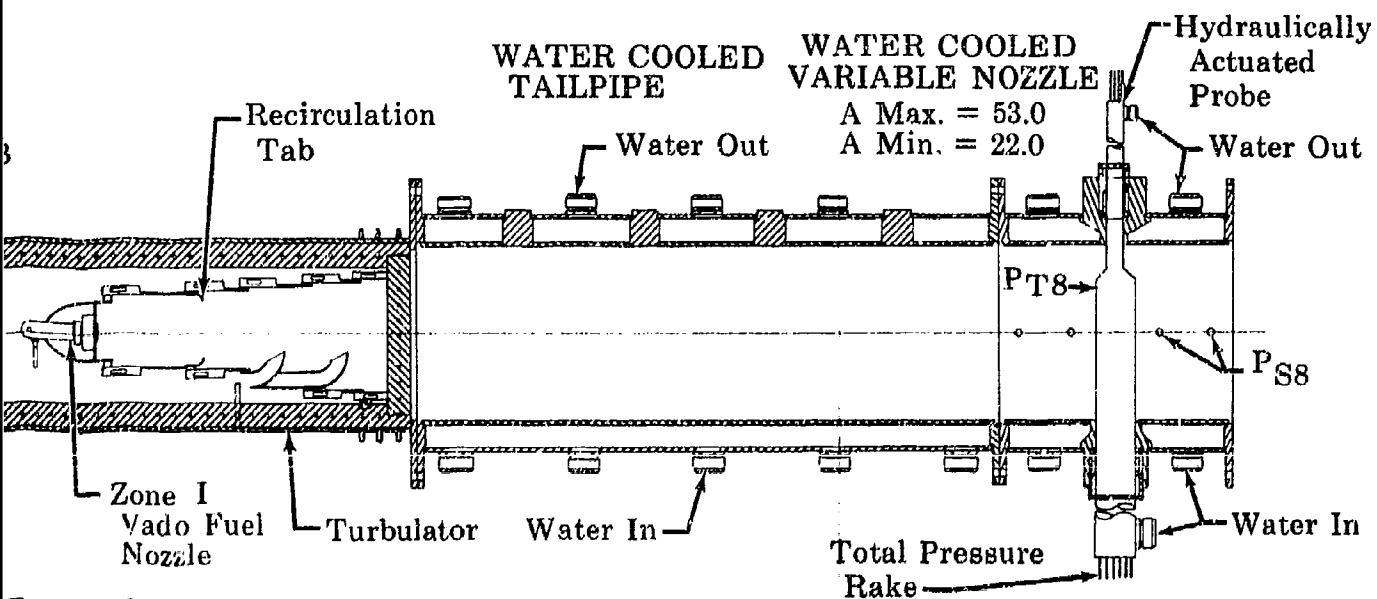
$P_{S3}$

$P_{T3}$

Zone I  
Vado Fuel  
Nozzle

Type A Combustion Chamber  
(With External Vortex Generator)





Type A Combustion Can  
(with External Vortex Generator)

13

**CONFIDENTIAL**

Pratt & Whitney Aircraft  
PWA FR-1855  
Appendix A

FC 7196

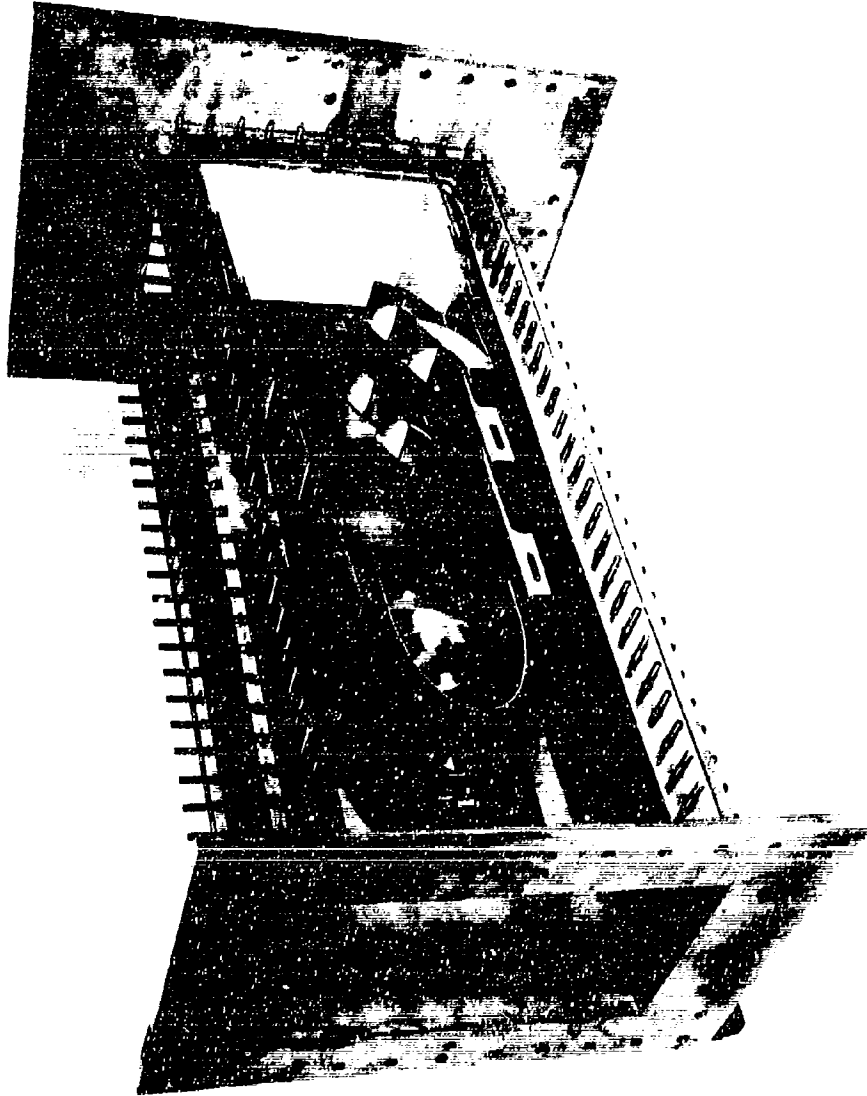


Figure A-III-2. Mod A Duct Heater Sector Installed in Rig Support Section

A-III-9

**CONFIDENTIAL**

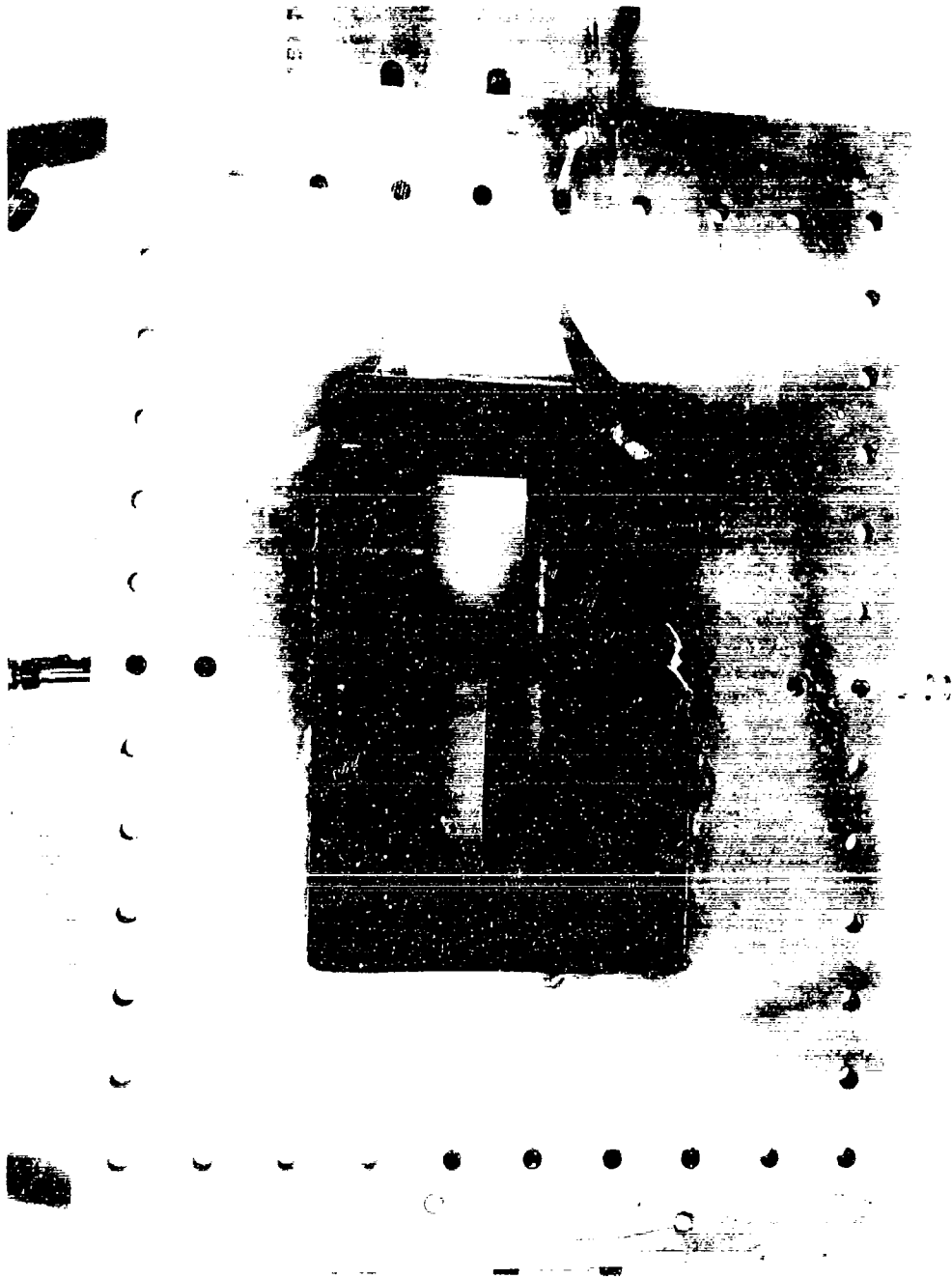


Figure A-III-3. Variable Area Nozzle

FE 39554

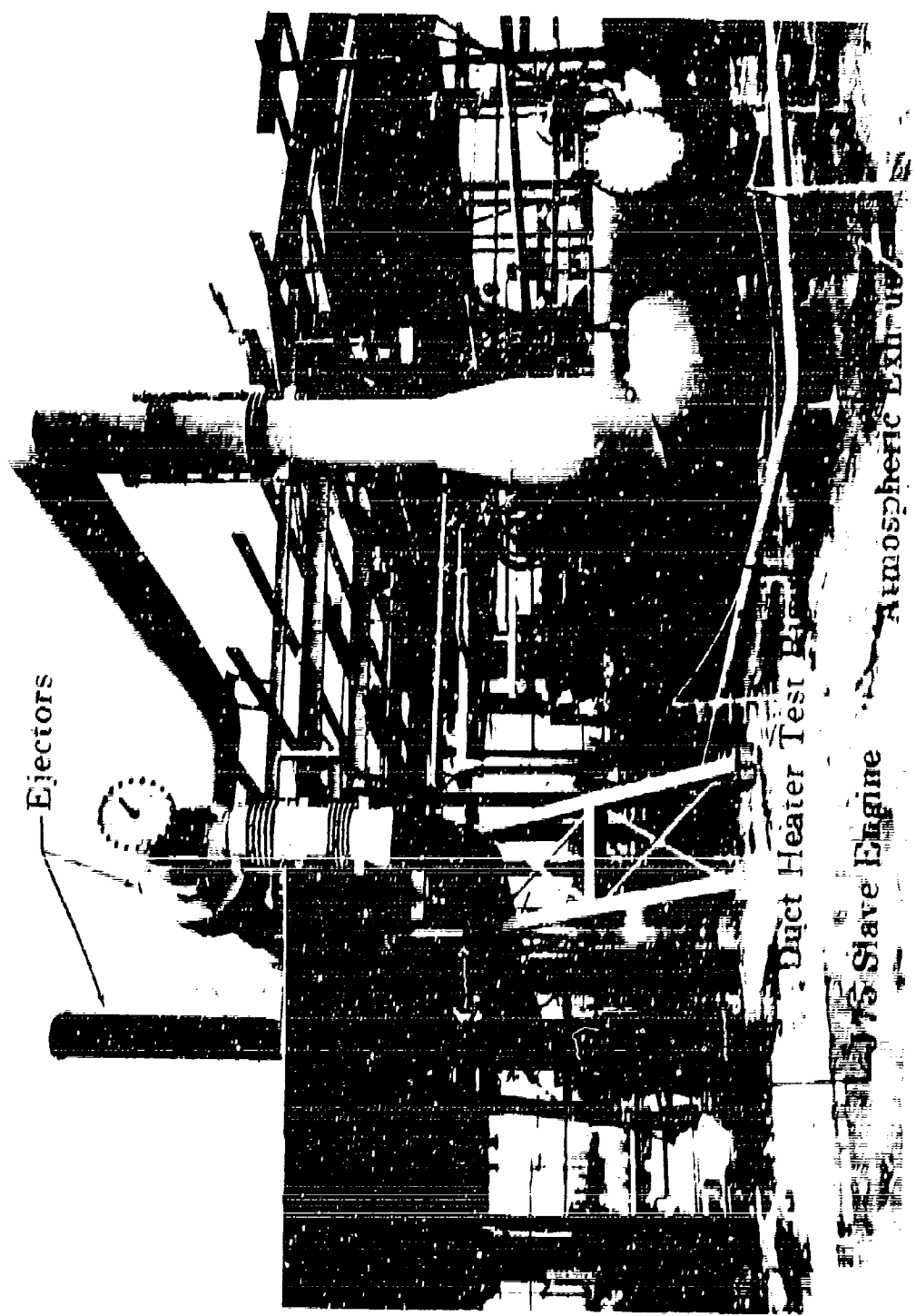
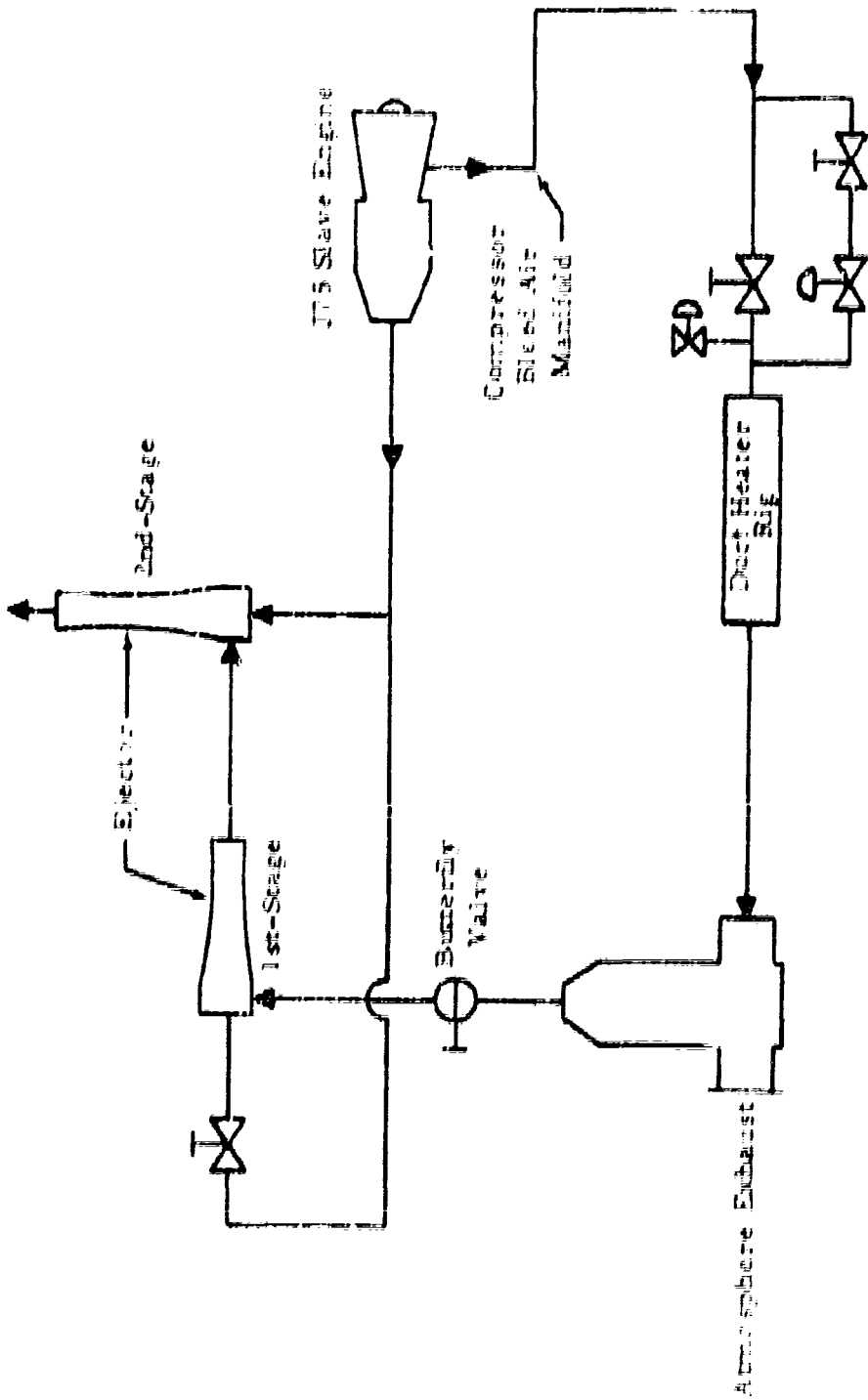


Figure 1. Slave Engine Test Cell. The Slave Engine Test Cell is a complex structure used for testing the slave engine. It consists of a duct heater test rig, an atmospheric exhaust system, and various support structures. The slave engine is mounted on a test stand within the cell.



8, 10, 11, 12

Figure A-111-12. 1st Stage Turbine Bleed Air System Schematic

Pratt & Whitney Aircraft  
IWA PR-1005  
Appendix A

100  
101  
102

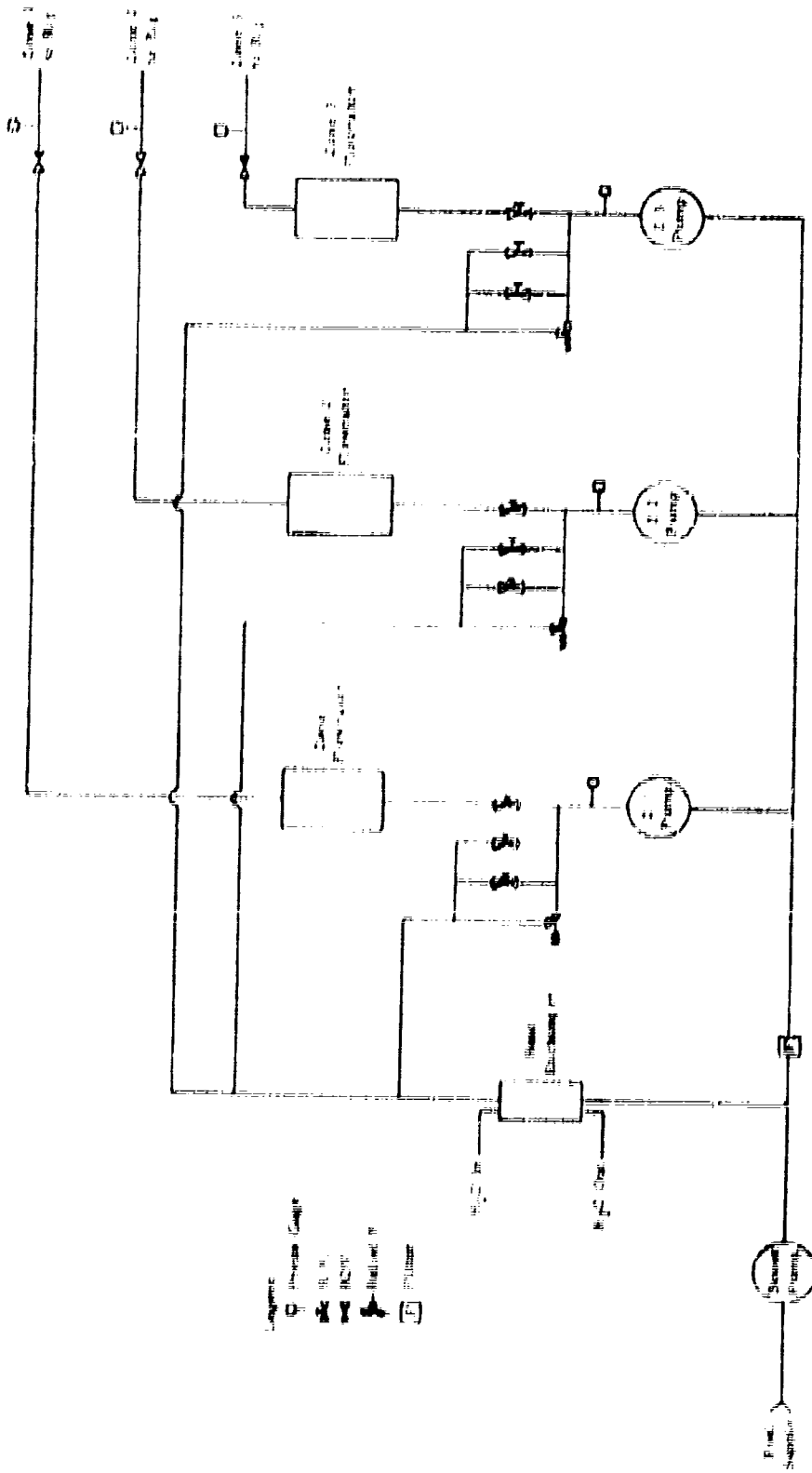
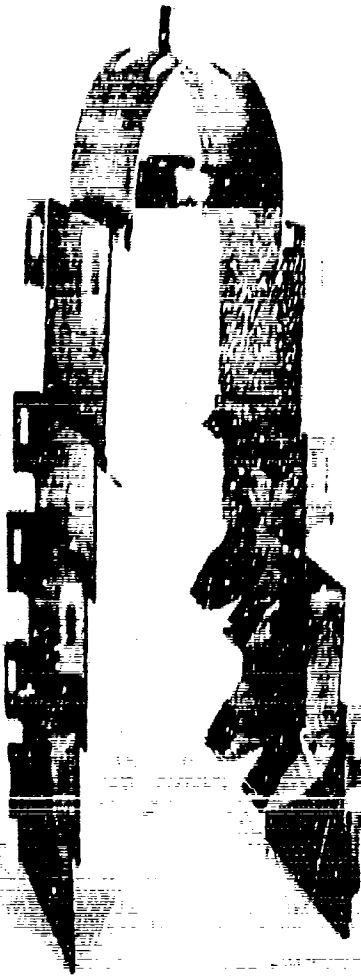


Figure A-111-1. Fuel System Schematic

**CONFIDENTIAL**

**Pratt & Whitney Aircraft**  
PWA PR-1855  
Appendix A



*[Faint, illegible technical text or notes, possibly bleed-through from the reverse side of the page.]*

Figure A-11-7. Hod A Duct Heater

PC 7195

A-11-14

**CONFIDENTIAL**



Figure A 111-B, Duct Heater

FR 61411

A 111 B



**CONFIDENTIAL**

**Pratt & Whitney Aircraft**

PWA PR-1855

Appendix A

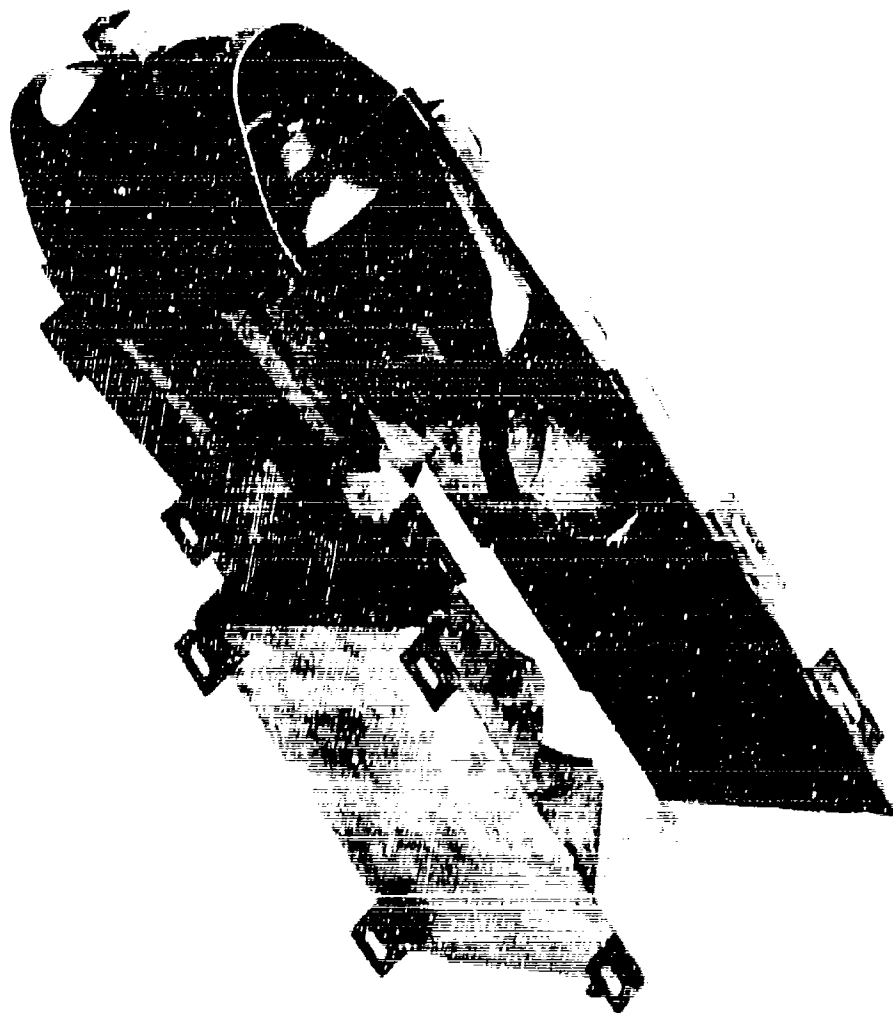


Figure A-111-9. Model C Duct Heater

PR 52378

A-111-16

**CONFIDENTIAL**

**CONFIDENTIAL**

Pratt & Whitney Aircraft  
PWA FR-1855  
Appendix A

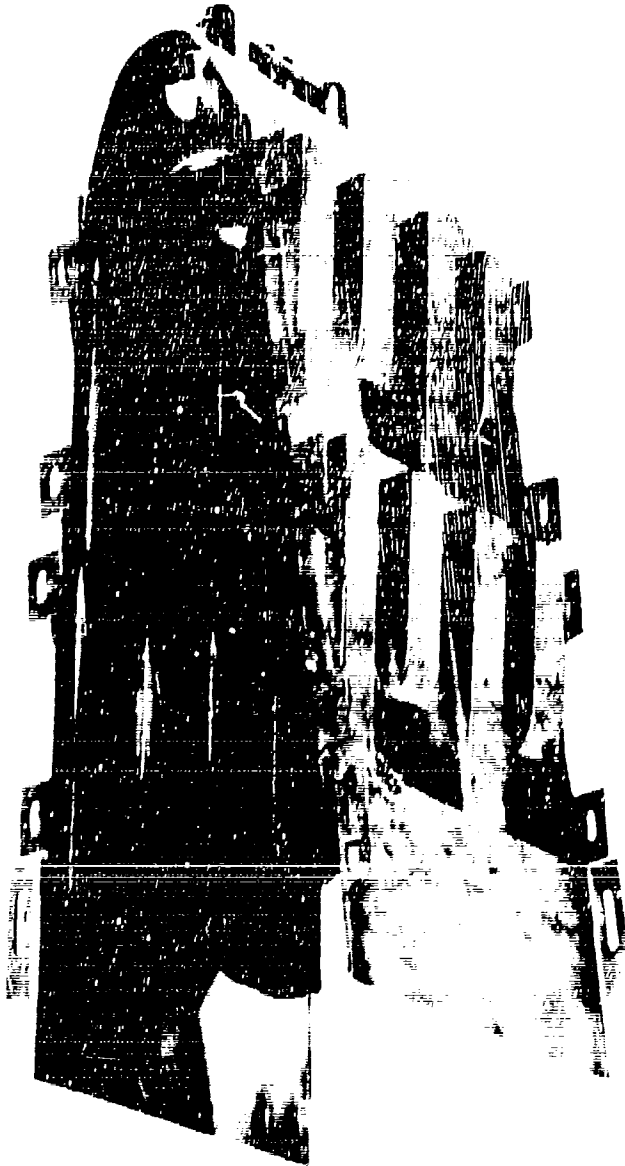


Figure A-111-10. Mod D Duct Heater

FR 1855

A-111-17

**CONFIDENTIAL**

**CONFIDENTIAL**

Pratt & Whitney Aircraft  
PWA FR- 855  
Appendix A

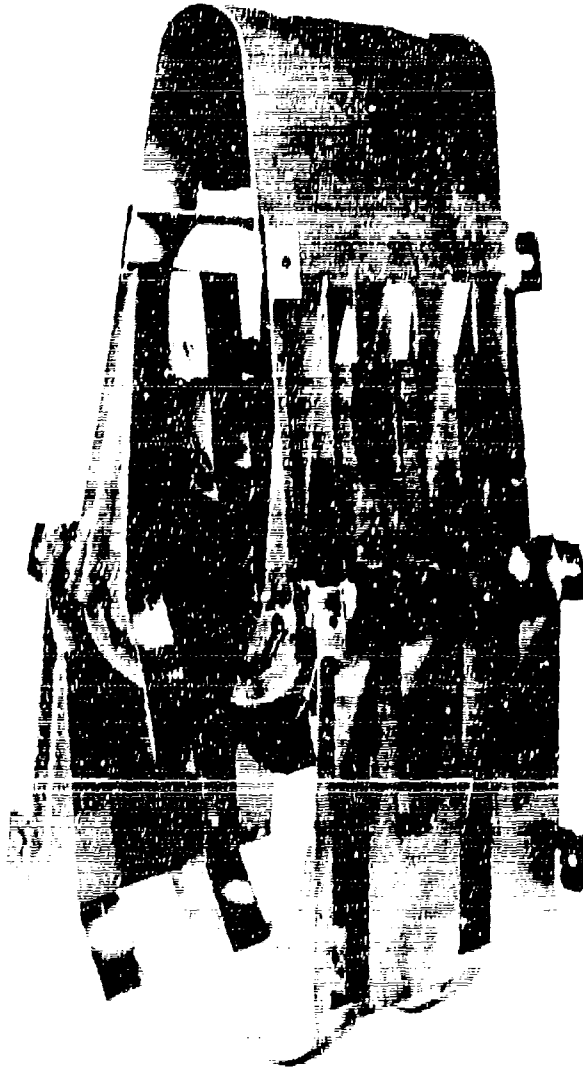


Figure A-111-11. Mod. E. Duct Heater

A-111-15

FE 34,992

**CONFIDENTIAL**

**CONFIDENTIAL**

Pratt & Whitney Aircraft  
PWA PR-1855  
Appendix A

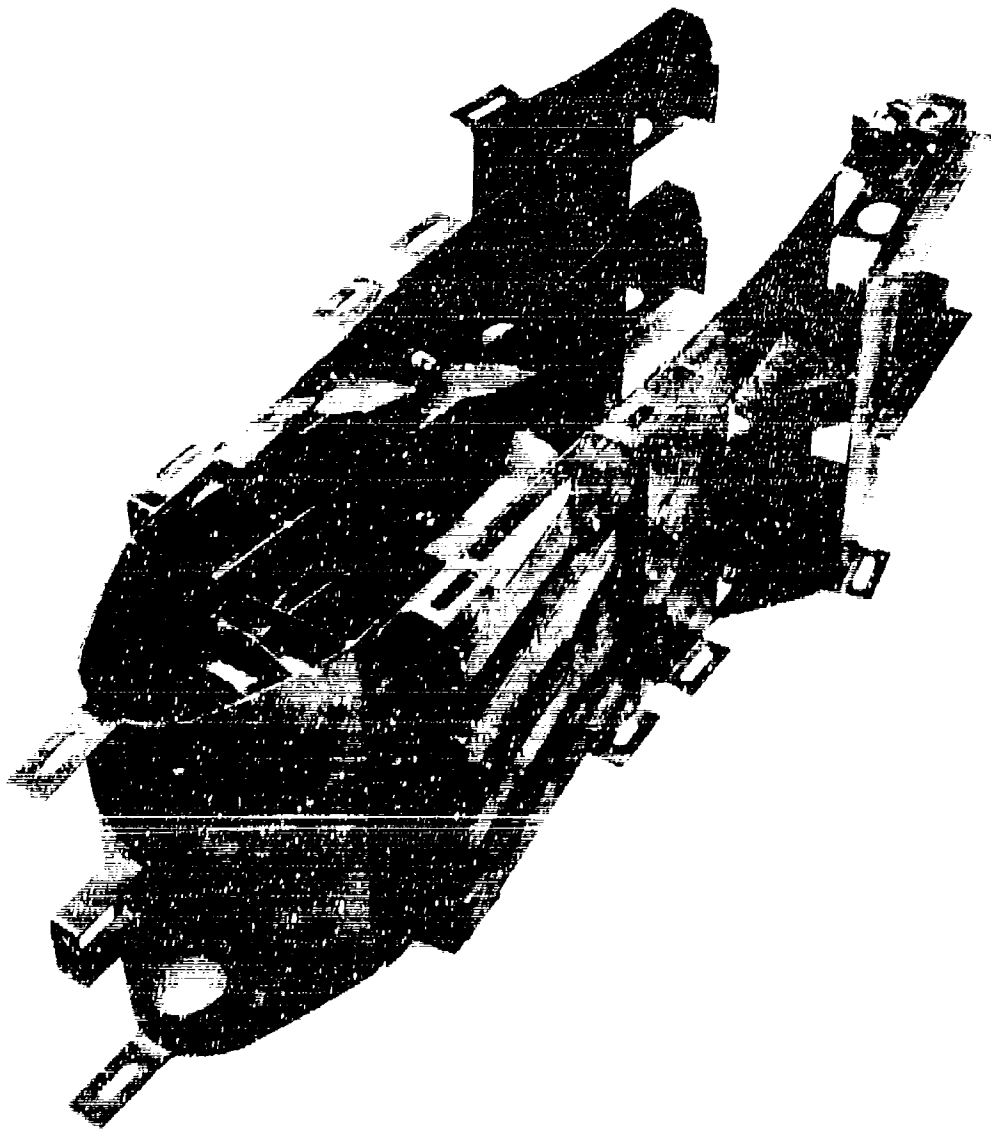


Figure A-111-12. Mod II Duct Heater

FE 54232

A-111-19  
**CONFIDENTIAL**

**CONFIDENTIAL**

Pratt & Whitney Aircraft  
IWA FR-1855  
Appendix A

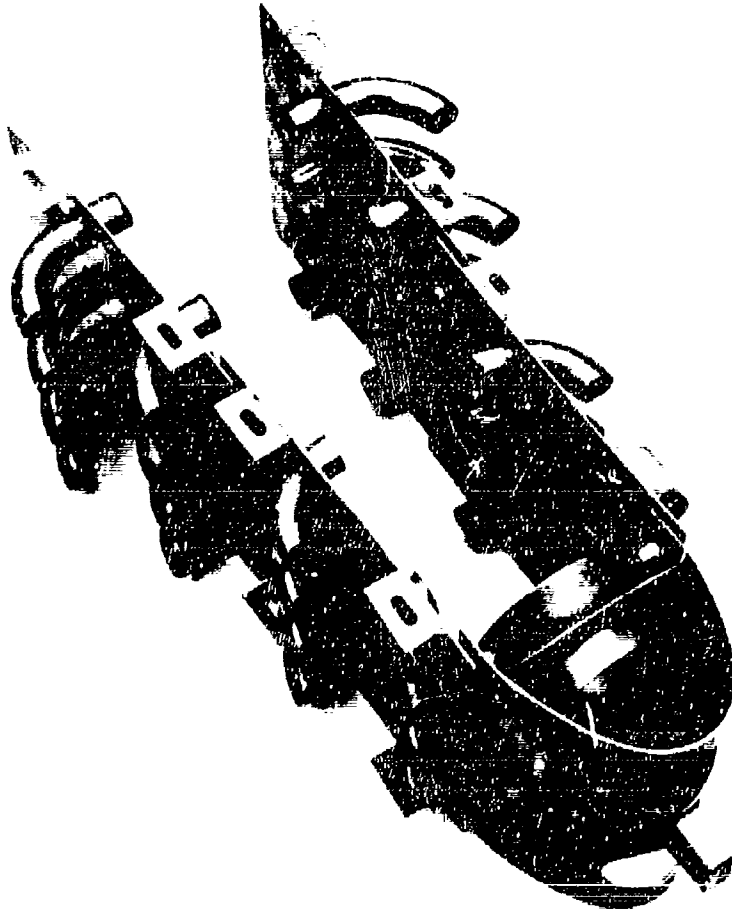


Figure A-111-13, Mod J Duct Heater

PR 52470

A-111-20

**CONFIDENTIAL**

**CONFIDENTIAL**

Pratt & Whitney Aircraft  
PWA FR-1855  
Appendix A

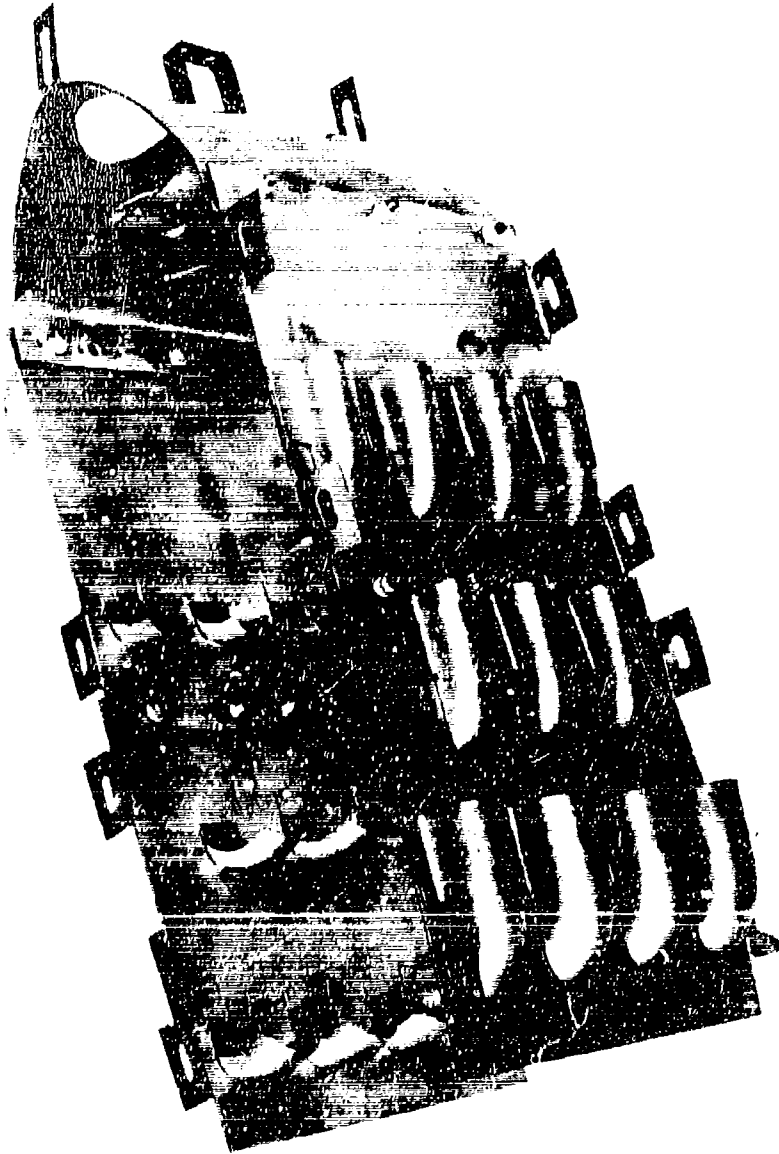


Figure A-III-14. Modified Mod J Duct Heater

FE 57227

A-III-21

**CONFIDENTIAL**

**CONFIDENTIAL**

**Pratt & Whitney Aircraft**  
PWA FR-1855  
Appendix A

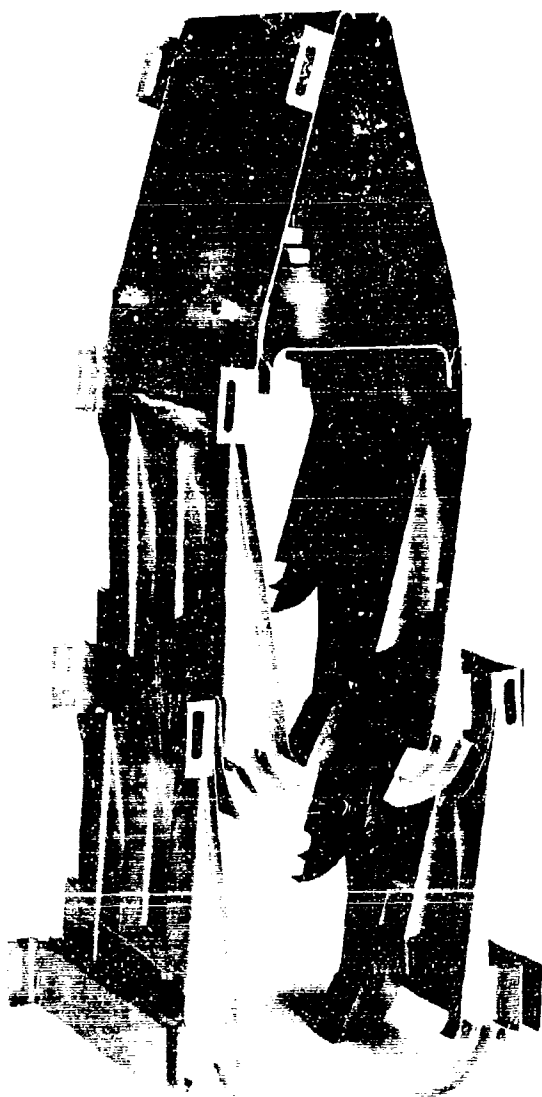
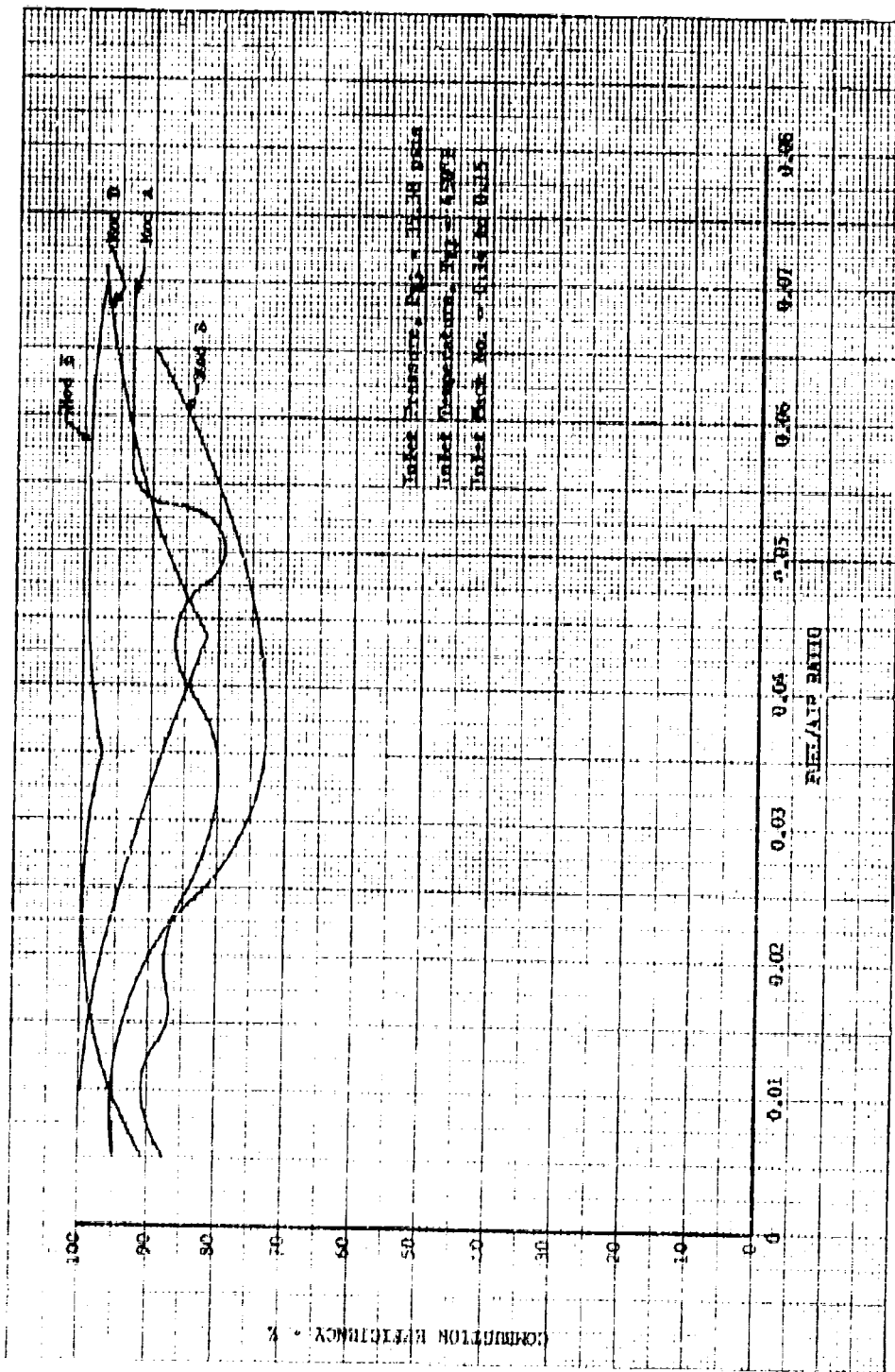


Figure A-III-15. Mod K Duct Heater

FE 54059

A-III-22

**CONFIDENTIAL**



DF 47190

Figure A-III-16. Duct Heater Combustion Efficiency (Inlet Temperature = 450° F)



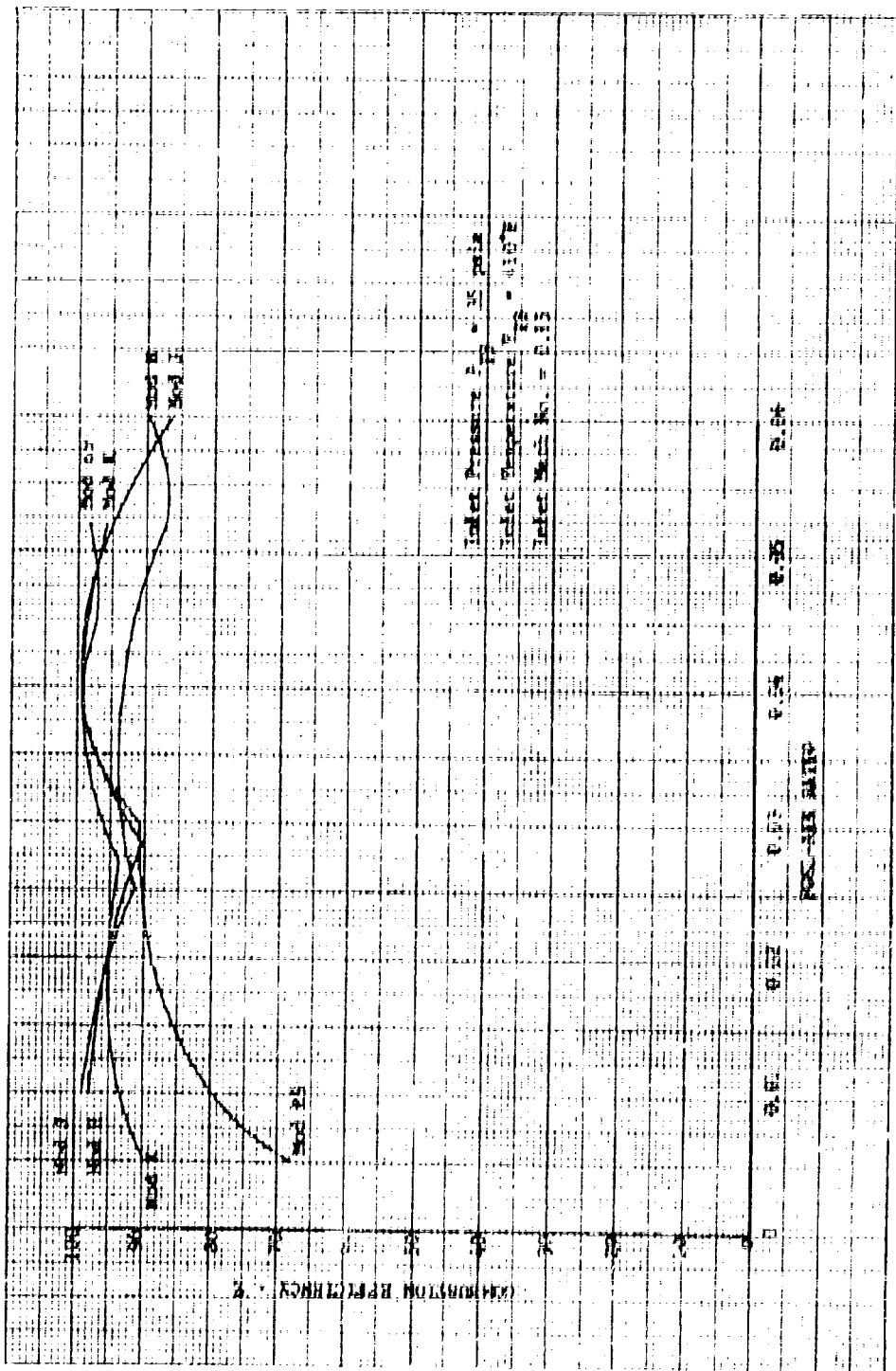
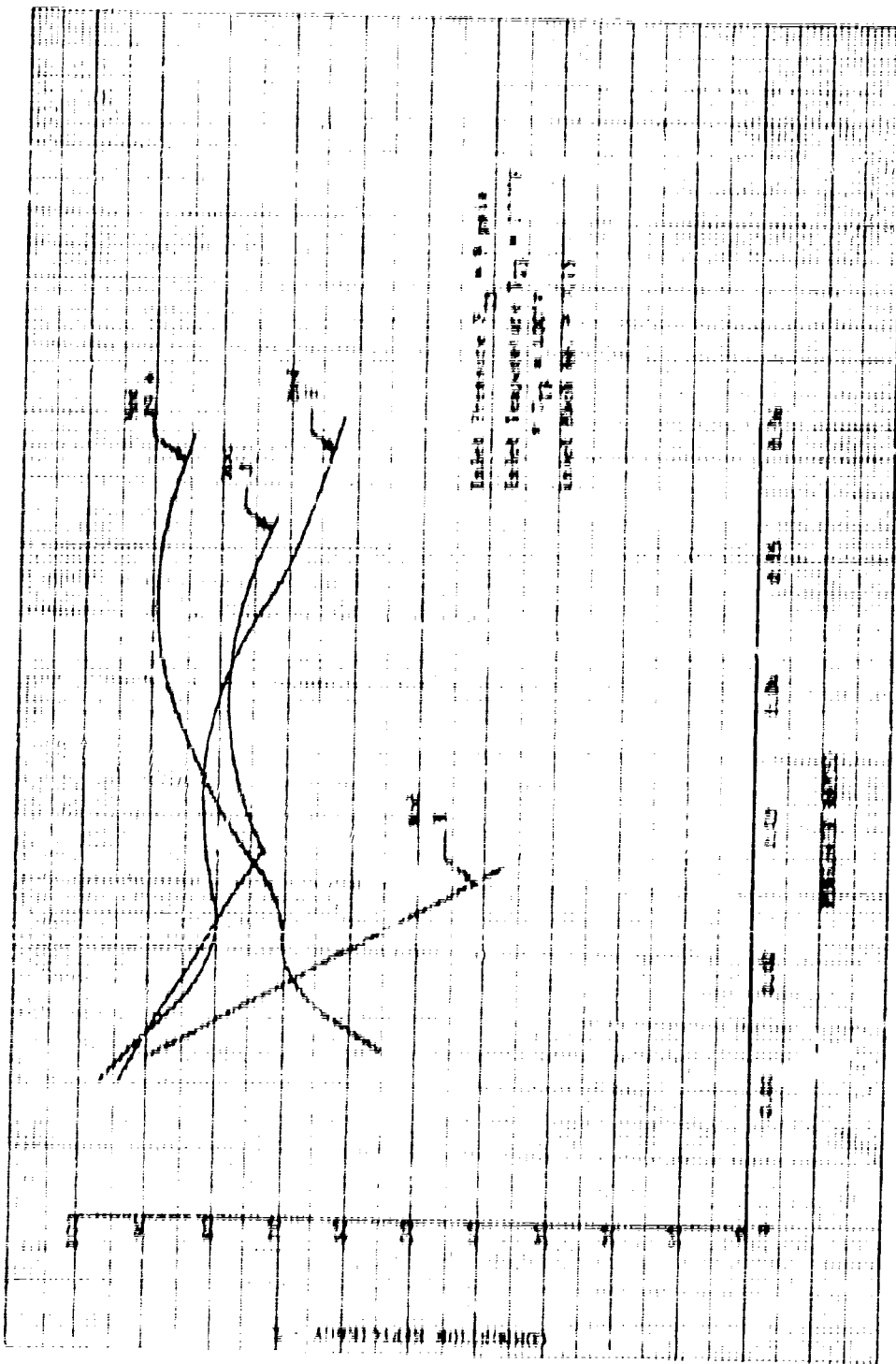


Figure A-11-17. Dual Heater Compressor Efficiency (35-psia Inlet Pressure) 03-1191

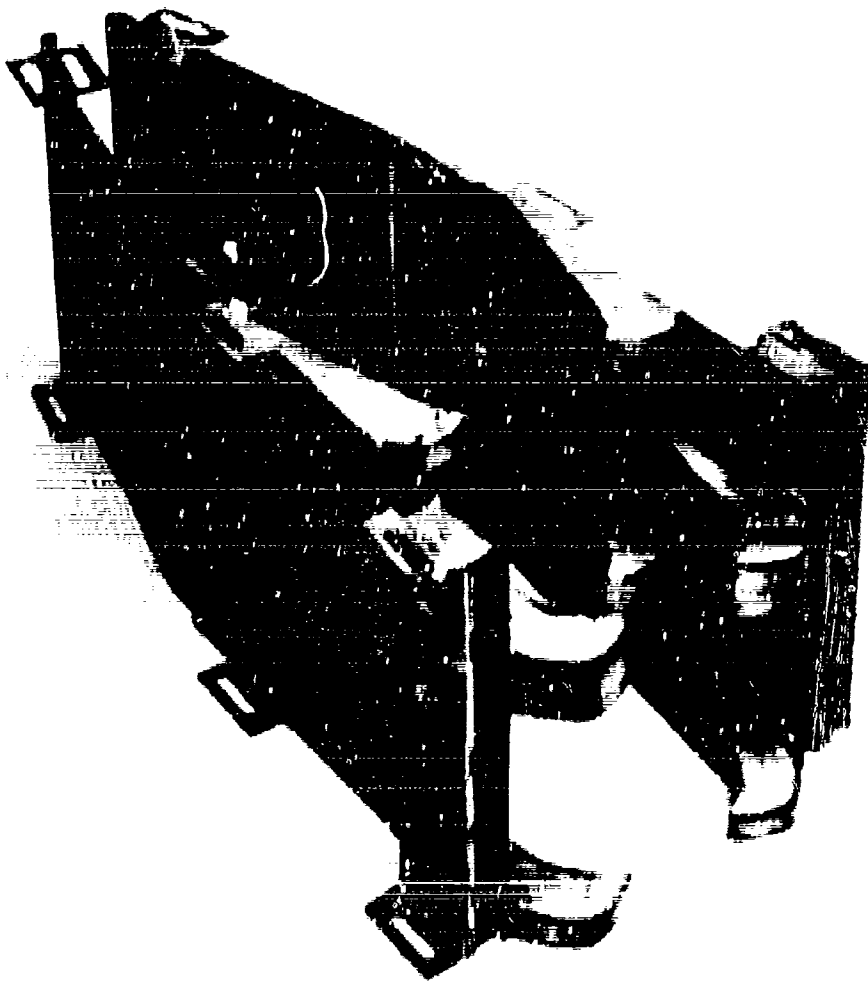
Pratt & Whitney Aircraft  
 PWA PR-1455  
 Appendix A



**CONFIDENTIAL**

Pratt & Whitney Aircraft  
PWA PIC-1A55  
Appendix A

1  
2  
3  
4



CONFIDENTIAL

A 111 06

**CONFIDENTIAL**

SECTION IV  
DIFFUSER TEST

## A. GENERAL

A two-dimensional water table was used to study the flow characteristics of the fan duct passage. Emphasis was placed on obtaining a better understanding of the flow in the diffusing regions of the fan duct. These water table studies were helpful in developing a qualitative understanding of the flow phenomena and aided in the analysis of the data obtained from the 0.6-scale annular duct diffuser rig.

## B. RIG DESCRIPTION

The diffuser rig simulated the actual duct heater flow path from the fan exit to the combustor inlet. The rig was constructed of laminated wood and was made on a 0.6 scale of the actual diffuser. The scale was selected to coincide with that of the existing two-stage fan rig, allowing for the possibility of combined testing of the diffuser and fan at a later date if results warranted. Forward of the diffuser section there were two cylindrical instrumentation sections and a flow straightening bellmouth. Flow profile generating plates, when utilized, were added between the two instrumentation sections. (Figures A-IV-1 through A-IV-3.)

The bellmouth at the forward end of the rig was open to the atmosphere and the aft end was connected to a high capacity exhaustor. Air supplied to the rig was at ambient conditions; by varying exhaustor speed, any selected Mach number could be established in the rig.

The variables determined during testing of this rig were inlet and exit Mach number, diffuser total pressure loss, and static pressure recovery. Individual diffuser characteristics such as separation tendencies were also studied in this program.

## C. INSTRUMENTATION

The diffuser rig instrumentation consisted of static and total pressure measuring devices. Wall static pressure taps were constructed from brass plugs and mounted flush with the inner walls. These plugs assured accurate static pressure, which could not be obtained from holes drilled

directly in the wood. Four types of probes were used to obtain total pressure and free stream static pressure.

#### 1. "Banjo" Probes (Figure A-IV-4)

Both total and static pressure can be obtained from this type of probe. To measure accurate static pressure with the banjo probe, it is necessary to null the static pressure readings, i.e., rotate the probe until static pressures on each side of the probe read the same value. At this point the measured angle of attack with the airstream is zero and the side pressure ports measure true static pressure.

#### 2. Kiel Probes

This probe is an inherently accurate probe for measuring total pressure, and it also has a large air acceptance angle. For this reason the total pressure used in calculations was obtained with this type of probe.

#### 3. Pitot-Static Probes

This probe did not prove accurate enough for traversing the airstream because of sensitivity to air angle and wall influence. This probe did, however, prove useful in establishing and maintaining a constant airflow when held in a fixed position sufficiently far from the rig walls.

#### 4. Boundary Layer Total Pressure Probes

These probes consisted of several total pressure pickups at incremental distances from the wall of the diffuser, and were used for boundary layer determination.

The location of traverse planes in the rig is shown in figure A-IV-1.

1. Instrumentation located in the first instrumentation section consisted of two, three-element pitot-static probes, positioned circumferentially at  $45^\circ$  and  $270^\circ$ , and wall static pressure taps adjacent to these probes. This instrumentation was used primarily to hold a steady-state condition after an airflow point had been established.

2. In the second instrumentation section, there were five axial traversing planes and three axial planes of wall static. The five traversing points would accept Kiel, banjo, or pitot-static probes.
3. Diffuser Section: Instrumentation in this section consisted of five axial traversing planes at which both Kiel and banjo probes were used. Static pressure instrumentation was present on both inner and outer walls adjacent to each traverse point. All of the above diffuser instrumentation was installed at two different angular planes in the rig.

Two total pressure probes and static pressure taps were installed at the bleed cavity entrance to determine bleed airflow rate.

#### D. TEST PROCEDURE

##### 1. Profile Determination and Development

Before any flow profile generating scheme development could be initiated to simulate fan discharge conditions, tests were conducted to establish the diffuser inlet profile with no profile generating device.

The stream blockage required to simulate a predicted fan discharge profile (figure A-IV-5) was calculated and an aluminum plate corresponding to the calculated blockage was inserted between the first and second instrumentation sections for testing (figure A-IV-6). This position was well forward of the measurement plane to allow the profile to stabilize. A series of tests with the instrumentation plane moved relative to the profile generating plate verified that the position used was properly selected. The Mach number profile produced by the plate may be seen in figure A-IV-5.

A second profile generating plate simulated the fan discharge profile from early experimental 0.6-scale fan rig test data. The fan rig exit profile differed by a considerable amount from the design prediction (figure A-IV-7). It should be noted that this profile is representative of the engine fan during the early stages of development only; these three diffuser inlet Mach number profile generating plates were used to evaluate the diffuser.

## 2. Diffuser Evaluation

Diffuser testing was performed by establishing Mach number profile for a given profile generating plate, and by traversing in the second instrumentation section to determine that the desired profile had been achieved.

The diffuser was then traversed at each of its five axial positions with both the Kiel and banjo probes. The number of points taken at each position varied with the intent of the specific program. Data from all instrumentation were taken periodically with each traverse.

The data taken during the test program were used to assess the following parameters:

### a. Determination of Diffuser Pressure Loss.

The expression of total pressure loss is

$$\frac{\Delta P_t}{P_t} = \frac{\text{Change in total pressure from inlet to exit of diffuser}}{\text{Total pressure at the diffuser inlet}}$$

In the pressure loss analysis, the Kiel probe data from traverse stations No. 1 and No. 4 were used.

The average total pressure at both the inlet and the exit of the diffuser was obtained by averaging the total pressures over equal mass areas in the diffuser for both the inlet and exit.

### b. Static Pressure Recovery

The expression for static pressure recovery is

$$\frac{P_{s4} - P_{s3}}{P_{s4(\text{theoretical})} - P_{s3}} = \frac{\text{Actual exit static pressure minus actual inlet static pressure}}{\text{Theoretical exit static pressure minus actual inlet static pressure}}$$

Theoretical exit static pressure is calculated on the basis of the isentropic expansion of an ideal gas over a given area ratio.

The static pressures used in these recovery calculations were obtained from banjo probes and wall static pressures. The values of static pressure at stations No. 0 and No. 4 were mass averaged.

## c. Diffuser Characteristics

## (1) Diffuser Wall Separation

Flow separation was assumed to have occurred when total pressure was the same or near static pressure, thus indicating zero velocity. All diffuser data at each traverse point were reviewed with this criterion.

## (2) ID Diffuser Cooling Airflow Bleed

The percent of diffuser flow passing through the annular bleed air extraction louver in the inner wall was calculated as follows:

$$\begin{aligned} \text{percent bleed flow} &= \frac{\frac{\omega_2 \sqrt{T}}{\Lambda_2 P_t} \times A_2 \times C_{d2}}{\frac{\omega_1 \sqrt{T}}{\Lambda_1 P_t} \times A_1 \times C_{d1}} \\ &= \frac{\text{Weight flow of air through bleed}}{\text{Total diffuser weight flow}} \end{aligned}$$

Discharge coefficients for diffuser and bleed cavities were assumed to be 0.96 and 0.83, respectively.

## B. TEST RESULTS

The total pressure loss and the static pressure recovery for the fan duct diffuser is shown in Figure A-IV-8. The losses are extremely low with a flat inlet profile and with the profile peaked near the outer wall. This fact is particularly encouraging because the two-stage fan of the JTP17A-20 engine is expected to produce a flat profile at cruise conditions. With the discharge profile of build No. 5 of the fan rig, the total pressure losses were below the 3% level for inlet Mach numbers corresponding to cruise conditions.

The static pressure recovery data confirmed the low total pressure losses. Even with a severely inboard peaked inlet profile, the static pressure recovery is an acceptable 70%, and approaches 85% with a flat inlet profile.



The average Mach number at the diffuser exit (combustor inlet) is shown in figure A-IV-9. The low diffuser exit Mach number and the high static pressure recovery were the primary contributors to the lower than predicted cold pressure loss of the JTF17A-20 augmentor. (See Appendix A, Section V.)

The total pressure loss of the diffuser with build No. 5 inlet profile is attributed primarily to flow separation at the outer wall. Separation of the OD wall was predicted by the water table tests. (Refer to Paragraph A-III-E.) Evidence of flow separation is shown in figure A-IV-10. The region near the outer wall becomes more deficient in flow after the initial turn, but tends to recover near the entrance to the combustor. This type of separation produced a somewhat higher total pressure loss, but would not be expected to result in operational problems (i.e., instability). Flow separation was not observed with the more uniform inlet profiles.

#### F. CONCLUSIONS

1. The fan duct heater diffuser as designed is satisfactory for engine testing.
2. The diffuser pressure loss is lower than predicted.

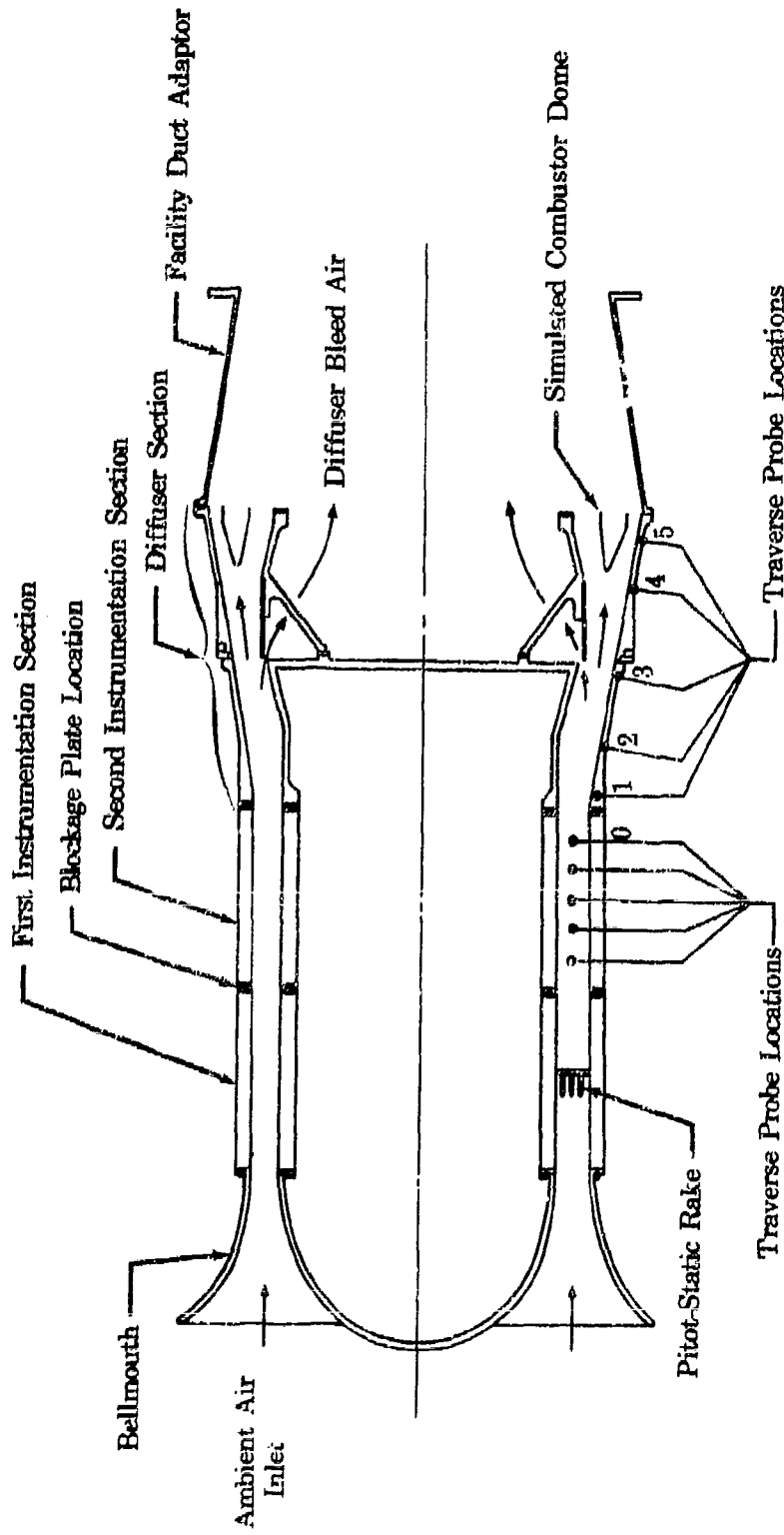


Figure A-IV-1. Schematic of 0.6-Scale Duct Diffuser Rig

FD 15370

FE 53436

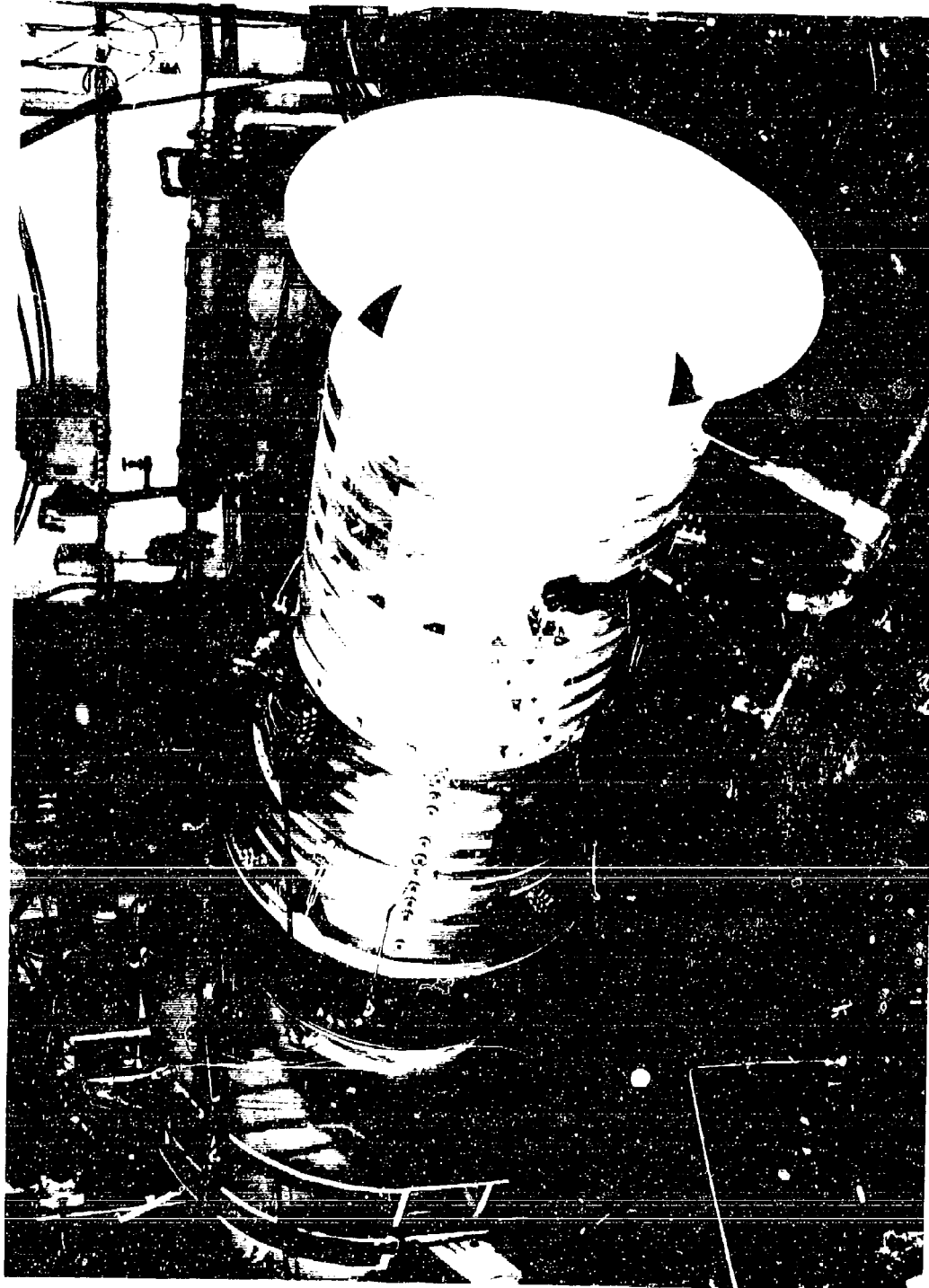


Figure A-IV-2. 0.6-Scale Duct Diffuser Rig

FE 53488

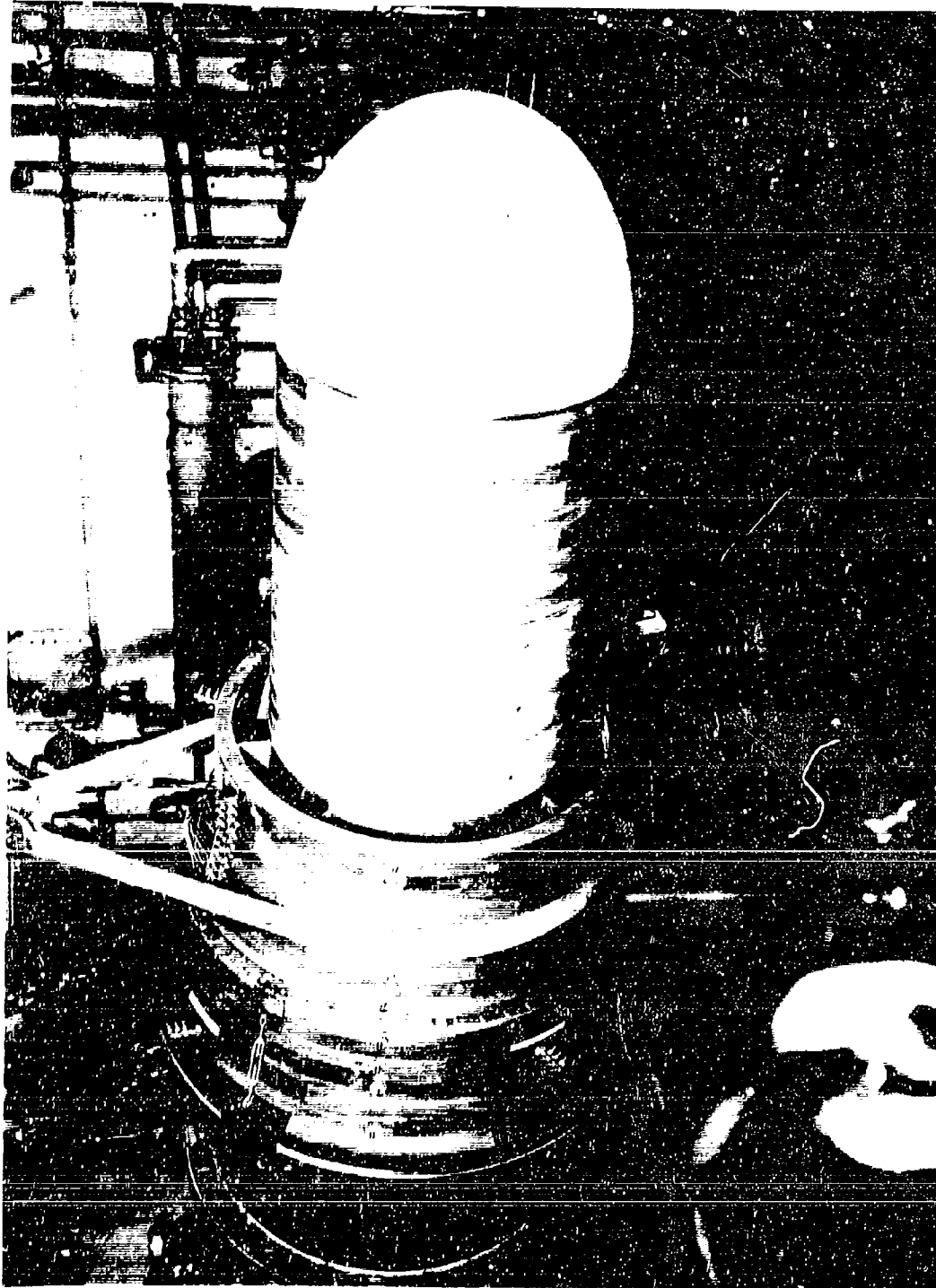


Figure A-IV-3. Diffuser Rig Centerbody

FD 15305

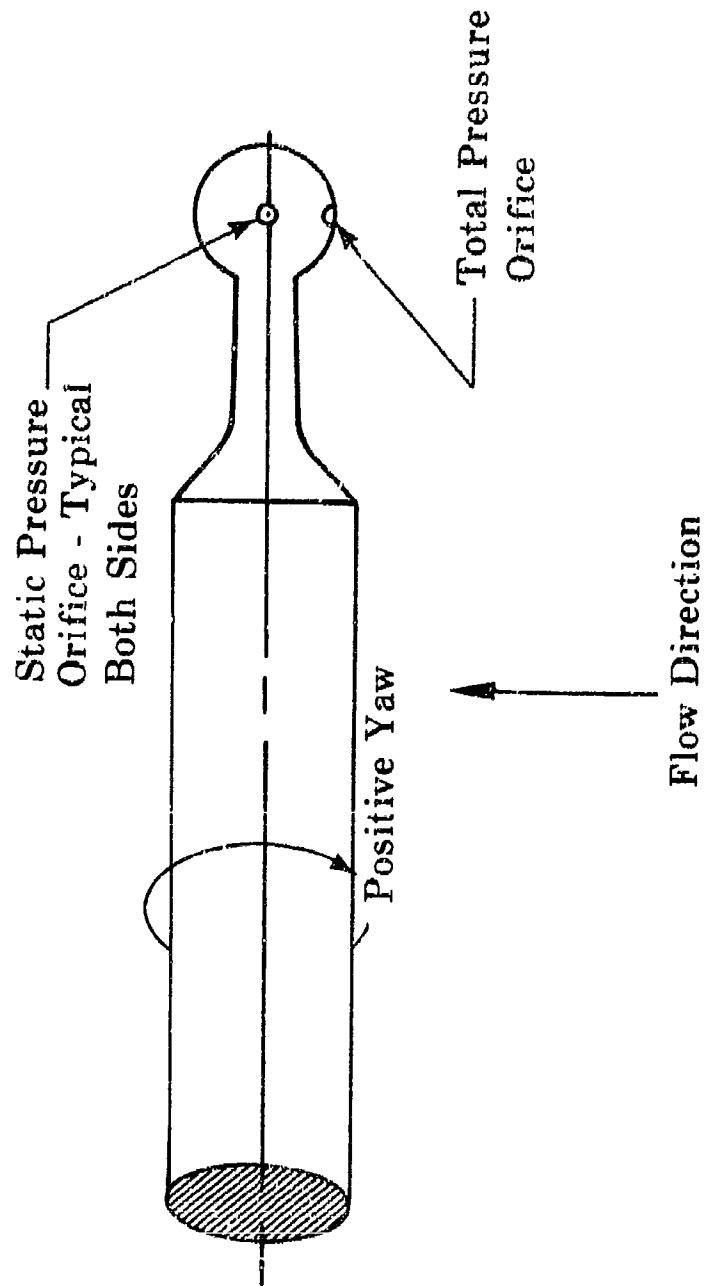
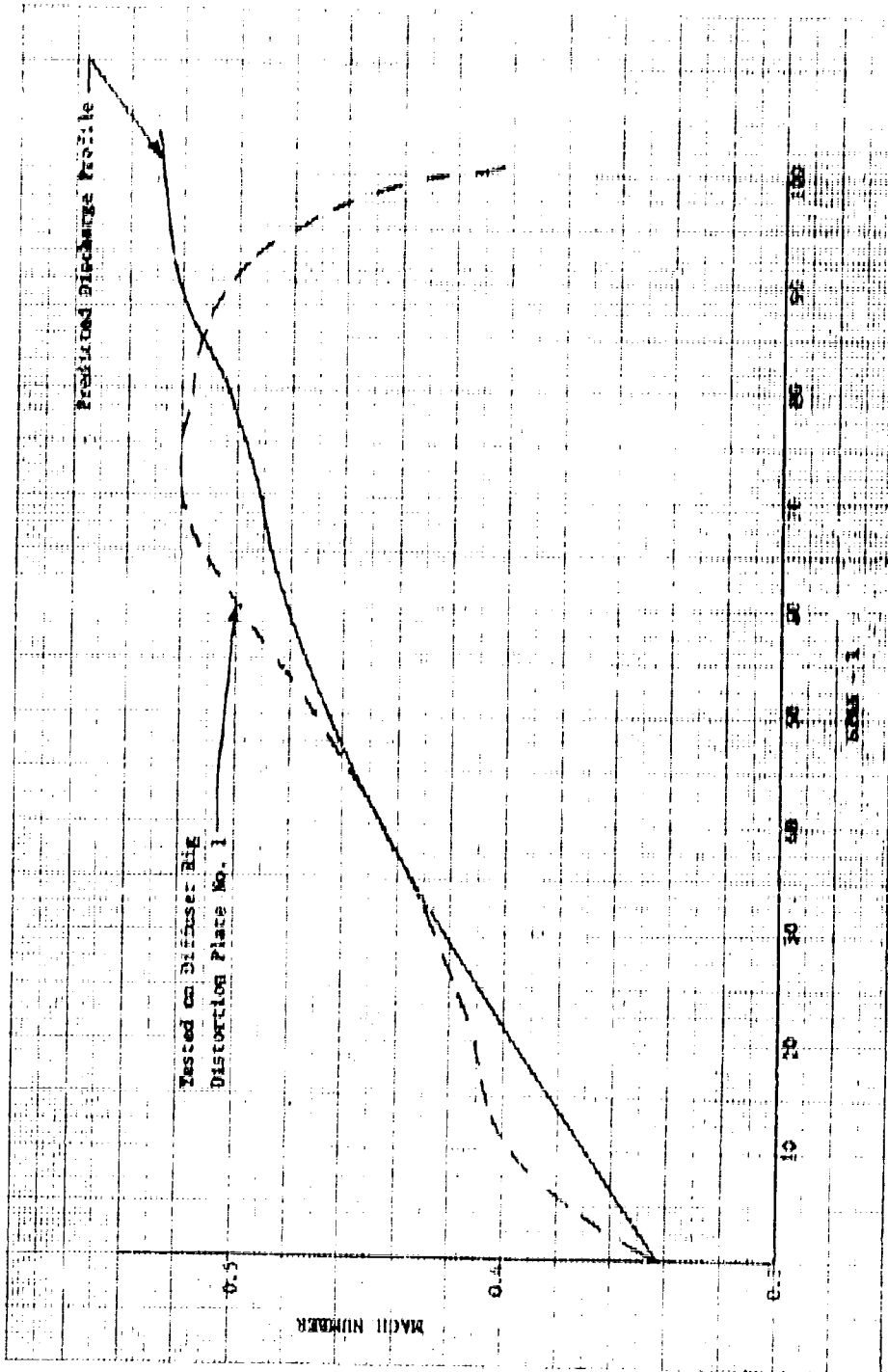


Figure A-IV-4. Banjo Traverse Probe



DE 1874

Figure A-IV-5. Predicted Fan Discharge Profile

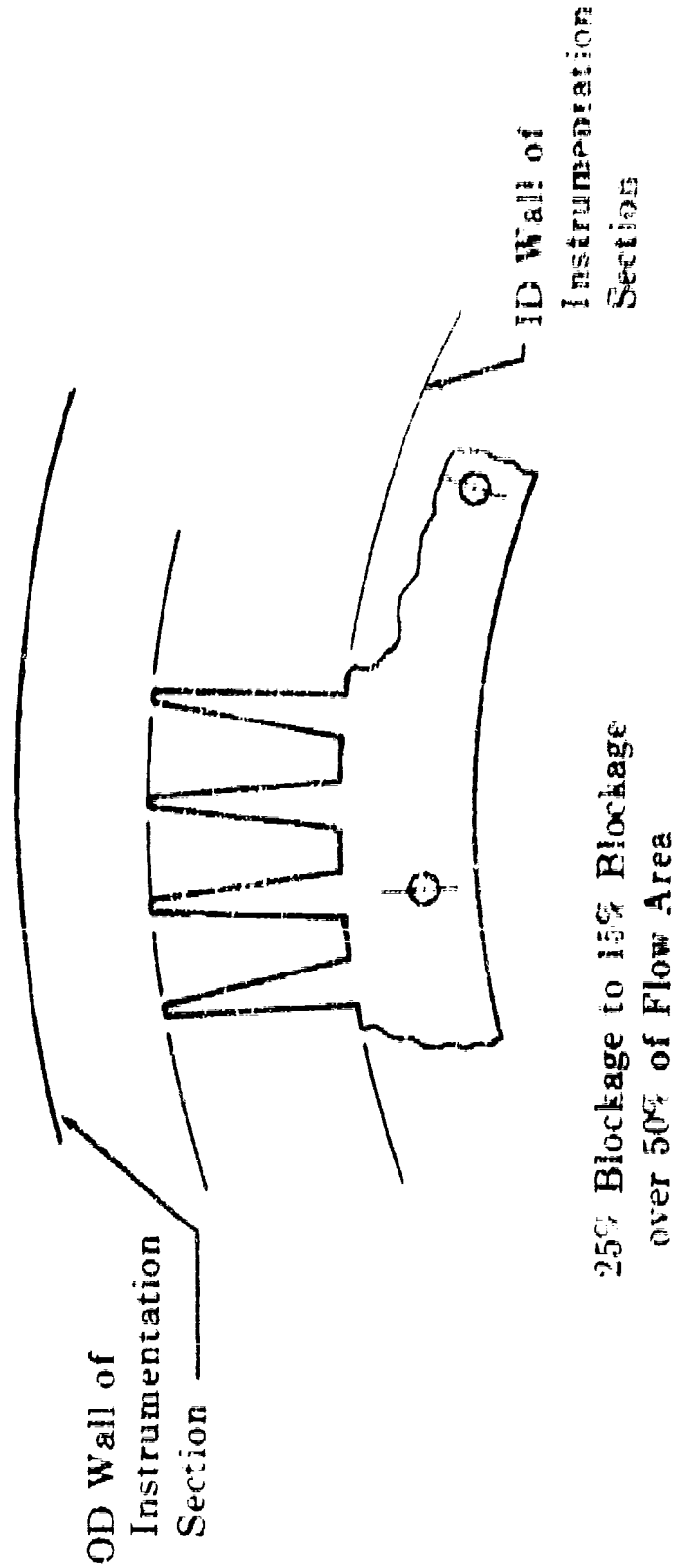


Figure A-IV-6. Diffuser Rig Flow Profile Generating Plate

DE 44675

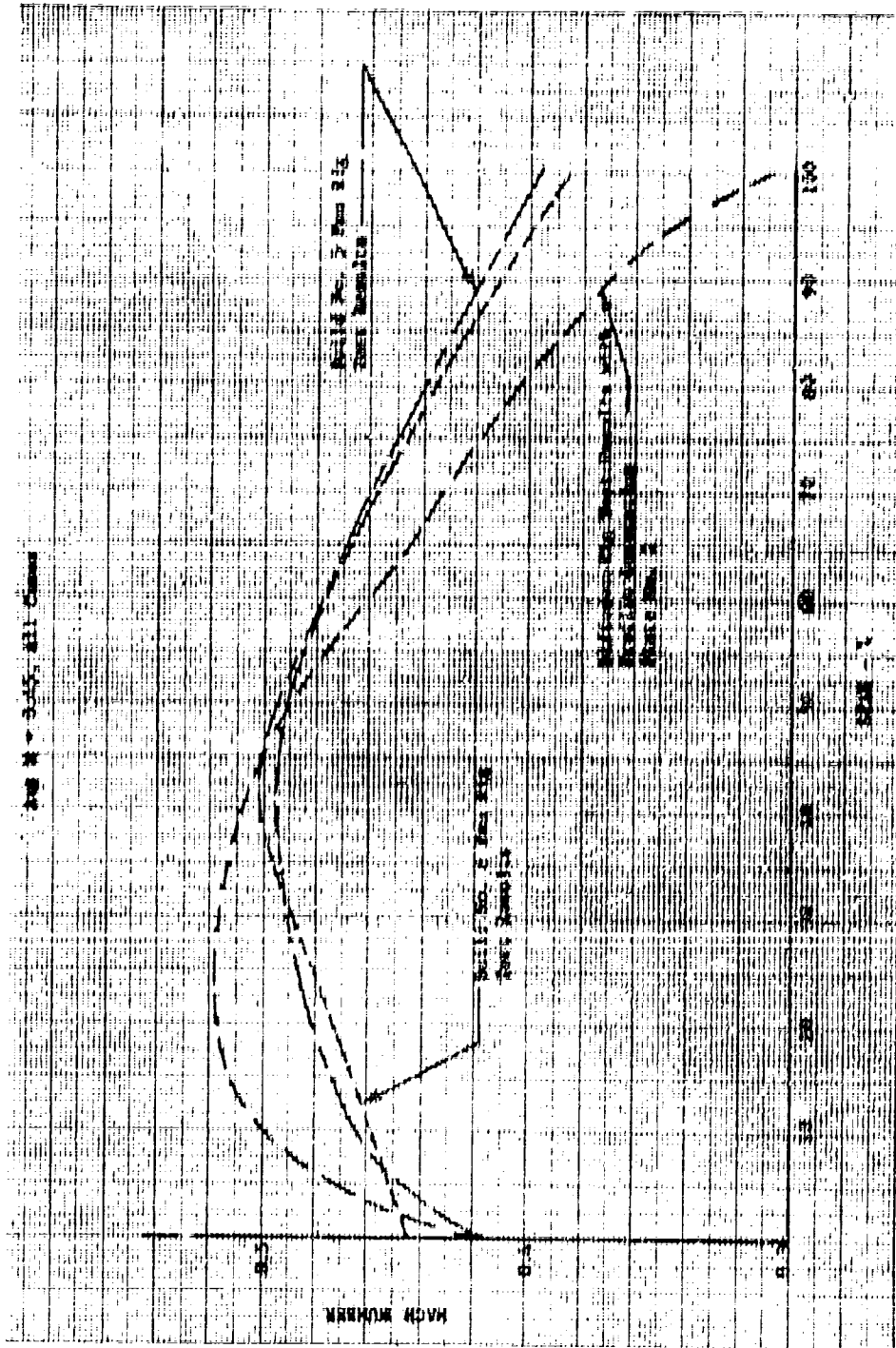


Figure A-IV-7. Duct Diffuser Mach Number Profiles



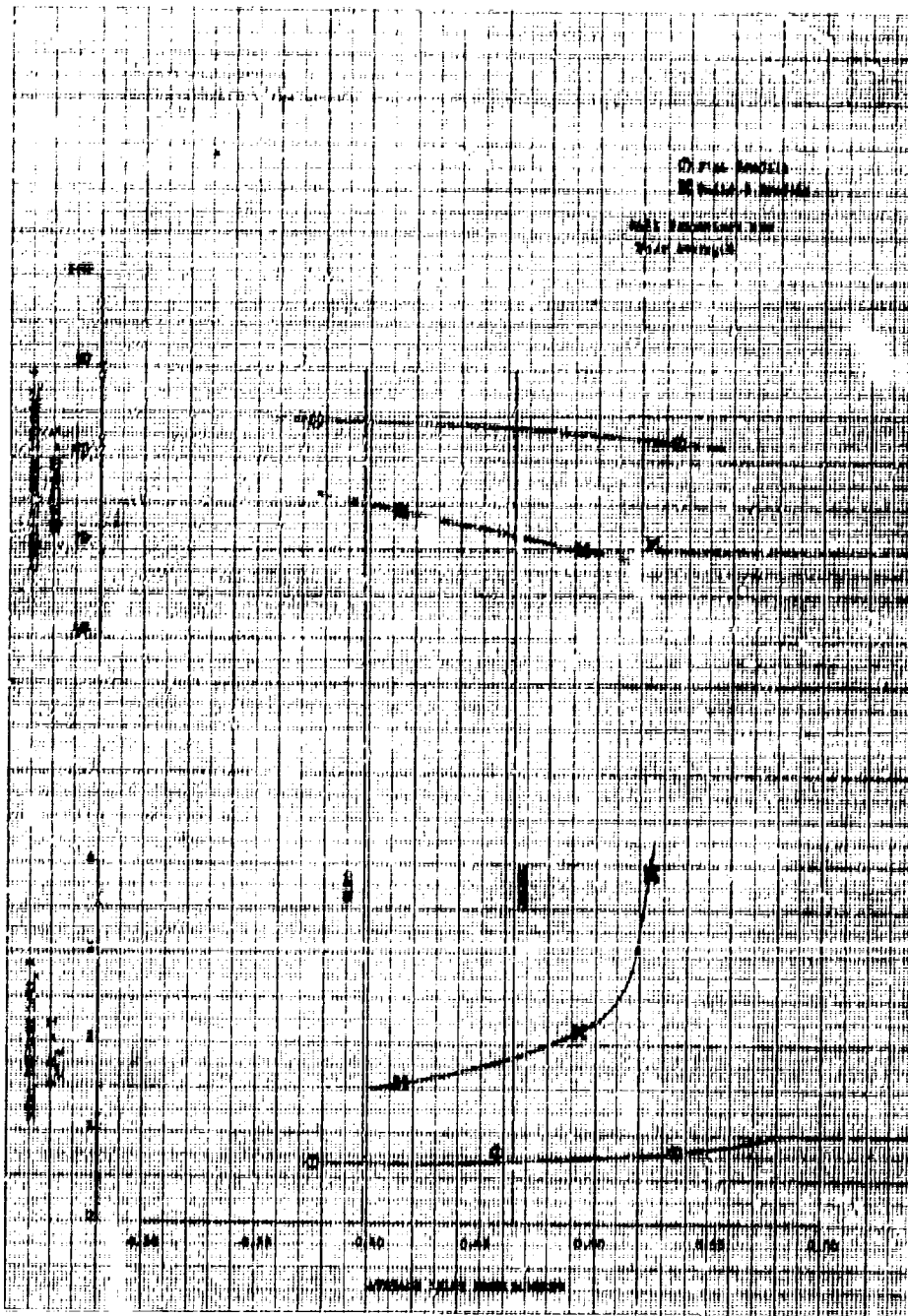


Figure A-IV-8. Total Pressure Loss and Static Pressure Recovery for Fan Duct Diffuser

DF 46676

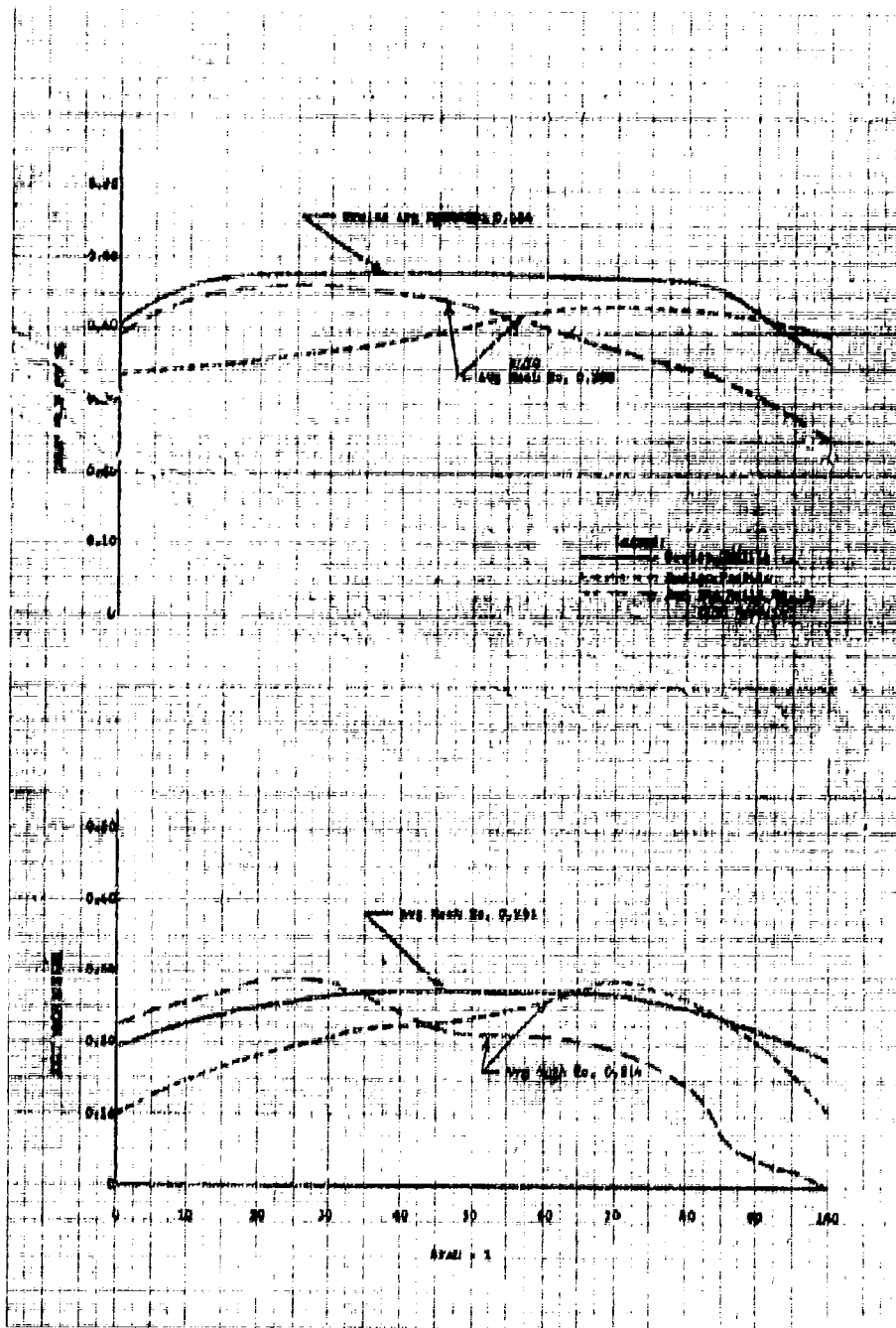


Figure A-IV-9. Interpolated Mach No. Profiles

DF 46677

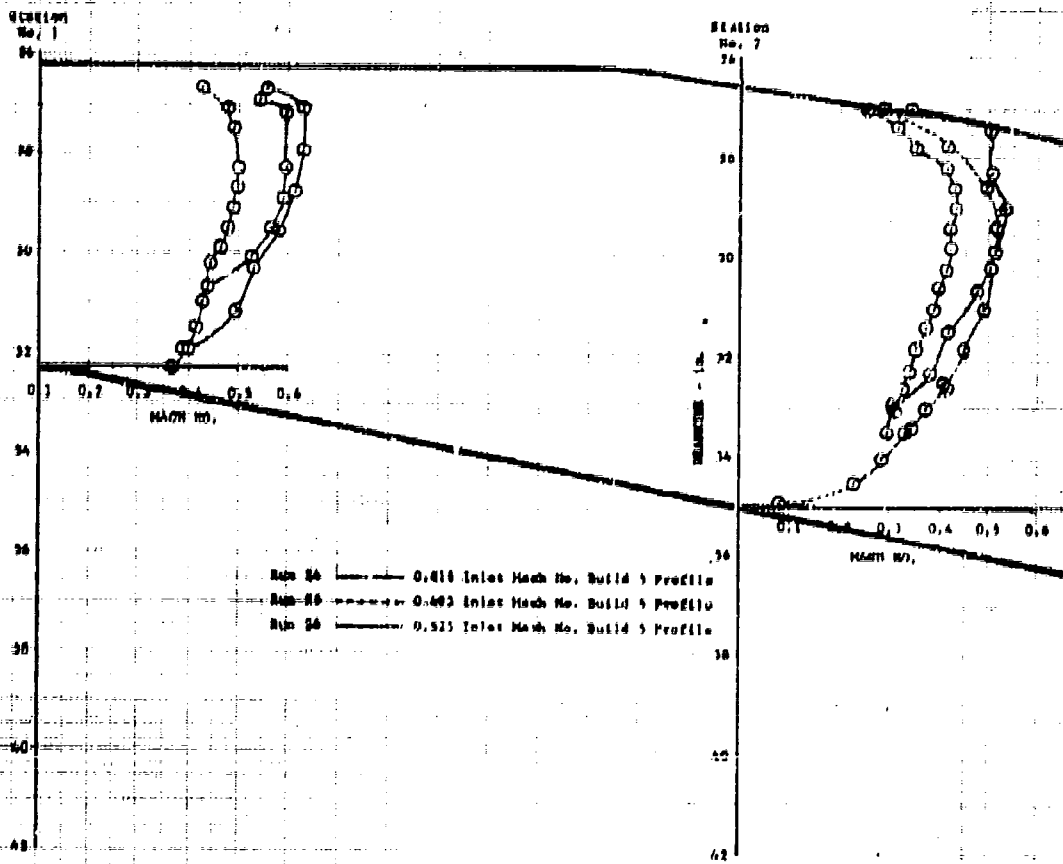
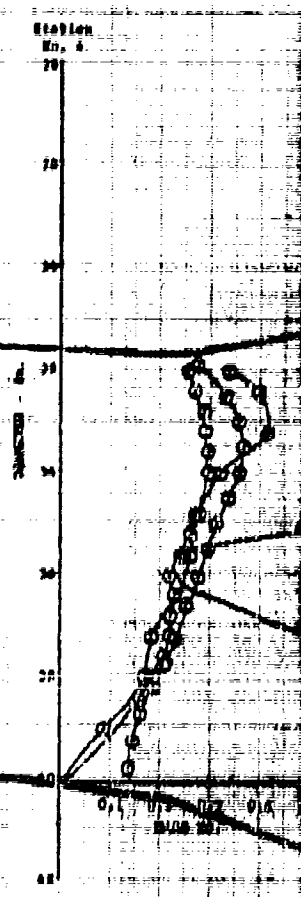
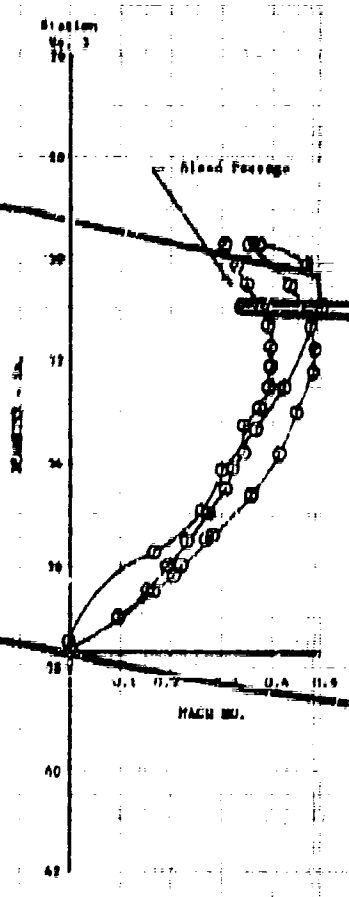
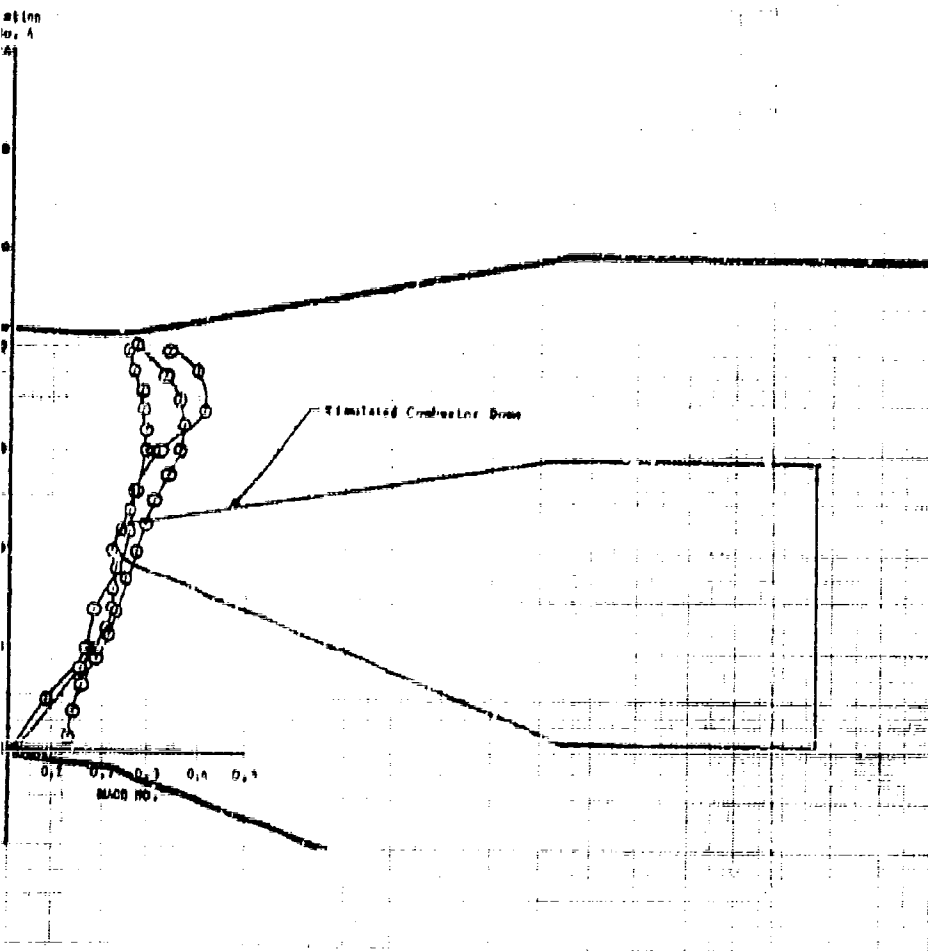


Figure A-IV-10. Mach No. Profiles



2

Pratt & Whitney Aircraft  
FWA FR-1855  
Appendix A



DF 46678

A-IV-16

3

SECTION V  
FULL-SCALE ANNULAR DUCT HEATER TESTS  
RIG TESTING

A. RIG DESCRIPTION

The full-scale annular duct heater rig consisted of the following sections, as shown schematically in figure A-V-1:

1. Adapter section
2. Diffuser section
3. Combustor section
4. Tailpipe section
5. Fixed-area nozzle
6. Variable-area nozzle.

The adapter section consists of the front bullet and the inlet case that adapts the diffuser section to the facility plenum chamber. The front bullet has a 10-inch diameter vent hole to provide for a positive outward pressure across the inner cylinder during rig operation.

Although of heavier construction, the diffuser section is aerodynamically the same as the engine, and consists of an annular diffuser with eight struts supporting the inner body. Instrumentation and cooling water for the rear bullet are fed through these struts.

The combustor section consists of the combustor support case, combustor and tailpipe. Cooling air for the ID liner is bled from the diffuser by an annular stepped slot in the diffuser case inner wall. This cooling flow accounts for approximately 10% of the total inlet flow. The combustor is cantilevered from eight support struts.

The duct heater combustor in the combustor support case, shown in figure A-V-2, is of the ram-induction design. Scoops and turning vanes and a slot at the front of the burner dome direct air into the combustor. The scoops are staggered to provide for uniform mixing of air and fuel. Fuel is introduced through two zones of injection. Zone I consists of 40 variable-area, dual-orifice nozzles incorporating a swirler around each nozzle. These nozzles are inserted through the outer case and into the dome of the combustor. Zone II consists of 10 manifolds (6 outer and 4 inner) that have a total of 272 injection elements. Figure A-V-3

shows a cross section of the Zone II fuel injector. Fuel pressure deflects the diaphragm, thus allowing increased flow. Slots in the seat impart a swirl resulting in a hollow cone spray. Fuel flow-pressure characteristics for the Zone I nozzles and Zone II injectors are shown in figures A-V-4 and A-V-5. Turbulators behind the fuel injectors direct some fuel into the "pilot" flame from the combustor and also promote additional turbulence and mixing with the duct heater combustor discharge air.

The outer cooling liner is composed of 60 pressure-loaded catenary segments, each having forward, intermediate and rear liner portions. These segments are mounted individually in axial tracks to provide support, allow for thermal expansion, and enhance maintainability. The rear and intermediate liners are corrugated to allow for differential axial expansion (i.e., the center of the catenary can expand more than the edges). The forward liners are perforated to provide for sound suppression and to damp combustion instability. Two configurations of front liners were tested. The original design (figure A-V-6) contained punched holes that provided a 9.0% open area for the first 9 inches of the liner. For improved absorption, the holes in the second liner configuration, shown in figure A-V-7, were plunged to increase the effective thickness of the air mass in the apertures. Air through the outer liners was metered by the discharge area of the rear liner segments. The inner liner was film cooled by three slots through which air was injected axially along the circumference of the inner liner.

A fixed annular nozzle is used to calculate duct heater discharge temperature through use of the continuity equation. This nozzle consists of a water-cooled inner bullet and a water-cooled outer housing. Three outer housings were fabricated to provide a range of exhaust nozzle areas. An 11.0-ft<sup>2</sup> nozzle was used during the sea level test and a 6.1-ft<sup>2</sup> nozzle was used for the altitude tests. Eight total temperature and pressure radial traversing probes were mounted on the case (extensive redesign of the mounting brackets was necessary to minimize leakage around these probes; the modified design incorporated a seal cavity with an external pressure supply to balance against burner pressure).

A variable nozzle (figure A-V-8) was used downstream of the fixed nozzle to establish inlet Mach number and burner pressure independent of burner outlet temperature. The variable nozzle is a modified J58 afterburner nozzle installed in a water-cooled housing. The J58 nozzle was modified by adding extensions to the flaps to provide a minimum area of 3.5 ft<sup>2</sup>. Cooling air, amounting to approximately 3% of the total airflow, was bled downstream of the airflow measurement orifice to cool the flaps.

Ignition was accomplished by utilizing two spark igniters and two 4-joule low-tension exciters with a 28-volt d-c input voltage. The spark igniters were mounted on the combustor support case and extended through the combustor outer wall. The igniters were located approximately 2-1/2 inches downstream and in line with the Zone I fuel nozzles.

#### B. TEST STAND DESCRIPTION

The duct heater rig was mounted in C-4 test stand (figure A-V-9). This facility has the capability of operating the duct heater within the engine operating envelope in the areas of principal interest. Figure A-V-10 shows the operational capabilities of the test stand.

The separate fuel supply systems for Zone I and Zone II are shown schematically in figure A-V-11. The fuel, commercial aviation kerosene, is pumped by a constant displacement pump. The fuel bypassed sets the amount of flow into the rig; vernier valves permit fine control of the bypass flow. A three-way valve either directs the flow to the rig or through a recirculating loop. A typical starting sequence is to establish the starting flow with the three-way valve in the closed position. The back pressure is established by the recirculating system back pressure control valve to the back pressure on the Zone I nozzles; thus, when the three-way valve is opened, flow remains constant.

An automatic abort system is electrically connected to two ultra-violet sensing photoelectric cells. If ignition does not occur within 20 seconds after an attempt, i.e., if both "fire eyes" show no output, the three-way valve closes and a 5-minute air purge sequence is started.



### C. INSTRUMENTATION

The rig was fully instrumented to measure temperatures and pressures within the duct heater, as well as pressures, acceleration, velocity, and displacement of various components of the burner. Figure A-V-12 shows the location of the temperature and pressure measurements.

The primary purpose of the instrumentation was to measure combustion efficiency, pressure loss and cooling liner flow. Efficiencies were calculated from the measurements of airflow through a standard 40-inch orifice, fuel flow through turbine flowmeters, and exit temperatures and pressures from eight traversing probes. Each of these burner exit temperature probes incorporated aspirated, shielded, irridium-irridium-rhodium, dual-element thermocouples and total pressure sensing elements. These probes were mounted on a mechanism that radially traverses the exit area in 10 equal area steps. The traverse control automatically stopped at each position, stabilized for a preset time period, provided the automatic data recording system with a record signal, and then proceeded to the next point.

Data were recorded by a CEC Millisadic Recording System. Each channel was recorded 10 times and averaged; 21 seconds were required for a complete scan of all channels. This average constituted the measurements utilized in the analysis of data. After the data were recorded on tape, they were transmitted to the data recording center, which programed the channels into an IBM 1410 computer. Efficiency, diffuser inlet Mach number, airflow, fixed-area nozzle pressure ratio, and burner exit temperatures were then transmitted back to the test stand control room via teletype. Manometers, gages, flow counts and temperature readouts were provided in the control room to monitor rig operation.

High-frequency-response pressure crystal pickups monitored pressure oscillations in the combustor tailpipe, diffuser, and in the facility plenum. Accelerometers are placed in the rear portion of the centerbody. Accelerometers were also mounted on the burner case in the vertical plane. These measurements were recorded on a CEC magnetic tape recorder. In addition, the displacement and vibration were monitored on meters in the control room during rig operation. Starting transients and Zone II ignition were monitored on an oscillograph.

#### D. ANALYSIS OF DATA

With the instrumentation provided, combustion efficiency can be calculated by several methods. Two methods, one of which was a check on the other, were used to determine exit temperatures needed for calculating the combustion efficiency:

1. Mass weighted exhaust temperature from exhaust pressure and temperature measurements. This method provides an assessment of the chemical combustion efficiency.
2. Calculate exhaust gas temperature based on total and static pressures and flow at the fixed-area nozzle through the use of the continuity equation. The effective area of the fixed nozzle was determined from 0.6-scale model calibration tests. This technique provides a "thrust equivalent" combustion efficiency.

The efficiencies calculated were based on total airflow through the diffuser and take into account a radiation loss of the rig to ambient conditions. Redundant instrumentation was used on all performance parameters to decrease error.

#### E. OBJECTIVES

The objectives of the test program using the full-scale annular burner were as follows:

1. Demonstrate the combustion efficiency of the duct heater at cruise and sea level conditions
2. Determine the combustion efficiency lapse rate with altitude
3. Demonstrate the durability of the combustor and cooling liners
4. Determine the total pressure losses of the diffuser and duct heater
5. Demonstrate duct heater ignition and determine the pressure rise at ignition of both Zone I and Zone II fuel flow.

## F. TEST RESULTS

The full-scale annular duct burner was tested for a total of 45.0 hours. The range of simulated flight conditions at which the burner was tested is listed in the following table:

Parameter	Maximum	Minimum
Burner pressure, psia	11.0 (80,000 ft)	40.0 (Sea Level)
Inlet temperature, °F	650	270
F/A ratio	0.058	0.001

The condition of the duct heater after test, as shown in figure A-V-13, was excellent, no evidence of overheating existed and a minimum of carbon was deposited inside the dome. The turbulators on the outside of the annulus were in good condition; however, the outer vane of several of the inner turbulators overheated. This is believed to have been caused by impingement of hot gases from the combustor. The inner liner was adequately cooled with no sign of overheating. At all conditions tested, approximately 6.0 to 8.5% of the total airflow entered the inner cooling liner.

The convoluted OD liners were properly cooled. Approximately 7.5 to 11% of the total airflow entered the outer liners. Of this, 2.5 to 3.5% of total airflow discharged from the rear cooling liners. Some intermediate and rear liners did, however, crack during the tests. The failure of these liners was attributed to stress concentrations and vibration resulting from pressure oscillations in the tailpipe. Figure A-V-14 shows typical liner failures.

The design of the OD liner segments has been revised to eliminate rapid changes of material cross section and to provide more generous radii at the corners of the segments. The forward OD liner segments have been redesigned by increasing the length of the apertures to increase the sound absorption capability of the liner. The design procedure followed is described in \*Utvik et. al., and was incorporated into an IBM computer program. Increasing the depth of the liner apertures increases the

---

\*Utvik, D.A., H.J. Ford and A.W. Blackman, "Evaluation of Absorption Liners for Suppression of Combustion Instability in Rocket Engines." AIAA Preprint. Propulsion Joint Specialist Conference, Colorado Springs, Colorado, June 1965.

acoustical mass of the Helmholtz resonator formed by the space between the liner segment and the outer wall of the duct. This provides a higher sound absorption coefficient at low frequencies. A measure of the effectiveness of this modification can be seen by the fact that the pressure oscillations in figure A-V-15 were reduced to one-half as shown in figure A-V-16. Further reduction in the amplitude of the pressure oscillations is expected to be achieved with a liner configuration now being fabricated having a longer aperture and increased resonator volume. This configuration will be evaluated in engine tests.

The combustion efficiency of the duct heater as determined by the exhaust temperature measurements is shown in figure A-V-17. The results of the sector rig tests are also shown in figure A-V-17 to demonstrate the excellent agreement with the annular rig results. The duct heater efficiency was over 95% in the expected cruise conditions (Mach No. = 2.7, Altitude = 65,000 ft) and at SLTO. A reduction in combustion efficiency at altitudes above 65,000 ft was observed in the 7 x 11-inch sector rig. Considerable improvement was made to the low pressure operating characteristics of the sector combustor (Section III) by rescheduling the airflow into the combustor and improving flow recirculation in the rear portion of the combustor. Changes to the front end of the full-scale duct heater combustor in a similar manner would rectify this. Temperature and pressure measurements across the rig exit plane furnished data at  $F/A = 0.025$ , Mach No. = 2.7, and altitude of 65,000 feet; these data are shown in figure A-V-18. The same parameters at SLTO conditions with Zone I fuel flow only, and with Zones I and II are shown in figures A-V-19 and -20, respectively.

It should be noted that the temperature profile peaks close to the inner wall during Zone I only operation because in the original design the combustor was positioned closer to the inner wall to provide air to the OD cooling liners. The outer liner cooling airflow was reduced by decreasing the height of the convoluted liner segments at a time when changing the combustor dimensions was deemed impractical.

The SLTO combustion efficiency at fuel-air ratios above 0.042 were not valid because of nonuniform Zone II fuel distribution. Foreign material in the test stand plumbing supplying the inner Zone II manifold partially plugged the inner fuel injectors. Figure A-V-21 shows the change in radial temperature profile as Zone II fuel flow was increased. The maximum temperature of the stream (i.e., the OD region) did not increase for fuel-air ratios above 0.049. These data indicate that the local fuel-air ratio at the OD was over stoichiometric and that the local fuel-air ratio at the ID was less than the desired value.

Total pressure loss of the diffuser section (Station 3 to 4) is shown in figure A-V-22. The very low level of total pressure loss resulted from high levels of diffuser efficiency, as was discussed in Section IV. Good agreement in the total pressure loss, as measured in the 0.6-scale diffuser rig and the full-scale duct heater rig, was obtained.

The cold total pressure loss between the diffuser exit and the combustor exit is shown in figure A-V-23. The loss is somewhat less than predicted because of the lower value of diffuser exit Mach number associated with the highly efficient diffuser. The overall cold total pressure loss for the duct heater system is shown in figure A-V-24. The results show the additive effects of the diffuser and combustor pressure losses.

The total pressure loss of the duct heater with combustion is shown in figure A-V-25. The hot losses are a strong function of temperature rise and generally were slightly lower than the levels predicted by "Reyleigh line" or momentum change relations where the Mach number is assumed to be the "Reference" Mach number of the duct heater. This result would imply that the principal heat addition is in a region of the combustor where the velocities are lower than the reference values.

The duct heater was successfully ignited at all conditions attempted using the 4-joule electrical ignition system planned for the engine. Ignition was accomplished with a slight rise in duct heater pressure, as can be seen in figures A-V-26 and -27. Successful lights were obtained with combustor fuel-air ratios 0.0014 to 0.0048. The phasing-in of Zone II fuel in incremental changes produced no pressure discontinuity (figure A-V-28).

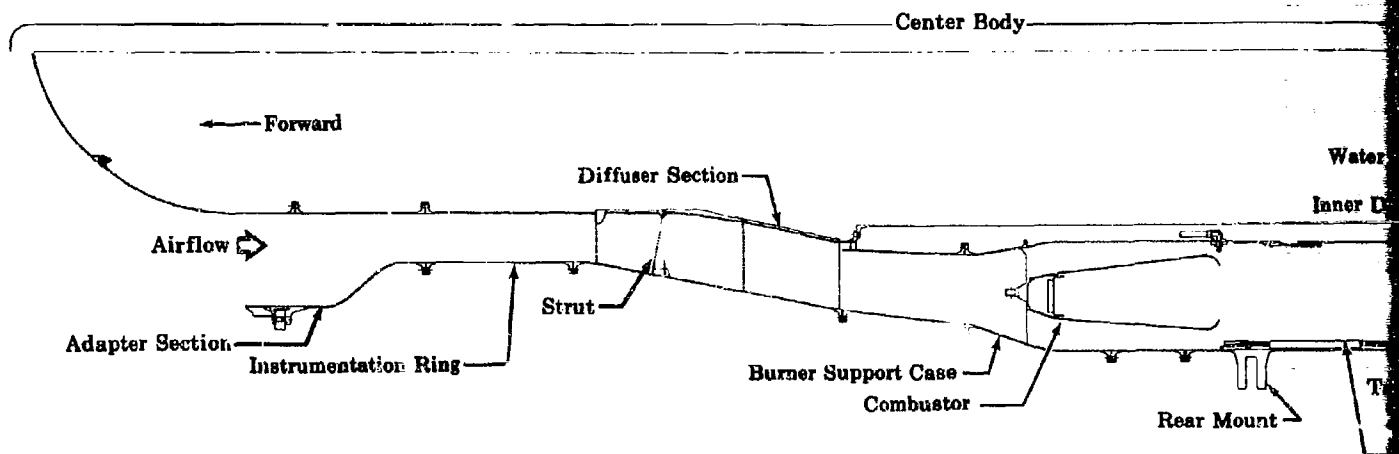
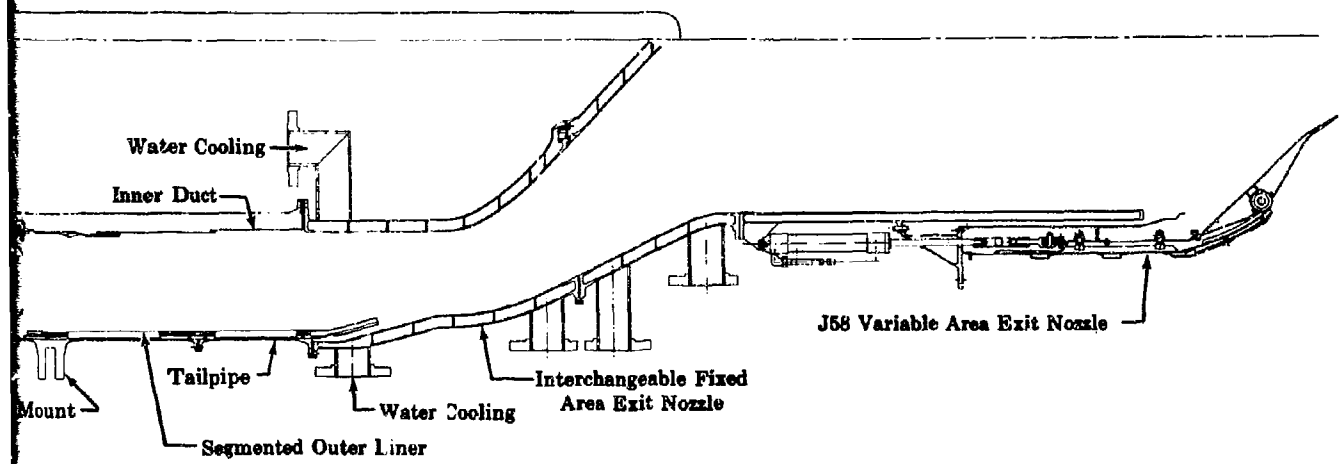


Figure A-V-1. JTF17A-20 Full-Scale Duct Heater Rig



FD 14486B

A-V-9

2

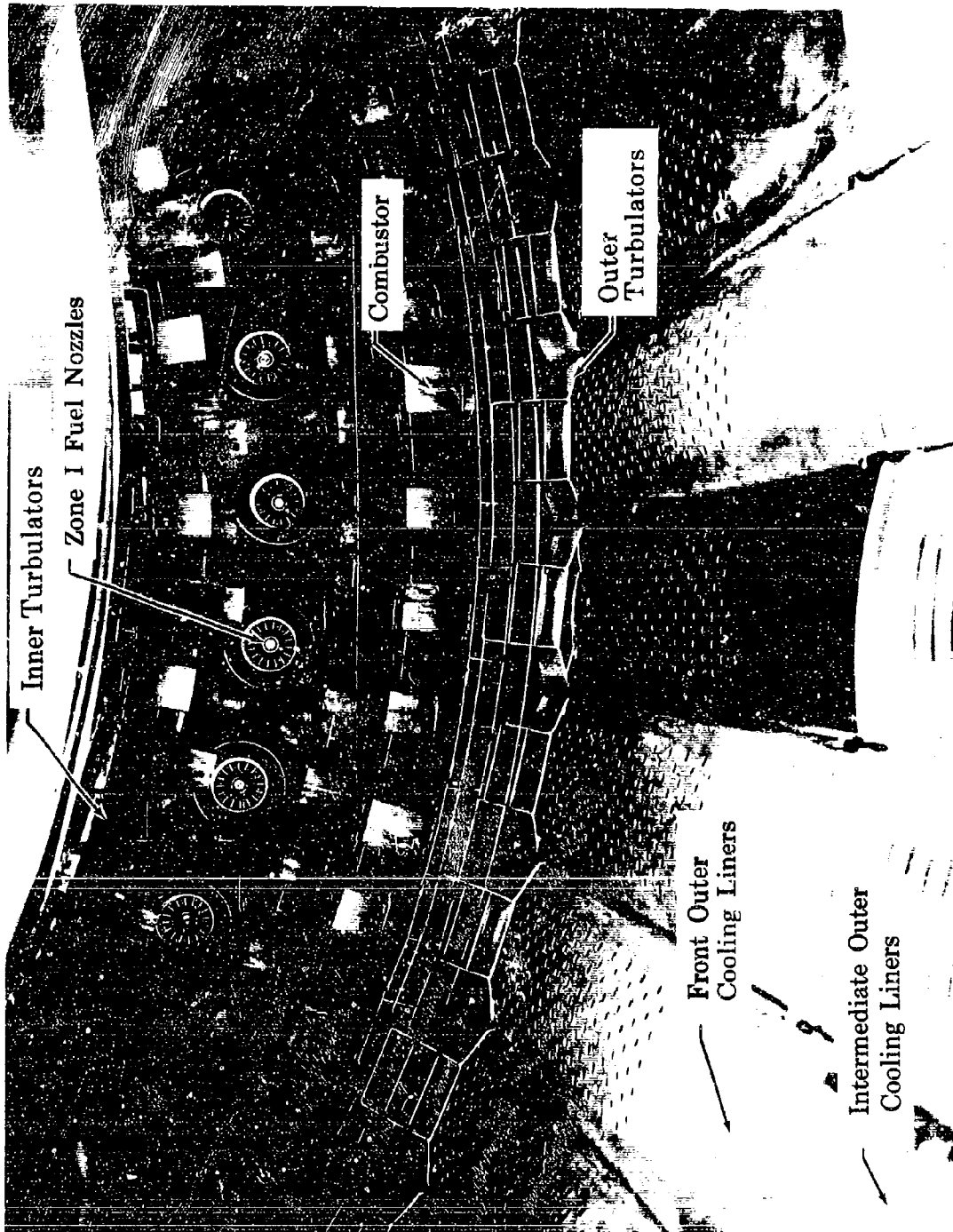


Figure A-V-2. Annular Duct Heater After Cruise Testing



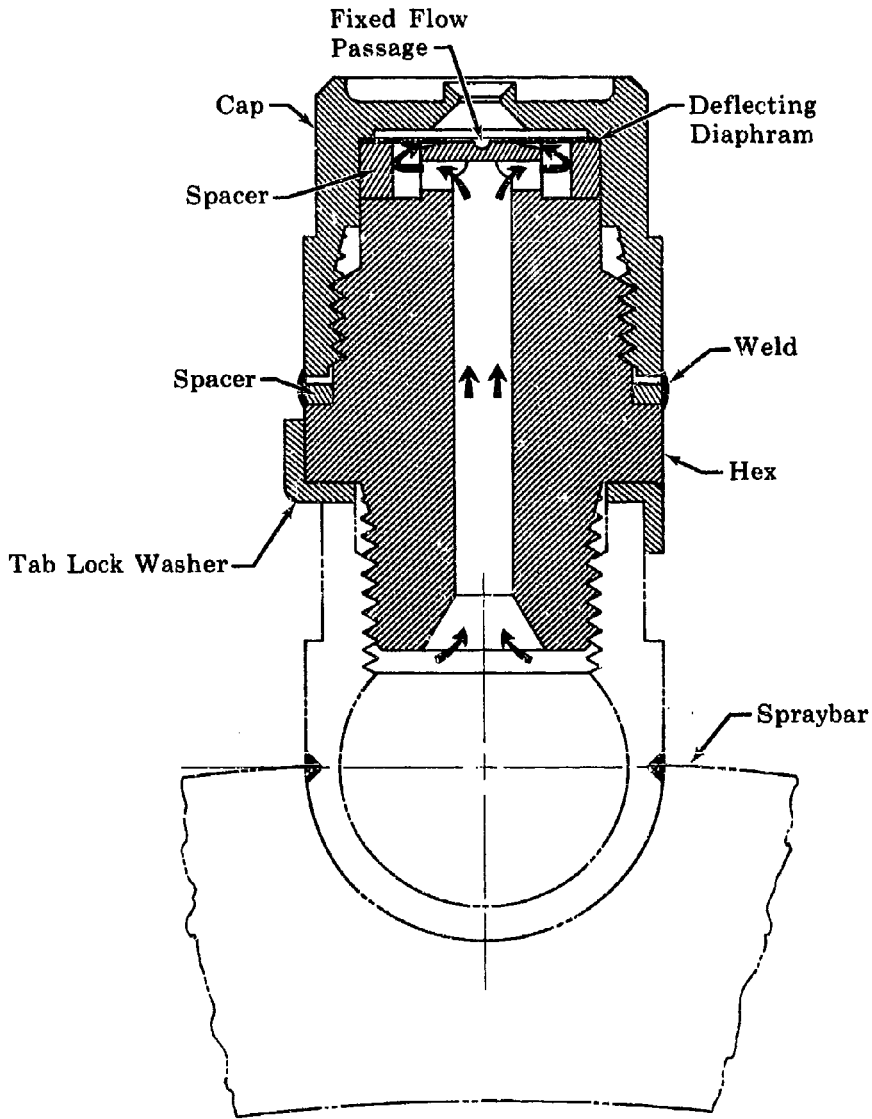


Figure A-V-3. JTF17A-20 Zone II Duct Heater Fuel Nozzle

FD 14324

DE 46730

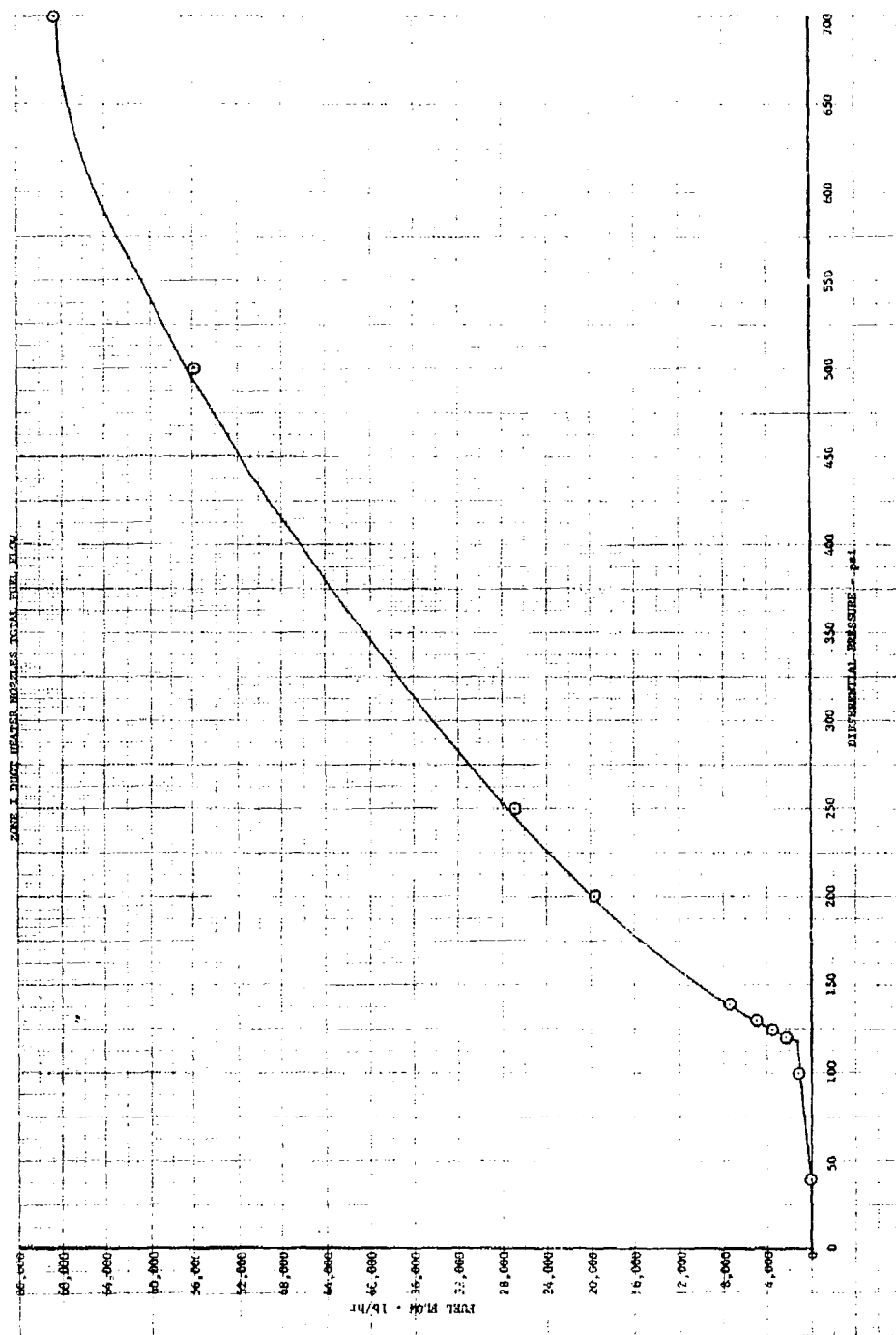


Figure A-V-4. Zone I Duct Heater Nozzles Total Fuel Flow

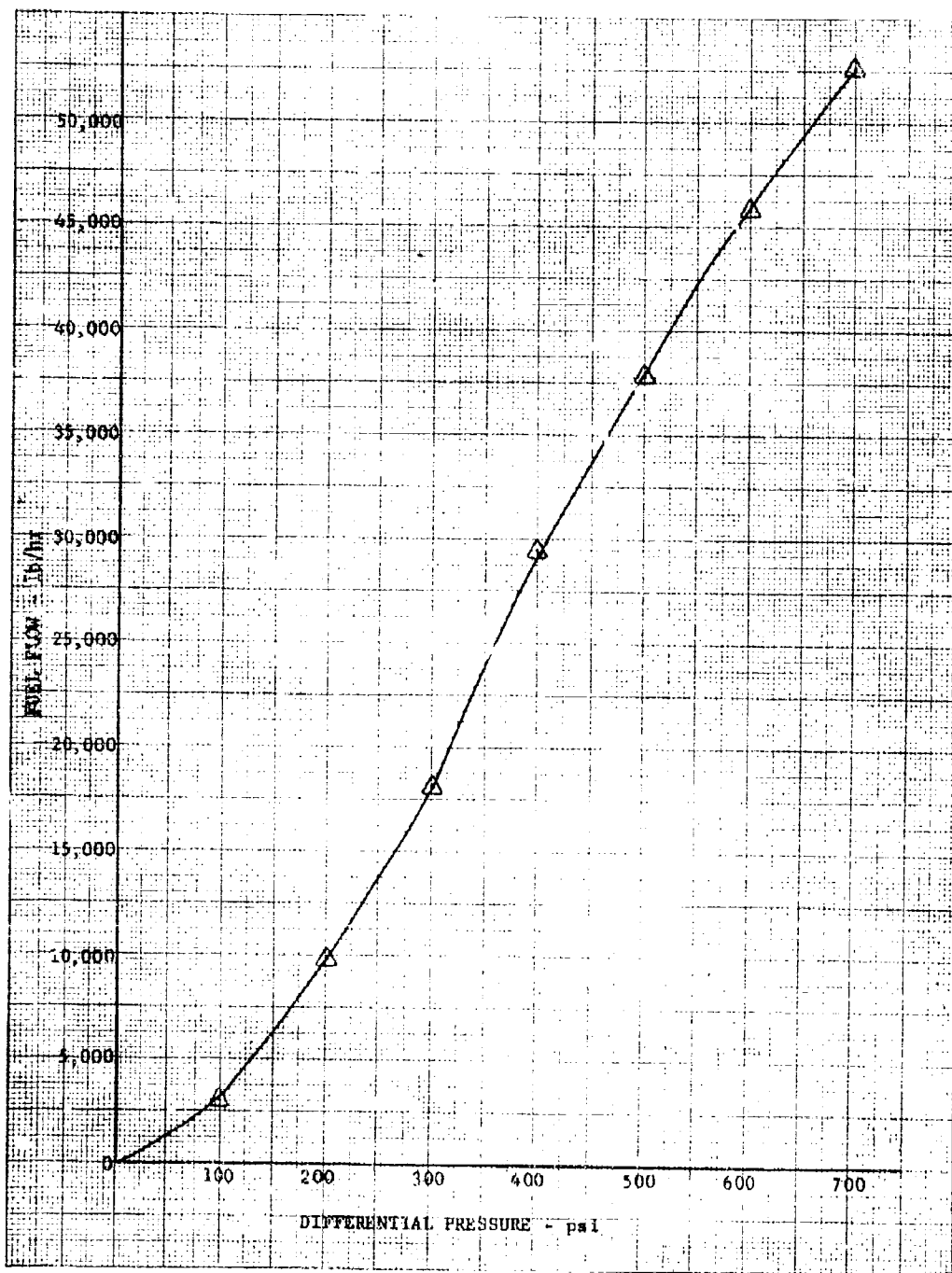
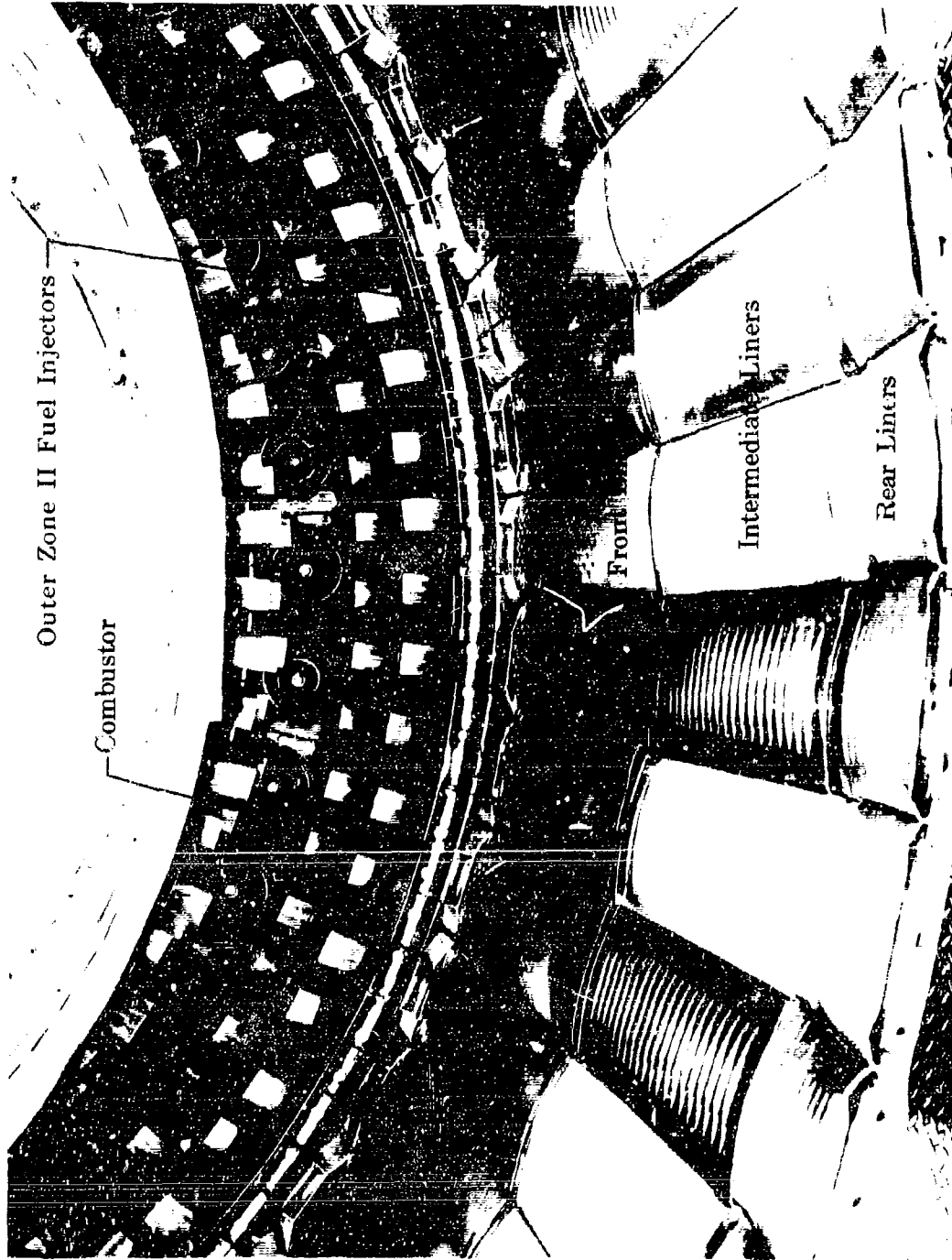


Figure A-V-5. Zone II Duct Heater Spraybar Total Fuel Flow

DF 46731

**CONFIDENTIAL**

Pratt & Whitney Aircraft  
PWA FR-1855  
Appendix A



FD 15312A

Figure A-V-6. Annular Duct Heater, Including Outer Cooling Liner Segments

A-V-14  
**CONFIDENTIAL**

**CONFIDENTIAL**

**Pratt & Whitney Aircraft**

PWA FR-1855

Appendix A

FD 15310

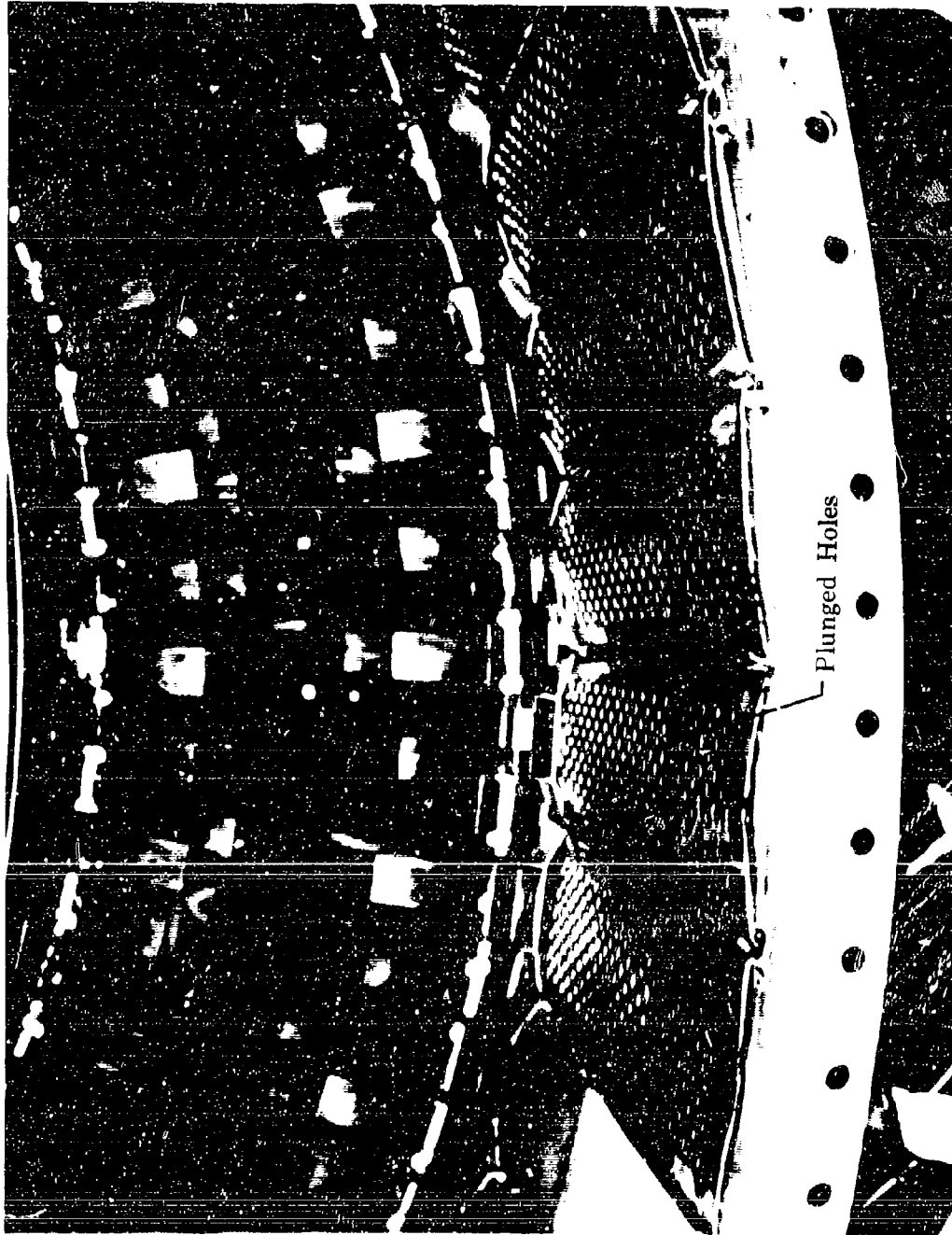


Figure A-V-7. Forward Outer Liner Segment Showing Plunged Sound Absorbing Holes

A-V-15  
**CONFIDENTIAL**

Pratt & Whitney Aircraft

PWA FR-1855

Appendix A

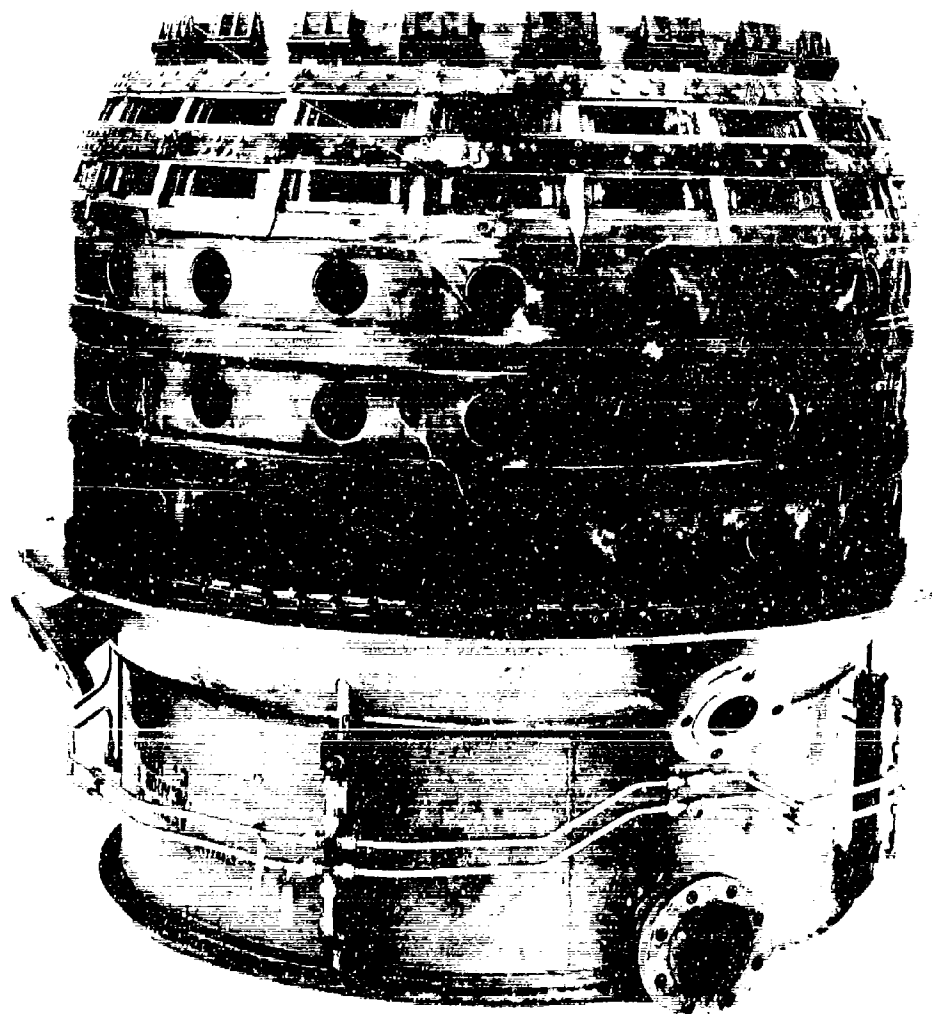
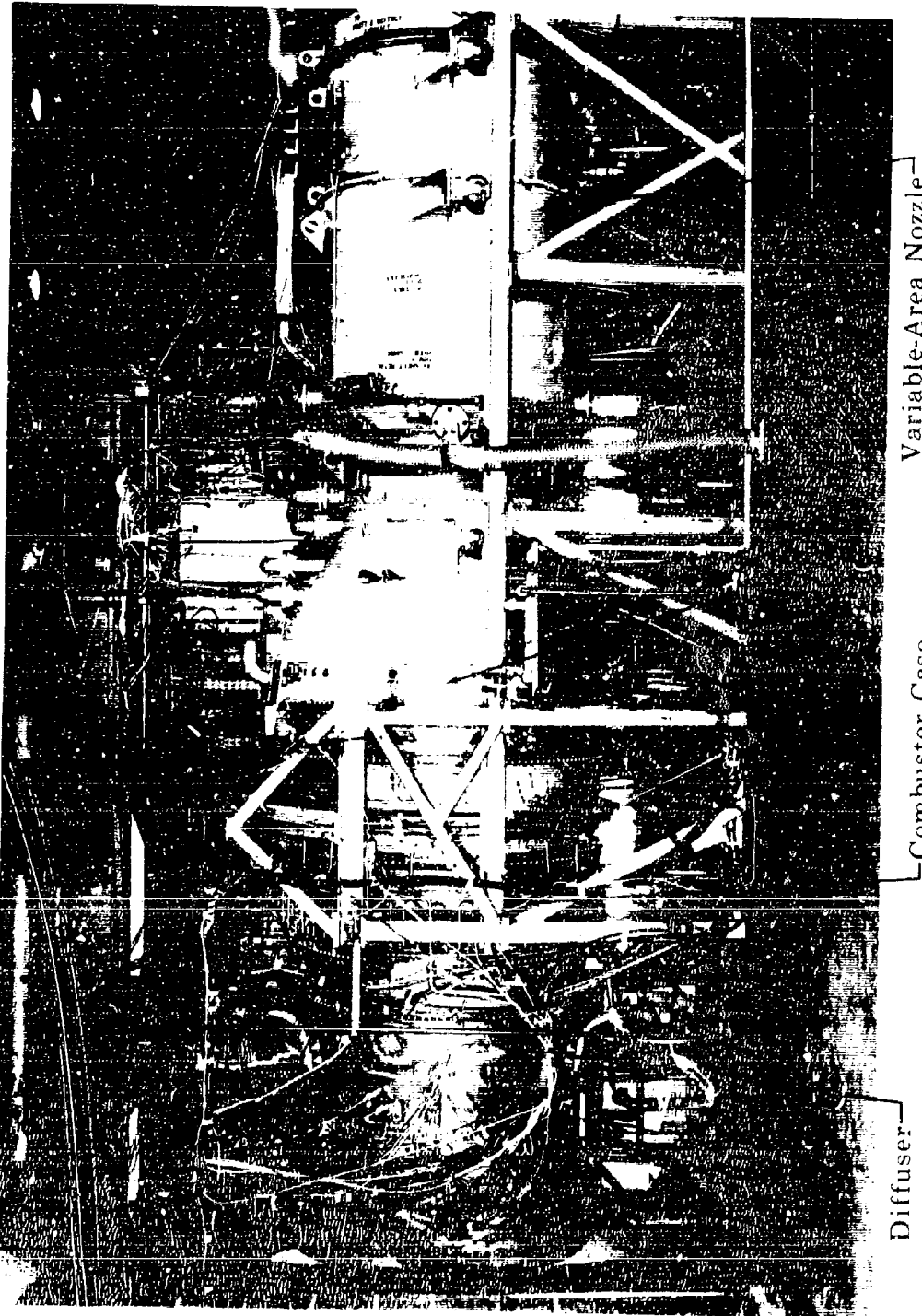


Figure A-V-8. Variable Exhaust Nozzle for  
Duct Heater Rig

FE 55129



FD15311

Figure A-V-9. Full-Scale Annular Duct Heater Rig

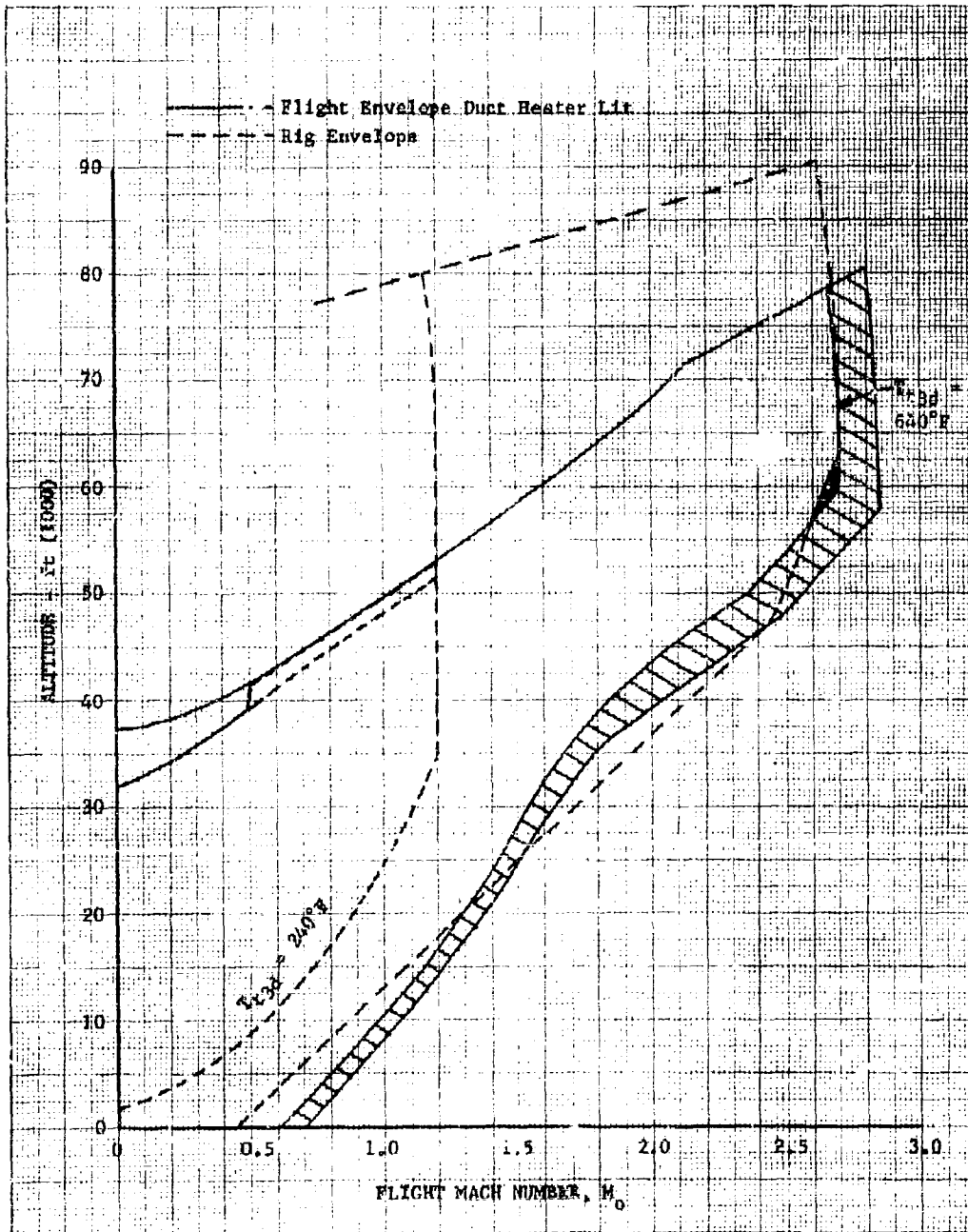


Figure A-V-10. Duct Heater Rig Operation Capability  
 (C-4 Stand)

DF 46732



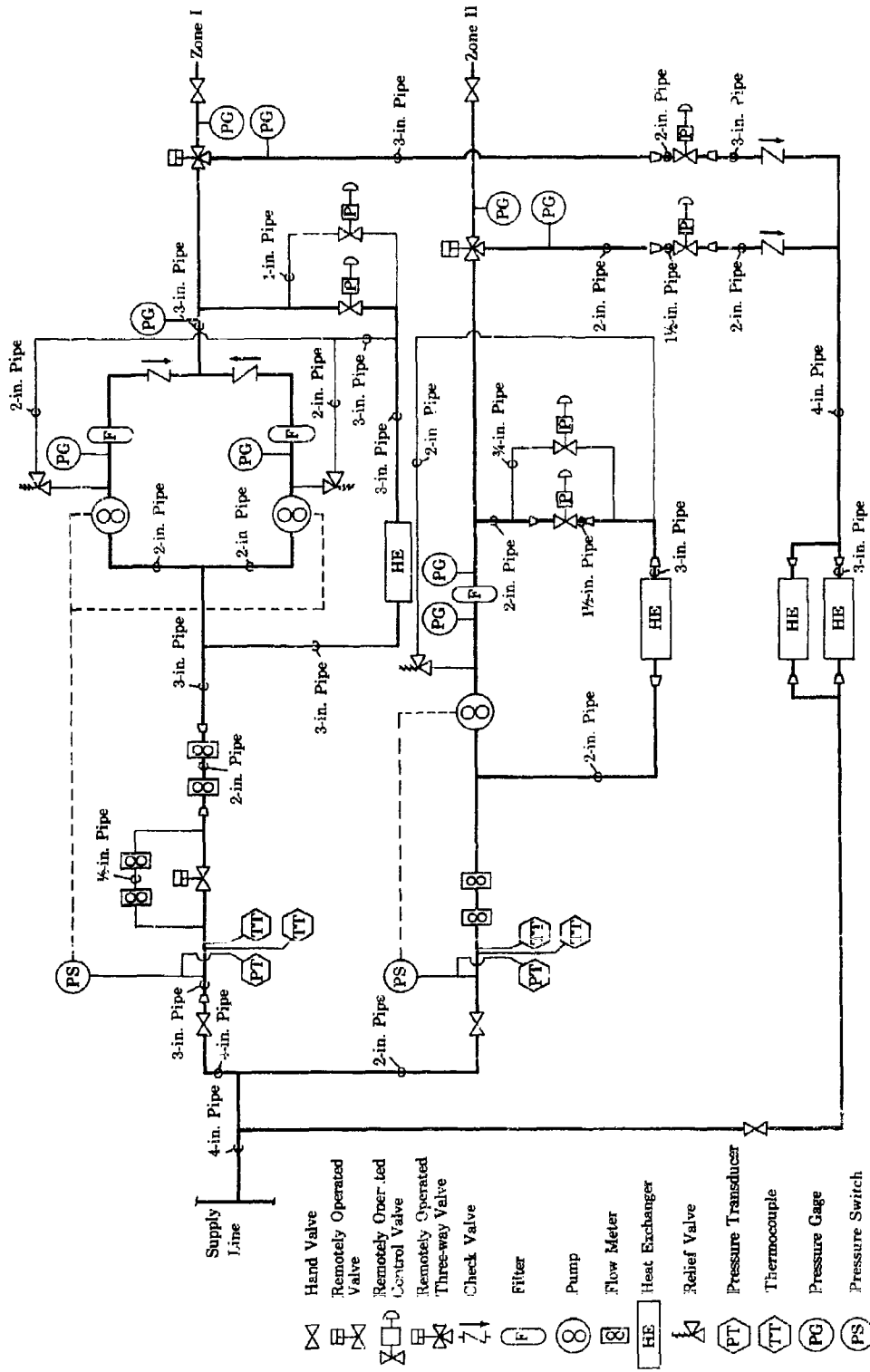


Figure A-V-11. Duct Heater Rig Fuel System Schematic

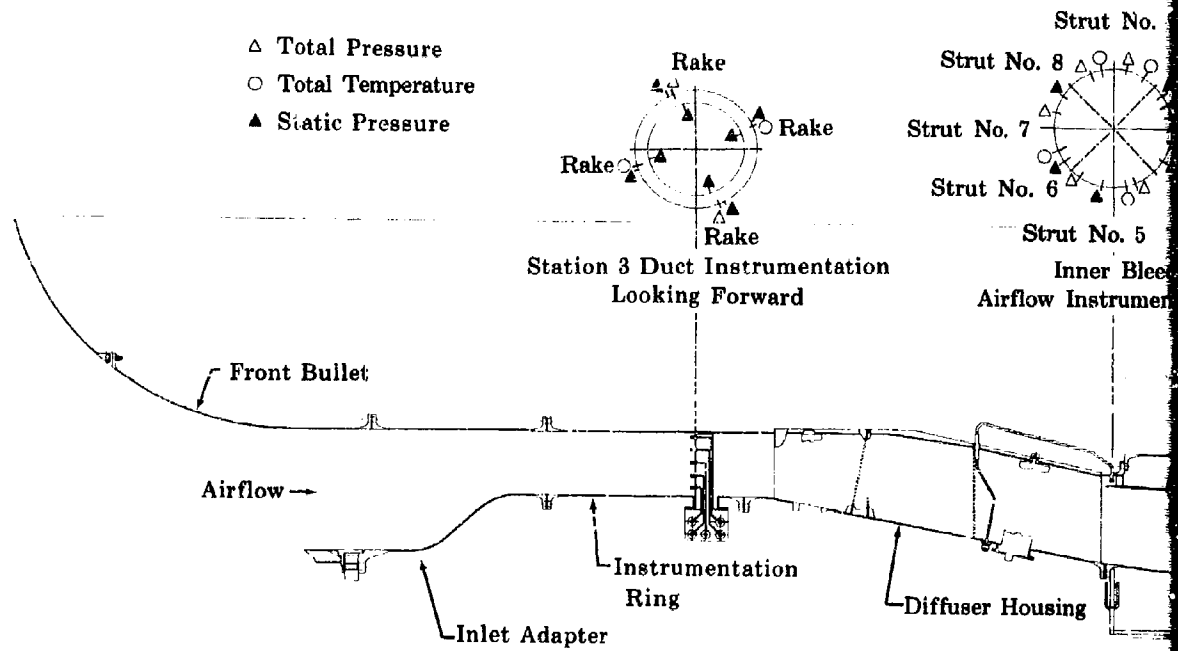
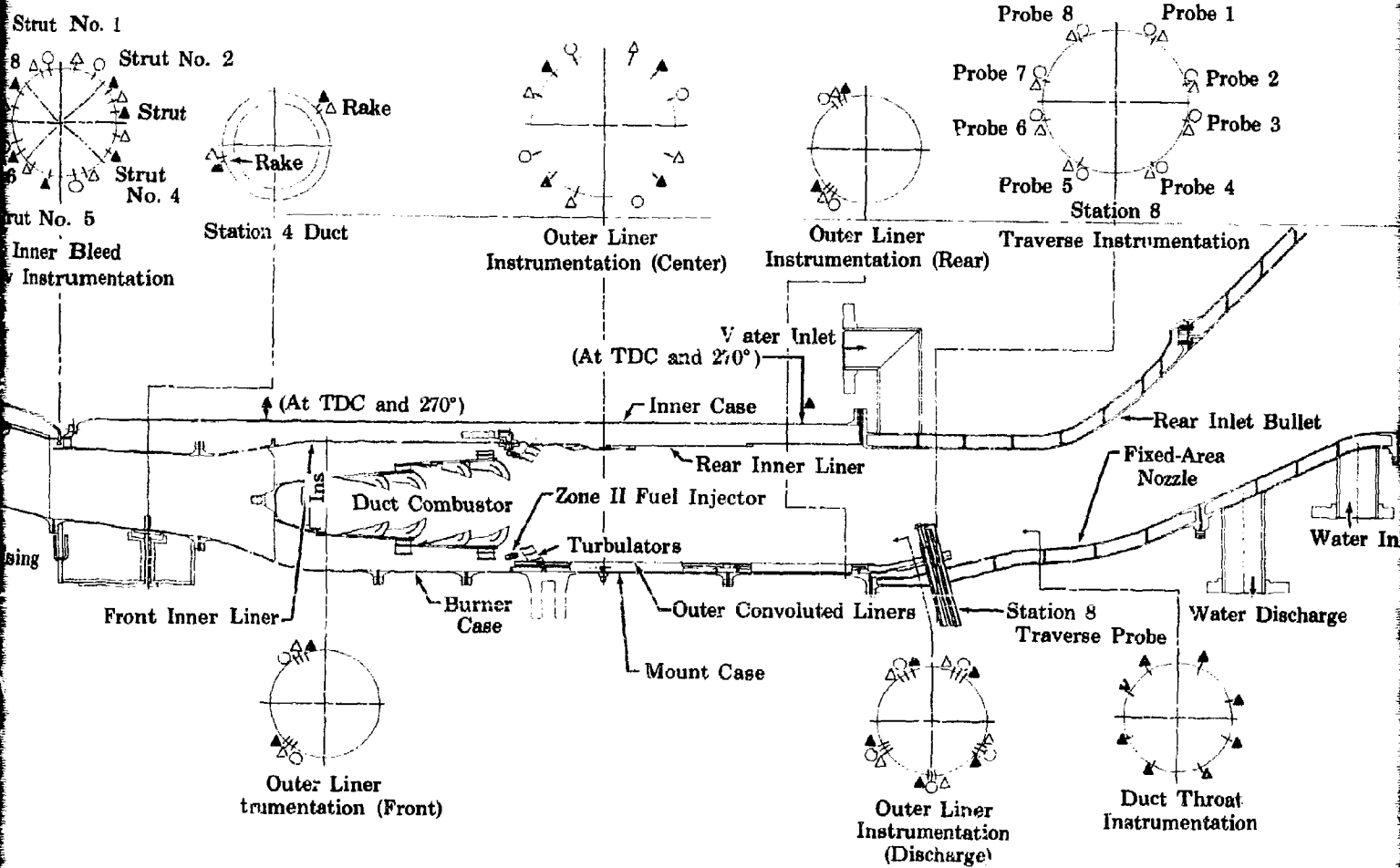


Figure A-V-12. Instrumentation Schematic



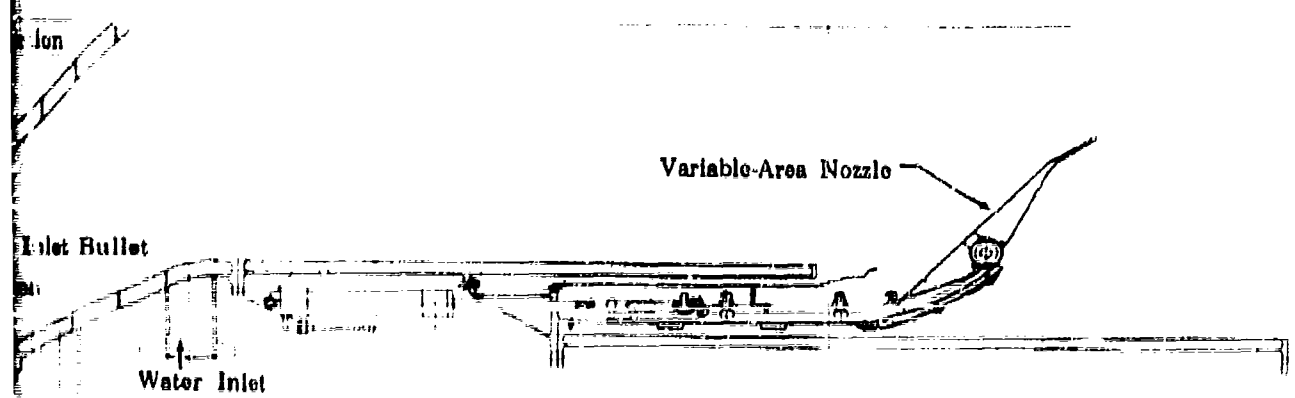
Pratt & Whitney Aircraft

PWA FR-1855

Appendix A

Probe 1  
Probe 2  
Probe 3  
4  
Inlet  
Inlet Bullet  
Water Inlet  
Exhaust Discharge  
Exhaust  
Exhaust

Variable-Area Nozzle



FD 15374A

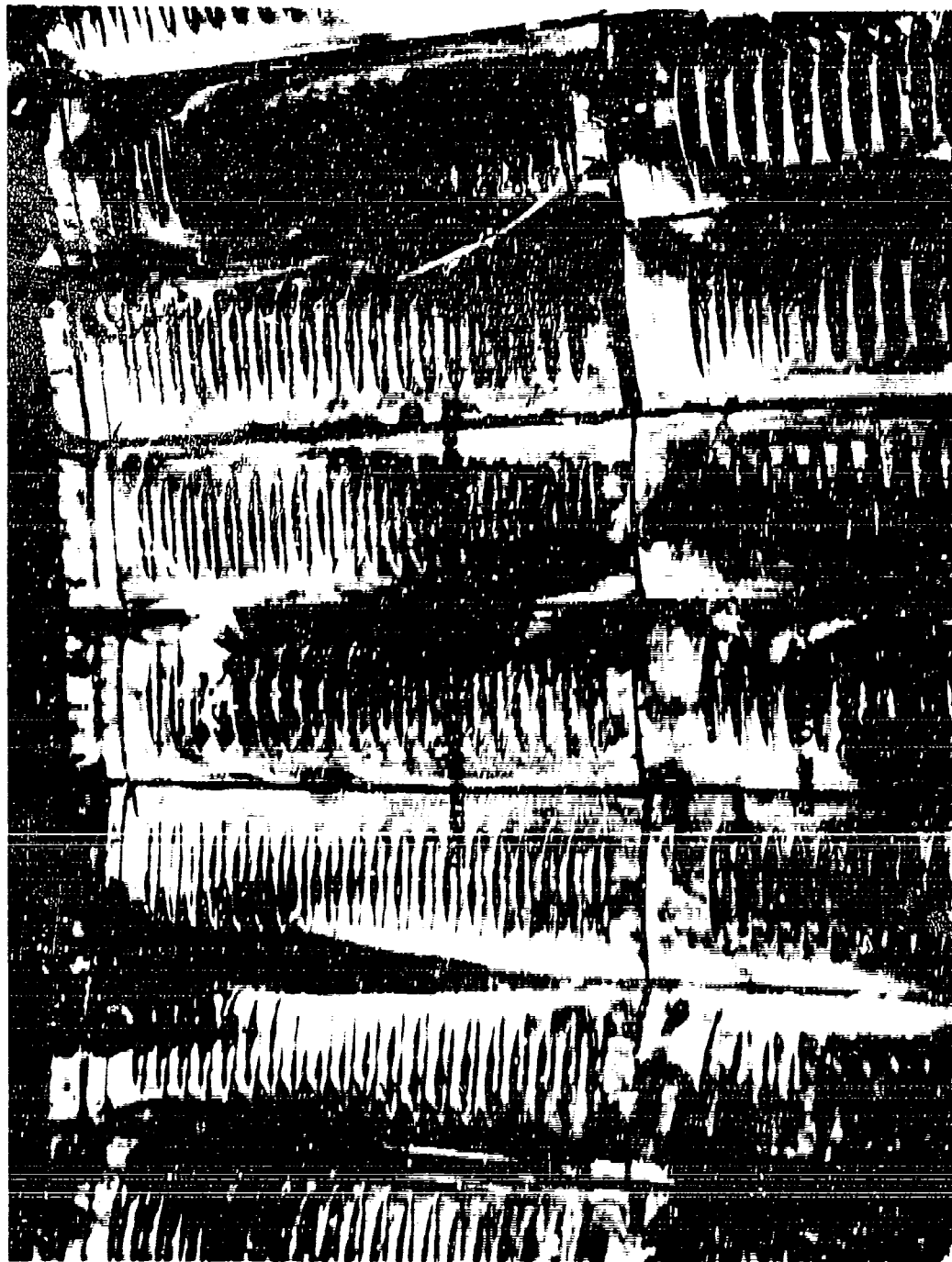
A-V-29

2

**CONFIDENTIAL**

Pratt & Whitney Aircraft  
WA PR-1855  
Appendix A

ED 15309

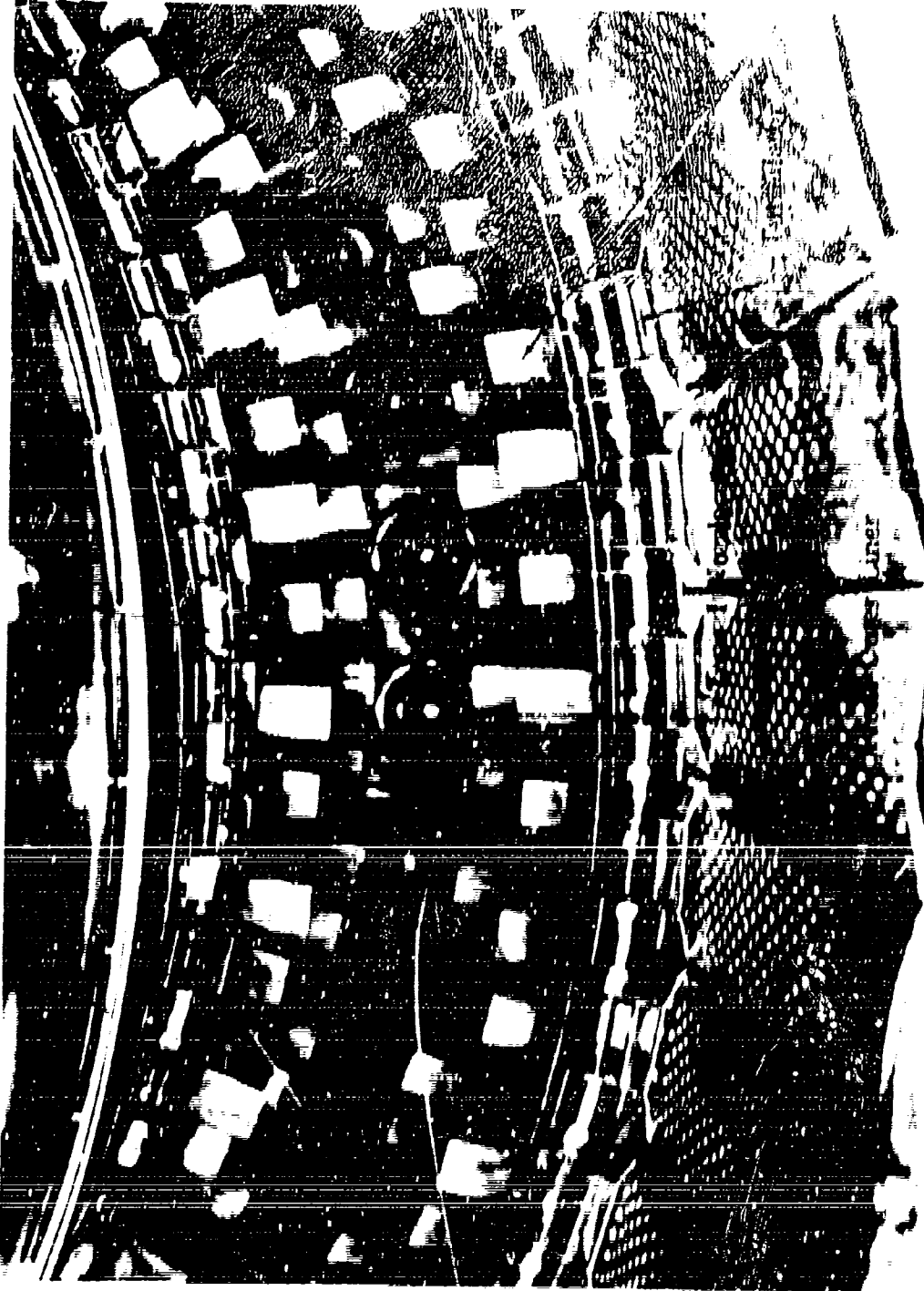


ED 15309

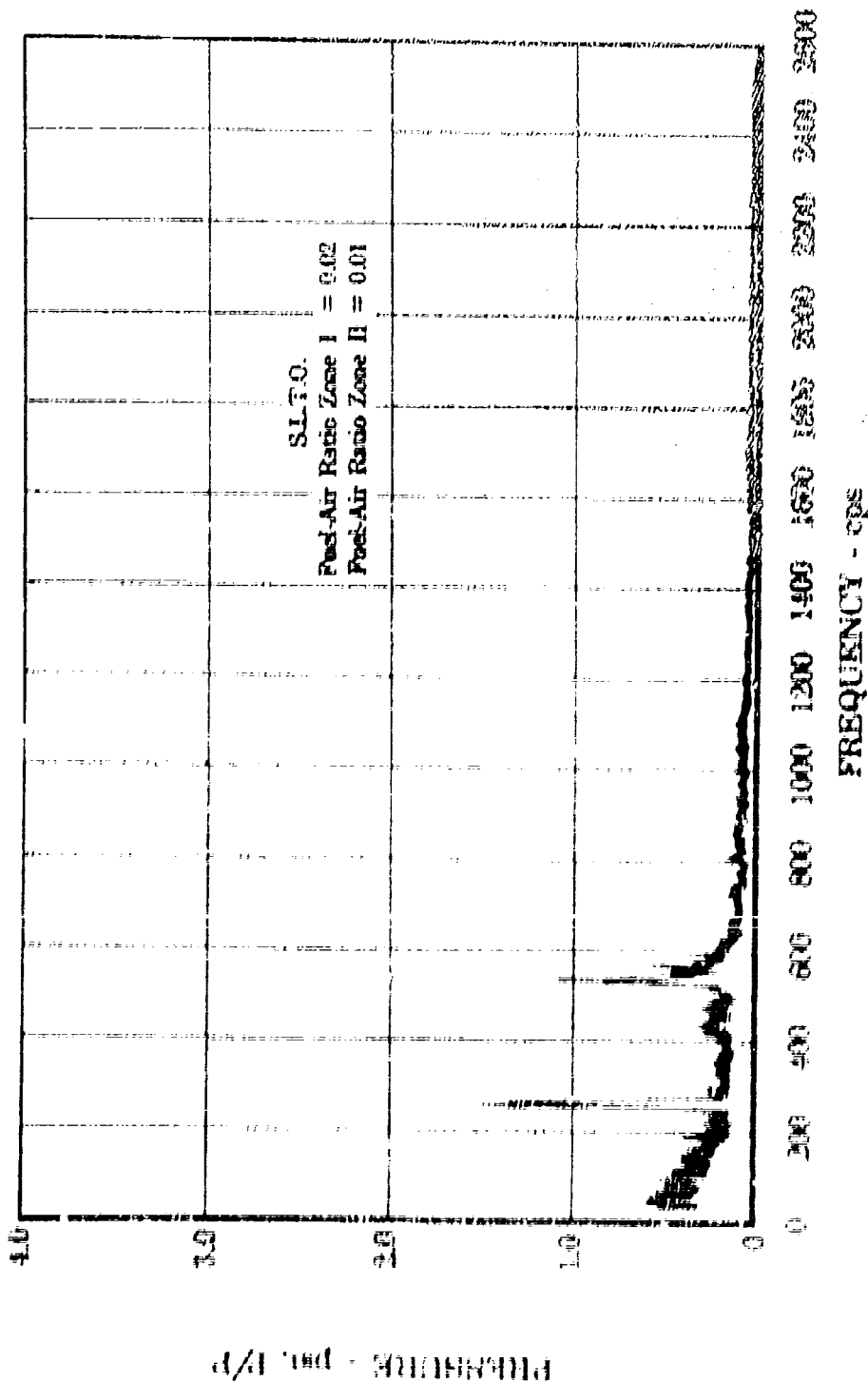
**CONFIDENTIAL**

CONFIDENTIAL

Pratt & Whitney Aircraft  
IWA F10-1855  
Appendix A



CONFIDENTIAL



Pressure Fluctuations in the Fuel-Air Ratio Zone I and Zone II of the Fuel-Air Ratio Control System  
 with Detuned Echo Input and Output Combinations

Pratt & Whitney Aircraft

FWA FR-1855

Appendix A

FD 15373

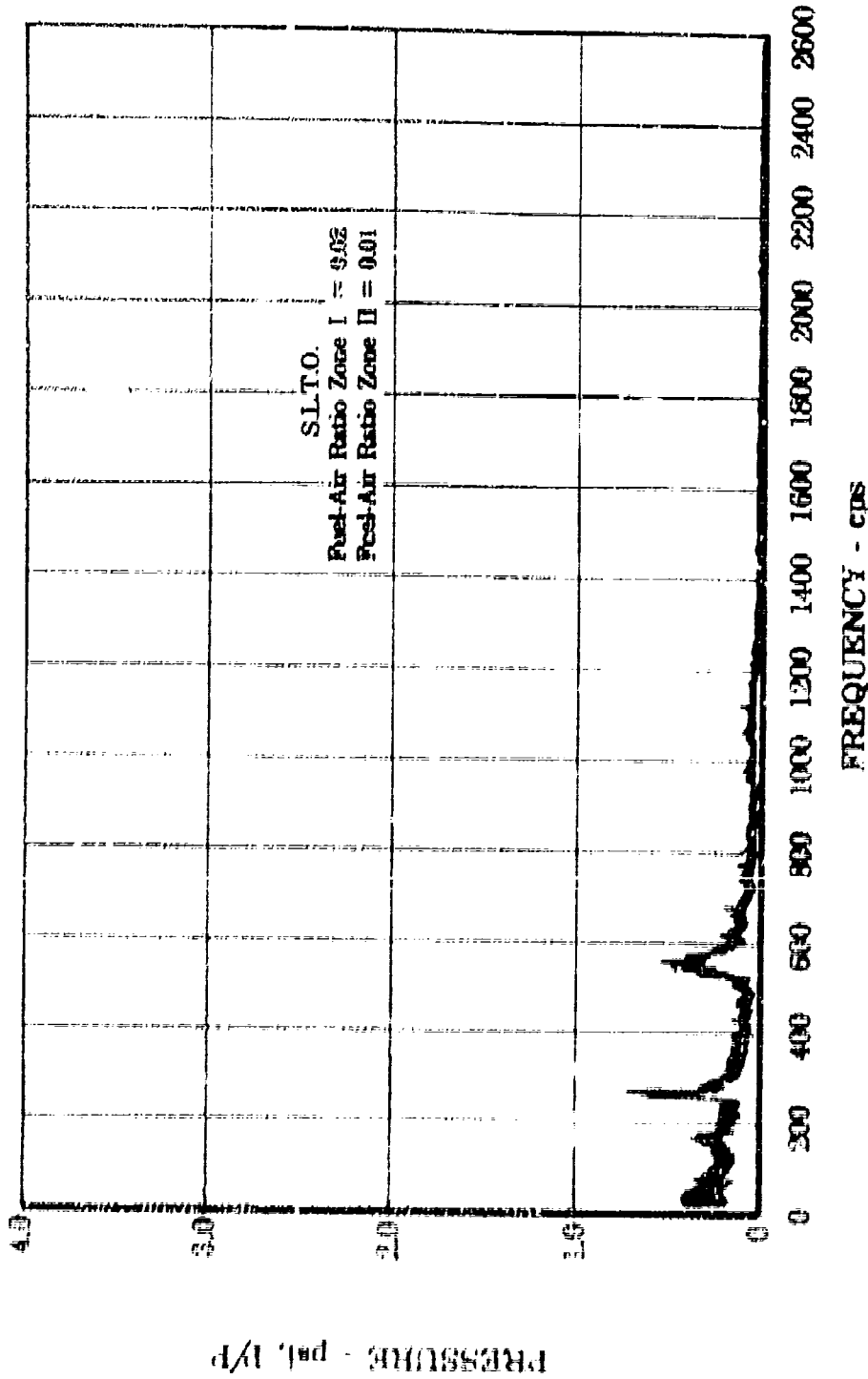


Figure A-V-16. JET14-20 Full-Scale Duct Heater Pie Varnier Pressure Oscillations with Plunged Hole From Outer Liner Configuration



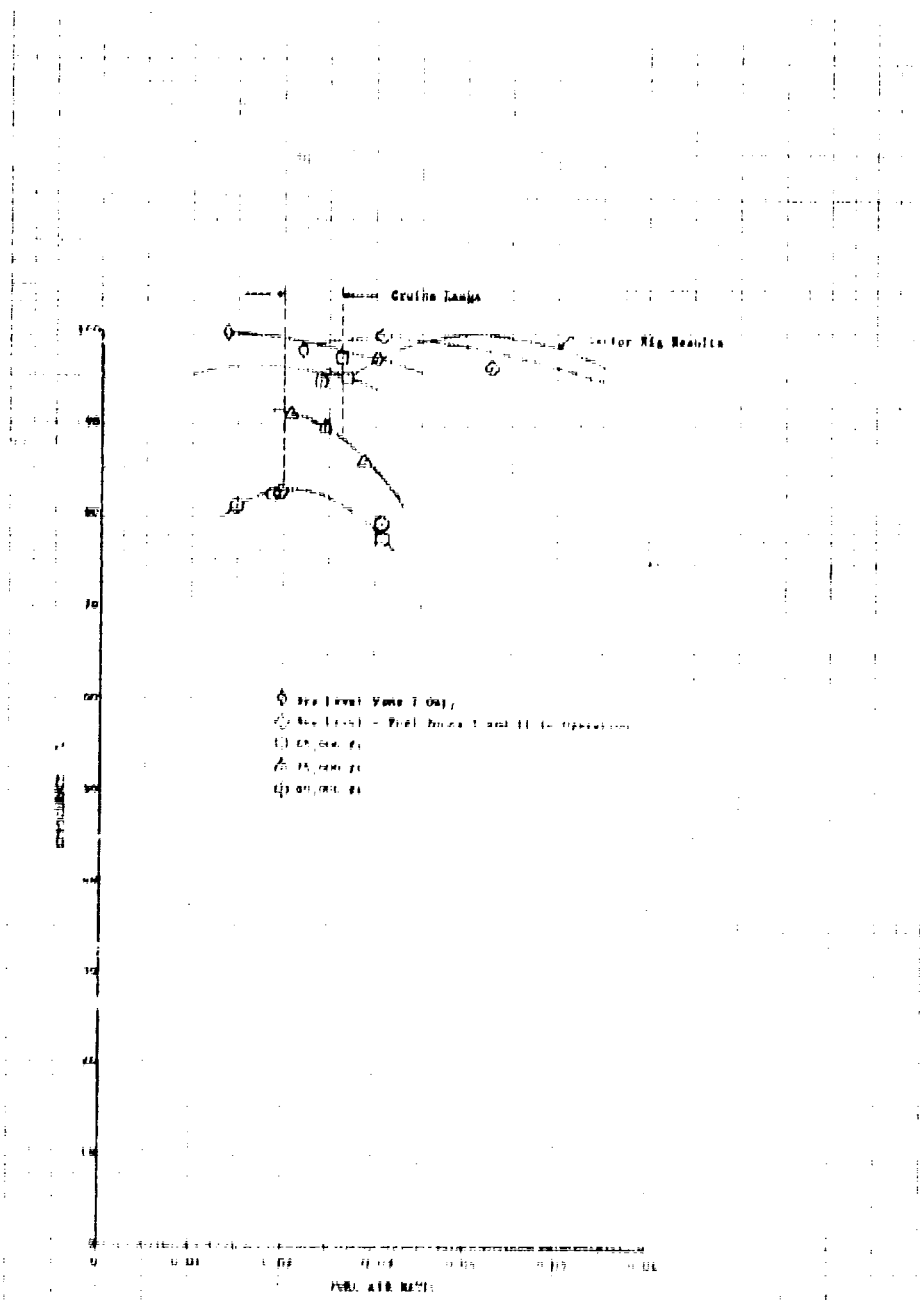


Figure A-V 17 PWA 20 Full Scale Duct Heater Rig Efficiency vs Fuel Air Ratio

DE 66733

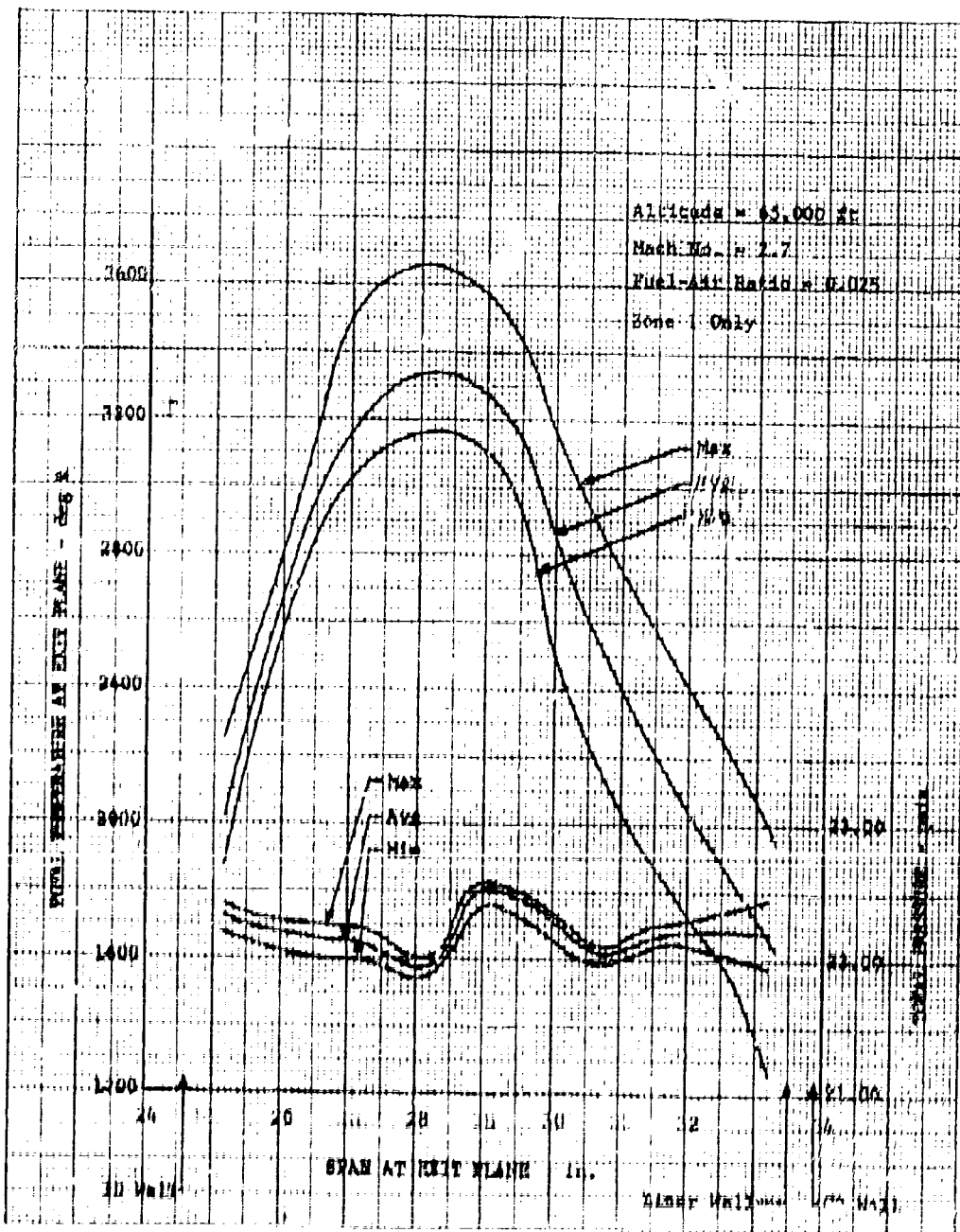


Figure A-V-10. JTF17A-20 Full-Scale Duct Heater Rig  
Radial Temperature Profiles at Cruise  
Conditions

DP 46738

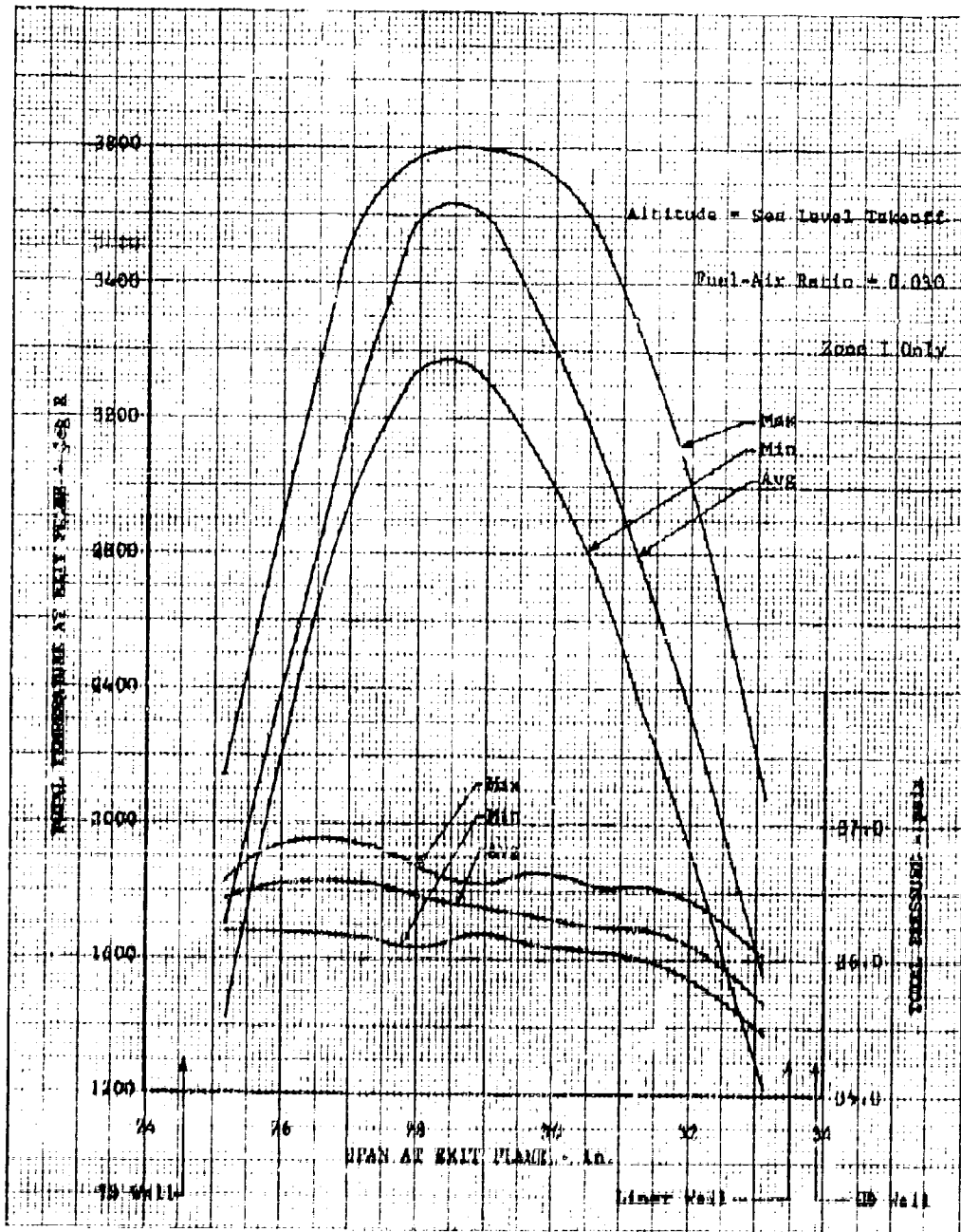


Figure A-V-19. JTP17A-20 Full-Scale Duct Heater Rig  
Radial Temperature Profiles at Sea  
Level Takeoff Conditions

DP 46736

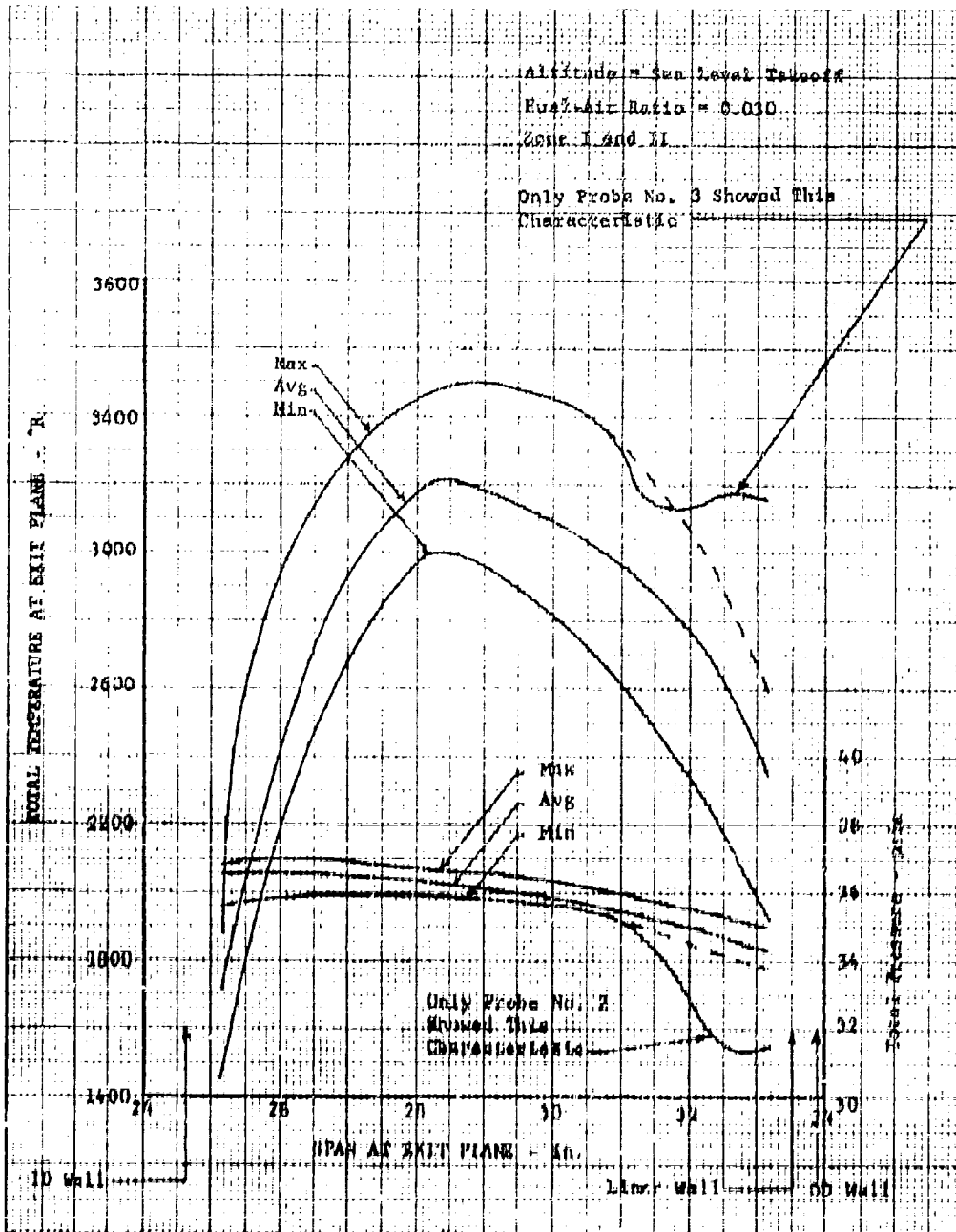


Figure A-V-20. JTF17A-20 Full-Scale Duct Heater Rig  
 Radial Temperature Profiles at Sea  
 Level Takeoff Conditions

DF 46737

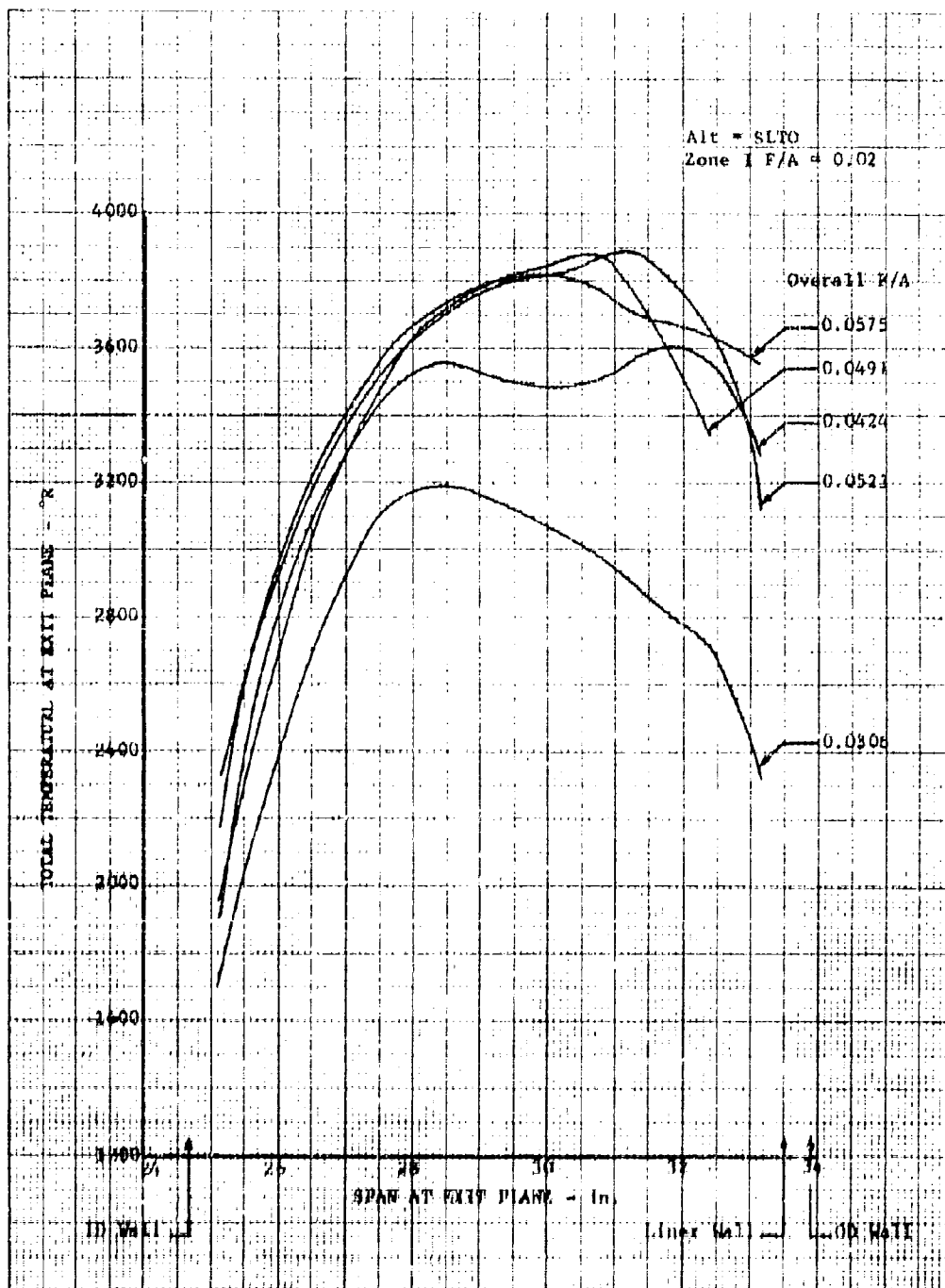


Figure A-V-21. JTP17A-20 Full-Scale Duct Heater Radial Temperature Profile with Zone II Fuel Operation

DF 46841

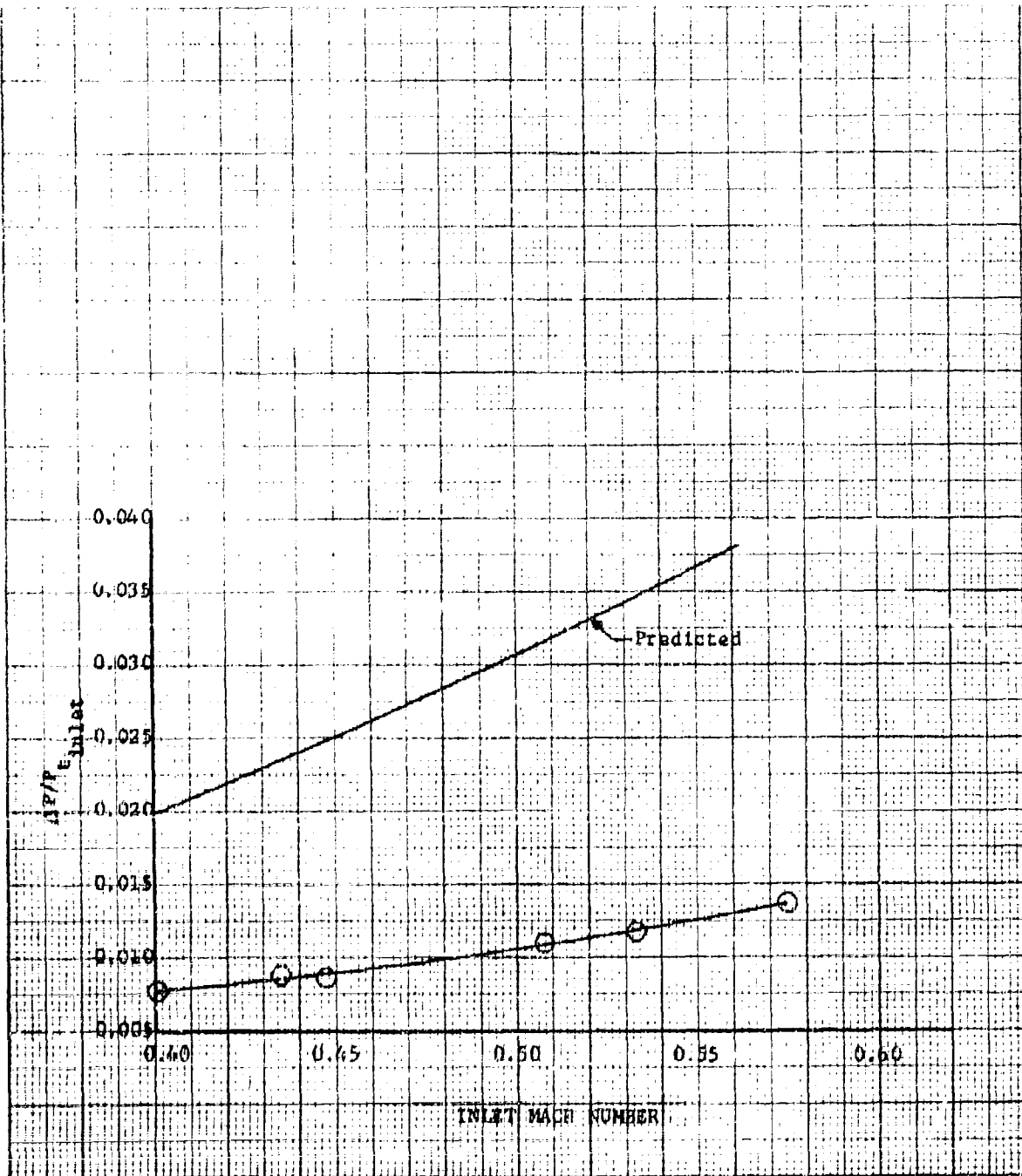


Figure A-V-22. JTF17A-20 Full-Scale Duct Heater Rig  
Total Pressure Loss for Diffuser Section

DF 46738

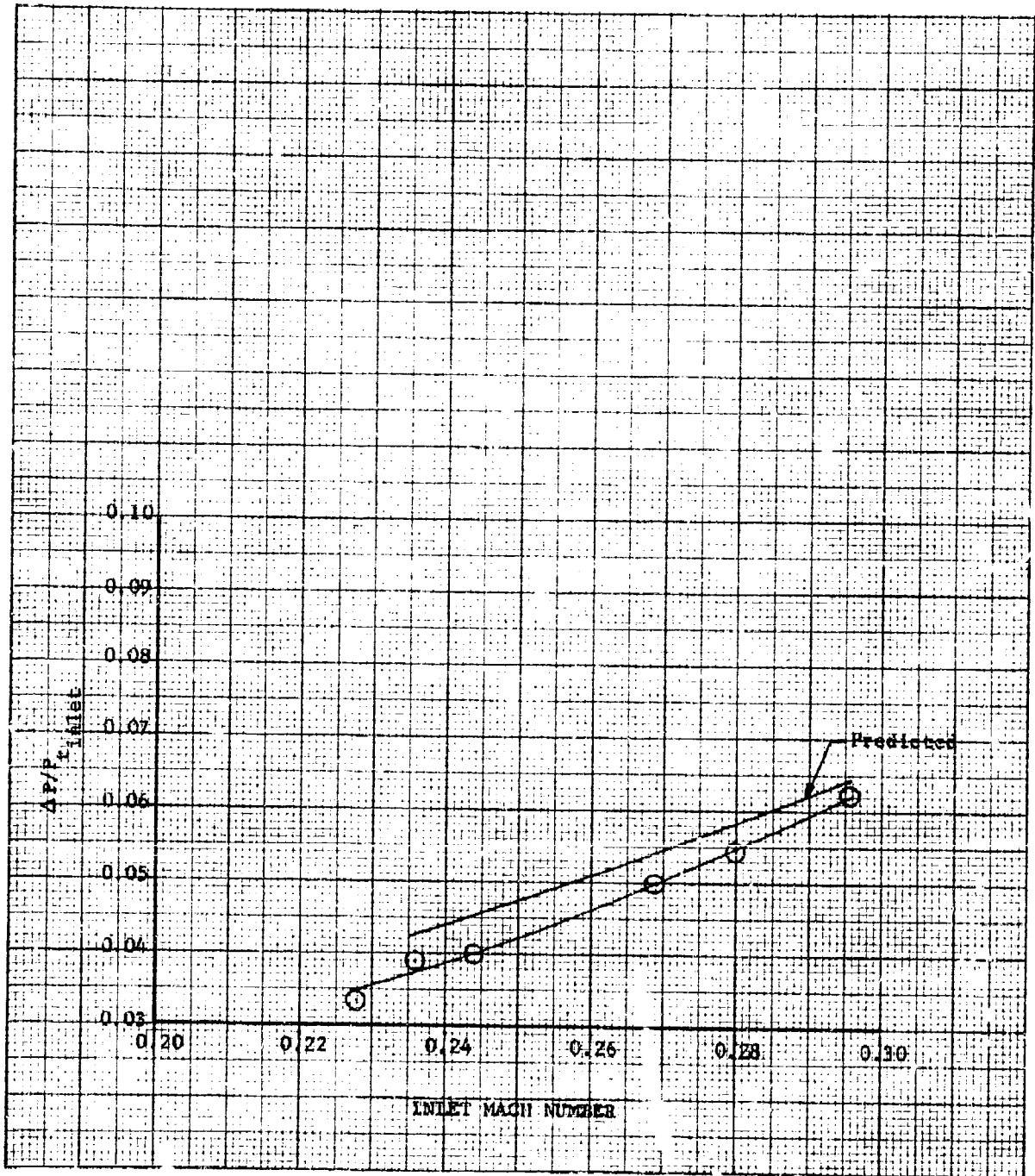


Figure A-V-23. JTF17A-20 Full-Scale Duct Heater Rig  
Isothermal Total Pressure Loss  
Through Combustor

DF 46739

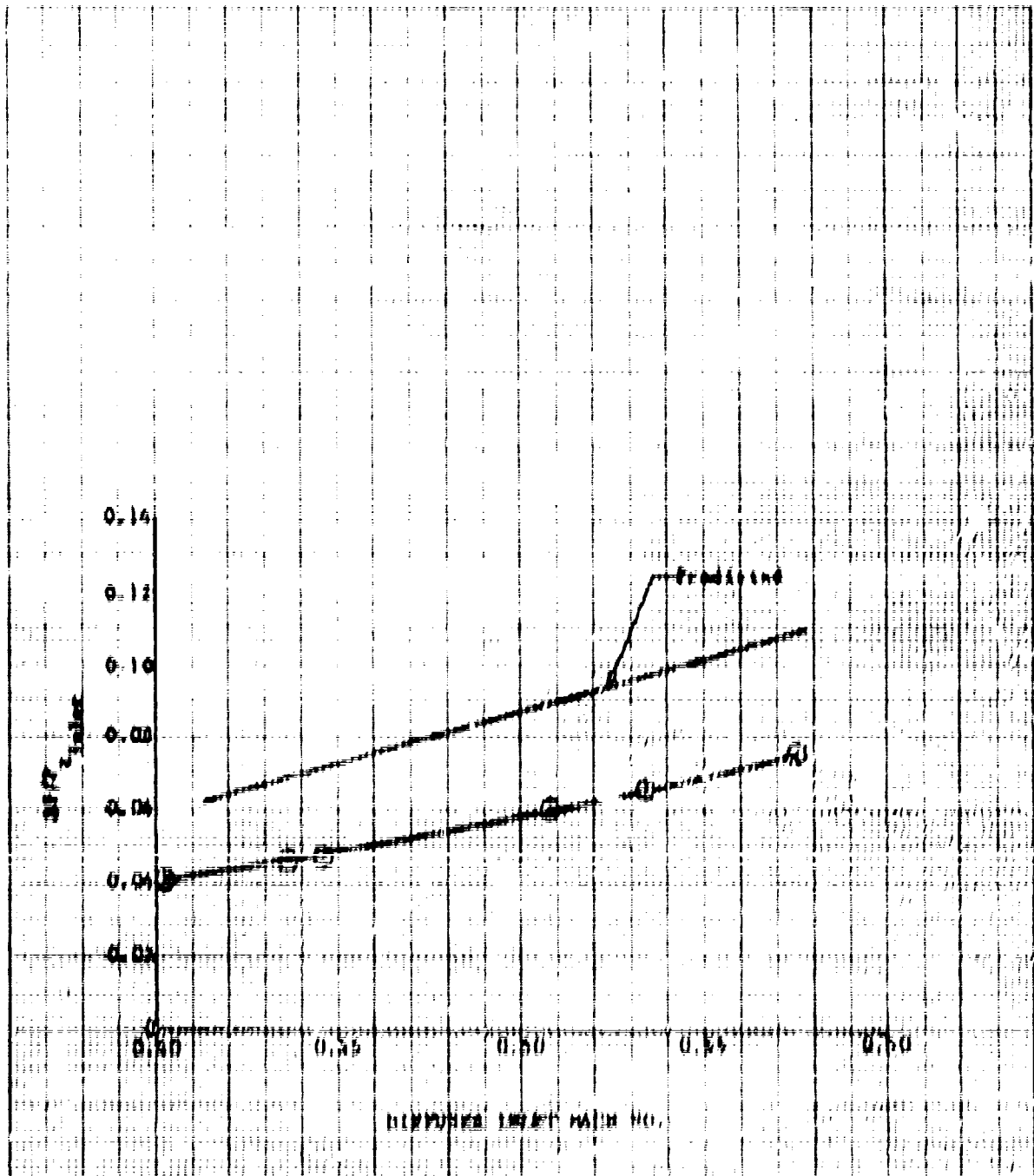


Figure A V 26, JTF/A 20 Full Scale Duct Heater Rig  
Overall Isentropic Total Pressure Loss  
for Duct Heater System

DF 467-0



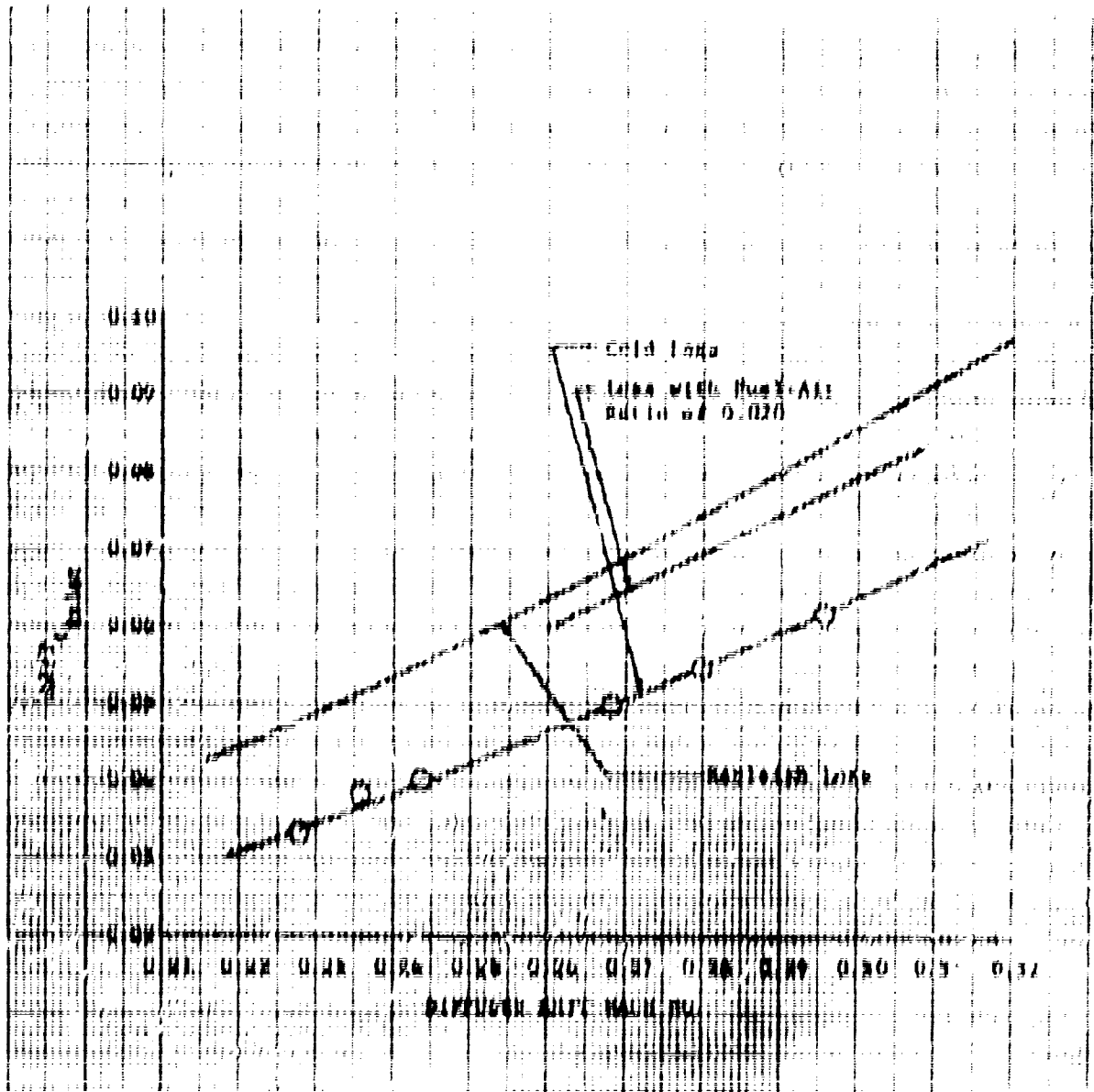
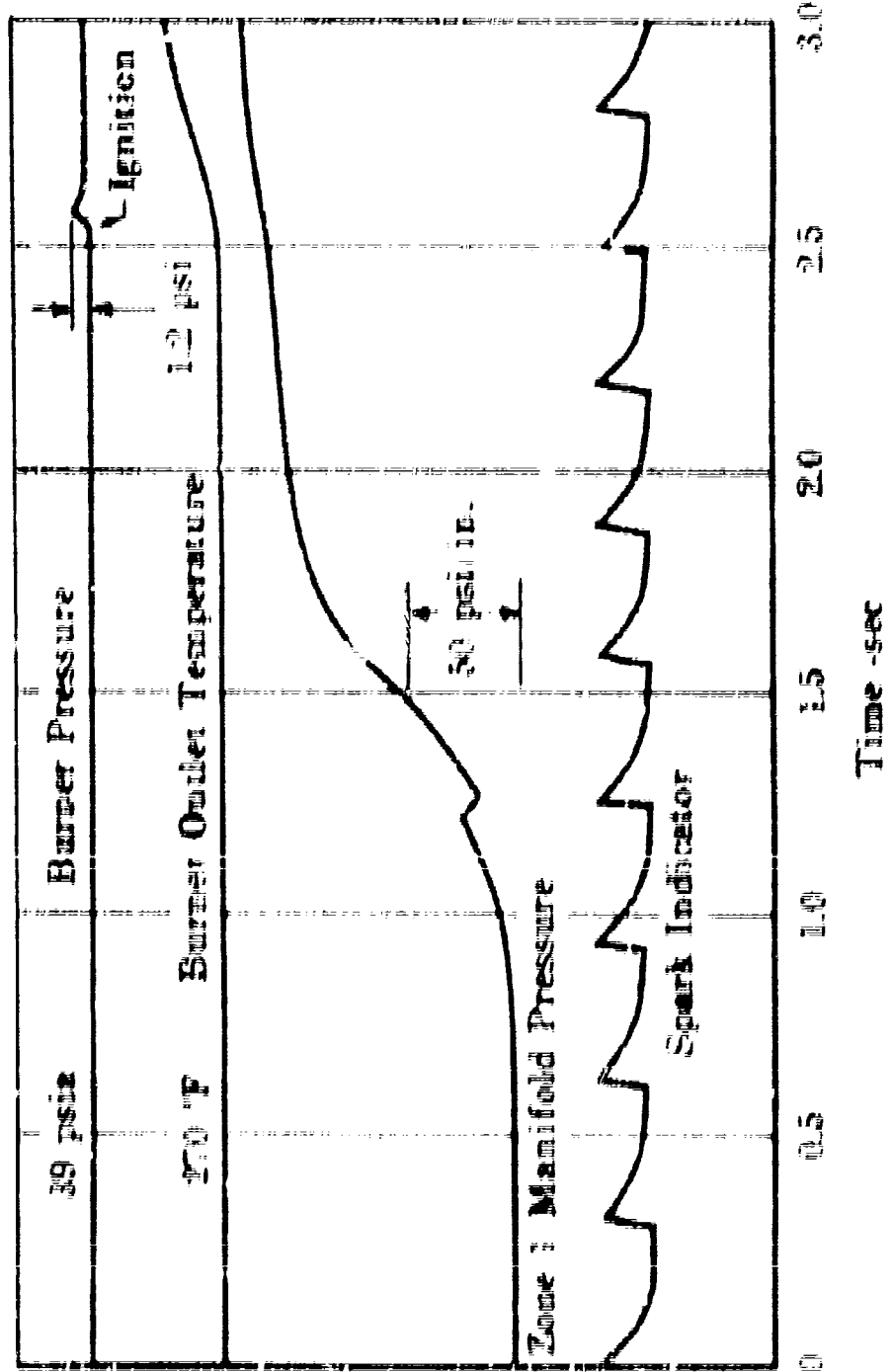


Figure A V 75. JT11D-20 Full Scale Dual Heaters Rig  
 Overall Total Pressure Loss at Cruise  
 Conditions



FR-1855

Engine Test Results

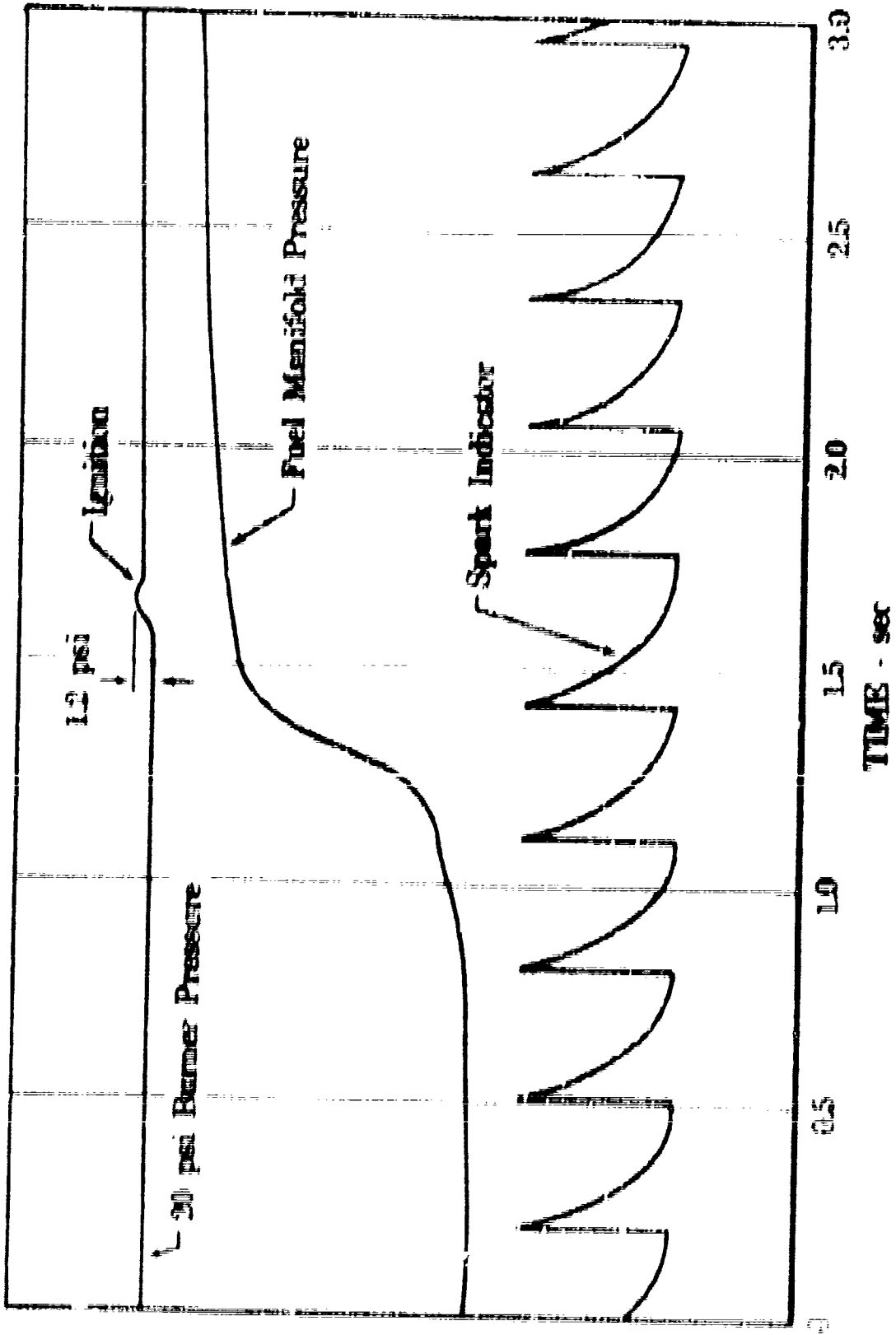


Figure 1-1. Fuel Manifold Pressure, Burner Pressure, and Spark Indicator Pressure vs. Time at 1000 RPM

TEST RESULTS

PR-1055

FD 146050

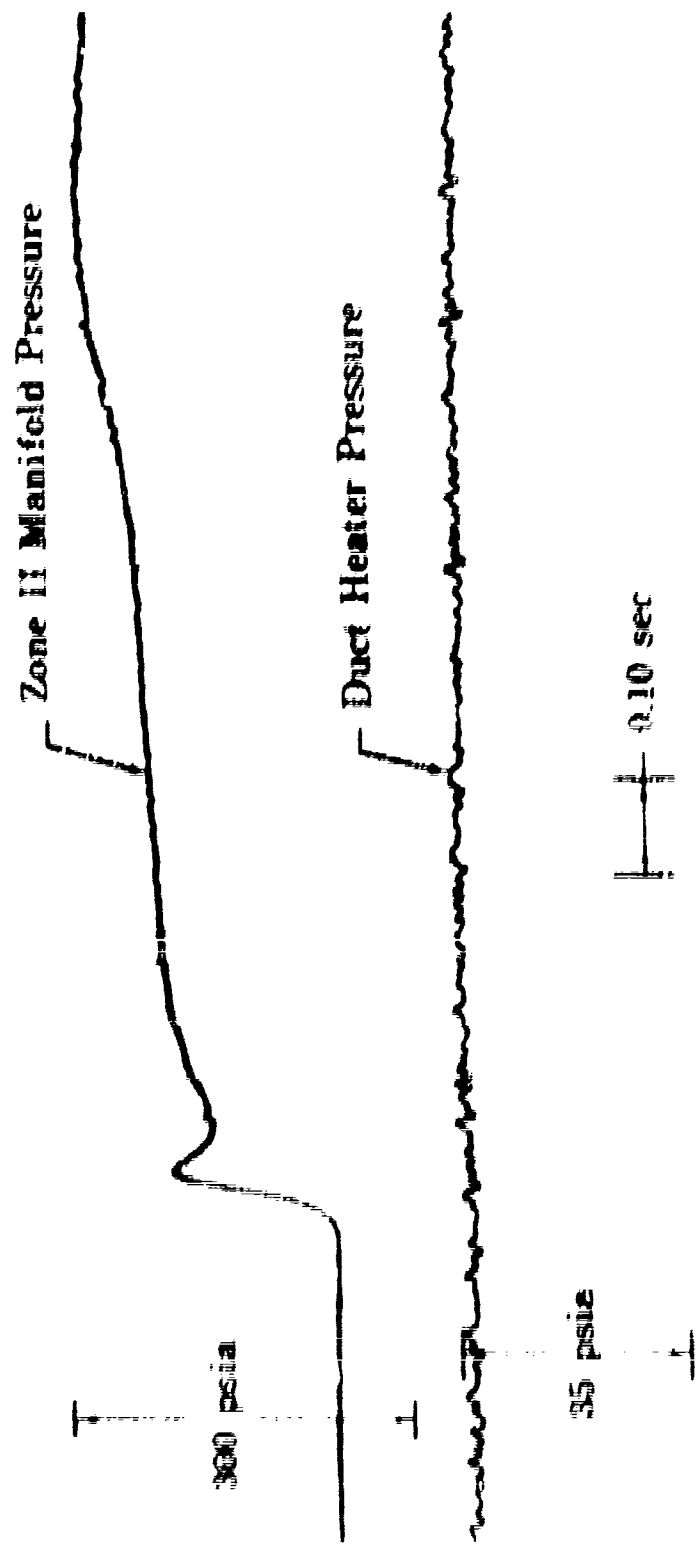


Figure 4-1-28. Rate of Duct Heater Pressure Rise with Addition of Case 12 Fuel (See Data)

A 4 16

SECTION VI  
CONCLUSIONS

The following conclusions have been drawn from the duct heater experimental program to date:

1. The duct heater combustor configuration selected from the full-scale sector rig tests for the JTPI7A-20 engine exhibited excellent performance characteristics in the full-scale annular rig.
2. The total pressure loss in the diffuser section of the augmentor was lower than predicted and was the primary reason for the low cold pressure loss of the augmentor system.
3. The results from the 7 x 11-inch sector duct heater rig and the 0.6-scale duct diffuser rig agreed well with those from the full-scale annular duct heater rig.
4. The combustion efficiency of the augmentor is greater than 95% for the expected cruise points and for MTO condition up to  $F/A = 0.06$ . Combustion efficiency at fuel-air ratios greater than 0.04 range between 85 and 95%. It was concluded from sector rig test (see Figure A-III-17) that better fuel coverage of the combustor bypass air will produce high combustion efficiency at the high fuel-air ratios.
5. The combustor demonstrated excellent ignition characteristics over all conditions tested at fuel-air ratios between 0.001 and 0.004.
6. The condition of the augmentor parts was, in general, excellent after 45 hours of hot testing. Some damage of the outer liners was encountered in areas of stress concentration. Design changes have been incorporated to eliminate areas of stress concentration and to improve the sound absorbing characteristics of the liners.

7. The duct heater results have demonstrated that the component can be developed to operate on the JT17A-20 engine over the required operating envelope with performance equal to or exceeding the goals to meet engine specification thrust and TSFC and with durability required for a long life commercial aircraft engine.

**APPENDIX B**

**Rusla Activity Review**

APPENDIX B  
JT17A-20 FUELS ACTIVITIES

## A. GENERAL

This appendix includes the material presented to the FAA Fuel Industry Advisory Committee at FAA headquarters in Washington, D. C. on 21 April 1966.

Six major sections are covered, as follows.

1. The current fuel specification - Discussion of the current Type A-1 aviation kerosene used to run the JT17A-20 engine and the shipping and storage controls maintained to ensure its quality.
2. Phase II-A and II-B work completed - Review of work from previous publications including the 1964 Field Survey of Jet Fuel Quality and the effect of the oxygen content on the thermal stability failure threshold.
3. Conditions to which the fuel will be exposed - Description of a selected mission profile established to show maximum estimated temperatures and fuel system schematic with fuel temperatures throughout the system for maximum allowable fuel inlet temperature at cruise conditions.
4. Phase II-C testing to date - Outline of the coker rig programs and descriptions of erosion and corrosion tests with the current delivered fuel, including accelerated erosion-corrosion tests by the addition of sulfur to the maximum allowable content and salt air atmosphere.
5. Related activities - This effort is related directly to Phase II-C testing to show the results of accelerated pump wear tests as a possible method for evaluating fuel lubricity.
6. Future Phase II-C program - The plan to run a J58 engine on Pratt & Whitney Aircraft's selected fuel was outlined.



## B. CURRENT FUEL SPECIFICATION

The current fuel specification for the JTF17A-20 engine is PWA 533. This fuel is the same as PWA 522, which is used in the current PWA commercial jet engines except for the thermal stability requirement of 350°F/450°F instead of 300°F/400°F. Purchase performance specification J-102 is used to maintain control of the fuel delivered to ERDC for experimental testing. This purchase performance specification was written to control the properties of the current fuel deliveries. In several areas, its requirements are tighter than PWA 533, but this is not to be interpreted as an engine requirement. This is being done to maintain the fuel at a specific reference, not release level. For example, the freeze point is given specifically at -58°F and the sulfur content is 0.05% maximum. If changes in the refinery processes should affect any of these properties they would be recognized at an early date and we would investigate at this time whether any other additional properties may also be affected. This would prevent an additional variable from showing up in any PWA tests at a later date. One example of this is the change in the freeze point from -58° to -50°F for future deliveries, which changes the fuel from Type A-1 to Type A.

The aviation kerosene, purchased to J-102 specification, used in the current experimental program is one of the fuels delivered to Miami International Airport, and it has been selected because of its low price. The existence of the airport delivery system is one of the reasons for the low price. Data on the fuel properties are sent by telegram to our Materials Control Laboratory as each barge is loaded at the Mississippi refinery. When each barge arrives at Port Everglades, Florida, a sample from the vessel is sent directly to our Materials Laboratory for analysis. When this sample has been checked to confirm its quality, Purchasing is informed and the fuel in storage at Port Everglades is released for delivery to ERDC by truck. Composite samples from the trucks are checked again as this fuel is delivered to the ERDC fuel farm. Periodic samples are also taken from these tanks to ensure that the fuel quality has not deteriorated during storage. (See Figure B-1.)

The 1964 Field Survey Jet Fuel Quality showed that ninety percent of these samples had a thermal stability break point of 350°F/450°F or higher as specified in PWA 533 fuel specification, as shown in figure B-2. This survey covered the entire United States and consisted of 49 samples taken from 13 major oil companies and 4 airports.

#### C. PHASE II-A AND II-B WORK COMPLETED

In Phase II-B, a program was conducted to investigate the effect of low pressure in releasing dissolved oxygen in the fuel. The dramatic effect of maintaining the fuel at 1 psia for a period of 1 hour on the fuel oxygen content can be noted in figure B-3.

Eleven fuel samples were tested at pressures of 1 psia and 1.5 psia. The oxygen content during these tests dropped to 4 ppm and 9 ppm. A summary of the effects is shown in figure B-4.

A table (figure B-5) of the summarized data showed a consistent gain in the fuel thermal stability with the oxygen content as low as 4 ppm at 1 psia. If the pressure on the fuel is as much as 1/2 psia higher, the dissolved oxygen content would remain as high as 9 ppm and a consistent gain in fuel thermal stability would not be obtained. The effect was very random; no attempt was made to indicate a requirement for this apparent improvement.

#### D. CONDITIONS TO WHICH THE FUEL WILL BE EXPOSED

The mission profile shown in figure B-6 was selected to expose the fuel system to extreme conditions. The climb portion of this profile includes maximum duct heat for takeoff with a cutback to a nonaugmented condition until the aircraft is out of the airport area and has reached approximately Mach 1. At this time, maximum duct heat is resumed for the remainder of the climb to Mach 2.7 and 65,000 feet where the power is then cut back to partial duct heat. The Mach number of 2.7 is maintained for cruise and the climb is continued to an altitude of 72,000 feet where power is then cut back to idle for the descent. The range of approximately 4000 miles and the high altitude of 72,000 feet along with an extreme power reduction from partial duct heat to minimum-flow idle were combined to demonstrate maximum estimated temperature effects.

The JTF17A-20 fuel system schematic is shown in figure B-7 with calculated bulk fuel temperatures noted at the end of cruise condition for the maximum fuel inlet temperature of 250°F established from the engine specification. The temperatures on this schematic are the maximum estimated for steady-state operation. The boost stage in the main fuel pump raises the fuel temperature to 263°F. Recirculation from other fuel systems will raise the temperature into the main stage to 348°F, and fuel into the main control will be 355°F at the thermal bypass temperature-sense valve. With the main engine at cruise power, an additional rise of only 10°F to 365°F will occur at the primary combustor nozzles. On the duct heater fuel system, the pump discharge will be 265°F with a rise of 35°F through the duct fuel-oil cooler. While the duct heater is in operation, the fuel-oil cooler in this system will carry the majority of the engine oil cooling requirements. The temperature at the duct heater Zone I nozzles will be 310°F. This is actually lower than the primary combustor nozzles, which are the same design. The duct heater nozzles will have a temperature environmental advantage that is not present in afterburning engines. Zone II in this schematic does not show a fuel temperature because cruise is on Zone I fuel only. The return line to the airframe does not show a fuel temperature because no heat will be returned to the airframe at the cruise conditions.

The engine fuel inlet temperature represents the maximum estimated during the climb, cruise, and descent. (See figure B-8.) A temperature of 250°F at the end of cruise was chosen for its maximum effect on the remainder of the engine system. During other time periods of the mission, the curve shows a typical contour to establish a basis for other temperatures through the engine.

The effect of the typical mission profile and the fuel inlet temperature is shown on the fuel temperature at the primary nozzles. (See figure B-9.) During the climb a step upward in the fuel temperature reflects the change from maximum augmented to nonaugmented power and the pickup of oil cooling by the main fuel-oil cooler. During the cruise portion of the mission, the altitude will be increasing and the main engine fuel flow decreasing. This is reflected in an increased temperature rise between the fuel inlet and the nozzles during the cruise

period up to a maximum of 365°F at the end of cruise. Experience with a high supersonic cruise engine operating with hot fuel has shown that at the end of cruise a peak calculated temperature rise will not actually occur because of system dynamics, and the maximum nozzle fuel temperatures will decrease during the descent. The calculated maximum peak is shown as a dashed line reaching 450°F.

The duct heater nozzle fuel temperature is shown relative to the mission time. (See figure B-10.) The low rise in temperature above the fuel inlet temperature at the beginning of the climb reflects the high duct flows. This line breaks during the nonaugmented portion of the climb and picks up again at maximum augmentation. As the duct heater fuel flows drop with increasing altitude, the temperature rise above fuel inlet temperature increases to a point where cruise begins on Zone I only. Zone I will reach a peak of only 310°F at the end of cruise. This low temperature for the augmentor fuel is possible only because the air around the duct heater combustor is as much as 1470°F cooler than in an afterburning engine. For the descent, a dump valve drains this system and no fuel will remain in the manifolds.

The heat return rate to the airframe is shown relative to the mission time in figure B-11. The outstanding point is the fact that no heat will be returned to the airframe during climb or cruise. At the end of cruise, when the power condition changes from partial duct heat to a minimum-flow idle for the descent, the heat return rate will rise to a maximum of 8500 Btu per minute and rapidly drop off.

The accumulation of total heat return is shown during the descent portion of the mission in figure B-12. The accumulated total will reach approximately 43,000 Btu per engine.

#### E. PHASE II-C TESTING

The coker rig has been used to monitor the fuel delivery and to ensure no deterioration below 350°F/450°F while the fuel is in storage. A series of coker tests was run on the current fuel, and the breakpoint was found to be 375°F/475°F. The addition of a hydrocarbon lubricity additive did not affect the thermal stability in samples used for Ryder gearing lubricity tests. An additional series of coker tests is in process to

establish the effect of low pressure and low oxygen on the current fuel delivery for comparison with II samples tested in Phase II-B. A series of tests is also in process to establish the effect of a thermal stability additive on the fuel breakpoint.

Erosion and corrosion tests have been run on turbine materials with the current fuel up to 1000 hours of testing. Figure B-13 shows that testing will be continued on certain materials while other materials have already been rejected. The photograph in this figure shows the turbine samples, at temperature, rotating in front of a hot gas nozzle.

Accelerated erosion and corrosion tests were run with the current PWA 533 specification fuel including sulfur added to the maximum of 0.3%. (See figure B-14.) The salt air atmosphere at 10 parts per million has also been used to accelerate this program. These tests will continue with the fuel maintained at the maximum sulfur content. This is one area in the Phase II-C program where fuel quality has been changed to approach a referee level.

Lubricity is a fuel property which does not have a good test measuring method at the present time. The results of a series of tests on the Ryder gear rig demonstrate why this test method may not be the best one to adopt. A neat fuel sample and three additional samples with 150, 250, and 350 ppm of a hydrocarbon lubricity additive were tested at the standard rig temperature of 165°F and at elevated temperatures of 300° and 400°F. The results of the neat fuel sample and two of the hydrocarbon lubricity additive samples showed an increase in the load-carrying capability with an increase in temperature (figure B-15). The odd curve at 350 ppm of the lubricity additive had several points rechecked with the same unexplained results. The general trend of increasing load-carrying capacities with increasing temperature was not expected and may be due to other variables occurring during the testing, such as the deposit of fuel degradation products or oxidative matter held in suspension.

#### F. RELATED ACTIVITIES

Fuel lubricity has been investigated under another program with accelerated pump wear tests. The simplified schematic in figure B-16 shows a high pressure piston pump system for endurance testing on hot fuel. The three tests run with the current fuel, PWA 533, show that a hydrocarbon lubricity additive will permit running for longer periods of

time at a higher temperature. These tests also show that with the same fuel and the same concentrations of lubricity additive, the pump will show increased life at lower fuel temperature. With these trends in the results, this test method may actually be more applicable to the measurement of fuel lubricity, although the tests are expensive and doubts have already been raised as to the repeatability or standardization of the pump used in this program.

Steady-state fuel temperatures of 365°F were shown at the primary combustor nozzles in the JTF17A-20 fuel system schematic. To demonstrate our confidence in operating with this temperature at the fuel nozzle, related activities were reviewed. Figure B-17 is a schematic of a rig test with heated fuel. The fuel used in these programs was the same as PWA 533. This fuel was raised to a temperature above 480°F where a mixing valve tempered it to 480°F so that, with a 30°F loss, the temperature going into a six-nozzle cluster was 450°F. Within the combustor rig, the fuel temperature continued to rise to a temperature greater than 550°F.

After a 50-hour hot fuel endurance test, one fuel nozzle configuration would not repeat its required flow schedule, as shown in figure B-18. The secondary portion of this nozzle stuck in the open position and the nozzle acted as though it were a dual, fixed-orifice nozzle.

Another nozzle configuration operated for 50 hours at the same fuel temperatures and still repeated the required flow schedule close enough to not affect engine operation. The nozzle configuration used in the JTF17A-20 is based on this technology and the extreme difference in the temperatures expected in our engine and those run in this related program should provide a degree of permissiveness in engine operation. This permissiveness could be interpreted as something occurring during the aircraft operation such that the engine may be subjected to extreme increases in fuel temperatures for nonstandard operation. It would mean that although engine life may be affected and increased maintenance may be required, the engine will not have to shut down but can continue to operate for short periods of time.

The series of tests run on the full-scale, North American rig indicated that fuel nozzles would be one of the regions suffering during engine operation. The tests in our related program show that although fuel nozzles could be a problem it is possible to design a fuel nozzle in such a manner that these effects of high temperature fuel operation can be reduced. (See figure B-19.)

The measured high temperature rise is shown in figure B-20 for various areas in a fuel nozzle cluster. Our design will keep a very low residence time for the fuel, and the temperature rise in the JTF17A-20 nozzle holder will be lower than the temperature rise in the first nozzle of a cluster.

The only carbon deposits seen (figure B-21) inside the accepted nozzle configuration following runs at temperatures much more extreme than expected in our engine, were in the secondary swirl chamber and did not have a significant effect on the nozzle flow schedule. Other surfaces inside the nozzle were clean.

#### G. FUTURE PHASE II-C PROGRAM

J58 engine testing at simulated JTF17A-20 conditions is scheduled to begin this summer and it is planned to run simulated mission climb, cruise, and descent profile for the JTF17A-20 engine with heated fuel.

GS 2299

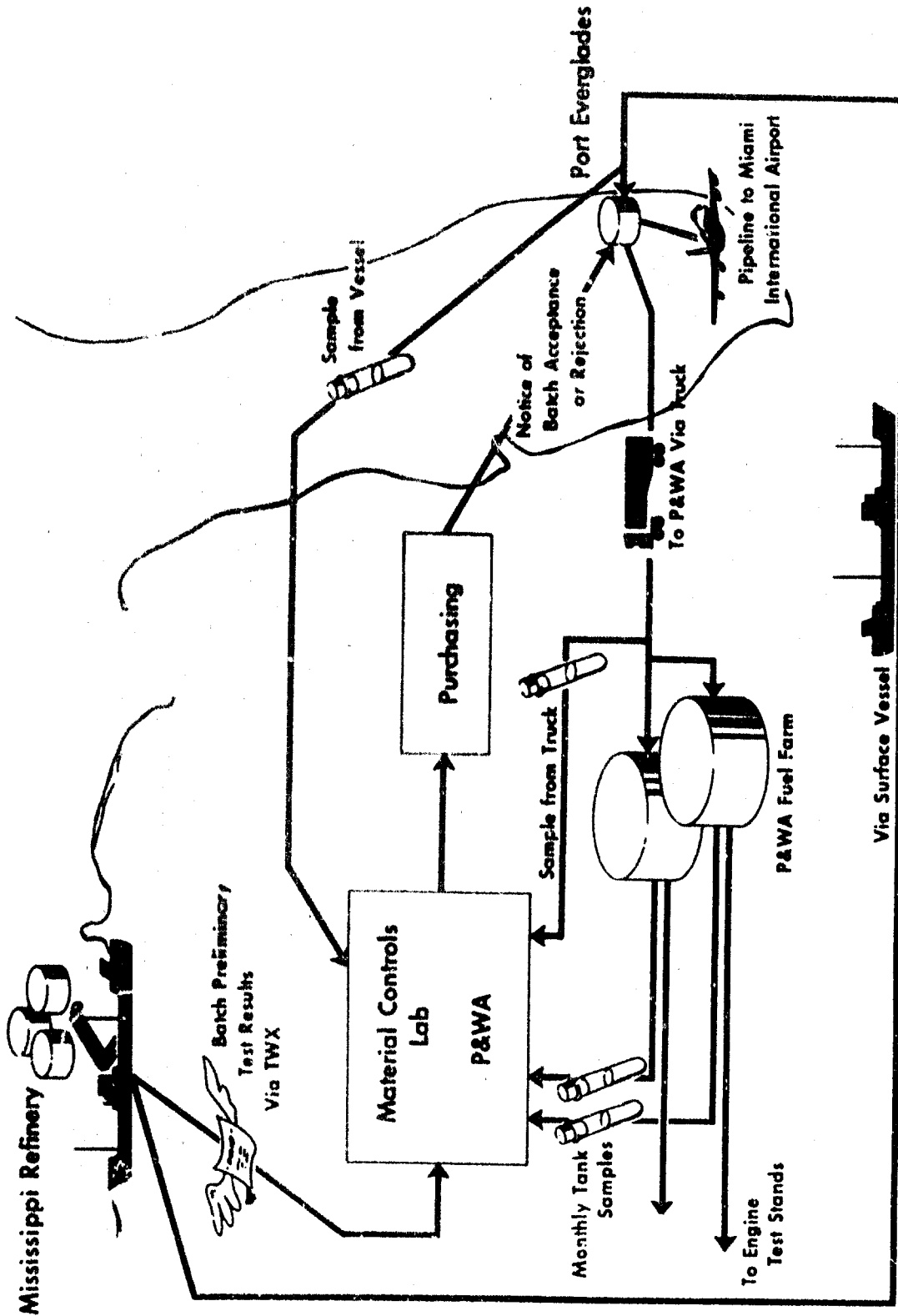
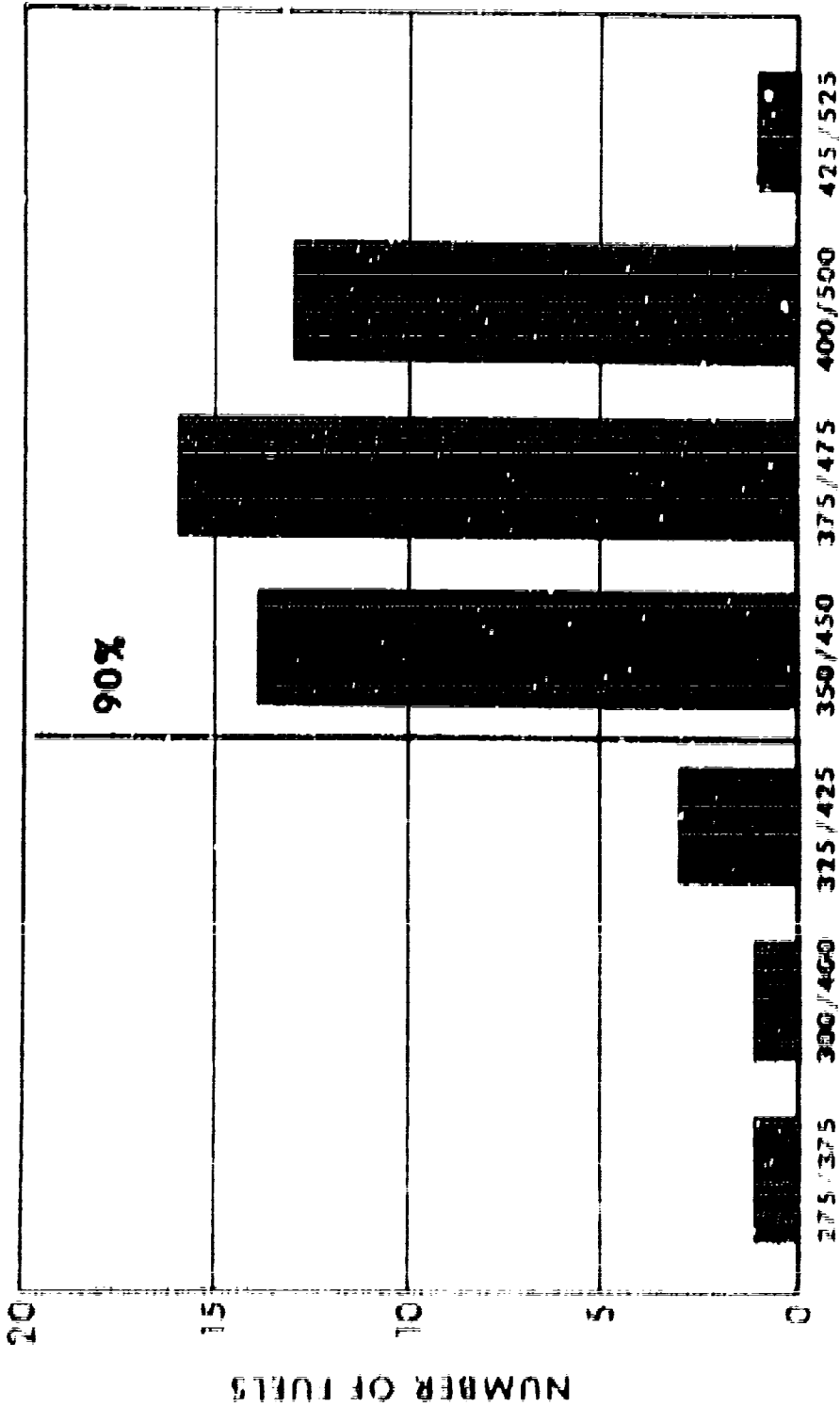


Figure B-1. Shipping and Storage Controls



Pratt & Whitney Aircraft

PWA PR-1A55  
Appendix B



PREHEATER/FILTER TEMP CONDITIONS - °F

Figure 1-1. Thermal Stability Summary

CS 2318

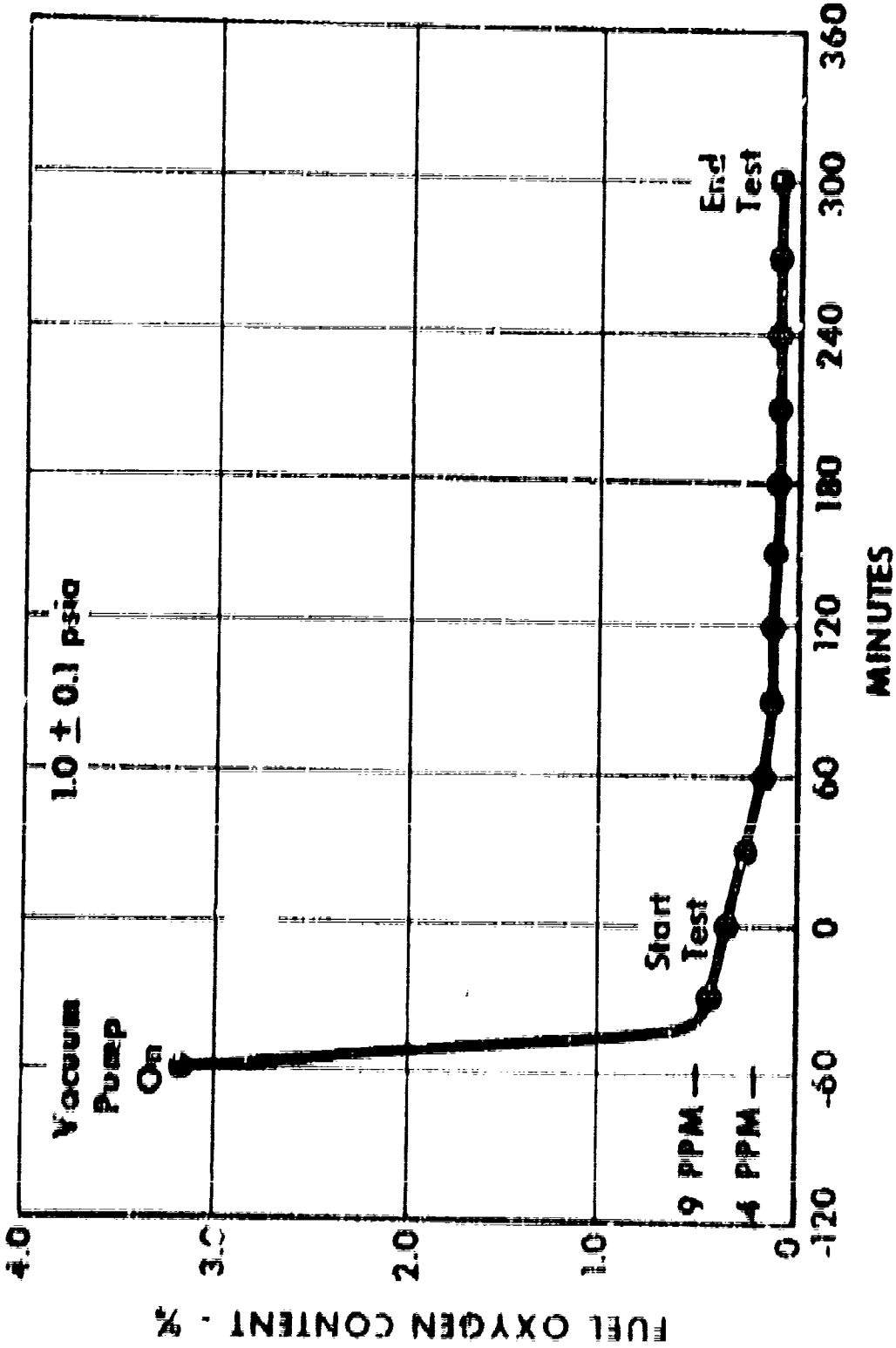


Figure 1-3. Oxygen Content at Low Pressure

Threshold Failure Temperature °F	
Standard Coker	Gain 1.5 psia 9 ppm O <sub>2</sub>
11 PWA Samples  300/460 to 375/475	Gain 1.0 psia 4 ppm O <sub>2</sub>  25° to 175°  -50 to 125

Figure B-4. Effect of Low Oxygen Content on Threshold Failure Temperatures

PWA Sample No.	Threshold Failure Temp °F		
	Standard Coker	Gain 1.0 psia 4 ppm O <sub>2</sub>	Gain 1.5 psia 9 ppm O <sub>2</sub>
1564	325	25	0
1565	325	75	-25
1566	350	75	50
1567	325	150	-50
1568	325	175	125
1569	350	25	-50
1573	325	25	25
1595	375	175	-25
1596	350	150	0
1597	300	150	-25
1598	350	125	50

GS 2391

Figure B-5. Effect of Low Oxygen Control on Threshold Failure Temperature.

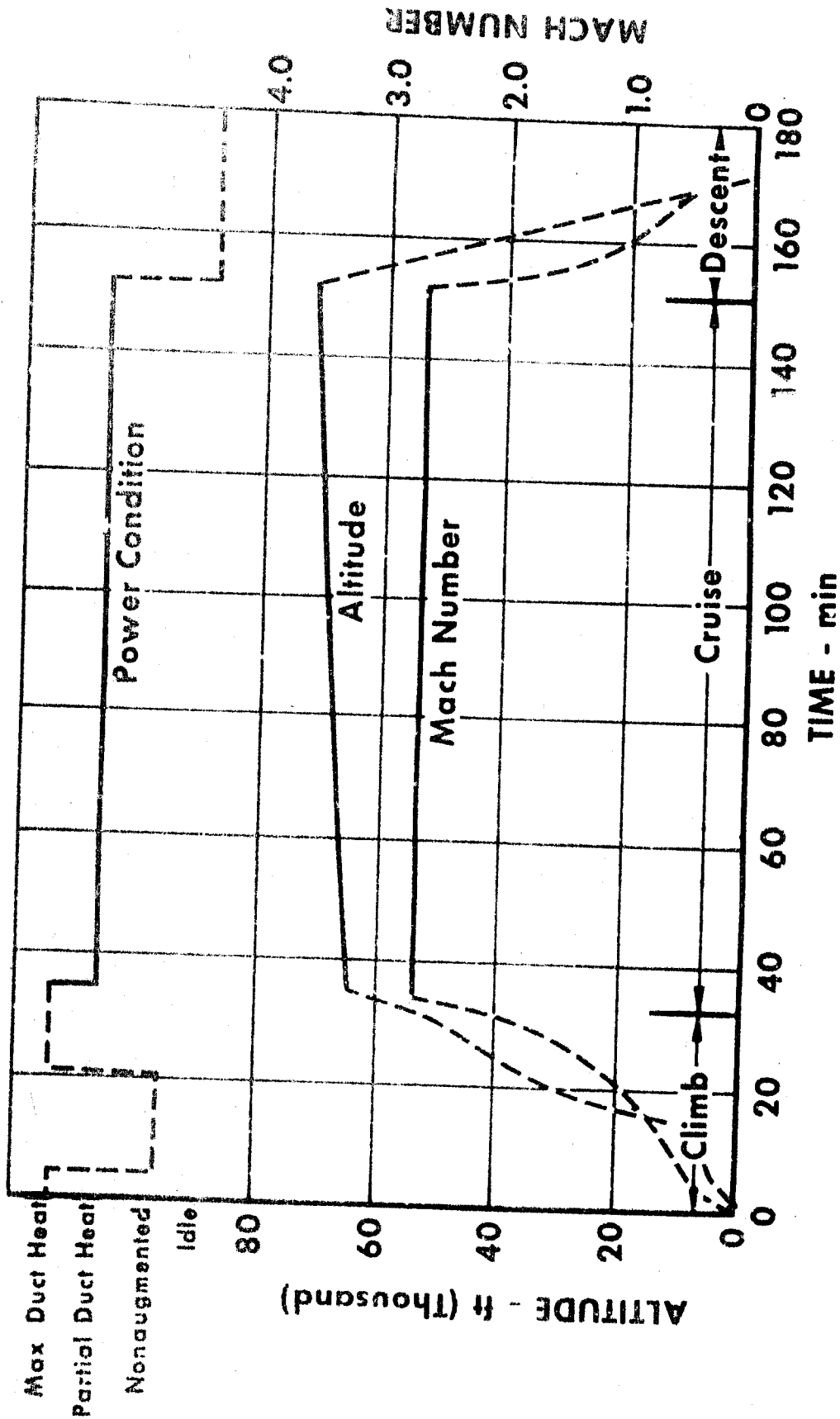
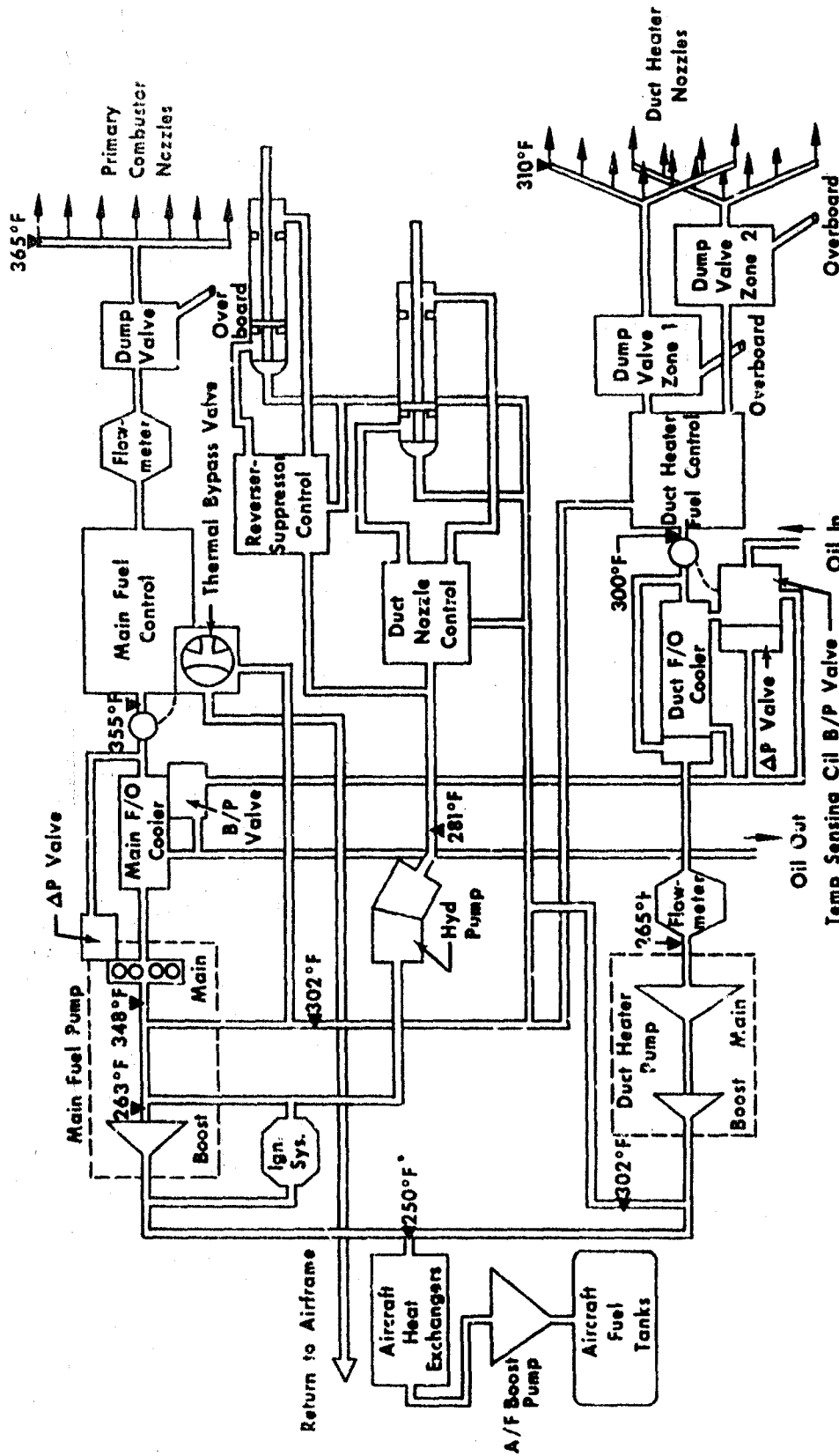


Figure B-6. Typical Mission Profile



\*Maximum fuel temperature allowed by engine specification

Figure B-7. JTF17A-20 Fuel System Schematic (Calculated Bulk Fuel Temperatures)

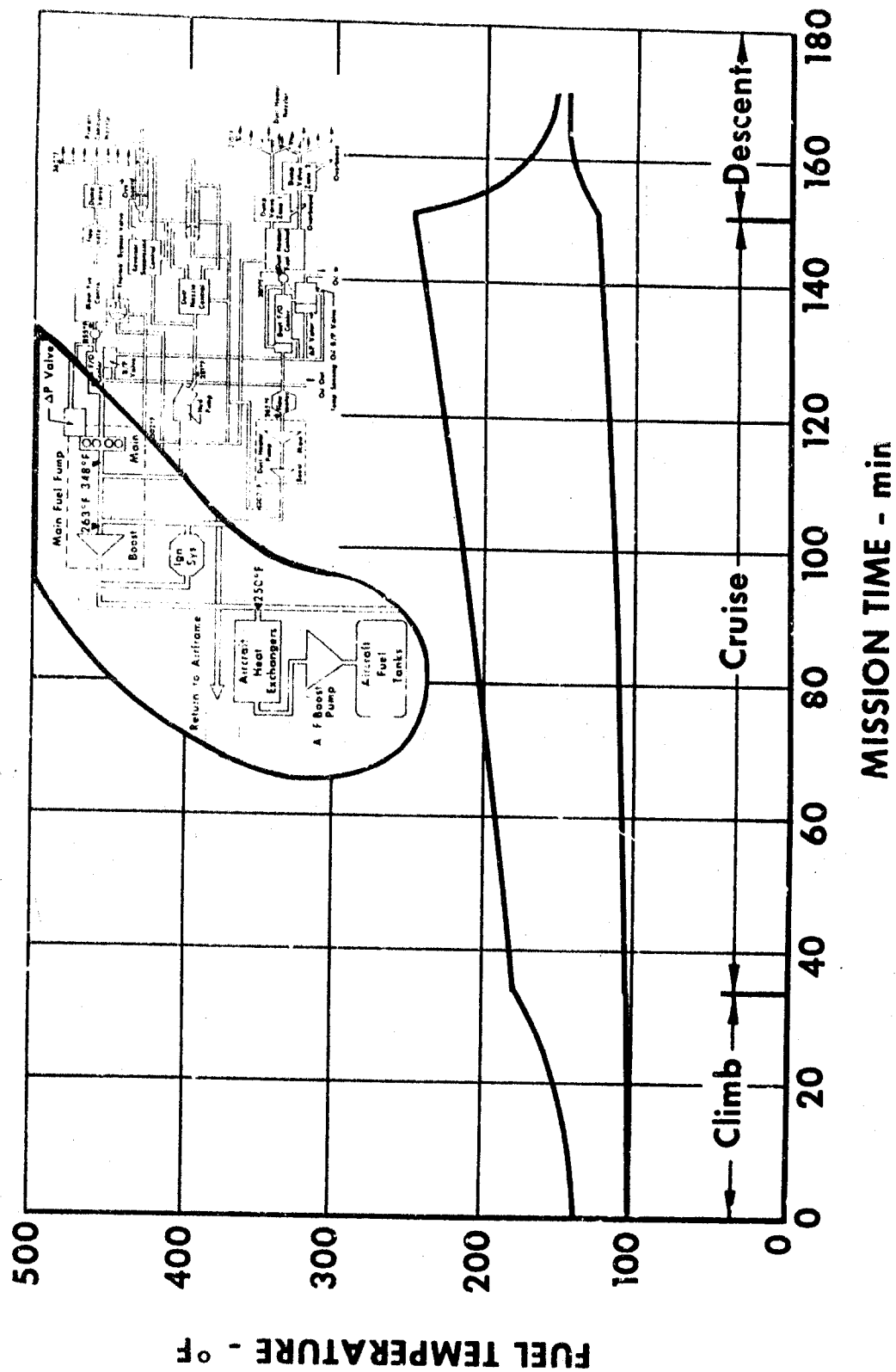


Figure B-8. Engine Fuel Inlet Temperature (Estimated Maximum)

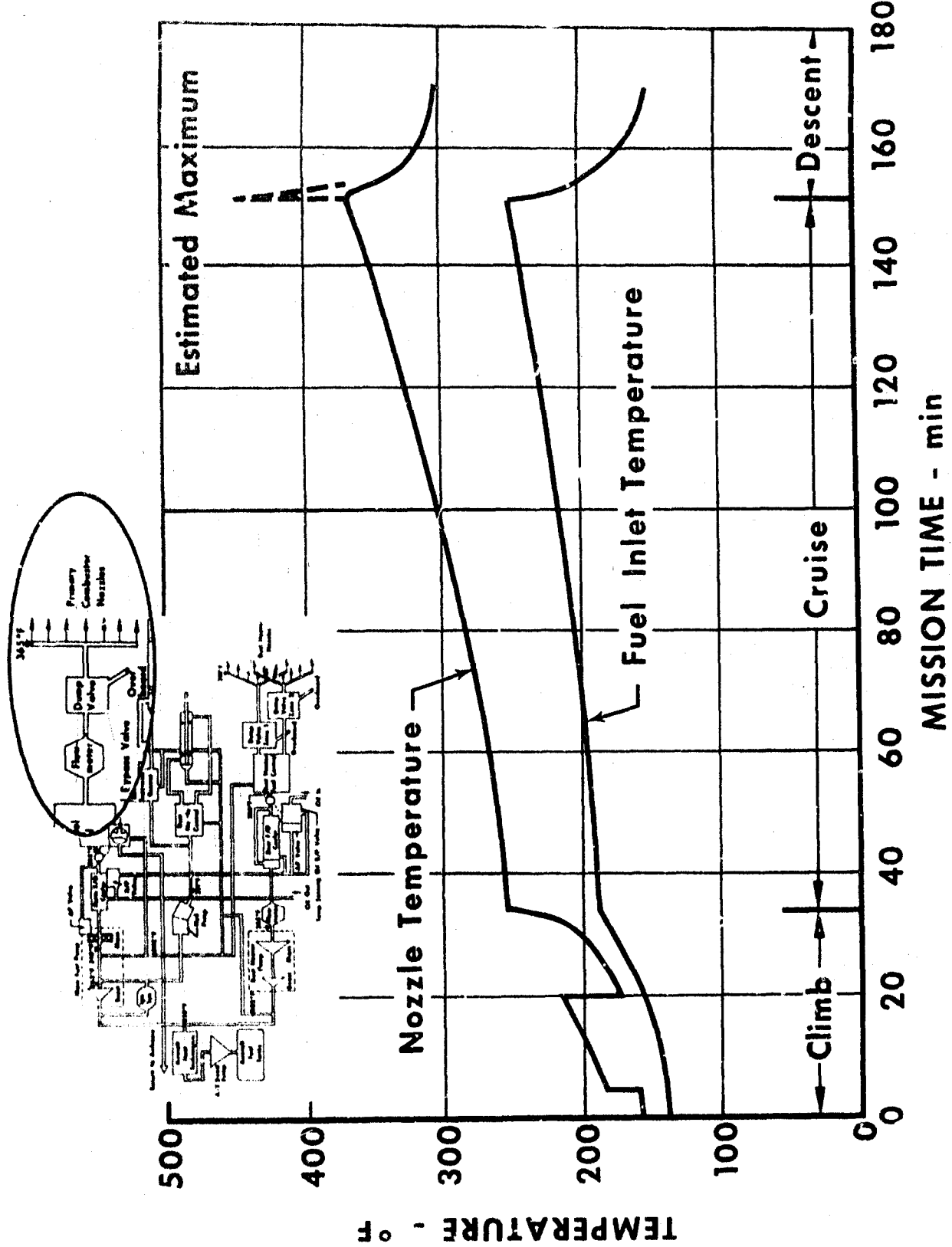


Figure B-9. Primary Nozzle Fuel Temperature (Estimated Maximum)



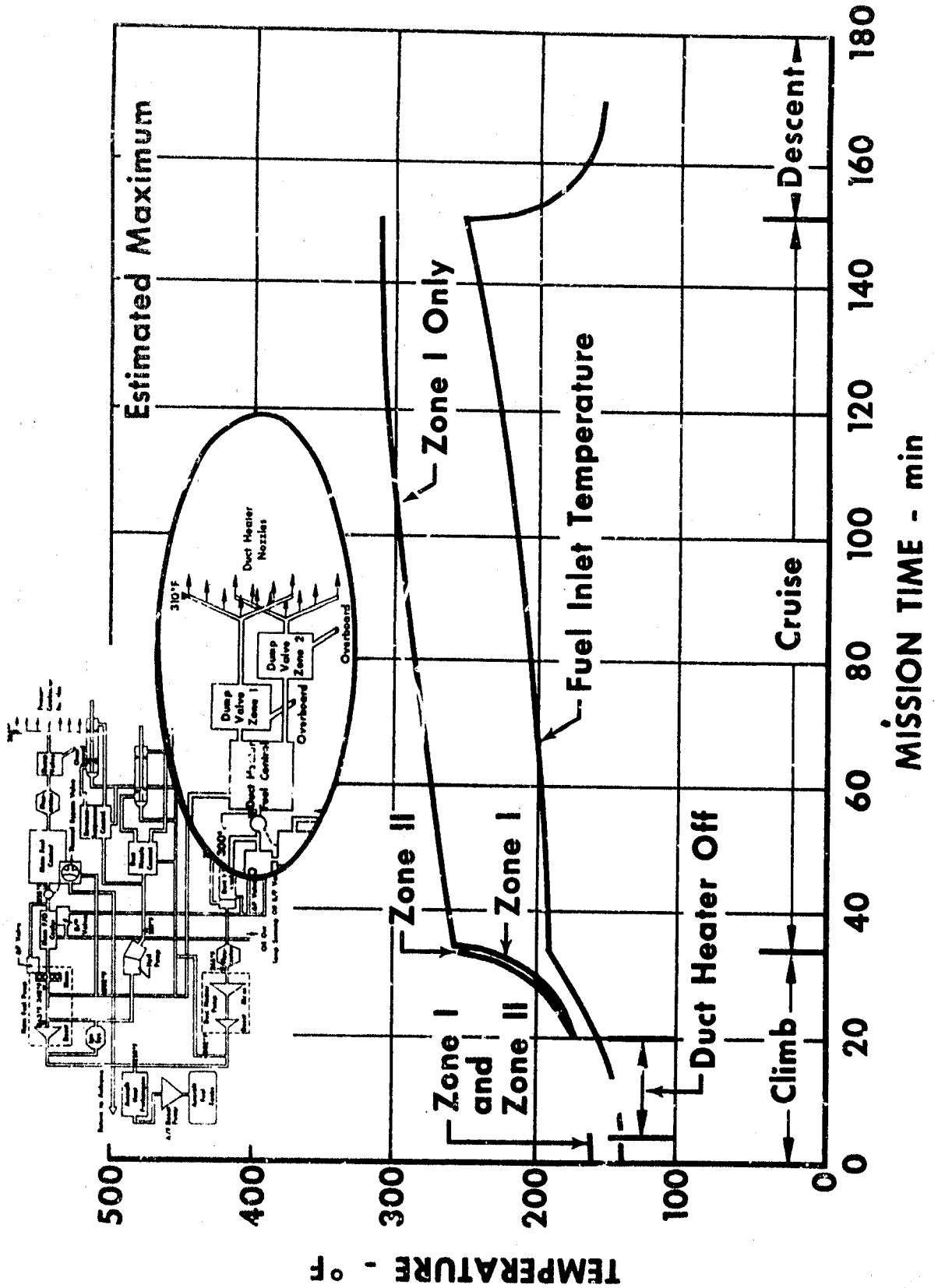


Figure B-10. Duct Heater Fuel Temperature (Estimated Maximum)

GS 2376

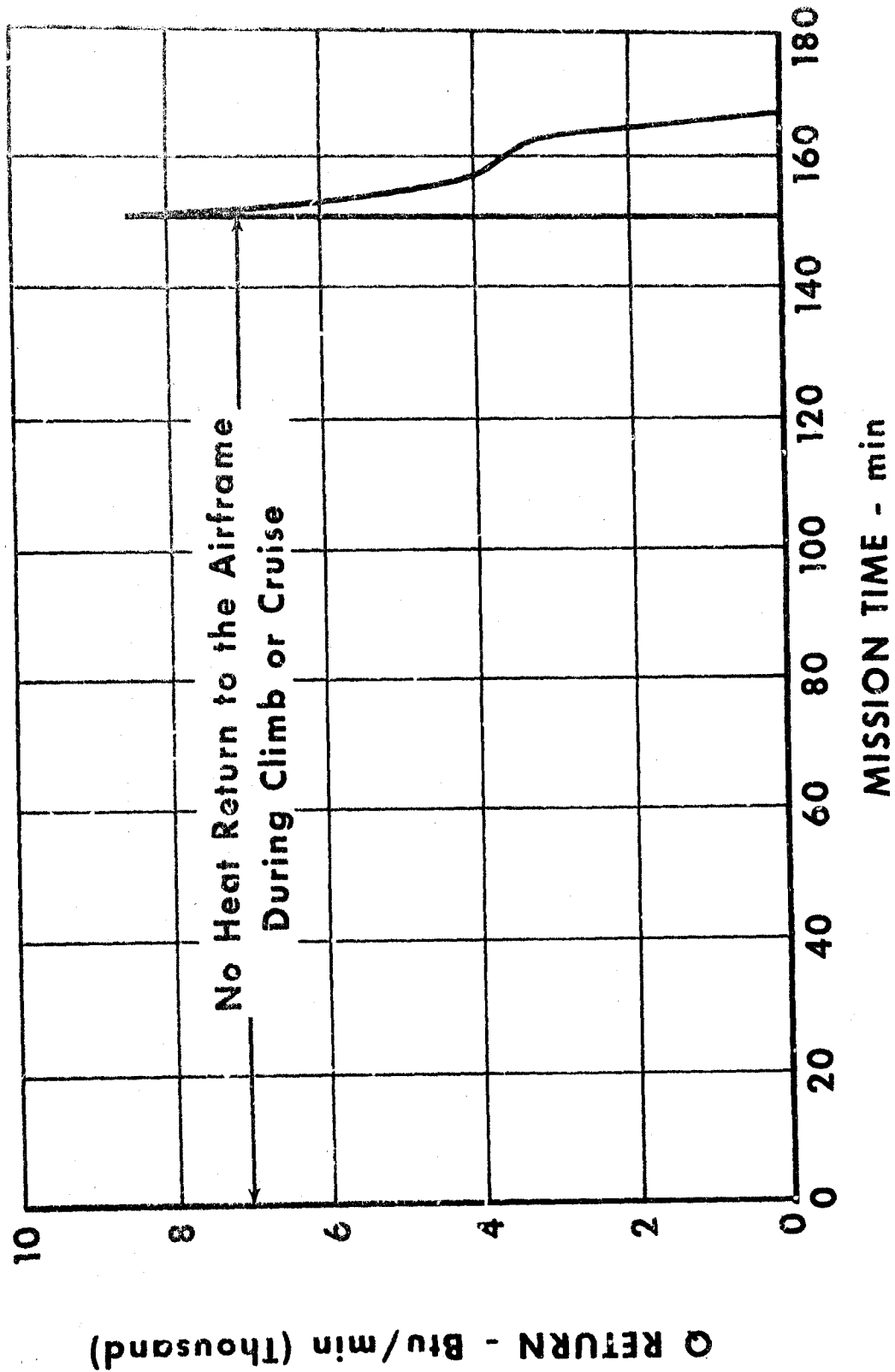


Figure B-11. Heat Return Rate to Airframe

GS 2377

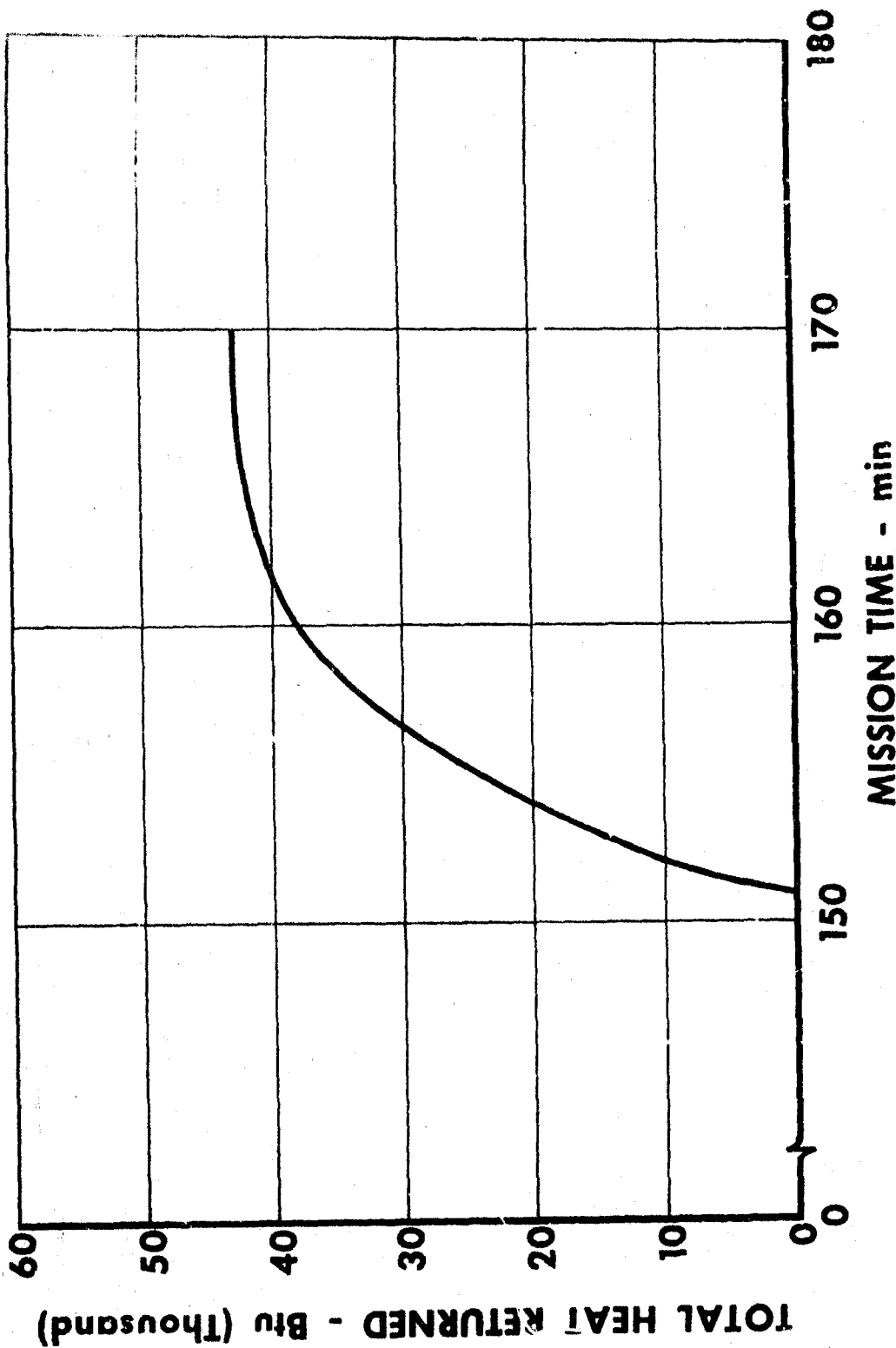


Figure B-12. Total Heat Return to Airframe

ES 2315

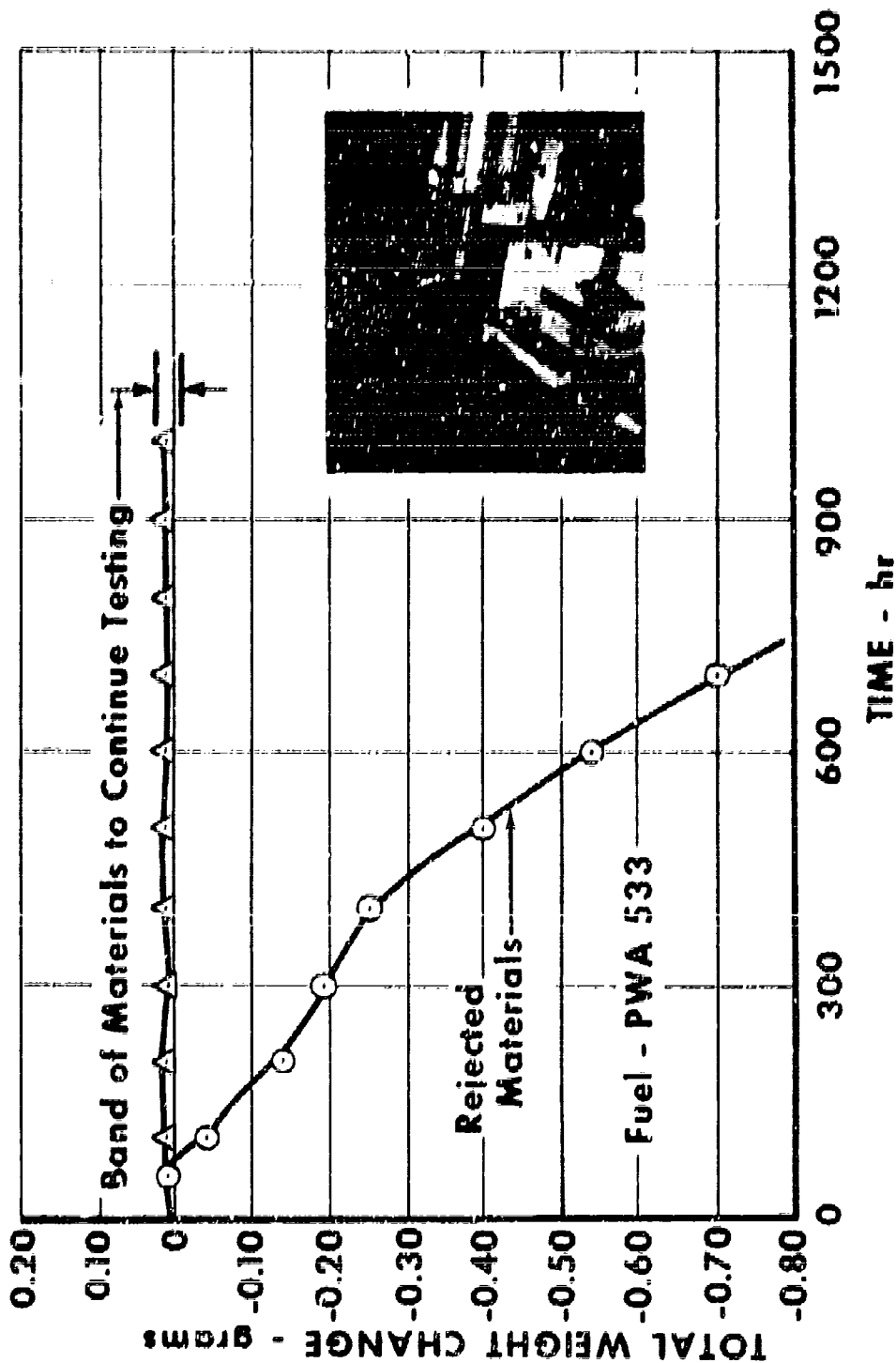


Figure B-13. Erosion-Corrosion Tests

SS 1368

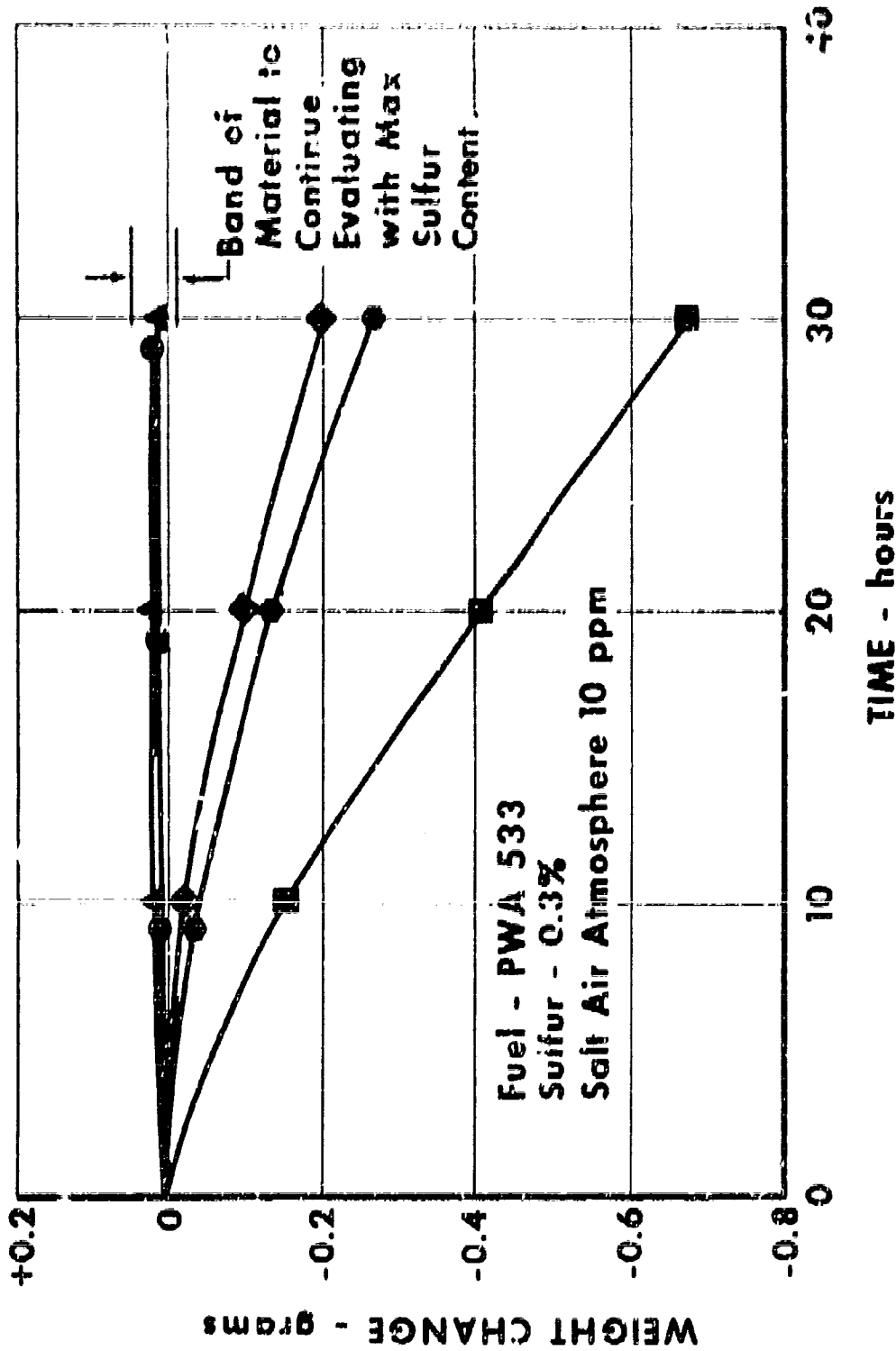


Figure B-14. Accelerated Erosion-Corrosion Tests

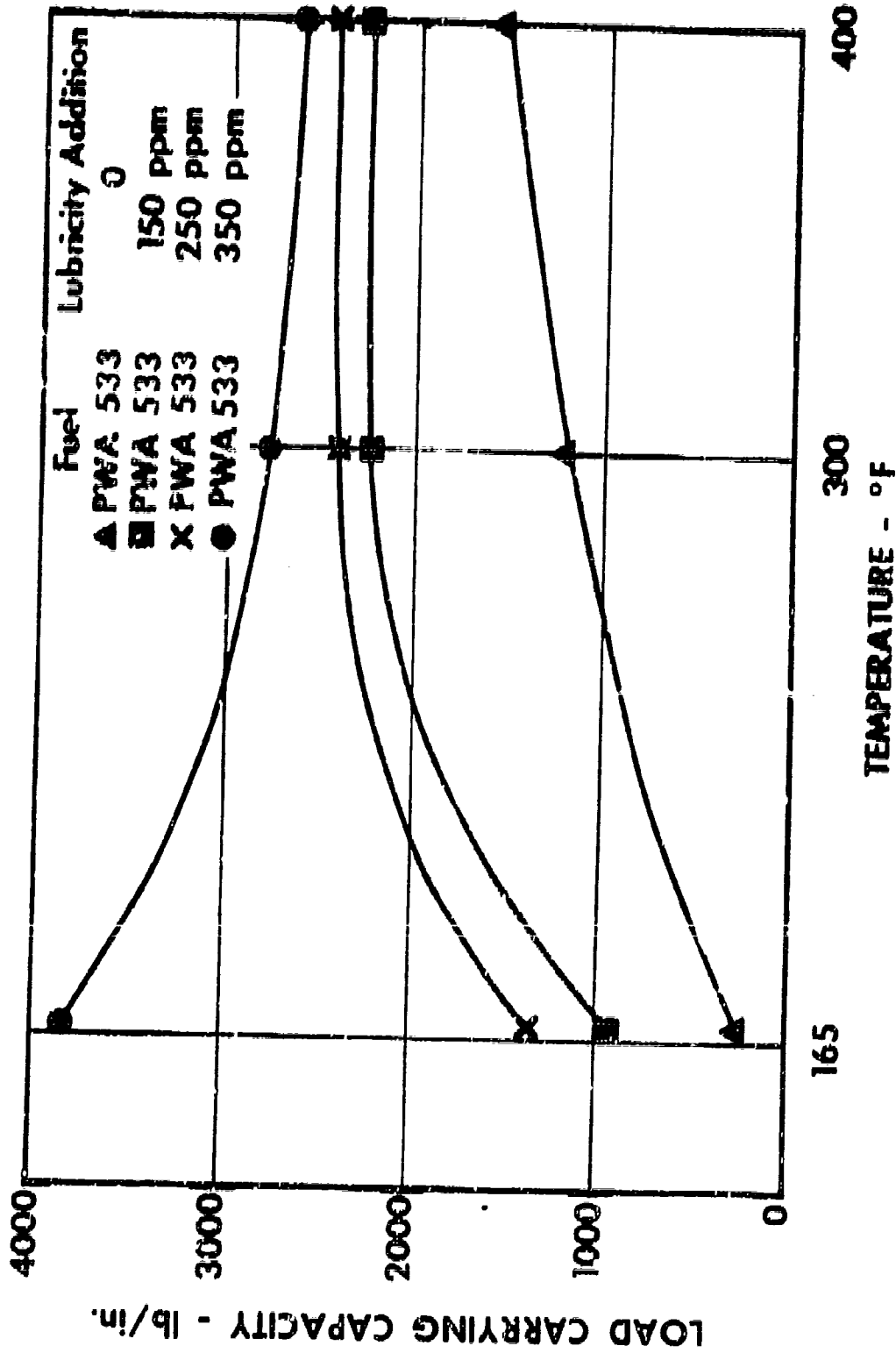


Figure B-15. Lubricity - Ryder Gear Rig

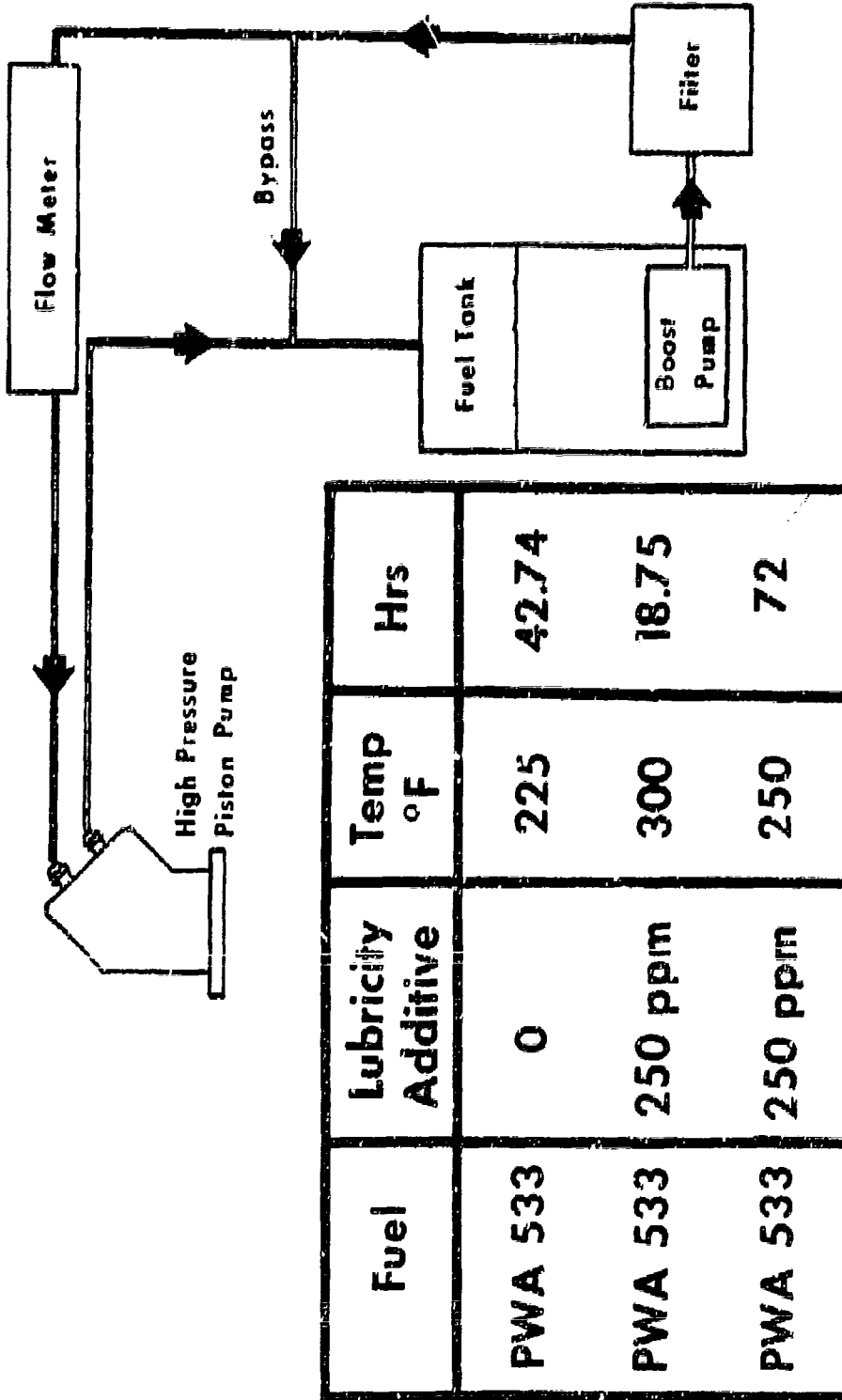


Figure B-16. Lubricity - Accelerated Pump Wear Test Related Activity

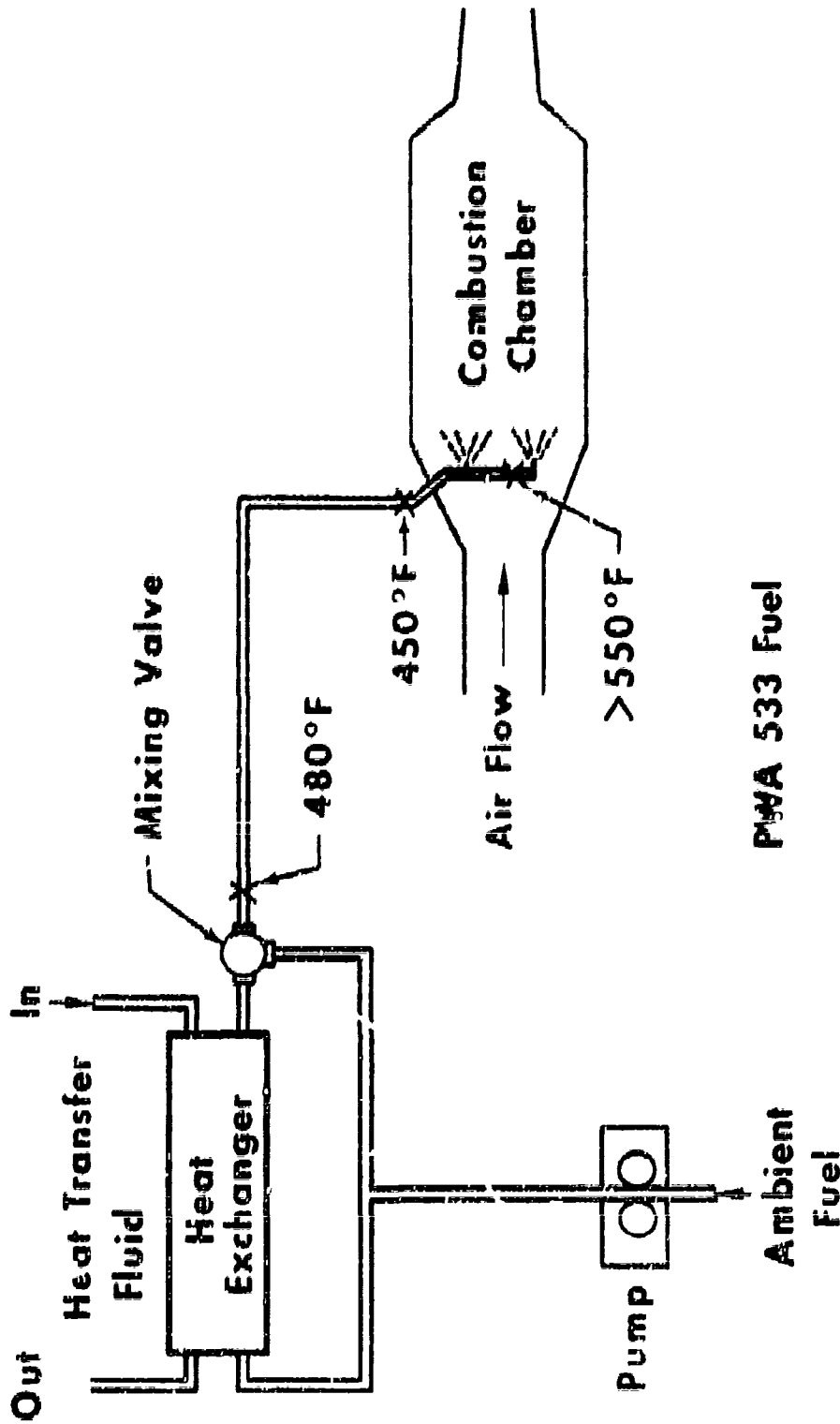


Figure B-17. Nozzle Tests with Heated Fuel Related Activity



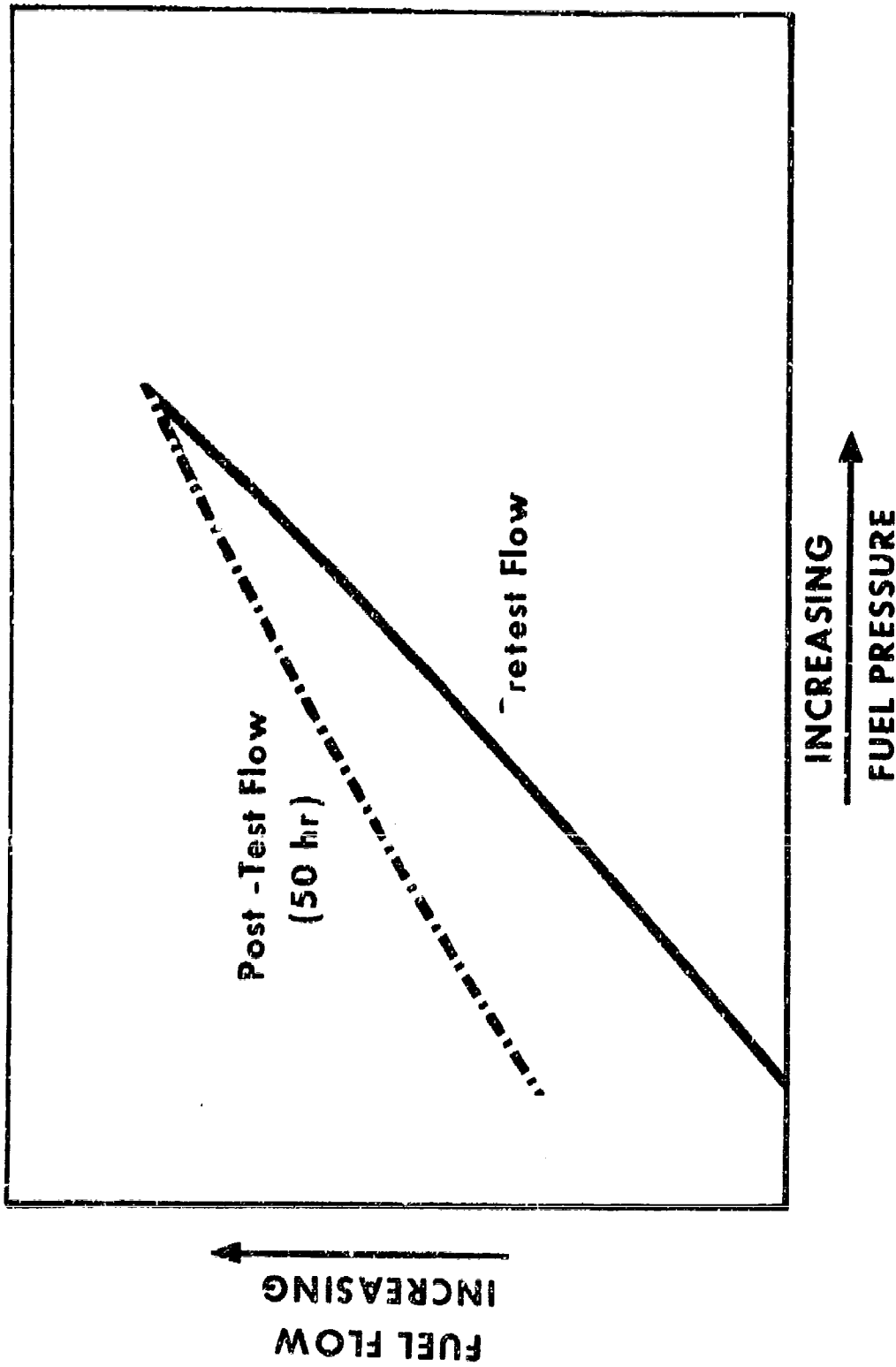


Figure B-18. Hot Fuel Test on Rejected Nozzle Configuration

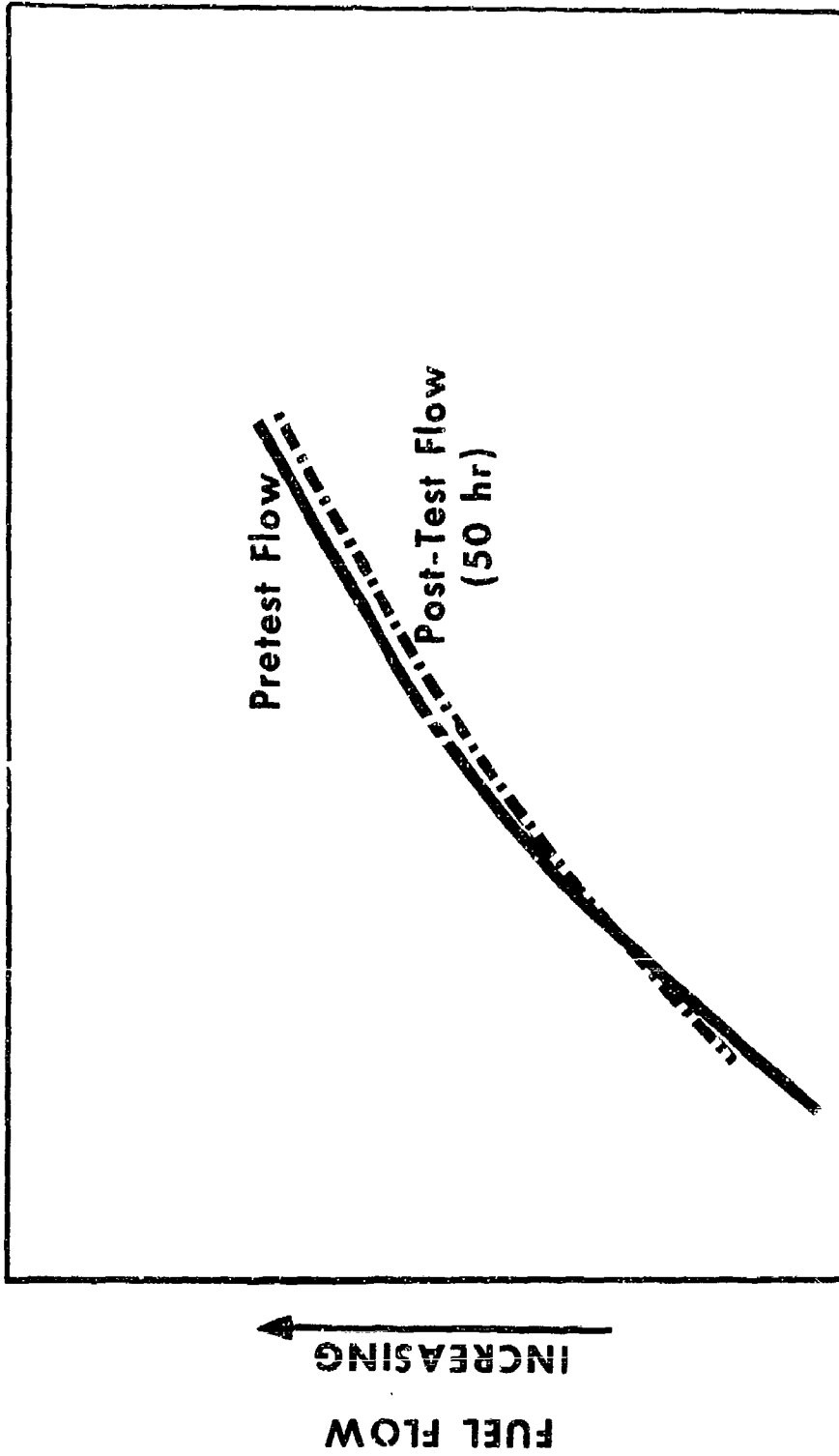
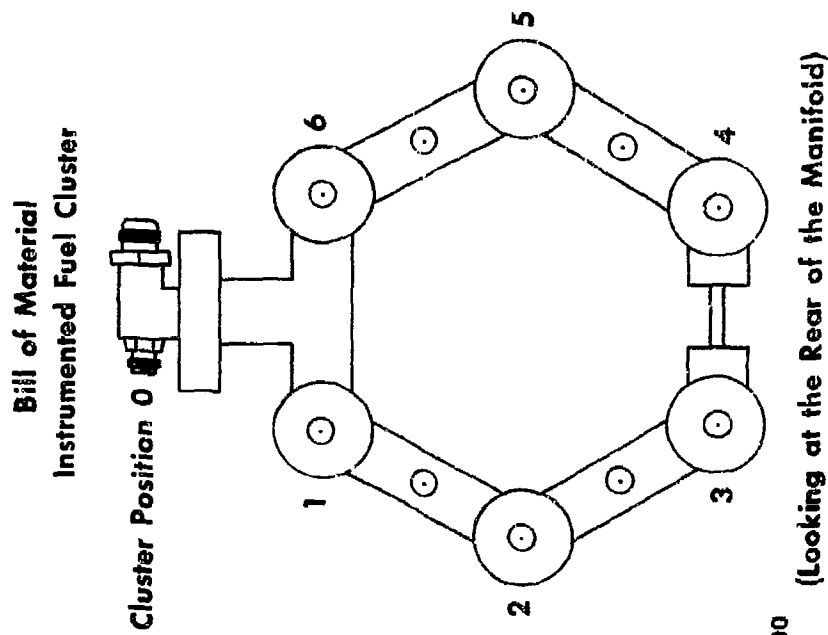


Figure B-19. Hot Fuel Test on Nozzle Configuration Accepted



**Temperature Rise in Internal Fuel  
Manifold (Heatshielded)**

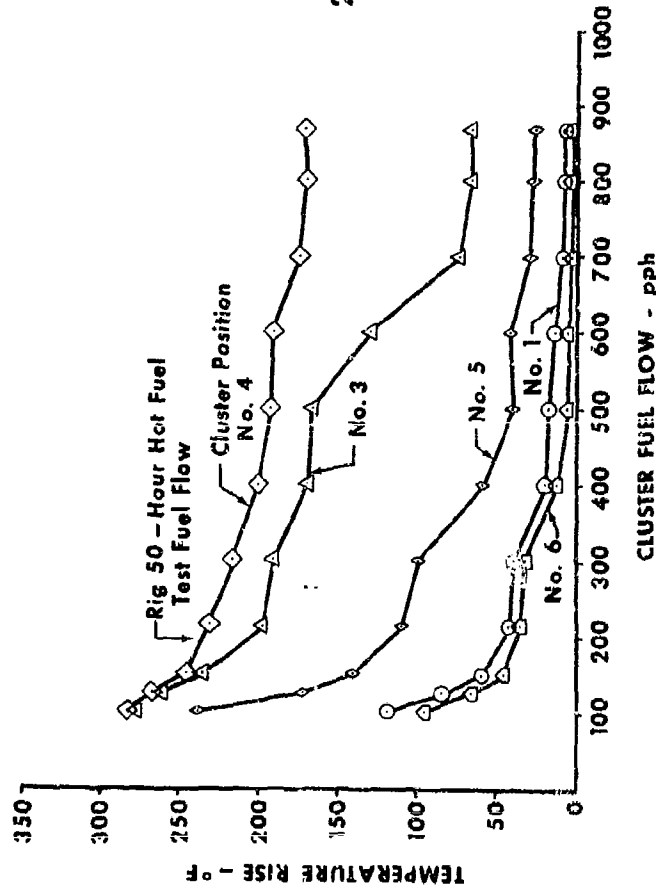


Figure B-20. Internal Manifold Fuel Temperature Rise

Pratt & Whitney Aircraft

PWA FR-1855  
Appendix B

GS 2375

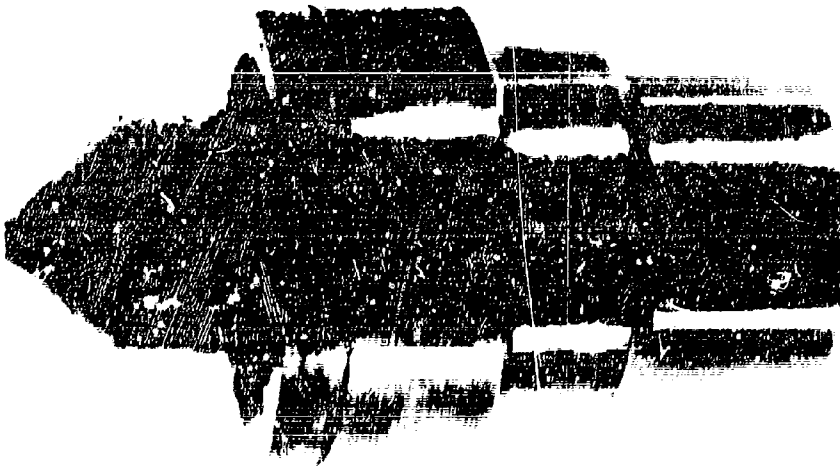
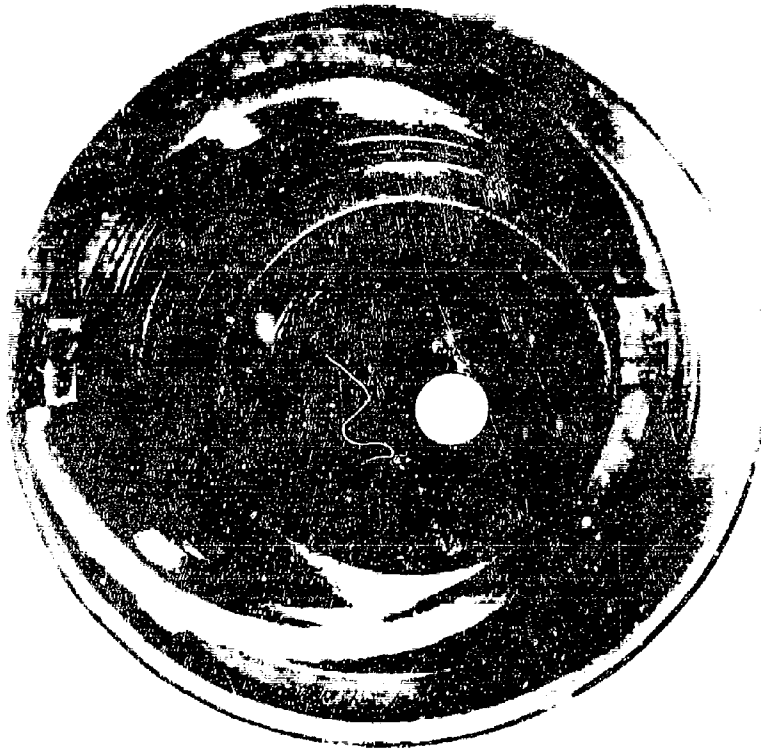


Figure B-21. Nozzle Secondary Swirl Chamber Deposits